AD

USAAVLABS TECHNICAL REPORT 68-31

HOT CYCLE ROTOR/WING COMPOSITE RESEARCH AIRCRAFT

By

C. R. Smith

August 1968

U. S. ARMY AVIATION MATERIEL LABORATORIES
FORT EUSTIS, VIRGINIA

CONTRACT DA 44-177-AMC-338(T)
HUGHES TOOL COMPANY, AIRCRAFT DIVISION
CULVER CITY, CALIFORNIA

Disclaimers

The findings in this report are not to be construed as an official Department of the Army position unless so designated by other authorized documents.

When Government drawings, specifications, or other data are used for any purpose other than in connection with a definitely related Government procurement operation, the United States Government thereby incurs no responsibility nor any obligation whatsoever; and the fact that the Government may have formulated, furnished, or in any way supplied the said drawings, specifications, or other data is not to be regarded by implication or otherwise as in any manner licensing the holder or any other person or corporation, or conveying any rights or permission, to manufacture, use, or sell any patented invention that may in any way be related thereto.

Trade names cited in this report do not constitute an official endorsement or approval of the use of such commercial hardware or software.

Disposition Instructions

Destroy this report when no longer needed. Do not return it to the originator.

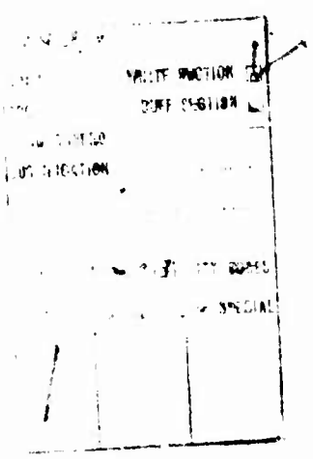

DISCLAIMER NOTICE

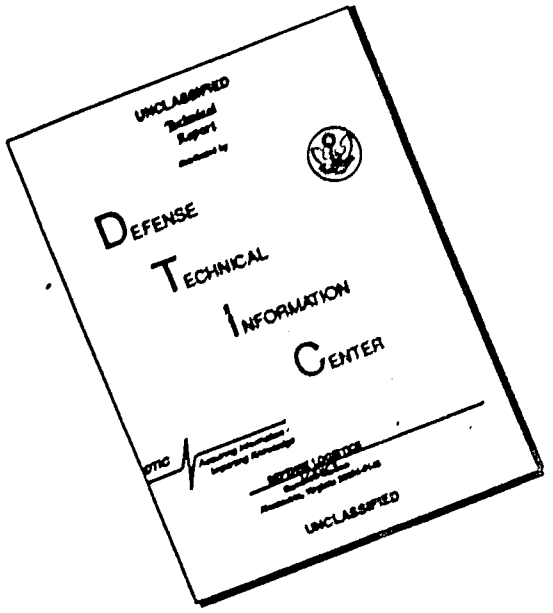

THIS DOCUMENT IS BEST QUALITY AVAILABLE. THE COPY FURNISHED TO DTIC CONTAINED A SIGNIFICANT NUMBER OF PAGES WHICH DO NOT REPRODUCE LEGIBLY.

DEPARTMENT OF THE ARMY
U. S. ARMY AVIATION MATERIEL LABORATORIES
FORT EUSTIS, VIRGINIA 23604

This report is a summary of the preliminary design study of a Hot Cycle Rotor/Wing Composite Research Aircraft (CRA) concept. The general objective of the CRA was to combine into one research aircraft the efficient hovering characteristics of a helicopter and the high-speed cruise characteristics of fixed-wing aircraft.

This study presents one approach to meeting the above objective. This report is published for the dissemination of information and the stimulation of new ideas.

Task 1F163204D15704
Contract DA 44-177-AMC-338(T)
USAAVLABS Technical Report 68-31

August 1968

HOT CYCLE ROTOR/WING COMPOSITE RESEARCH AIRCRAFT

HTC-AD 67-85

By

C. R. Smith

Prepared by

Hughes Tool Company, Aircraft Division
Culver City, California

for

U. S. ARMY AVIATION MATERIEL LABORATORIES
FORT EUSTIS, VIRGINIA

ABSTRACT

A preliminary design study conducted by Hughes Tool Company - Aircraft Division (HTC-AD) has defined the configuration and characteristics of the Hot Cycle Rotor/Wing aircraft shown in Figure 1. This design study was carried out, in accordance with the Army's Composite Research Aircraft (CRA) requirements, for the U. S. Army Aviation Materiel Laboratories (USAAVLABS).

The Hot Cycle Rotor/Wing combines, for the first time, the helicopter and the jet airplane in the form of the Hot Cycle Rotor/Wing lifting system. This is a tip-jet powered helicopter rotor with a very large hub. The Rotor/Wing can be stopped in flight to become a fixed wing (Figure 2), and the aircraft flies as a jet airplane.

The Hot Cycle Rotor/Wing CRA provides the advantages of hovering efficiency, low downwash velocity, and helicopter-like flying qualities for vertical and low-speed flight, in addition to the high-speed capability and cruise efficiency of the jet airplane. Its simplicity and light weight is made possible through the combined use of the all-pneumatic Hot Cycle drive system and the dual-purpose Rotor/Wing lift system. This eliminates the need for heavy and complex mechanical drive components and antitorque tail rotor; it permits flight as a helicopter and as an airplane without recourse to duplicate lifting systems or to folding, tilting, or retracting of lift systems to effect conversion.

With excellent hover and payload capabilities, a maximum speed of 490 knots, and maximum lift-to-drag ratio of 12, the Hot Cycle Rotor/Wing will exceed all CRA performance requirements and will make possible a major advance in vertical-lift aircraft technology.

Substantiation of all basic technical aspects of the CRA design is available from the results of the USAAVLABS XV-9A Hot Cycle Research Aircraft program and from extensive Hughes- and Government-sponsored analysis, whirl testing, and wind tunnel testing that have defined basic aerodynamic characteristics of the Rotor/Wing in all modes of flight. The Composite Research Aircraft based on the Rotor/Wing will further substantiate and refine the concept.

A convenient performance summary is provided as a foldout on page 307, Appendix V.

TABLE OF CONTENTS

LIST OF ILLUSTRATIONS

LIST OF TABLES

LIST OF SYMBOLS

(See note at bottom of page xxvii.)

A	area, sq in.
A	rotor disc area, sq ft
AR	wing aspect ratio, locked mode
A_d	rotor annulus area, sq ft
a	lift curve slope, lb/rad
B	rotor tip loss factor
B_l	lateral cyclic pitch, deg.
b	number of blades
b	fuselage average width, in.
C	torque
$\overline{C}$	mean aerodynamic chord
$1/C_{1/2}$	damping parameter, 1/cycle to 1/2 amplitude
C_D	drag coefficient
$\Delta C_{D \text{ at } C_L}$	increment in drag coefficient due to leading edge vortex generation
ΔC_{D_M}	increment in drag coefficient due to compressibility
C_{D_0}	minimum parasite drag coefficient
CF	centrifugal force, lb
CG	center of gravity
C_L	lift coefficient
C_{L_S}	lift coefficient at stall

C_{L_T}	tail lift coefficient
C_{L_α}	lift coefficient with respect to angle of attack, per rad or per deg
C_M	pitching moment coefficient
$\Delta(dC_M/dC_L)$	incremental pitching moment coefficient derivative with lift coefficient
C_N	yawing moment coefficient
C_{N_p}	yawing moment coefficient derivative with respect to roll rate, per rad
C_{N_r}	yawing moment coefficient derivative with respect to yaw rate, per rad
C_{N_β}	yawing moment coefficient derivative with respect to sideslip angle, per rad
C_Q	rotor torque coefficient, $Q/\rho\pi R^3 (\Omega R)^2$
C_T	rotor thrust coefficient
C_{Ve}	nozzle velocity coefficient
C_Y	side force coefficient
C_{Y_p}	side force coefficient derivative with respect to roll rate, per rad
C_{Y_r}	side force coefficient derivative with respect to yaw rate, per rad
C_{Y_β}	side force coefficient derivative with respect to sideslip angle, per rad
C_f	skin friction drag coefficient
C_ℓ	rolling moment coefficient
C_{ℓ_p}	rolling moment coefficient derivative with respect to roll rate, per rad
C_{ℓ_r}	rolling moment coefficient derivative with respect to yaw rate, per rad

C_{ℓ_β}	rolling moment coefficient derivative with respect to sideslip angle, per rad
$\partial C_m / \partial C_L$	pitching moment coefficient slope
c	rotor chord, ft
c	distance from neutral axis to extreme fiber, in.
c	fuselage average depth, in.
c_e	$\frac{\int_a^1 cx^2\,dx}{\int_o^1 x^2\,dx}$, effective blade chord, ft
cg	center of gravity
c_i	blade taper and twist factor
D	rotor diameter, in.
D	distance between centroids of span caps, in.
d	maximum width, in. or ft
E	modulus of elasticity, lb/sq in.
e	span efficiency factor
e	percent elongation
F_B	allowable bending stress, lb/sq in.
F_C	allowable compressive stress, lb/sq in.
FS	fuselage station, in.
Fc_{cr}	critical compressive stress, lb/sq in.
F_{cr}	critical stress, lb/sq in.
F_{cy}	allowable compressive stress, lb/sq in.
F_t	tensile stress, lb/sq in.

F_{tu}	allowable tension stress, lb/sq in.
F_{tu}/w	static strength/density, in.
F_{ty}	allowable tension stress, lb/sq in.
F_{ty}/w	static strength/density, in.
f	stress, lb/sq in.
f_b	bending stress, lb/sq in.
f_c	compressive stress, lb/sq in.
f_s	shear stress, lb/sq in.
G	modulus of rigidity, lb/sq in.
$\overline{GR}$	gear ratio
g	damping
H	horizontal
H	horizontal bearing load, lb
h	fuselage height, in. or ft
I	moment of inertia, $in.^4$
IGE	in ground effect
K	autorotational constant
KEAS	equivalent airspeed, kn
KIAS	indicated airspeed, kn
K_t	stress concentration factor
K_y	constant - depends on R/t ratio
L	fuselage length, ft

L	duct stiffener spacing, in.
L	length, in.
L/D	aerodynamic lift/drag ratio
LER	leading edge radius
LOH	light observation helicopter
$\partial L/\partial \beta$	rolling moment derivative with respect to sideslip angle, ft-lb/deg
ℓ/a	length-to-diameter ratio
M	Mach number
M	moment, in.-lb
MAC	mean aerodynamic chord
M_C	chordwise bending moment, in.-lb
M_{CF}	moment due to centrifugal force, in.-lb
M_D	drag divergence Mach number
M_F	flapwise bending moment, in.-lb
M_α	pitching moment derivative with respect to angle of attack, ft-lb/deg
$\partial M/\partial \alpha$	pitching moment derivative with respect to angle of attack, ft-lb/deg
N_R	rotor, rpm
$\partial N/\partial \beta$	yawing moment derivative with respect to sideslip angle, ft-lb/deg
n	ultimate load factor, g
n	rotor speed, rps

OGE	out of ground effect
P	pressure in duct, lb/sq in.
P	force, lb
PPF	profile power factor (empirical correction factor from test)
P_T/P_{T_7}	average blade duct pressure/engine exhaust total pressure
$\Delta P_t/P_{t_5}$	tail pipe pressure loss ratio
p	roll rate, rad/sec or deg/sec
p'	elastic constant, lb/in.
Q	low speed torque, ft-lb
q_T/q	ratio of dynamic pressure at tail to free stream dynamic pressure
q_{wake}	dynamic pressure corresponding to v_{wake}, lb/ft
$q_{a,b,c,d,e}$	shear flow as noted on Figure 142, lb/in.
q_{w_1, w_2, w_3, w_4}	shear flow as noted on Figure 142, lb/in.
q_{max}	shear flow, lb/in.
R	rotor radius, ft
R	stress ratio
R	duct radius, in.
RN	Reynolds number
$R_{1x}, R_{2y}, R_{2z}, R_{3y}, R_{3z}$	load applied to exhaust duct, lb.

r	yaw rate, rad/sec
r	duct radius
r	radial station along blade, ft
r	corner radius of fuselage, ft
r_c	radius of curvature, ft
S	area, sq ft
SFC	specific fuel consumption $\frac{\text{lb/hr}}{\text{lb thrust}}$
S_{disc}	rotor disc area, sq ft
S_T	total tail area, sq ft
S_{wet}	wetted area, sq ft
T	temperature, °R or °K
T	total rotor thrust, lb
T	torque, in.-lb
T_{net}	net rotor thrust after download is deducted, lb
t	time, sec
t	duct wall thickness, in.
Δt	change in temperature, °F
t/c	thickness-to-chord ratio
U_D	divergence speed, kn
U_F	flutter speed, kn
V	shear, lb
V	flight velocity, ft/sec or kn

V_F	flight velocity, ft/sec or kn
V_H	level flight velocity, ft/sec or kn
V_L	limit flight speed, kn
V_{S_L}	stall speed, landing configuration, kn
V_T	blade tip speed, ft/sec
V_{max}	maximum speed, mph
V_{ne}	never exceed velocity, kn
V_{tip}	blade tip speed, ft/sec
V_v	vertical climb speed, ft/sec
vt	vertical tail
v_{wake}	fully developed velocity in rotor slipstream, ft/sec
W_B	fuselage (or body) group weight, lb
W_g	design gross weight, lb
w	fuselage width, in. or ft
w	density, $lb/in.^3$
w	web thickness, in.
X	r/R nondimensional distance to radial blade station
$\overline{X}$	center of gravity, percent MAC
Z/D	ratio of vertical distance from rotor plane to rotor diameter
α	coefficient of thermal expansion, in./in./°F
α_F	fuselage angle of attack, deg
α_W	wing angle of attack, deg

α_T	tail angle of attack, deg
α_r	local blade section angle of attack, deg
δ_{ELEVON}	elevon deflection angle, deg
$\Delta\delta e$	differential elevon deflection angle, deg
$\delta_0, \delta_1, \delta_2$	coefficients in classical blade drag coefficient equation (see reference 20)
ϵ_T	downwash angle at horizontal tail, deg
$d\epsilon/d\alpha$	downwash angle derivative with respect to angle of attack
η_t	ratio of dynamic pressure at tail to free stream dynamic pressure
θ	collective pitch, deg
θ	pitching amplitude, deg
θ	rolling amplitude, deg
θ	variable angle for shear flow calculations, deg
Λ	leading edge angle of sweep, deg
μ	rotor advance ratio
ν	kinematic viscosity, sq ft/sec
ν_e	Poisson's ratio
ρ	radius of gyration, in.
ρ	mass density, slugs/ft^3
σ	rotor solidity ratio, $bC_e/\pi R$
σ	direct stress due to bending, lb/sq in.
σ_e	maximum combined stress, lb/sq in.

τ	shear stress, lb/sq in.
$\lvert\phi\rvert/\lvert V_e\rvert$	rolling parameter, roll angle/velocity, deg/ft/sec
Ω	rotor angular velocity, rad/sec
ΩR	blade tip speed, ft/sec
w	distributed pressure load, lb/in.
ω	natural frequency, rad/sec
ω/Ω_o	natural frequency/design maximum rotor rpm, cycles/rev
Ω_o	design maximum rotor rpm
Ω/Ω_o	rotor speed/full rpm

Subscripts

c	centerbody
e	equivalent
i	induced
o	profile
rotor	based on rotor disc area
s	segment
w	wing
wing	based on wing area (centerbody plus 2 blades)

NOTE: The integration of symbol lists for each of several appendixes has caused some duplication of symbols. The reader may determine the appropriate symbol from the context in which it is used.

INTRODUCTION

A preliminary design study has defined the configuration and characteristics of the Hot Cycle Rotor/Wing high-speed VTOL aircraft shown in Figure 1. This design study and the planning for a program to design, build, and test this aircraft have been carried out for the USAAVLABS in accordance with the Army's Composite Research Aircraft (CRA) requirements:

1. Payload - 3,000 pounds
2. Fuel - 3,000 pounds
3. Vertical takeoff and landing
4. Hover (OGE) at 95°F and 6,000 foot pressure altitude
5. Disc loading - 10 psf or less
6. Speed - 300 knots required (400 knots desired)
7. Lift/Drag ratio - at least 10
8. Cargo compartment size - 5.5 feet wide by 6 feet high by 14.5 feet long.

The Hot Cycle Rotor/Wing combines the two major advancements in aircraft technology of the past 25 years: the helicopter and the jet airplane. This is accomplished through the use of the Hot Cycle Rotor/Wing lifting system, which is a tip-jet-powered helicopter rotor with a very large hub. The Rotor/Wing can be stopped in flight to become a fixed wing.

The Hot Cycle Rotor/Wing CRA will provide the helicopter advantages of hovering and the high-speed capability and cruise efficiency of the jet airplane. It is characterized by simplicity and light weight, made possible through the combined use of the all-pneumatic Hot Cycle drive system and the dual-purpose Rotor/Wing lift system. This eliminates the need for heavy and complex mechanical drive components without recourse to duplicate lifting systems or to folding, tilting, or retracting of lift systems to effect conversion, and makes possible an advance in vertical-lift aircraft technology.

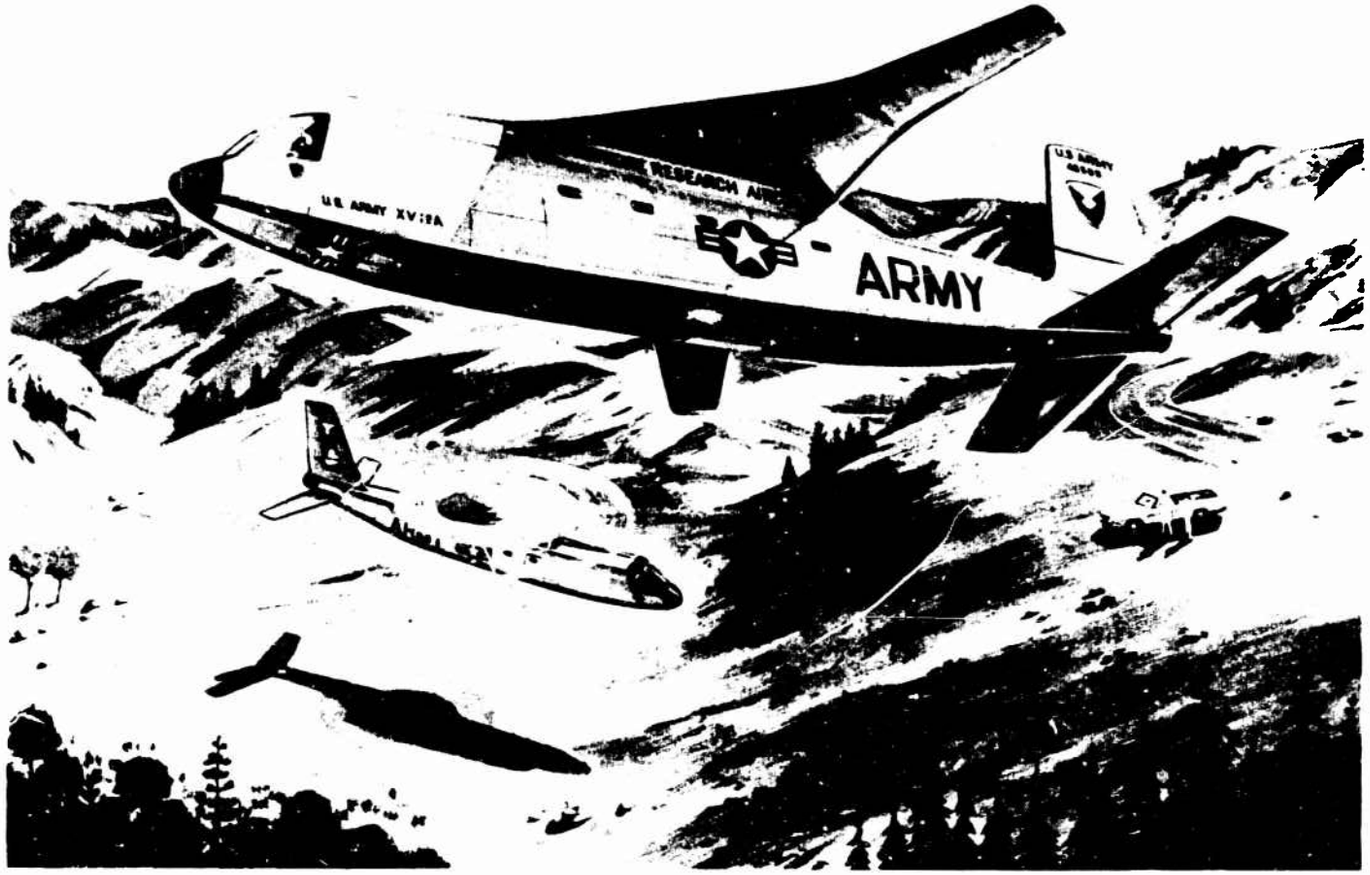

Figure 1. Hot Cycle Rotor/Wing Composite Research Aircraft.

Substantiation of the technical aspects of the CRA design is available from the results of the USAAVLABS XV-9A Hot Cycle Research Aircraft program and Hughes- and U. S. Government-sponsored analysis, whirl testing, and wind tunnel testing that have defined basic aerodynamic characteristics of the Rotor/Wing in all modes of flight.

The performance of this particular aircraft design, which is powered in cruise flight by a turbojet engine, should not be applied to all Hot Cycle Rotor/Wing vehicles since others will undoubtedly incorporate tip-turbine cruise fans or front-fan bypass engines for lower specific fuel consumption. Cruise flight will also be made at more optimum altitudes.

HOT CYCLE ROTOR/WING CONCEPT

The Rotor/Wing is basically a Hot Cycle rotor with a large triangular hub and short-span, wide-chord blades. It acts as a tip-jet-powered helicopter rotor for vertical and low-speed flight, autorotates during conversion, and stops during flight to become a swept-back fixed wing for cruise and high-speed flight.

The Hot Cycle system that powers the Rotor/Wing is the simplest possible propulsion system for aircraft with both rotary-wing and fixed-wing modes of operation. As shown in Figure 2, the Hot Cycle system transmits power pneumatically by lightweight ducting and a valve that direct high-energy gas from a turbine engine to the rotor blade tips to drive the rotor as a big reaction turbine for helicopter flight and to a jet nozzle to produce forward thrust for autogyro and airplane flight.

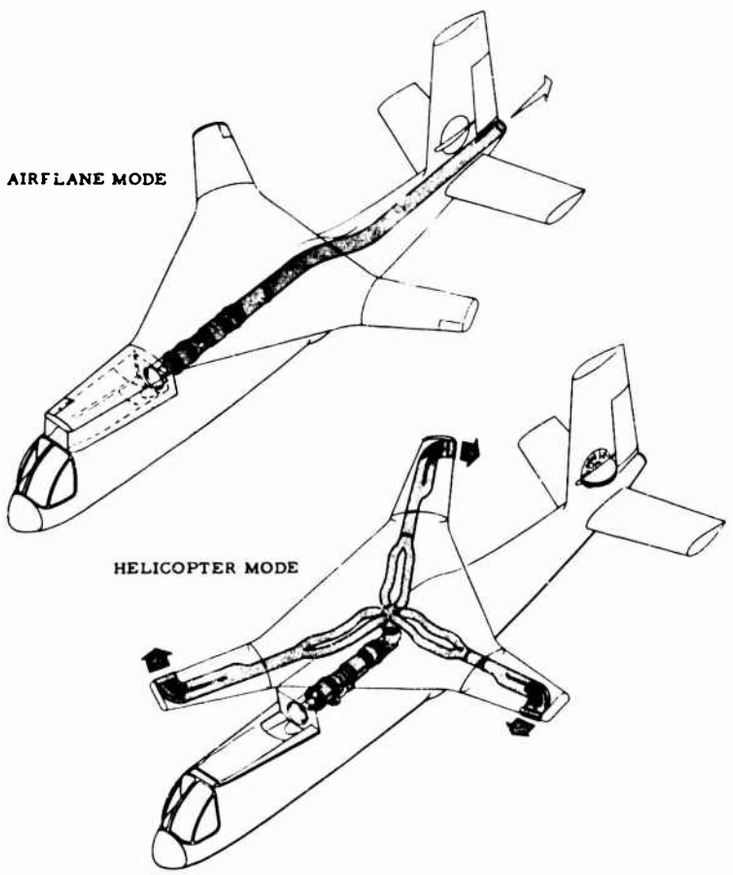

Figure 2. Propulsion System Schematic.

Operation of the Hot Cycle Rotor/Wing in its various modes of flight is illustrated in Figure 3. The Rotor/Wing aircraft takes off, hovers, and flies at speeds up to approximately 100 knots in the helicopter mode, with the rotor powered by its tip jets and with control from rotor blade cyclic and collective pitch and the yaw fan in the tail. To increase flight speed, power is shifted from the rotor to the jet nozzle to produce forward thrust, and the collective pitch is reduced to put the rotor into autorotation; control is from rotor cyclic pitch and yaw fan, augmented by airplane-mode control surfaces on the tail. As the speed reaches approximately 150 knots, the Rotor/Wing is slowed aerodynamically by raising the collective pitch and is stopped by a brake and locked to the fuselage to establish the fixed-wing airplane configuration. Airplane mode control is provided by horizontal tail surfaces (elevons) that act in unison for longitudinal (pitch) control and differentially for lateral (roll) control. Directional (yaw) control is provided by the rudder. Cockpit controls provide conventional helicopter characteristics during low-speed flight and conventional airplane characteristics during high-speed flight, with a smooth transition by using the stick and rudder pedals throughout. Engine power control is provided by rotor speed governing and the collective stick twist grip for

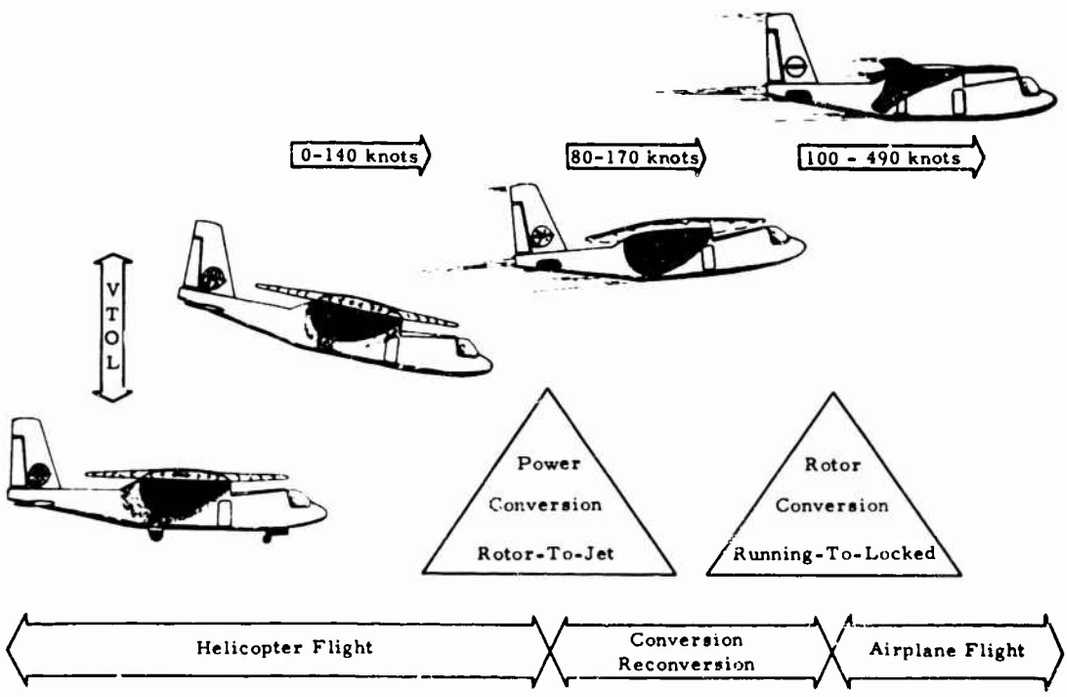

Figure 3. Flight Modes.

helicopter flight and by a throttle quadrant for airplane flight when the collective is not used. Both power controls function in parallel at all times. Two selector switches are used in the conversion process -- one to direct the power to either the rotor blade tip jets or the cruise jet nozzle, and the other to establish the rotor lock, fairing, and control configuration for either airplane or rotary-wing flight.

Conversion between helicopter and airplane modes of flight is a straightforward pilot procedure, not requiring recourse to automatic stabilization devices. It is accomplished by normal pilot control motions, is reversible at any point, and can be accomplished in climbing, diving, or level flight -- in smooth or turbulent air.

Mechanical simplicity of conversion between rotary-wing and fixed-wing operation with composite-type aircraft is of significance with regard to safety, reliability, weight, and cost. With the Rotor/Wing, this conversion is accomplished by merely starting or stopping rotation.

Since the Rotor/Wing provides lift for all flight regimes, the complexity and weight of separate low-speed and high-speed lift systems are avoided, as are the problems associated with transferring the lifting function from one system to the other. Also avoided are the duplicated structure for lift system support and other major load paths that must be provided with separate lift systems.

Unfavorable aerodynamic interference occurs between multiple lift systems such as separate wings and rotors, and can cause serious stability problems and performance losses, particularly in low-speed and autorotational flight. The use of the single Rotor/Wing lift system in the CRA precludes this problem area.

The Rotor/Wing is rigidly mounted on the fuselage through bearings that allow only rotational motion, and the blades are similarly mounted to the hub section, allowing only pitch motion. This arrangement provides efficient support of the short, stiff blades. The Rotor/Wing also serves as an aerodynamic fairing of the structure and equipment in the hub area, thus providing the aerodynamic cleanness required for efficient high-speed flight.

The Hot Cycle Rotor/Wing provides flexibility of operation. Safe landings can be made in helicopter, autogyro, and airplane flight configurations. Overload takeoffs can be made in either the helicopter mode (in ground effect) or the airplane mode.

In the event of power failure or other emergency, the Rotor/Wing aircraft has the capability of safe autorotational landing from any flight mode. From airplane flight, the rotor can be started by using only aerodynamic forces. Wind tunnel tests indicate that autorotational landing characteristics are comparable with those of current helicopters.

The Hot Cycle propulsion system used with the Rotor/Wing transmits power pneumatically through lightweight ducting, eliminating the weight and complexity of power turbines, shafts, gearboxes, clutches, and propellers of a turboshaft-driven composite aircraft. Since there is no rotor shaft drive torque reaction on the fuselage, there is no need for an antitorque tail rotor; directional control in helicopter flight is provided by a small yaw fan in the tail.

An extensive background of research and development exists that substantiates many technical areas involved in the Hot Cycle Rotor/Wing. By marrying the helicopter and the jet airplane, by retaining the best features of both, and by eliminating the basic limitation of each, the Rotor/Wing will open up a new spectrum of vertical-lift capability.

RESEARCH AND DEVELOPMENT BACKGROUND

The feasibility of the Hot Cycle propulsion system has been established through an extensive R and D program that culminated in the successful flight testing of the USAAVLABS XV-9A Hot Cycle Research Aircraft shown in Figure 4. During 160 hours of rotor operation and 35 hours of flight testing that were completed in August 1965, structural and mechanical design, weights, and cooling adequacy were verified. Gas leakage was found to be negligible (less than 1/5 of 1 percent), and noise was determined to be essentially equal to that of the quietest type of VTOL aircraft (turboshaft helicopters). The rotor performance prediction method used for the CRA was verified, and the reduction in maintenance requirements promised by the Hot Cycle system was illustrated by the low logistical requirements during XV-9A flight operations. The Hot Cycle propulsion system can be applied to the Rotor/Wing CRA with reasonable assurance of its successful application.

Figure 4. XV-9A Hot Cycle Research Aircraft.

The aerodynamic characteristics of the Rotor/Wing in all flight regimes have been established through model test programs carried out during a 3-1/2-year period. All essential aerodynamic parameters have been defined covering a broad range of configurations, including the configuration chosen for the CRA.

Figure 5. Rotor/Wing Whirl Tests.

Hovering performance was established in whirl stand tests (Figure 5) during which effects of various blade sections and hub planform shapes were investigated to establish appropriate Rotor/Wing geometry.

Under U. S. Navy sponsorship, an extensive wind tunnel test program was conducted that covered helicopter, autogyro, and airplane flight modes and conversion between stopped- and running-rotor regimes. These tests (Figure 6) indicated that the helicopter and airplane mode performance and flying qualities were satisfactory, that autorotational capability during both conversion and emergency

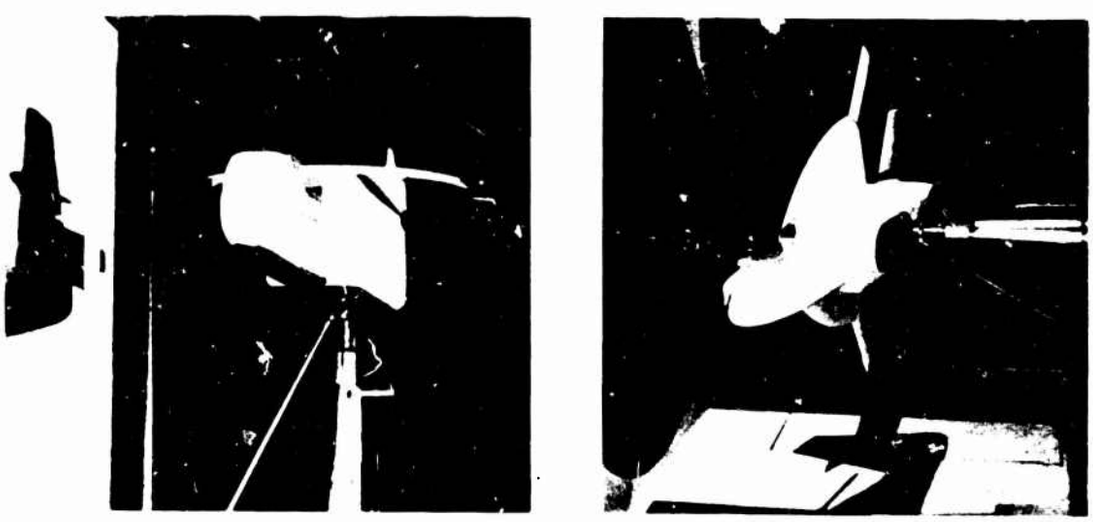

Figure 6. Rotor/Wing Wind Tunnel Tests.

landing was adequate, and that starting and stopping the rotor could be accomplished in a simple, straightforward manner by the pilot using only normal control motions and without recourse to automatic devices.

During the preliminary design program, additional aerodynamic testing was accomplished on models simulating the specific design of the Rotor/Wing chosen for the CRA. Wind tunnel tests (Figure 7) validated the fixed-wing lift, drag, and stability characteristics of the CRA configuration and verified the suitability of the low position of the horizontal tail chosen for the CRA. A transonic wind tunnel test (Figure 8) was carried out in cooperation with the U. S. Navy Bureau of Weapons, and the results show excellent lift, drag, and stability characteristics of the CRA design up to Mach 0.9. A model closely simulating the specific Rotor/Wing configuration selected for the CRA was recently tested on the whirl stand (Figure 9). Results of these tests show that hover performance is somewhat superior to that of earlier designs; the results provide an excellent validation of the CRA rotor design.

In addition to the testing briefly summarized above, design and analytical development applicable to the Rotor/Wing has been accomplished. Performance, dynamics, and flying qualities have received particular attention, and analytical methods have been developed and mechanized on high-speed computers (IBM 7094) to cover all modes of flight of the Rotor/Wing. A thorough analysis of the CRA configuration using these analytical tools has verified satisfactory dynamic characteristics -- vibration, flutter margins, and aircraft response -- and has established performance and flying qualities for all flight regimes.

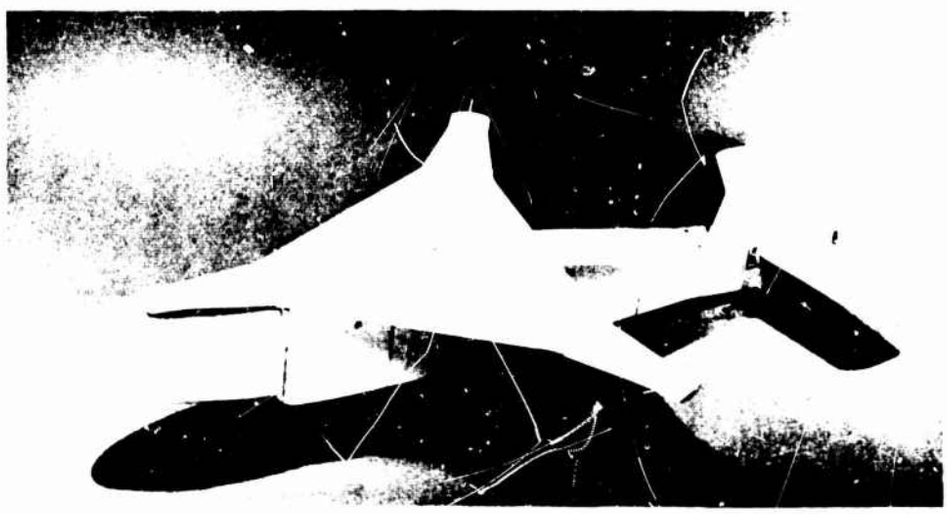

Figure 7. CRA Low-Speed Wind Tunnel Tests.

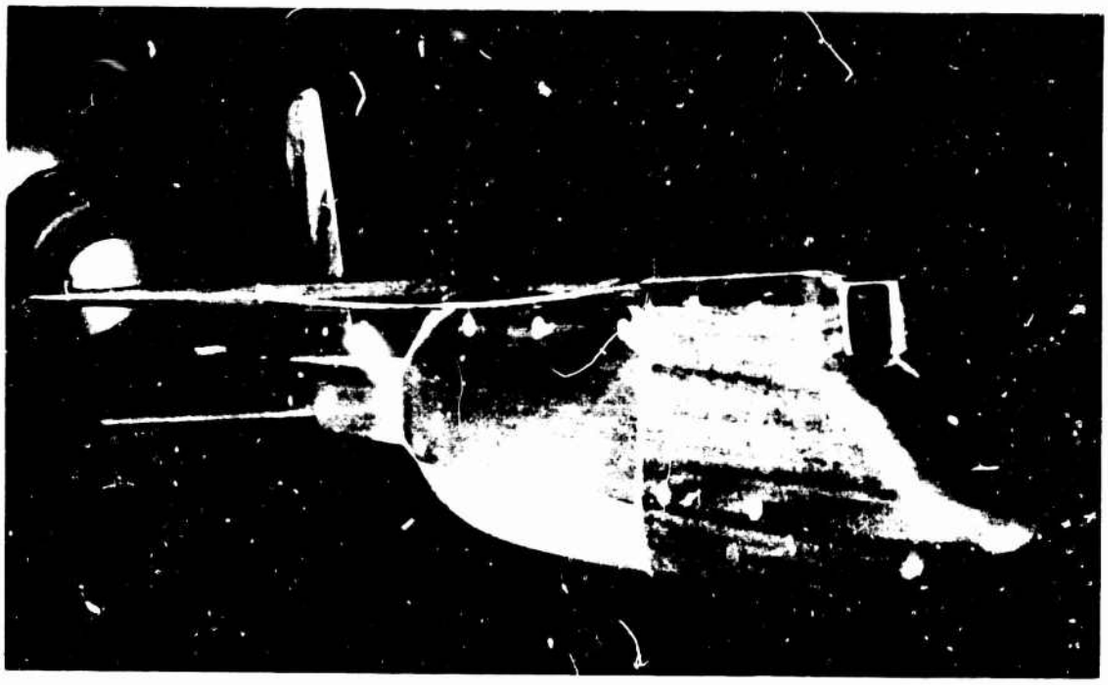

Figure 8. CRA Transonic Wind Tunnel Tests.

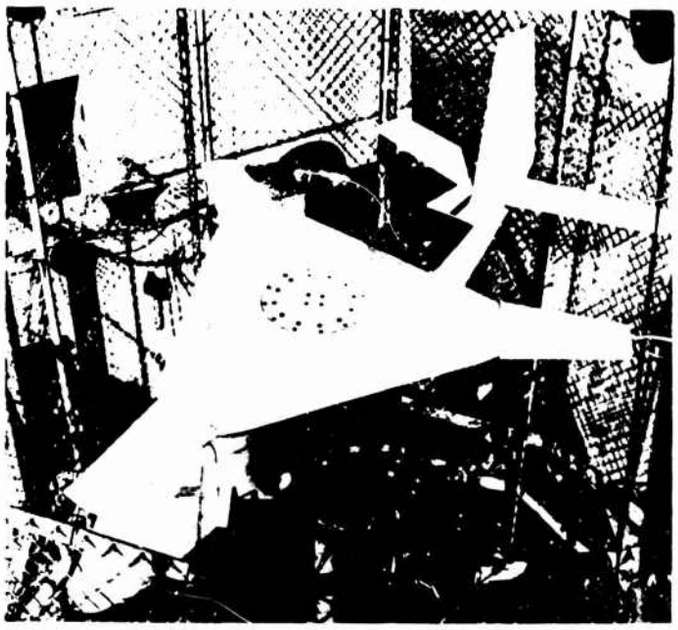

Figure 9. CRA Whirl Tests.

DESCRIPTION OF AIRCRAFT

In the definition of the preliminary design of a Hot Cycle Rotor/Wing aircraft to meet or surpass all of the stated CRA requirements, the following primary criteria were followed:

1. Performance and operational capabilities of greatest feasible scope and flexibility were to be provided to enhance the value and significance of the test results from the CRA flight research program.

2. Safety was to be maximized by placing major emphasis on simplicity, reliability, and fail-safe design. Proven zero-zero ejection seats were to be provided as an ultimate crew safety feature.

3. Maximum use of proven available components and technology was to be made to simplify and increase the reliability of the design and to minimize the cost of the aircraft development program.

4. Margins were to be provided on all basic CRA performance requirements to maximize assurance of program success.

5. The aircraft configuration was to be defined so that CRA test data would have maximum direct applicability to future development of operational composite aircraft.

The general arrangement of the selected CRA configuration is shown in Figure 10, and the basic features of the interior configuration are shown in Figure 11. Table I presents some of the leading particulars defining the CRA.

The overall configuration selected for the CRA provides a clean acrodynamic shape. Location of the cockpit forward of the rotor allows the application of qualified zero-zero ejection seats as an ultimate safety factor during exploratory research with the aircraft. The use of a single engine simplifies the installation and the operational characteristics of the power plant system. A high degree of engine reliability is predicted for the J52 turbojet engine, which has been proven in more than 10 years of successful service in a variety of military and commercial aircraft. The placement of the engine just below the rotor allows an unobstructed cargo compartment of nearly twice the minimum size specified in the CRA requirements. Location of the jet nozzle at the extreme rear of the aircraft avoids any possible problems from jet impingement, and its vertical and angular

Rotor/Wing

Disc Area (25-ft radius)	1964 sq ft
Wing Area (wing plus 2 blades)	526 sq ft
Blade Airfoil	Modified Circular Arc

Empennage

Vertical Tail Area	137 sq ft
Horizontal Tail Area	184 sq ft

Power Plant

Pratt and Whitney J52-P-8A
Gas Generator

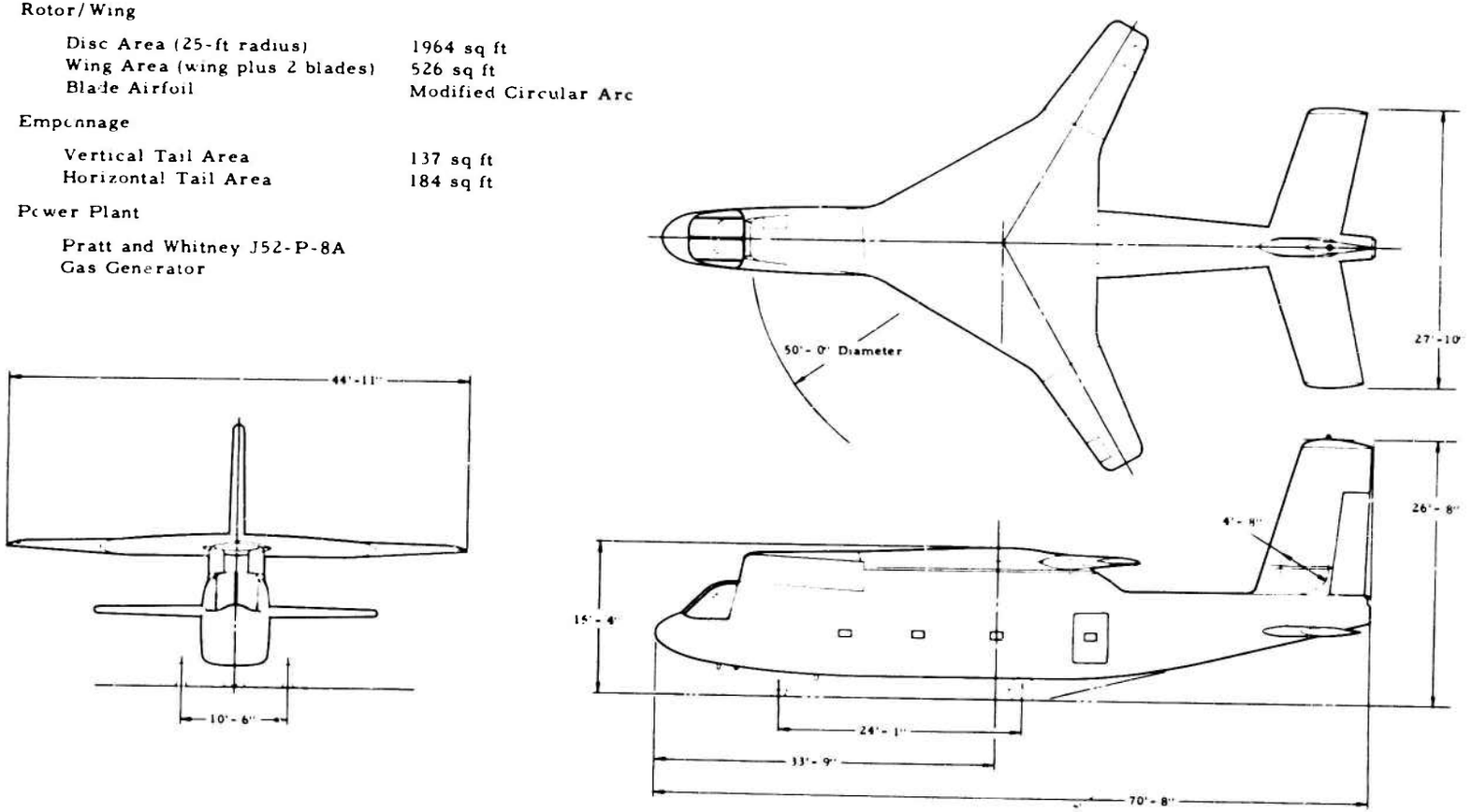

Figure 10. CRA General Arrangement.

TABLE I. BASIC CHARACTERISTICS

Rotor/Wing diameter	50.0 ft
Wing span	44.9 ft
Overall length	70.7 ft
Overall height	26.7 ft
Cargo compartment height x width x length	6.0 x 5.5 x 29.1 ft
Empty weight	13,169 lb
Design gross weight	19,635 lb
Alternate gross weight	30,000 lb
Design maneuver load factors	
Helicopter	+3.0, -0.5
Airplane	+4.5, -1.0
Power plant	One Pratt and Whitney J52-P-8A turbojet

orientation assures minimal trim changes as a result of power changes in autogyro or airplane flight.

The design of structure and systems of the CRA is based on conventional application of established helicopter and airplane technology and practice. The fuselage and empennage are typical of conventional subsonic fixed-wing aircraft structures using semimonocoque construction of skin, frames, longerons, and spars. The major structure of the Rotor/Wing consists of a central box beam in each blade section and two parallel box beams in the wing section adjacent to each blade. Leading and trailing edge structures are of aluminum alloy honeycomb or truss-core sandwich material. Major frames occur only at the root transition structure between the blade and wing. A nonrotating space frame pylon structure provides support of the main rotor bearing inside the Rotor/Wing hub itself. The pylon in turn is supported from the fuselage at four points that are the intersections of the rugged main fuselage frames and the upper fuselage longerons.

Conventional airplane-type tricycle landing gear employed on the CRA is designed for use in either the helicopter or the airplane mode. A powered irreversible flight control system is supplied by two completely independent hydraulic systems, with each system serving as a continuous backup for the other.

Empty weight of the CRA has been established during the preliminary design program. Since the CRA employs available systems and components to a high degree, actual weight is known for approximately 35 percent of the total empty weight. The remaining weight has been established from

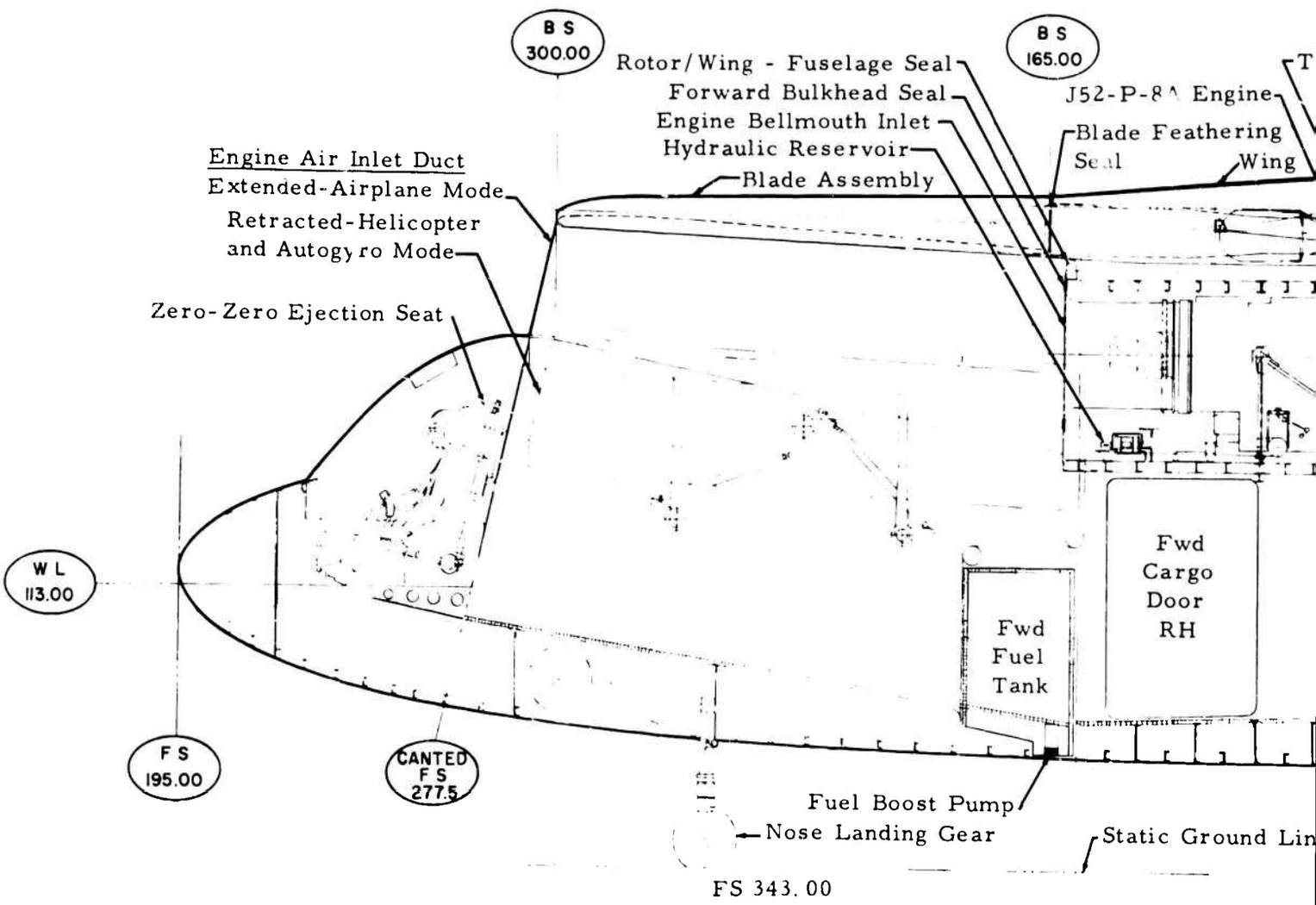

Figure 11. CRA Inboard Profile.

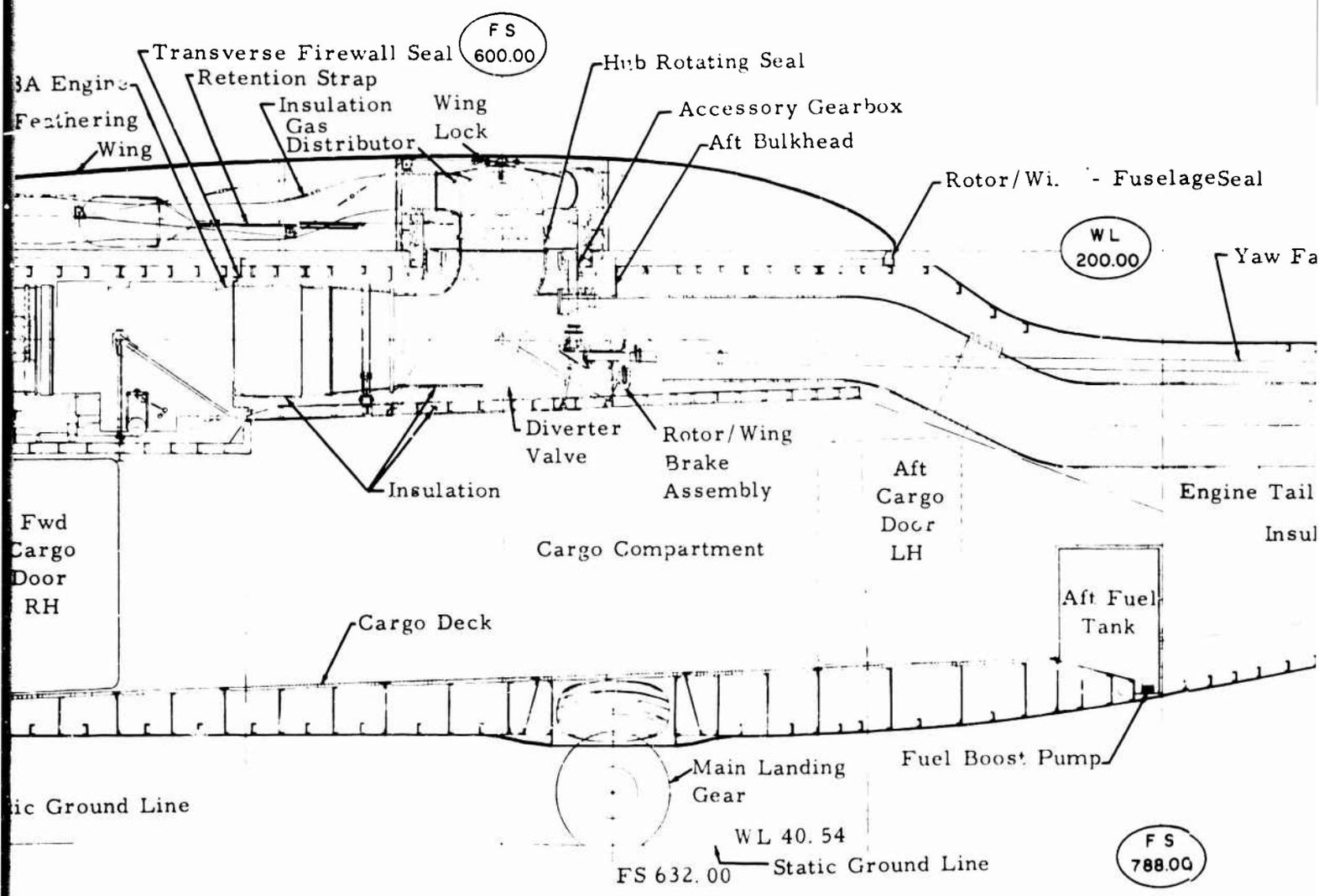
FS 600.00
Transverse Firewall Seal
Retention Strap
Insulation Gas Distributor
Wing Lock
Hub Rotating Seal
Accessory Gearbox
Aft Bulkhead
Rotor/Wi. - FuselageSeal
WL 200.00
Yaw Fa
Diverter Valve
Rotor/Wing Brake Assembly
Insulation
Aft Cargo Door LH
Engine Tail
Insul
Fwd Cargo Door RH
Cargo Compartment
Aft Fuel Tank
Cargo Deck
Fuel Boost Pump
Main Landing Gear
WL 40.54
Static Ground Line
FS 632.00
FS 788.00

E

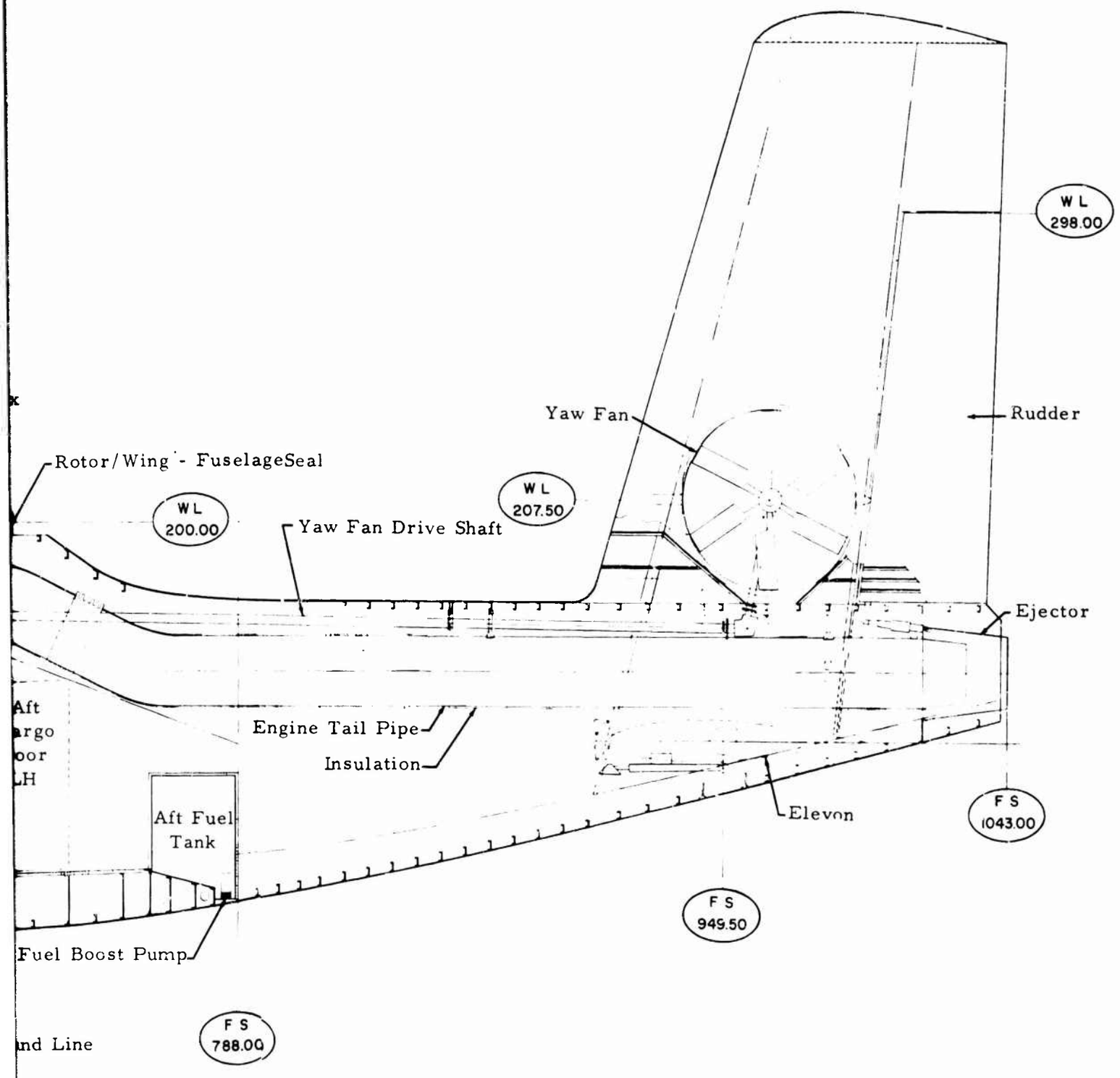
W L
298.00
Yaw Fan
Rudder
Rotor/Wing - FuselageSeal
W L
207.50
W L
200.00
Yaw Fan Drive Shaft
Ejector
Aft
rgo
oor
LH
Engine Tail Pipe
Insulation
Aft Fuel
Tank
Elevon
F S
1043.00
F S
949.50
Fuel Boost Pump
nd Line
F S
788.00

the design and stress analysis and is substantiated by comparative statistical analysis.

The CRA is designed for operation by one pilot. However, cockpit accommodations and controls are provided for both a pilot and a copilot, as may be desired for test operations and pilot familiarization.

Provisions are made in the design of the CRA for installation of instrumentation to measure, record, and telemeter flight test data on performance parameters, strains, positions, accelerations, temperatures, pressures, and so forth. A panel for control and monitoring of flight test instrumentation is located in the cockpit.

A parametric study was the basis for sizing the major components of the CRA.

PERFORMANCE DATA

The J52-P-8A turbojet, in a single-engine installation, was chosen to power the CRA.

Hughes has accumulated extensive data directly applicable to the design of the Hot Cycle Rotor/Wing CR[illegible] The performance described in this section has been determined directly from these data by using accepted standards for converting model test data to full scale. Hughes' experience with Hot Cycle propulsion encompasses 10 years of design, whirl stand, and flight test activities. This experience has provided detailed documentation of the characteristics of the Hot Cycle system.

Rotor/Wing aerodynamic studies have extended over nearly 4 years and include model whirl stand investigations and wind tunnel tests covering all modes of flight, from low-speed helicopter flight, through conversion, to airplane flight at Mach numbers up to 0.9.

Performance characteristics have been established through the use of wind tunnel data corrected to full-scale Reynolds numbers.

Table II summarizes the major performance items.

TABLE II. HOT CYCLE ROTOR/WING CRA PERFORMANCE SUMMARY

At Design Gross Weight Except as Noted	
Hover ceiling, out of ground effect, 95°F, ft	13,100
Hover ceiling, out of ground effect, standard day, ft	19,500
Disc loading, lb/sq ft (based on 25-ft radius)	10
Maximum speed, sea level standard, kn	400
Maximum speed, 13,000 ft standard, kn	490
Range* with 3,000-lb payload (cruise at 35,000 ft), n mi	460
Ferry range** (cruise at 35,000 ft, takeoff gross weight - 30,000 lb), n mi	2,575

*Based on engine specification fuel flow -- no fuel reserves included.

**Engine SFC increased 5% -- fuel reserve equals 10% of initial fuel.

The CRA is capable of hovering out of ground effect at 6,000 feet, 95°F, at a gross weight of 26,000 pounds, which is 6 365 pounds more than the design gross weight. At an alternate gross weight of 30,000 pounds, the CRA can hover OGE at 6,500 feet, standard day, and can carry fuel and payload of 16,365 pounds.

Conversion from helicopter to airplane in level flight can be carried out at any altitude up to 15,000 feet at design gross weight on a standard day.

The capability and versatility of the Hughes CRA are summarized in the overall flight envelope shown in Figure 12. At the design gross weight of 19,635 pounds, the hovering ceiling is 19,500 feet on a standard day. The airplane mode ceiling is in excess of 35,000 feet, and the maximum airspeed is 490 knots. Conversion from helicopter mode to airplane mode takes advantage of an autogyro flight envelope that extends to '7,500 feet under standard conditions.

The conversion from helicopter mode through autogyro mode to airplane mode is made in the following manner. After takeoff, the ship is flown as a helicopter up to a speed of approximately 100 knots. The power divert switch is then placed in the AIRPLANE position, the collective pitch is lowered to maintain approximately 85 percent of normal rpm for autogyro flight, and the forward speed is increased to approximately 150 knots by adjusting engine thrust. The mode selector switch is then set to AIRPLANE position, and, while roughly constant forward speed is maintained, the collective pitch is increased to approximately 10 degrees to slow the Rotor/Wing. As Rotor/Wing speed decreases, the angle of attack of the aircraft is increased to transfer the lift from the blades to the wing. When the rpm slows to approximately 40 percent, the Rotor/Wing brake is applied with the toe pedals and the collective pitch control is lowered to the zero blade angle position as the Rotor/Wing stops. When the Rotor/Wing reaches 5 rpm, the Rotor/Wing locator rises automatically and engages the locking pin, which stops the Rotor/Wing. Wing and blade locks then engage, the Rotor/Wing controls are deactivated, the inlet duct is raised, and the yaw-fan doors are closed. The aircraft is now in airplane flight.

To reconvert from airplane to autogyro flight, basically the reverse sequence is followed. After the aircraft is slowed to the conversion airspeed of approximately 150 knots, the mode selector switch is placed in ROTOR position. This unlocks the Rotor/Wing and blades, activates the Rotor/Wing controls, opens the yaw-fan doors, retracts the inlet duct, and retracts the Rotor/Wing locator. The collective pitch is lowered to full down (-10 degrees) and, as the rpm increases, is raised gradually to obtain approximately 85-percent Rotor/Wing rpm. Level flight is maintained by

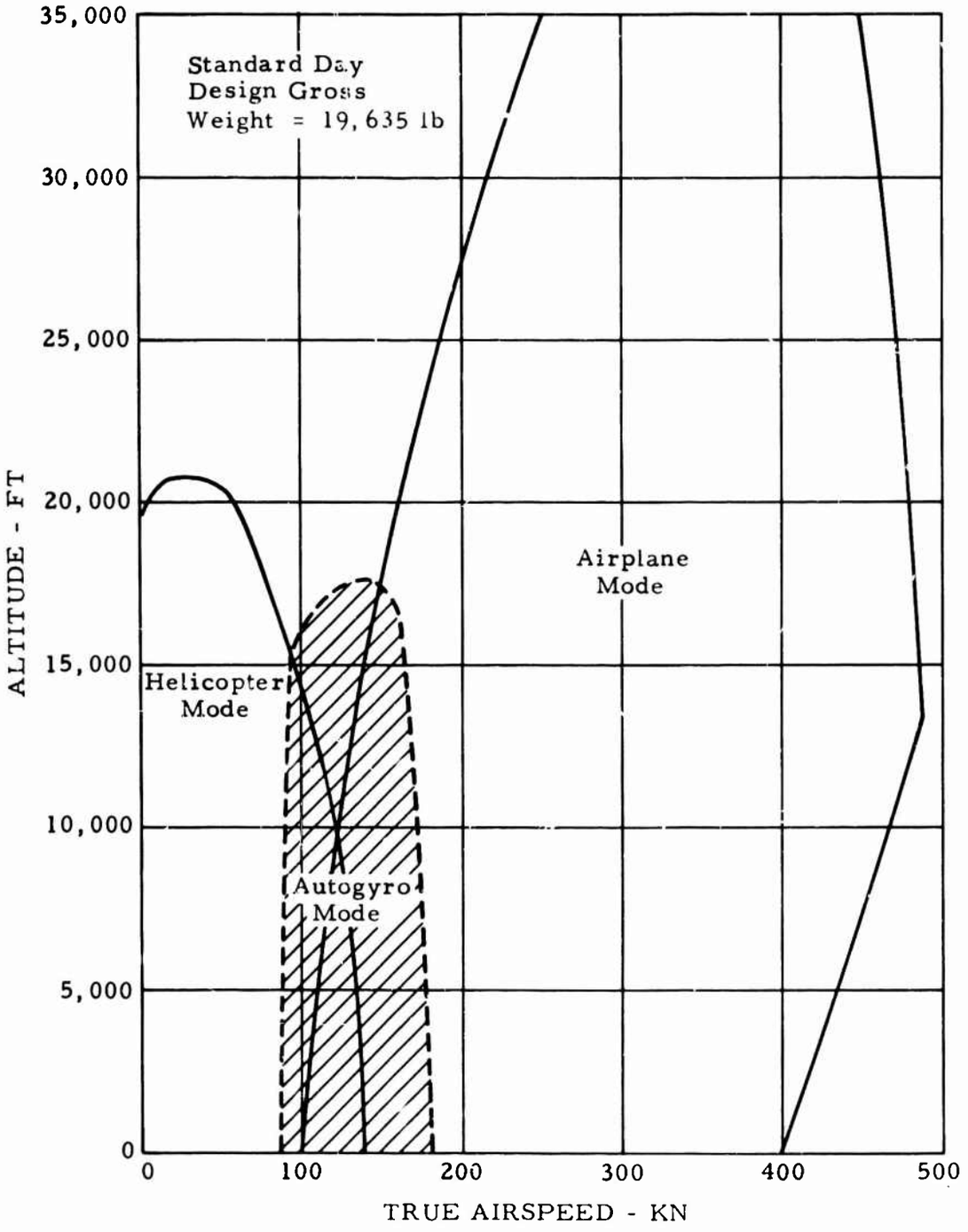

Figure 15. Overall Flight Envelope.

lowering the angle of attack of the wing as the rpm is increasing to transfer the lift from the wing to the blades. After steady autogyro flight is achieved, the forward speed is reduced to approximately 100 knots while constant collective pitch is maintained.

At the forward speed for conversion to helicopter flight, the power is diverted to the Rotor/Wing and the collective pitch control is raised to achieve level helicopter flight.

The feasibility of the above procedure has been substantiated in wind tunnel tests and is discussed further in this report under Stability, Control, and Flying Qualities. The section entitled Structures shows that the Rotor/Wing is free from flutter and aeroelastic divergence during the conversion and throughout the flight envelope.

AIRPLANE MODE PERFORMANCE

Flight Envelope

Figure 13 presents the flight envelope in the airplane mode. Six curves are shown on this plot. The maximum and minimum airspeeds with military power are based on the drag polars shown in Appendix I. Both stall and minimum trim speeds are less than the military power minimum speed, and therefore are not shown. Curves of speed for best climb and speed for best range are included. Speed for best range is defined as maximum speed for 99 percent of maximum specific range. The V_{ne} design limit is 400 knots equivalent airspeed (KEAS). The intersection of the military power limit and V_{ne} curves at a 13,000-foot altitude shows a maximum true airspeed of 490 knots.

Takeoff and Landing - Airplane Mode

Takeoff and landing can be accomplished in the airplane mode with the Rotor/Wing locked and the engine producing thrust as a turbojet.

The angle of attack for takeoff and landing is limited by the tail clearance angle, which is 14 degrees. To be conservative, a maximum angle of 12 degrees is assumed. The lift curve slope as obtained from wind tunnel tests is 2.49 per radian, or 0.0434 per degree. C_L maximum for this angle is 0.521.

Figure 4-27 of Reference 1 was used to estimate the takeoff distance to clear a 50-foot obstacle. At sea level standard and design gross weight,

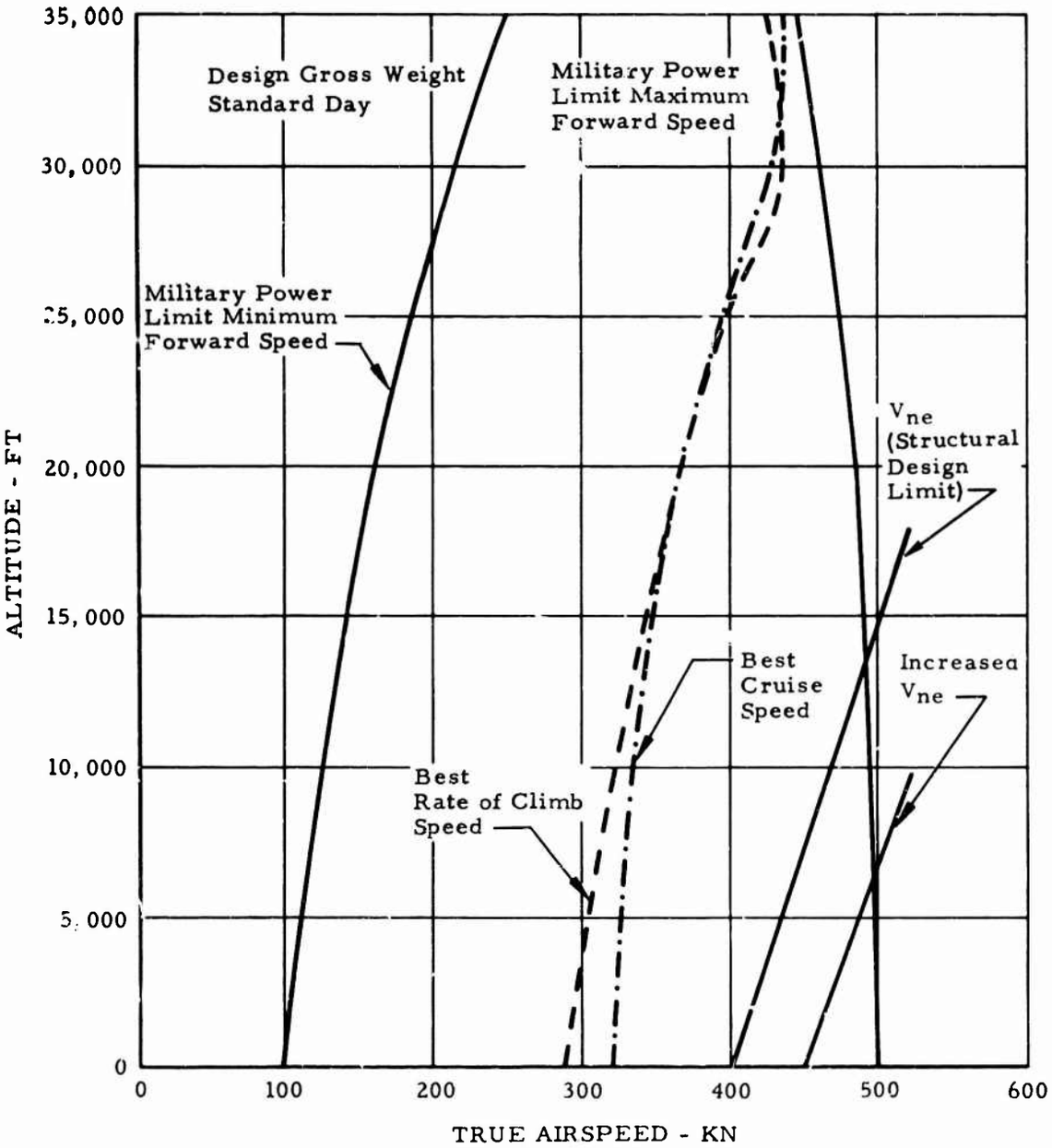

Figure 13. Flight Envelope, Airplane Mode.

this distance is 3,100 feet and the takeoff speed is 145 knots. At 3,000 feet, standard temperature, and design gross weight, the distance is 3,800 feet and the takeoff speed is 152 knots.

The total landing distance over a 50-foot obstacle at design gross weight is computed using equation 4.55 of Reference 1. This distance is 8,850 feet at sea level, standard temperature and 9,640 feet at 3,000 feet, standard temperature. This distance can be reduced to approximately 4,000 feet with the addition of a drag chute.

Rate of Climb

Figure 14 presents rates of climb versus altitude with military and normal power for a standard day in airplane mode. The graph shows that the rate of climb exceeds 7,500 feet per minute at design gross weight.

Payload-Range

Figures 15 and 16 present payload-range data for cruise altitudes up to 35,000 feet. In computing these curves, to the 2-minute allowance at normal power for warm-up, takeoff, and climb required by MIL-C-5011A is added another 2-minute allowance for conversion to airplane flight; no allowance for distance is considered. The climb to cruise altitude was assumed on course; no distance allowance was made at the destination for descent. Two minutes at normal power was assumed for reconversion to helicopter flight and landing at the remote base. No fuel reserve is included. Specific fuel consumption (SFC) is taken from engine specifications, and installation losses are accounted for.

Ferry Mission

The ferry mission is computed with takeoff at the alternate gross weight of 30,000 pounds. The power requirements at this weight in each mode of flight are shown in this section under Composite Power Available, which indicates that there is sufficient overlap in the flight envelope to convert easily in level flight from helicopter through autogyro to airplane flight. For the ferry range computation, the SFC is increased by 5 percent and a reserve of 10 percent of the initial fuel is assumed. As required by MIL-C-5011A, 2 minutes at normal rated power at sea level is assumed for starting the engines, taking off, and accelerating to climb speed; an additional 2 minutes at normal rated power is added for conversion. The mission profile is: climb on course with military power (30-minute rating) to reach a 35,000-foot altitude, continue cruise at speed for best range at 35,000 feet to destination, and land without distance credit for descent to sea level. Based on the above assumption, the ferry range is 2,575 nautical miles. This distance provides worldwide ferry capability.

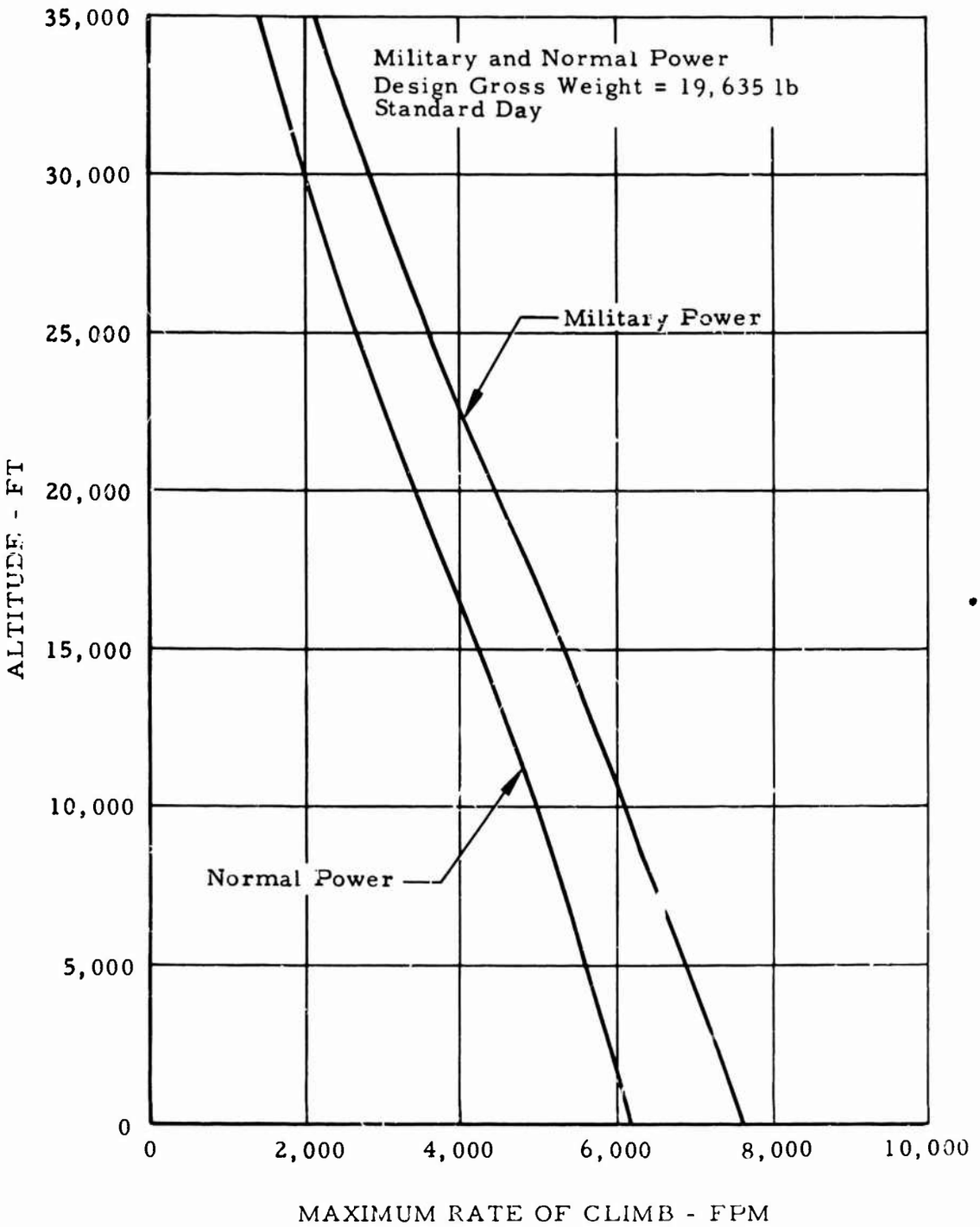

Figure 14. Maximum Rate of Climb, Airplane Mode.

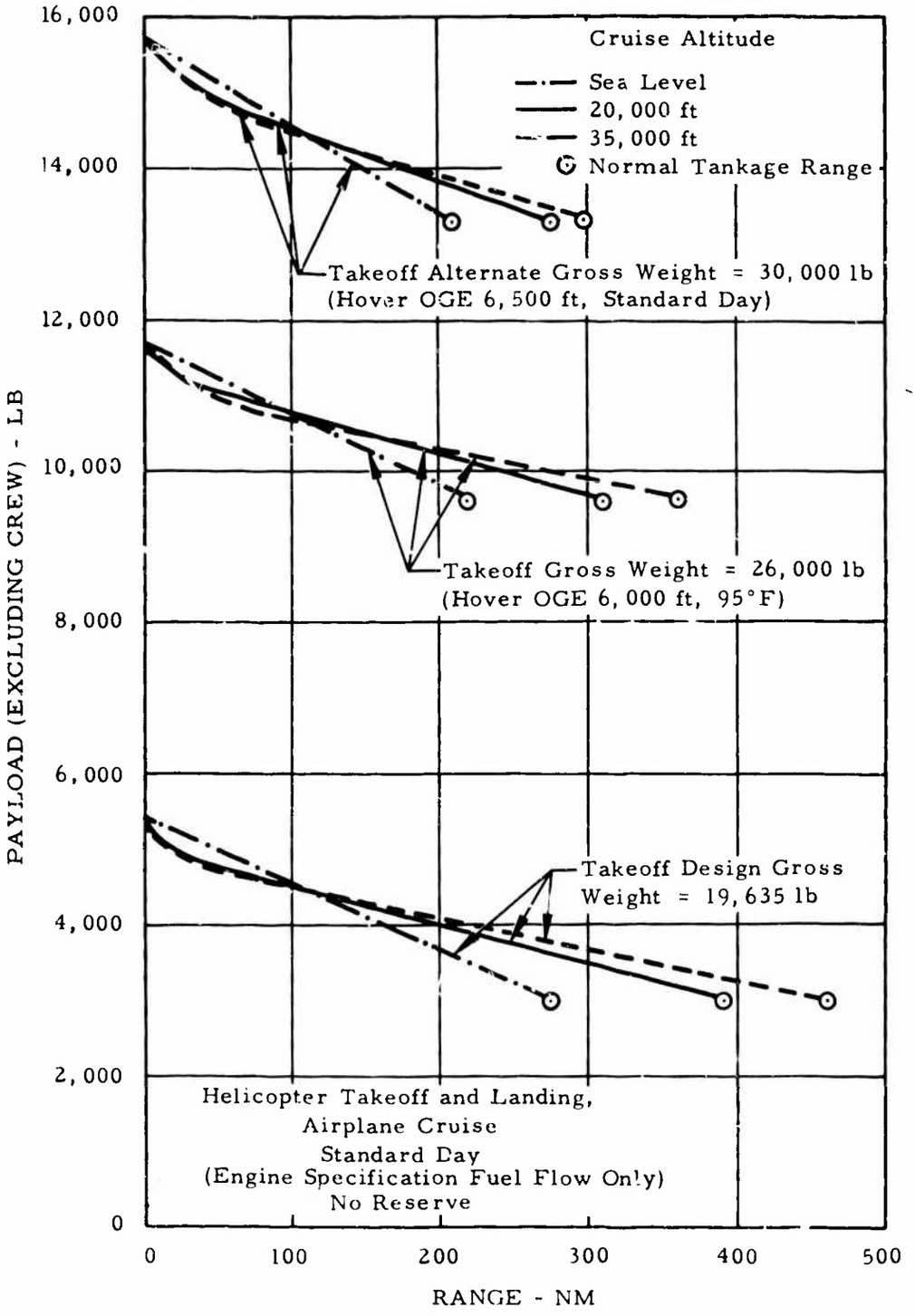

Figure 15. Payload-Range.

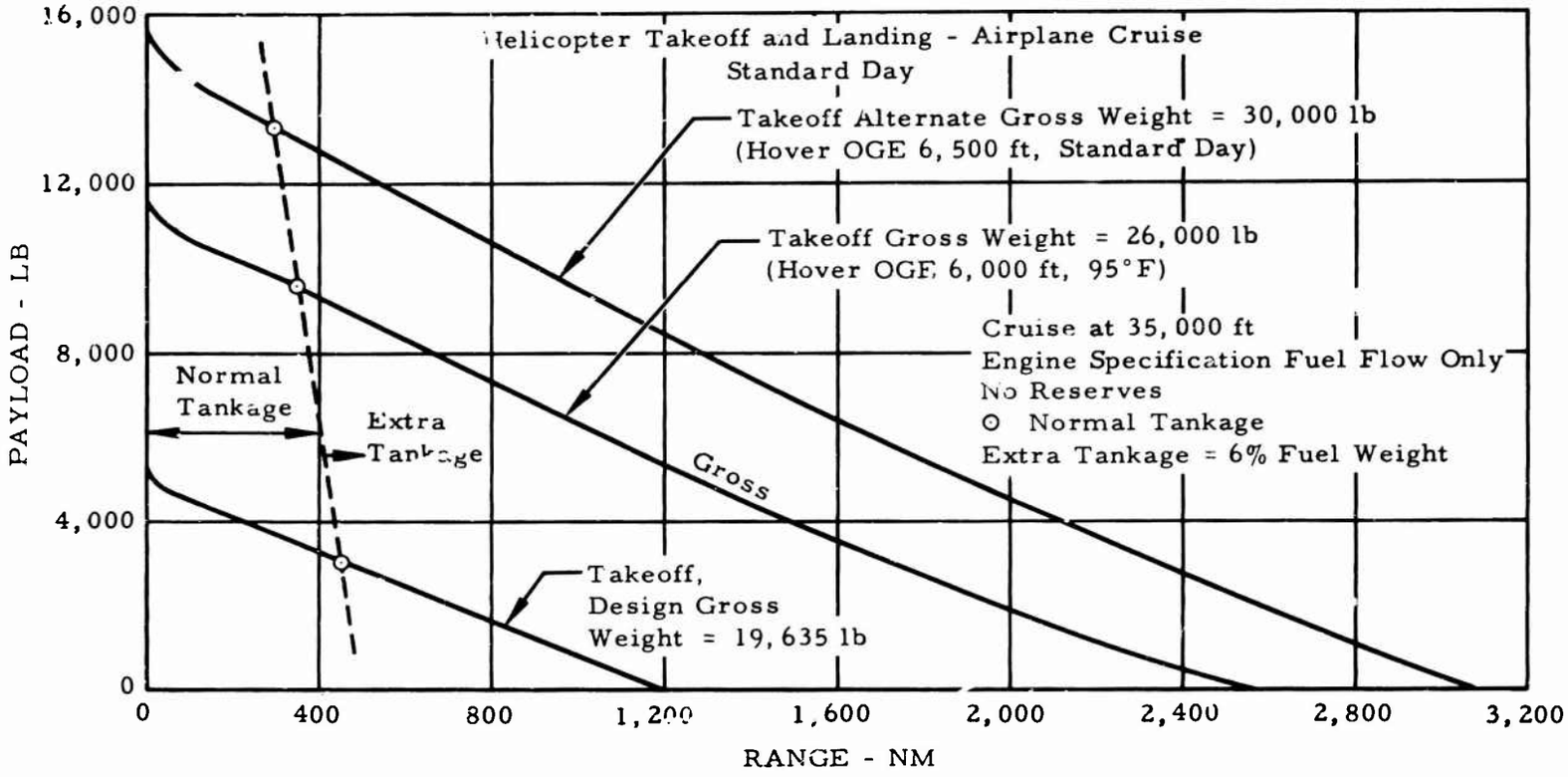

Figure 16. Payload Extended Range.

HELICOPTER MODE PERFORMANCE

Flight Envelope

Helicopter operation under standard conditions is summarized in Figure 17. The maximum speed is established by blade stall considerations. A conservative criterion of 12-degree retreating tip angle has been used.

Hovering Performance

Hover ceiling out of ground effect is presented as a function of gross weight for both standard and 95°F temperature conditions in Figure 18. At 95°F, hover ceiling at design gross weight is 13,100 feet. At 95°F at 6,000 feet, hover OGE is possible at a weight of 26,000 pounds. The out-of-ground-effect hovering power at design gross weight is summarized in Table III.

TABLE III. SUMMARY OF HOVERING PERFORMANCE - OGE

	Sea Level	6,000 Feet
Ambient temperature, °F	59	95
V_T, fps	720	720
Download, lb	1,033	1,033
C_T	0.00855	0.01141
C_T/σ	0.0519	0.0692
C_Q, Rotor/Wing	0.000972	0.0013791
Figure of merit	0.521	0.568
Yaw fan thrust, lb	40	38
Yaw fan power, hp	30	25
Rotor/Wing power required, hp	3,077	3,270
Total power required, hp	3,142	3,329
Fuel flow, lb/hr	3,666	3,800
Total power available, hp	7,240	5,065
Fuel flow, lb/hr	8,114	5,648
Excess power, hp	4,098	1,736

Hover in ground effect is summarized in Figure 19. The Rotor/Wing configuration experiences a benefit from ground effect, better than that experienced by a conventional helicopter rotor.

Both the basic hovering performance and the effect of ground proximity are calculated by using parameters drawn from recent Hughes tests of Rotor/Wing models closely approaching the CRA configuration.

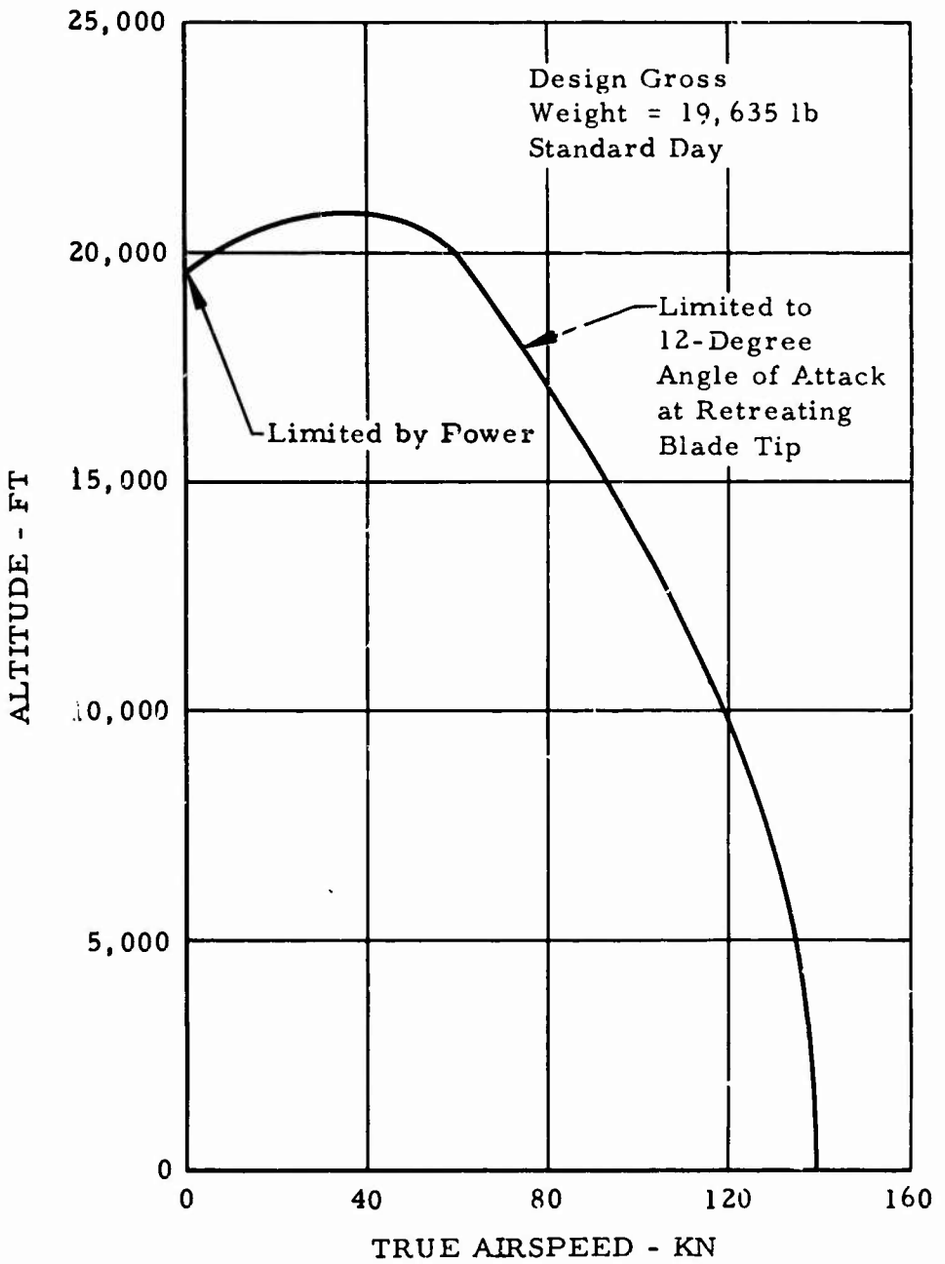

Figure 17. Flight Envelope, Helicopter Mode.

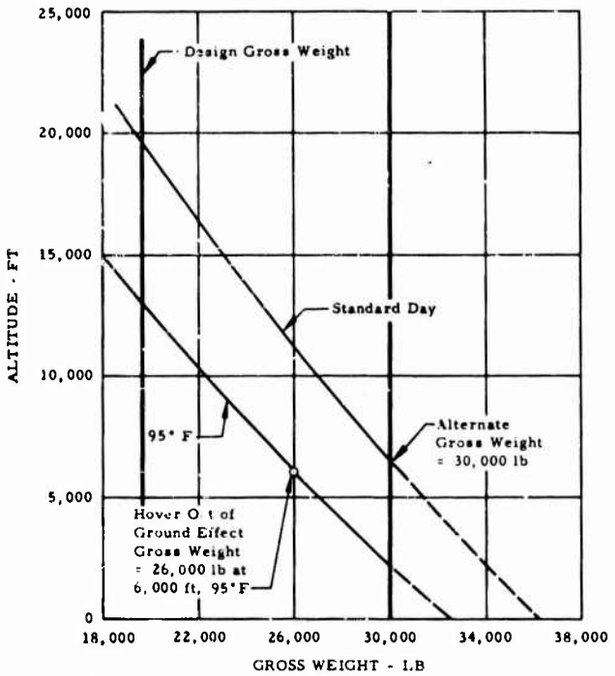

Figure 18. Hovering Ceiling OGE.

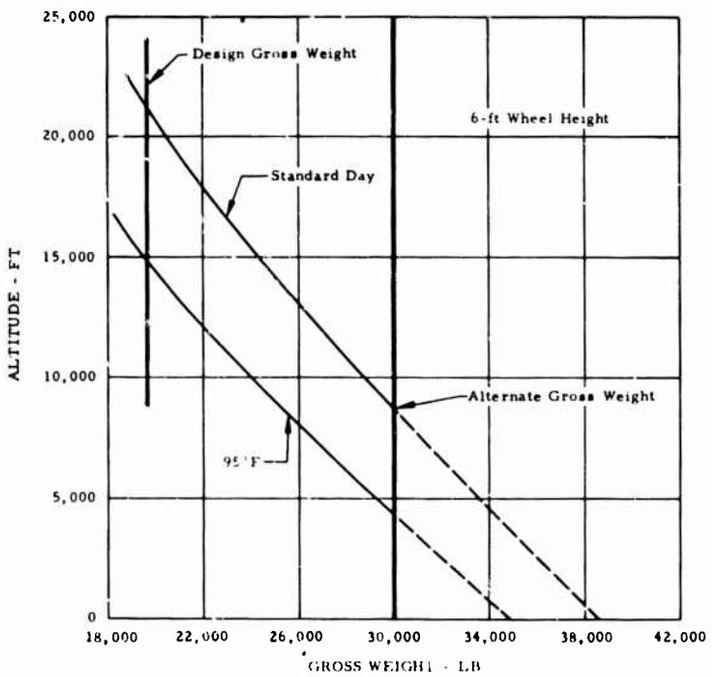

Figure 19. Hovering Ceiling IGE.

Vertical Rate of Climb

Helicopter mode vertical climb capability is summarized in Figure 20. Sea level rate of climb at design gross weight is 6,500 feet per minute.

AUTOGYRO MODE PERFORMANCE

Flight Envelope

Autogyro flight may be thought of as the key to the Rotor/Wing conversion process between helicopter and airplane operating modes. Since autogyro flight involves the propulsion mode of airplane flight combined with the lifting mode of helicopter flight, it permits a two-step conversion from one to the other. Accordingly, the autogyro flight envelope of Figure 21 is of interest since it controls the region wherein conversion can be effected. Note that autogyro flight is possible to an altitude of 17,500 feet on a standard day.

EMERGENCY LANDING CHARACTERISTICS

Figure 22 presents autorotational rate of descent versus forward speed for design gross weight at sea level standard. From helicopter flight, autorotation is entered by lowering the collective pitch to maintain the rotor rpm. Autorotation is entered from the autogyro mode by simply lowering the nose without changing the collective setting. At forward speeds of less than 90 knots, the rate of descent is computed assuming 85-percent rpm. For values greater than 90 knots, the collective pitch is assumed to be 2 degrees, which is the value used during the autogyro mode of flight.

In case of power failure during helicopter or autogyro flight, normal helicopter autorotational landings are performed. The regions marked "avoid" on Figure 23 represent those flight regimes where transition to autorotation is either difficult or impossible. These regions have been defined by calculating differences from Hughes OH-6A flight test results with the aid of the autorotational constant, K, as described in Reference 2.

In case of power failure during airplane flight, the pilot can elect to land the CRA as an airplane or to convert to autogyro mode and make an autorotational landing. This latter procedure is carried out as follows. The first phase, in airplane flight, is a speed reduction to roughly 150 knots. If at low height above terrain, a zooming climb is made in which altitude is gained and speed is reduced to 150 knots. The aircraft kinetic energy

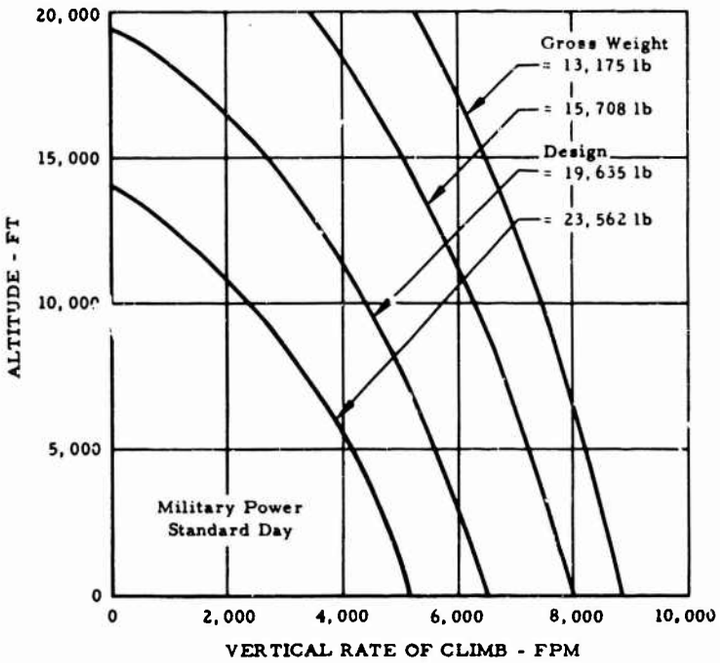

Figure 20. Maximum Vertical Rate of Climb, Helicopter Mode.

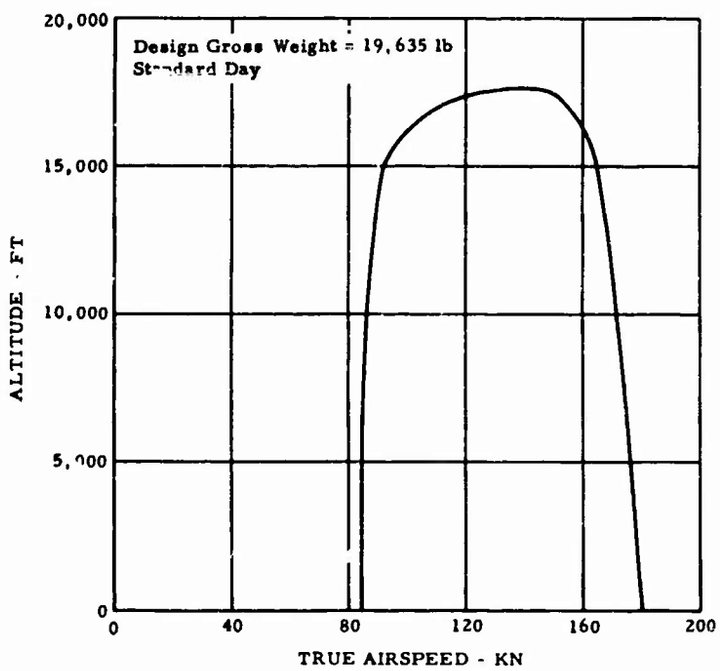

Figure 21. Flight Envelope, Autogyro Mode.

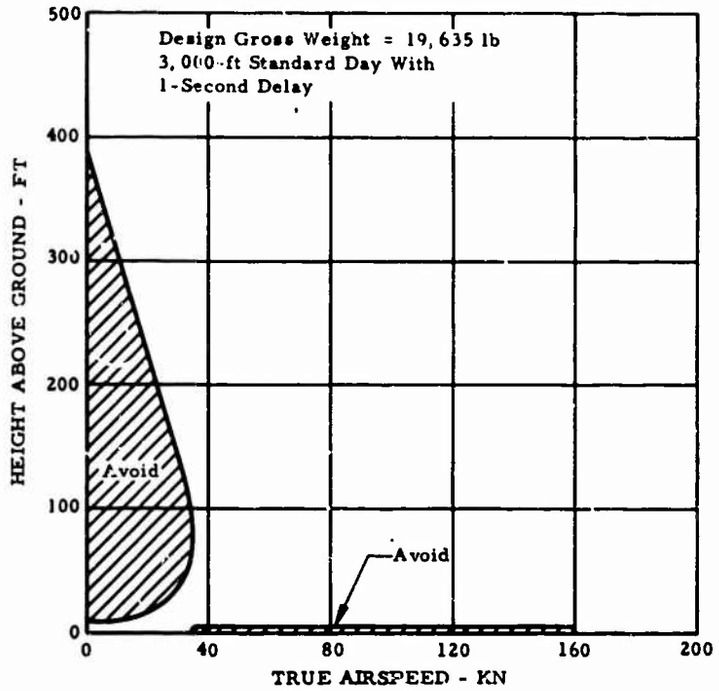

Figure 22. Autorotational Rate of Descent.

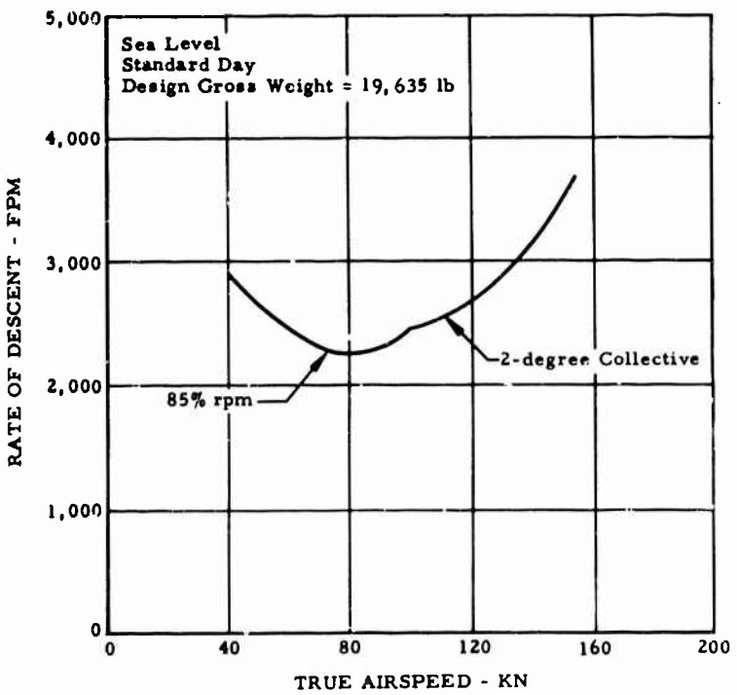

Figure 23. Predicted Height-Velocity Curve, Helicopter and Autogyro.

(less drag losses) is traded for a gain in altitude, followed by a pushover to approximately 150 knots. The conversion takes place at a roughly constant speed of 150 knots in a descent, during which potential energy is traded for the kinetic energy required to bring the Rotor/Wing up to normal rotational speed and to supply the aircraft drag losses. Following conversion to autogyro mode, airspeed is reduced to approach speed (60 to 80) followed by the final flare to an autorotative landing. Figure 24 presents the region in which conversion cannot be effected and an airplane-type power-off landing must be made.

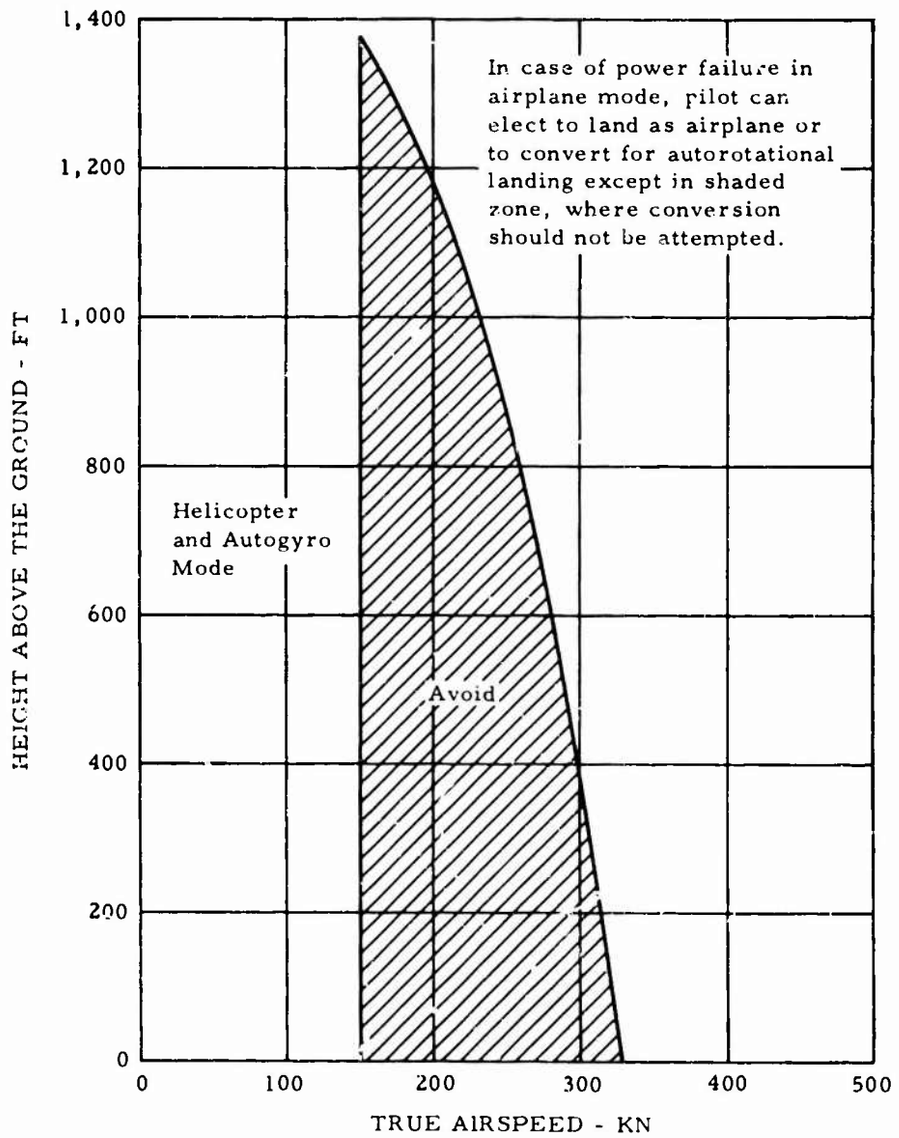

Figure 24. Emergency Landing, Airplane Mode.

PERFORMANCE PARAMETERS

The following pages summarize the essential parameters used in calculating the Hughes CRA performance. Comparison of these parameters with actual test data is shown wherever such a comparison can be made simply. In cases where parameter derivation from test results is more complex, full development will be found in the appropriate Appendix.

Dimensional Data and Performance Constants

Pertinent constants of dimensional and performance significance are presented in Tables IV through VII for airplane and helicopter modes. These constants, in addition to the graphs that follow, facilitate spot calculations to confirm or to extend the performance charts.

TABLE IV. AIRPLANE MODE DIMENSIONAL DATA AND PERFORMANCE PARAMETERS

Dimensions	
Rotor/Wing planform area	526 sq ft
Rotor/Wing aspect ratio	3.95
Rotor/Wing span	44 ft 11 in.
Fuselage length	70.0 ft 8 in.
Total wetted area	3,090 sq ft
Frontal area	171 sq ft
Aerodynamics	
Equivalent flat plate drag area	8.8 sq ft
Span efficiency factor, e	0.895
Maximum lift/drag ratio	12.0
Mach number for drag divergence	0.75
Propulsion	
Engine	One J52-P-8A
Tail pipe pressure loss ratio = $\Delta P_t / P_{t_5}$	6.4%
Engine accessory power extraction	19.7 hp
Engine air bleed	0.2%
Diverter valve leakage	0.7%
Inlet mass flow ratio at cruise	0.5
Inlet pressure loss at cruise	0.5%

TABLE V. DIMENSIONAL DATA AND PERFORMANCE PARAMETERS FOR HELICOPTER AND AUTOGYRO MODES

Dimensions	
Rotor/Wing diameter	50 ft
Rotor/Wing disc area	1,964 sq ft
Blade weighted equivalent chord	4.32 ft
Blade solidity	0.165
Normal rotor speed	275 rpm
Normal rotor tip speed	720 ft/sec
Yaw fan diameter	4.7 ft
Yaw fan moment arm	30.0 ft
Yaw fan normal speed	2,930 rpm
Power Required Parameters	
Equivalent flat plate drag area	16.35 sq ft
Rotor figure of merit (sea level standard, design gross weight)	0.521
Yaw fan thrust	40 lb
Rotor power extraction (sea level standard)	64 hp
Fuselage download (hover)	1,033 lb
Propulsion	
Autogyro - Same as airplane mode	
Helicopter	
Engine	One J52-P-8A
Overall pressure recovery at rotor tip nozzle	0.96
Tip nozzle velocity coefficient	0.96
Engine air bleed	0.2%
Diverter valve leakage	0.9%
Engine accessory power extraction	40.7 hp
Engine inlet pressure loss (hover)	0.2%
Engine inlet temperature rise (hover)	4°F

TABLE VI. GROSS WEIGHT BREAKDOWN (LB)	
Rotor/Wing group	2,753
Tail group	704
Body group	2,098
Landing gear	600
Flight control group	729
Engine section	240
Propulsion group	3,545
Auxiliary power unit	150
Instrument and navigation equipment group	120
Hydraulic group	205
Electrical group	300
Electronics group	900
Armament group (gunfire protection)	250
Furnishings and equipment group	412
Auxiliary gear group	8
Air conditioning and anti-icing group	40
Undefined weight	115
EMPTY WEIGHT	13,169
Crew (2)	400
Fuel (usable)	3,000
Fuel (unusable)	30
Oil	36
Cargo	3,000
DESIGN GROSS WEIGHT	19,635

TABLE VII. ENGINE DATA		
Guaranteed Sea Level Static Ratings - Pratt and Whitney J52-P-8A (Model JT-8B-3)		
Condition	Thrust (lb)	SFC (Maximum) (lb/hr/lb thrust)
Maximum	9,300	0.86
Military	9,300	0.86
Normal	8,200	0.81
90-percent cruise	7,380	0.79
75-percent cruise	6,150	0.76

Airplane Mode Aerodynamics

Airplane mode performance of the CRA has been calculated by standard techniques, using the family of drag polars presented in Appendix I. These calculations can be summarized in terms of overall lift/drag ratio versus lift coefficient as shown in Figure 25.

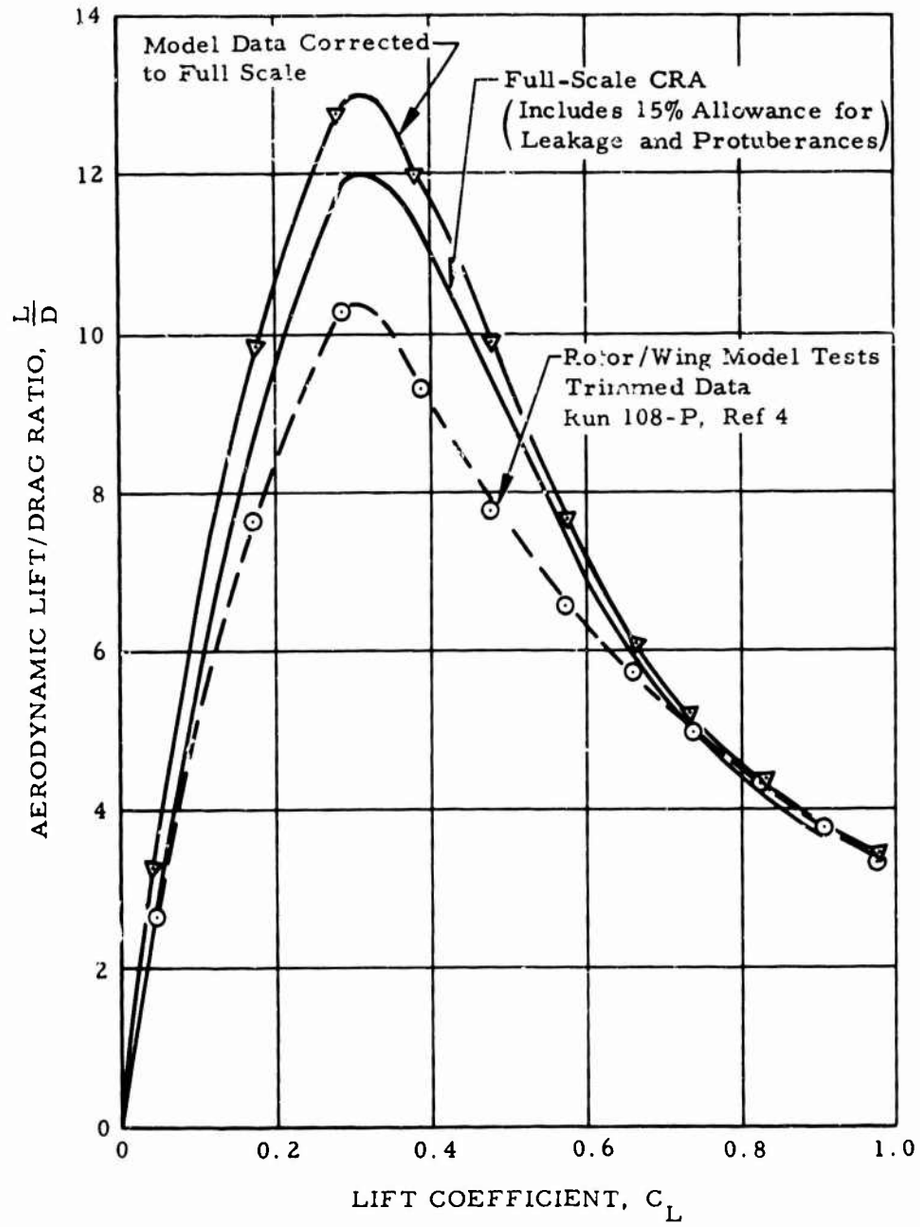

Figure 25. Airplane Mode Aerodynamic Efficiency.

Helicopter Performance

The helicopter mode performance reported herein has been calculated through a computer program containing all the terms and corrections available to modern rotary-wing technology as described in Appendix II. It is impossible to present a single performance parameter curve that adequately summarizes all of the factors that are involved in these calculations. However, the net result of the calculations is a series of power-required curves that can be related to the classical C_T versus C_Q curves of Figures 26, 27, and 28 for $\mu = 0$, 0.25, and 0.35, respectively. It must be recognized that these C_T - C_Q curves do not present the interactions of blade Mach number and C_T/σ in sufficient detail to permit extensions of the calculated helicopter flight envelope in terms of either altitude or maximum speed. This must be done during the complete analysis procedure.

Whirl tower test data from Reference 3 are included in Figure 26 as an indication of the excellent correlation between the CRA performance calculations and the actual test data. The difference that does exist represents a conservative value of scale and configuration effects. Helicopter forward flight aerodynamics are summarized and compared with model test data in Figures 27 and 28. At $\mu = 0.25$ (Figure 27), the CRA calculated performance is in even closer agreement with the wind tunnel results than was the case for hover performance in Figure 26. Note that the hovering model test results reported here are from whirl tower tests at the Hughes plant, whereas the forward flight data are from tests at the Navy Ship Research and Development Center Aerodynamics Laboratory.

At $\mu = 0.35$ (Figure 28), tip Mach number effects have assumed sufficient importance in the calculational procedure that the CRA predicted torque coefficients substantially exceed the model test values. The calculated values are considered to be conservative; however, helicopter maximum forward speed is a sensitive quantity in the conversion procedure, and conservatism is appropriate. All of the performance curves for the CRA include the effects of download on the fuselage in hovering and download on the tail in forward flight, in addition to the power extracted for the yaw fan and for cooling.

Autogyro Performance

The statements of the preceding paragraphs regarding the difficulty in presenting a parametric curve that adequately represents the helicopter performance calculational procedure are equally applicable to the autogyro situation. A significant overview of the autogyro performance situation

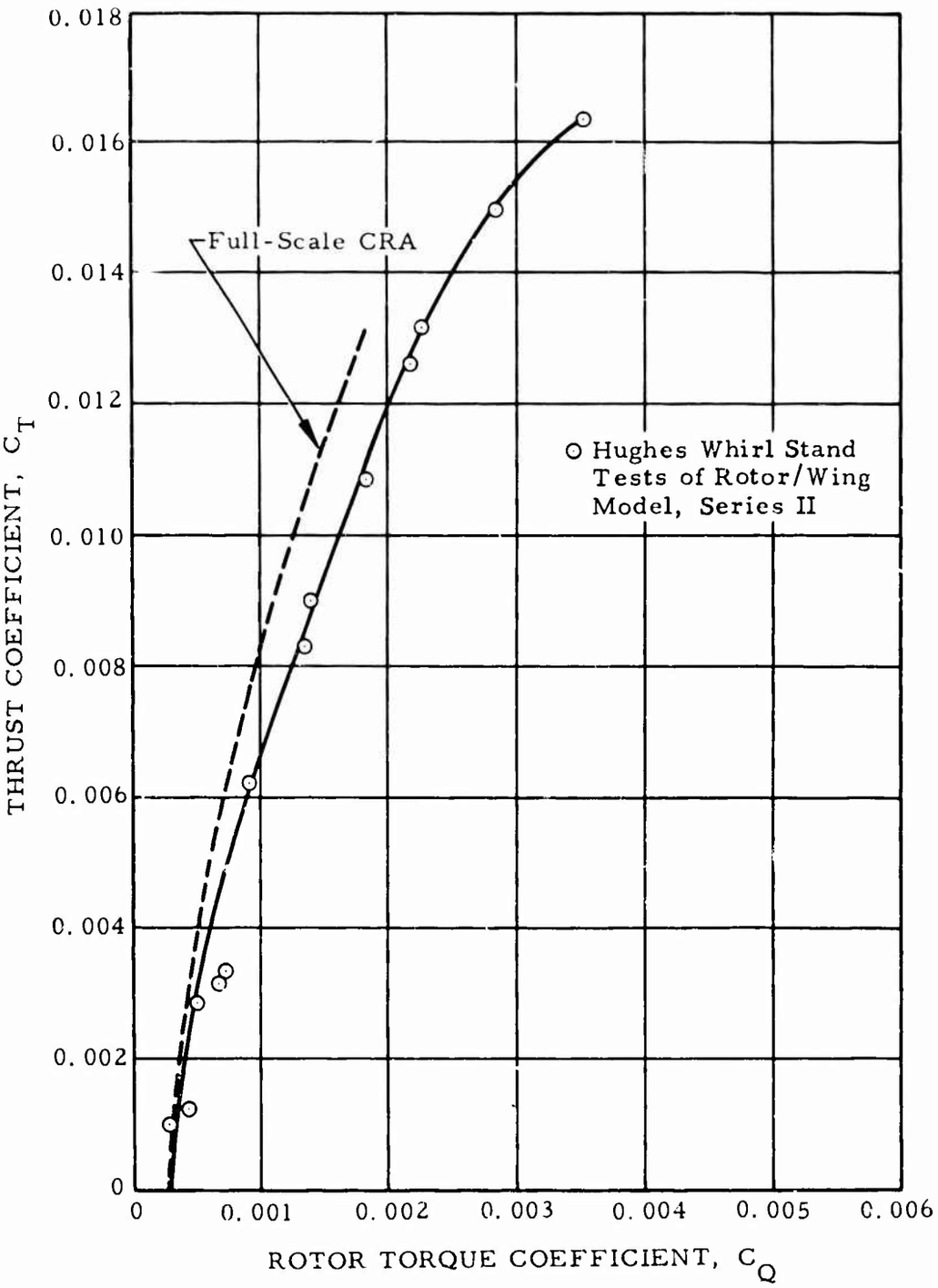

Figure 26. Hovering Rotor Performance, Helicopter Mode.

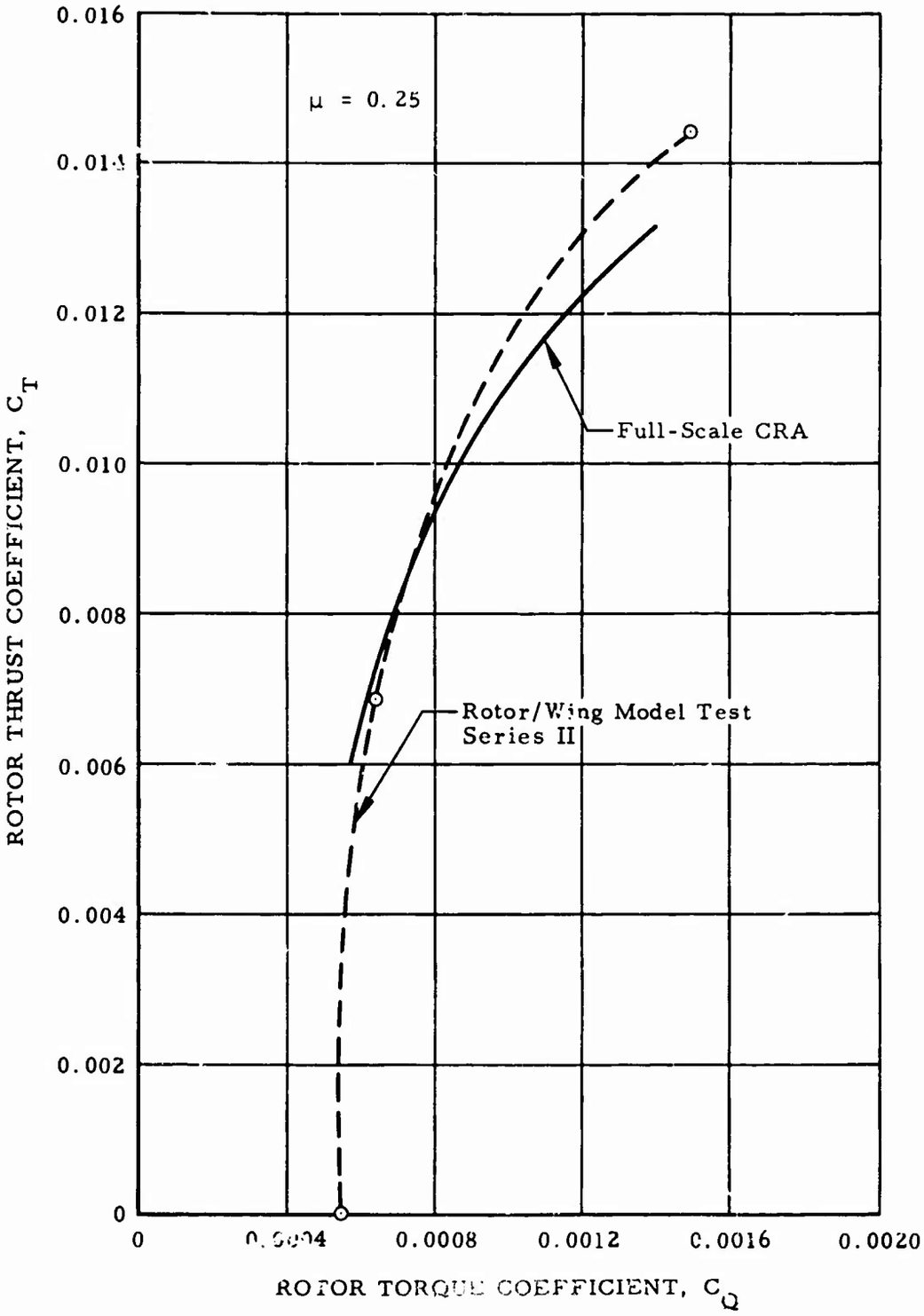

Figure 27. Forward Flight Performance, Helicopter Mode, μ = 0.25.

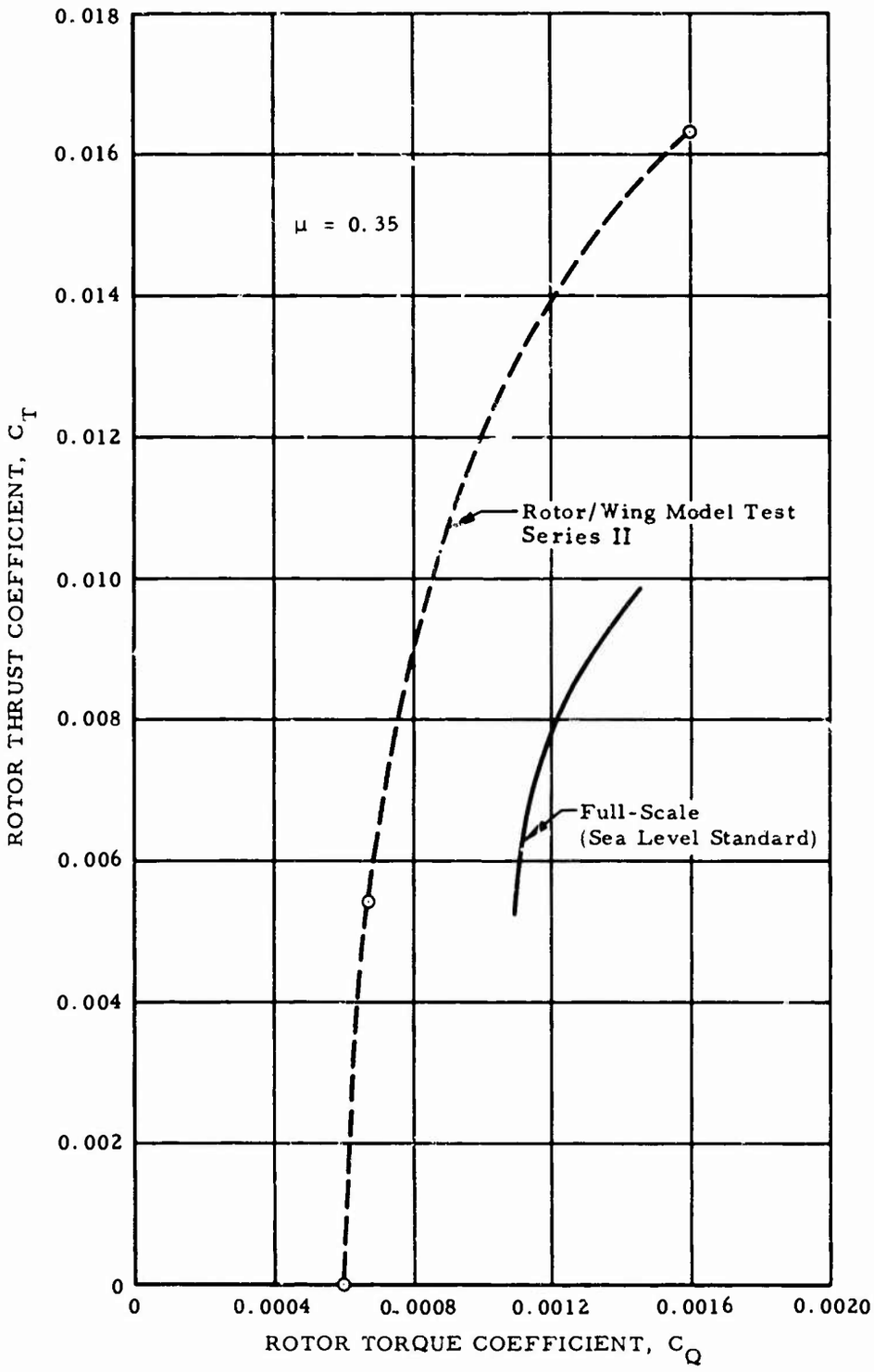

Figure 28. Forward Flight Performance, Helicopter Mode, $\mu = 0.35$.

can be obtained from a plot of overall autogyro lift/drag ratio versus advance ratio.

As shown in Figure 29, the CRA autogyro performance implies overall lift/drag ratios in the range of 3.0 to 4.5. Raw wind tunnel data from Rotor/Wing tests as reported in Reference 4 have been transferred to Figure 29 for comparison with the CRA calculations. The very close agreement between the small-scale test results and the full-scale calculations suggests that full credit has not been taken for Reynolds number effects in deriving the full-scale factors from the wind tunnel data. However, since autogyro flight is the key mode in the conversion of the CRA from helicopter to airplane flight, it is appropriate that the autogyro mode calculations be based on the most conservative performance parameters.

Hot Cycle Propulsion Performance

The helicopter mode propulsion system of the CRA is very closely related to that of the XV-9A Hot Cycle Research Aircraft, which was tested during 1964 and 1965.

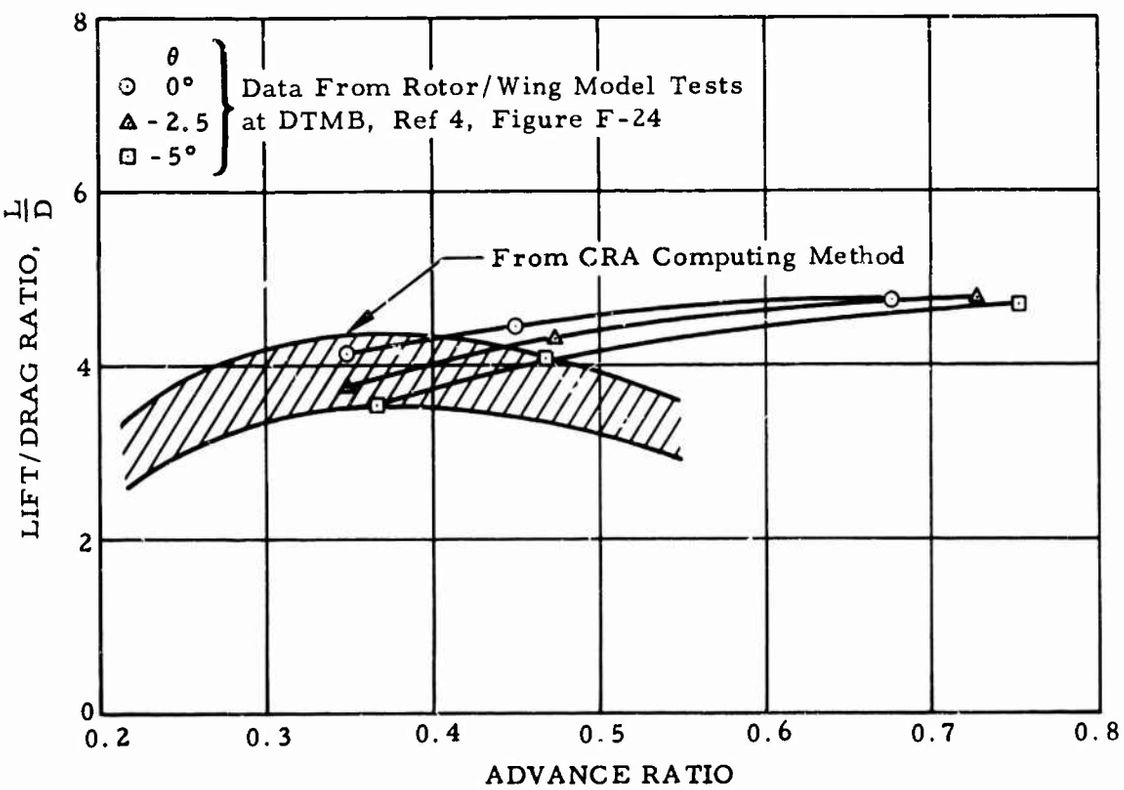

Figure 29. Lift/Drag, Autogyro Mode.

The performance of the Hot Cycle system depends primarily upon two parameters; namely, overall pressure recovery from the engine exhaust to the blade tip, and tip nozzle effective velocity coefficient. Both parameters have been identified during the XV-9A program, and the values used for the CRA represent a conservative application of the XV-9A test results as summarized in Figure 30.

Overall pressure recovery for the CRA is calculated to be slightly lower than for the XV-9A, as a result of somewhat higher duct Mach numbers in the CRA design. This effect is opposed by the effect of smaller duct length/diameter ratio in the CRA, and the net penalty shown in Figure 30 is conservatively stated.

In the XV-9A tip nozzle cascades, turning and accelerating losses could not be isolated. Accordingly, the tether test (Reference 6) C_{V_e} of 0.94 was based on flow conditions prior to the final turn. For the CRA configuration, it is easier to calculate the turning losses separately and to use a nozzle velocity coefficient based on conventional turbojet nozzle experience; the value used, $C_{V_e} = 0.96$, is again conservative. Complete details of the procedures for calculation of helicopter, autogyro, and airplane power available are included in Appendix III.

Composite Power Available and Power Required Curves

Power available and power required curves covering all three flight modes have been prepared for a variety of weights at sea level standard; 5,000 feet standard; and 6,000 feet, 95°F conditions. These curves are included here as Figures 31, 32, and 33, respectively. They represent the combined effects of the parameters just discussed.

Power required and power available calculations for the CRA are in every case built upon test data from closely related configurations. Any corrections to the test data for minor configuration changes and for the effects of small-scale test conditions follow accepted techniques.

Figure 34 presents curves of specific range versus true airspeed in the airplane mode for the two weights and various altitudes.

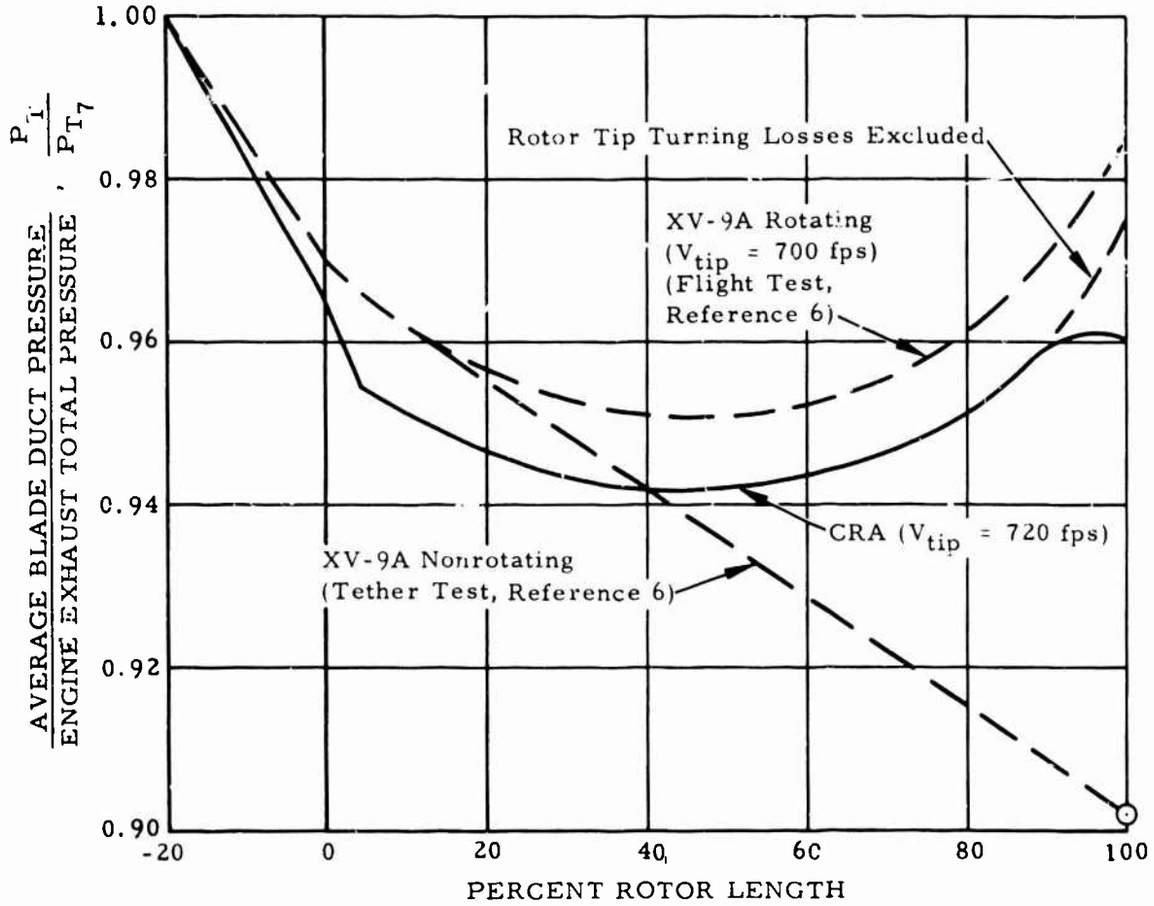

XV-9A Blade Tip

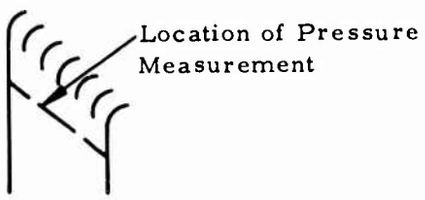

An effective nozzle coefficient C_{Ve} = 0.94 has been established based on the measured gas condition before the turning vanes.

CRA Blade Tip

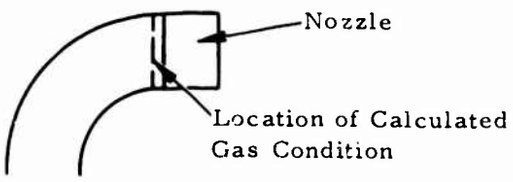

An effective nozzle coefficient C_{Ve} = 0.96 has been used for performance prediction based on the calculated gas conditions after the turn.

Figure 30. Overall Rotor System Pressure Recovery, Helicopter Mode.

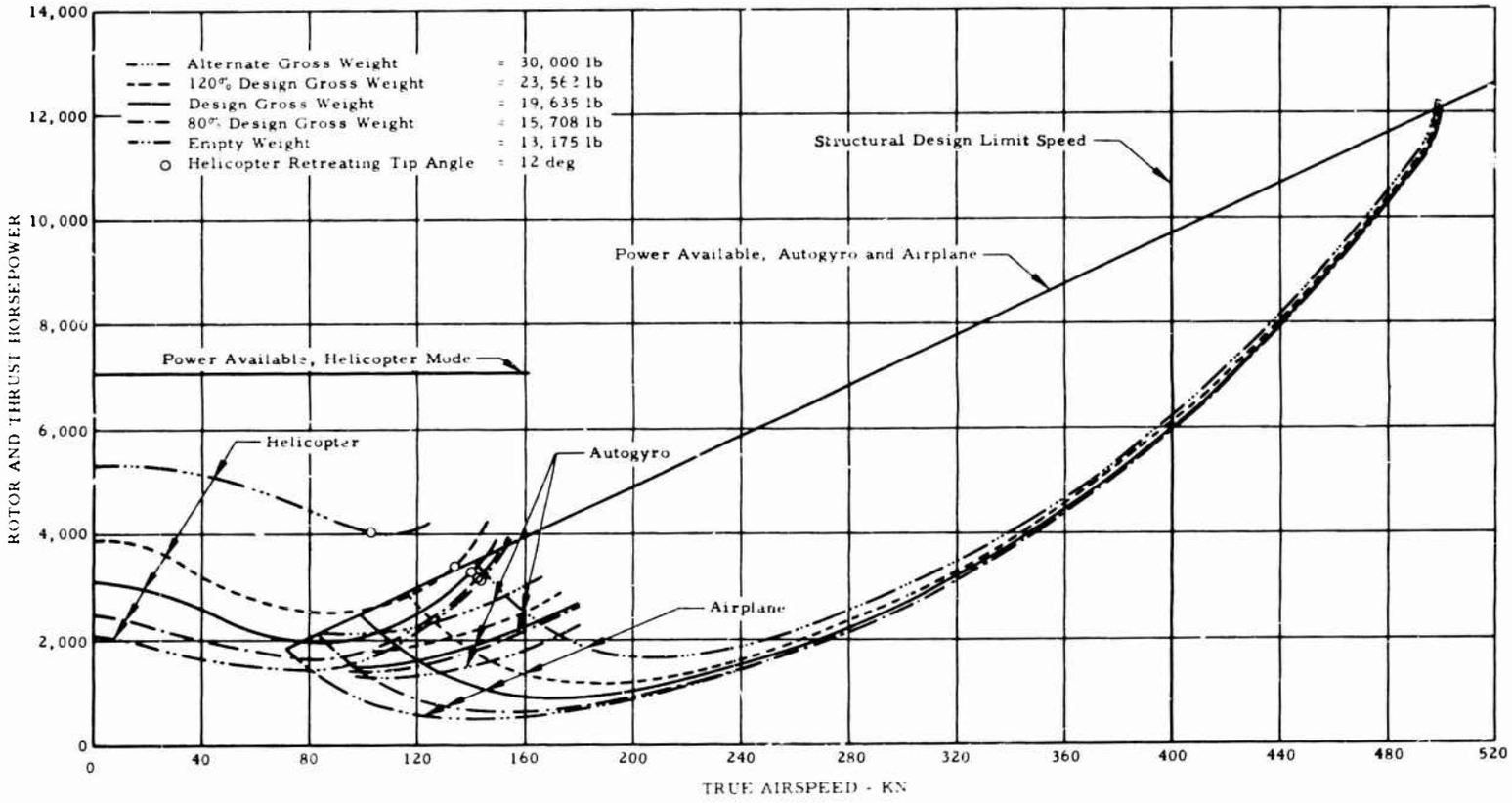

Figure 31. Power Required and Power Available, Sea Level Standard.

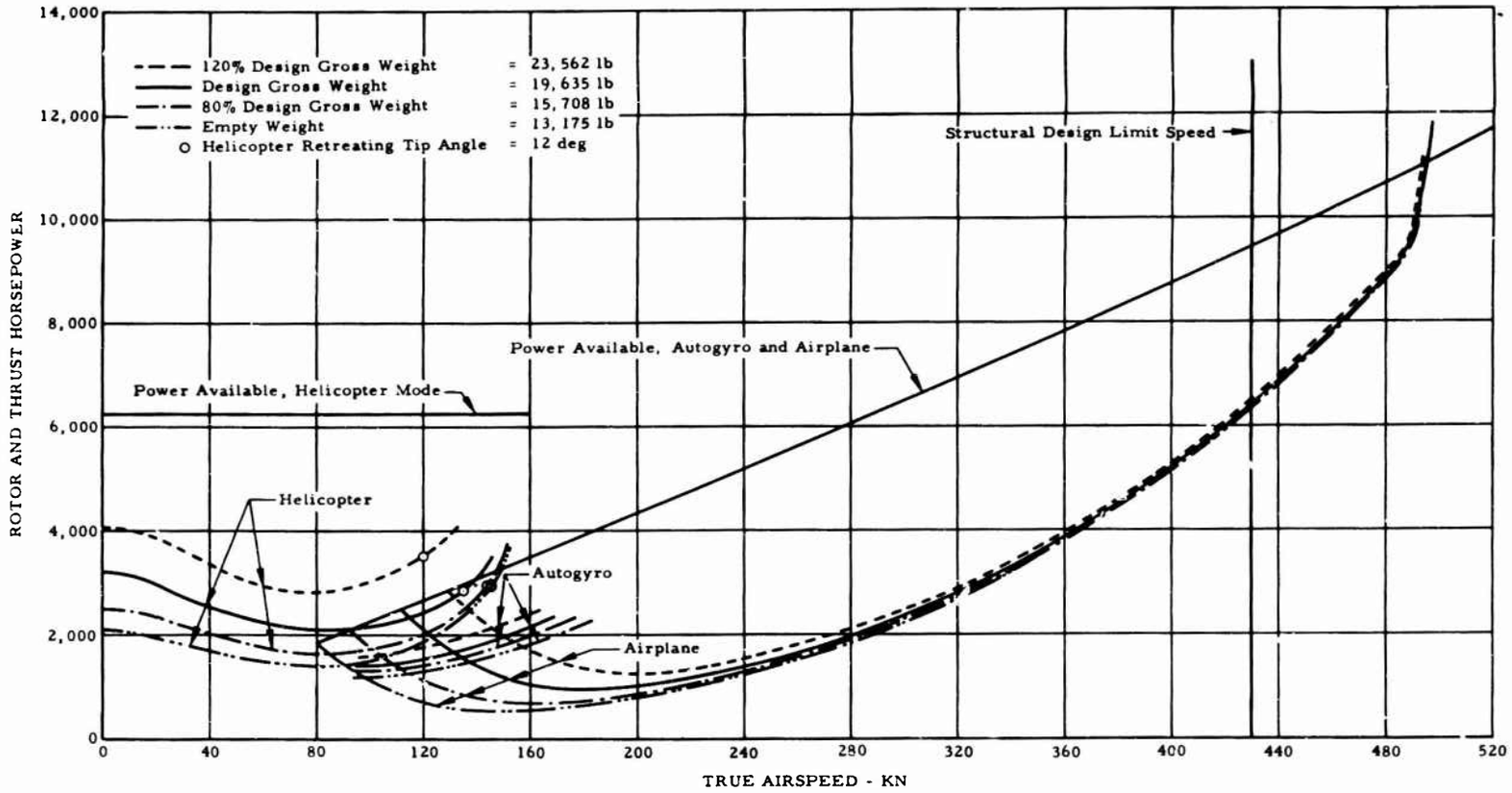

Figure 32. Power Required and Power Available, 5,000 Feet Standard.

Figure 33. Power Required and Power Available, 6,000 Feet, 95°F.

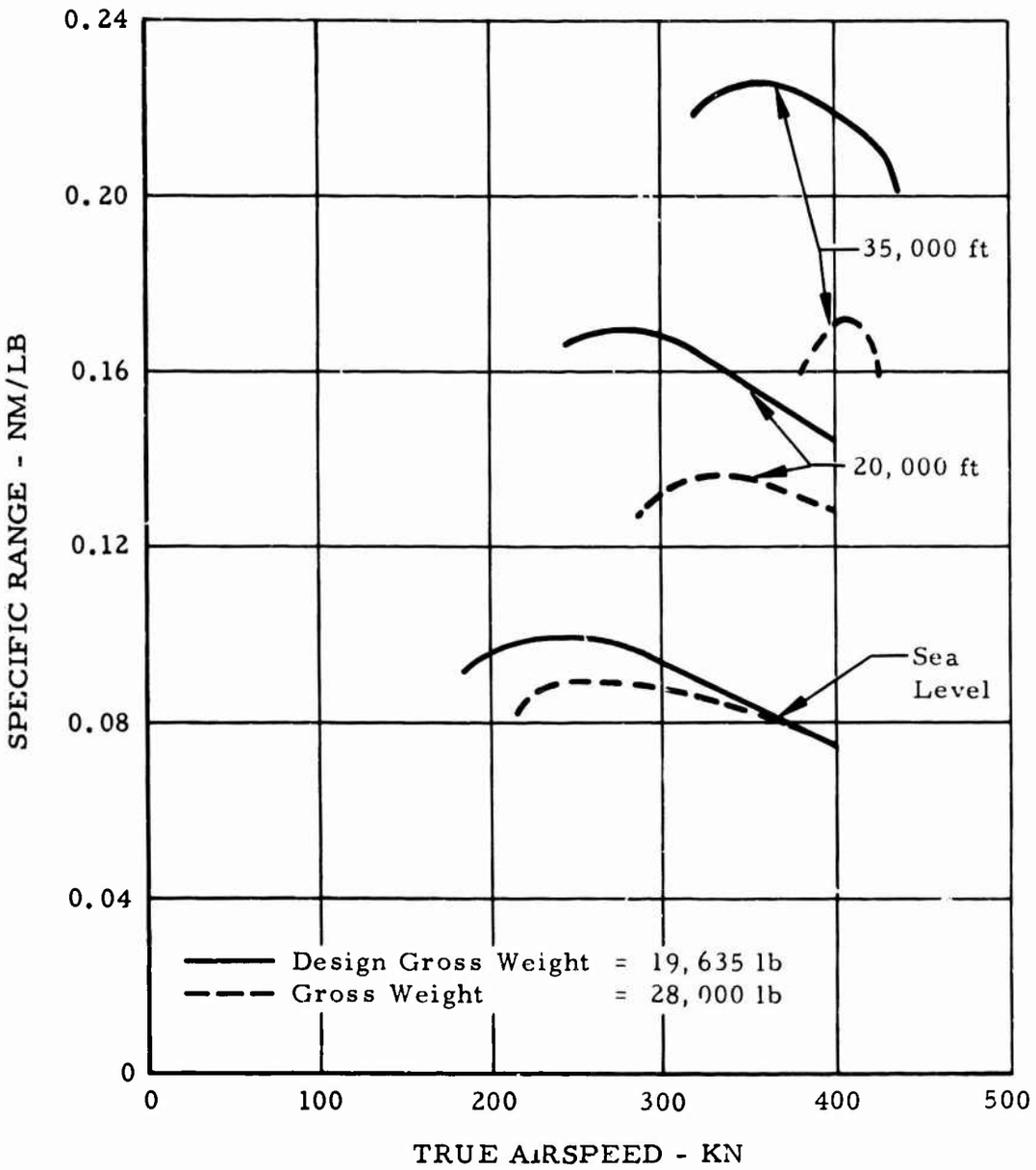

Figure 34. Specific Range Versus True Airspeed.

WEIGHT AND BALANCE

This section of the report presents the results of the weight and balance analysis performed during the CRA preliminary design study. It includes a Part I Summary Weight Statement that has been prepared in accordance with the format and content requirements of MIL-STD-451. Weight and balance calculations are also presented with substantiation for the estimated weight empty. The weight substantiation includes a detailed description of the design and the analytical methods used to determine CRA weights from the design.

Since the design employs proven, fully developed systems and components to the maximum practicable extent, actual weights were used to determine 35 percent of the total weight empty. The remaining 65 percent of weight empty was determined by using design analysis verified by comparative analysis and parametric study.

The estimated weights and center of gravity limits for the Composite Research Aircraft are as follows:

Weight empty	13, 169 lb
Design gross weight (with 3, 000-lb payload and 3, 000-lb usable fuel)	19, 635 lb
Forward cg limit	Sta 585 (at design gross weight)
Aft cg limit	Sta 600
Lateral cg limit	±8 in. from centerline

These data are based on the following design and weight considerations:

Rotor/Wing radius	25 ft
Speed	400 KEAS
Disc loading	10 lb/sq ft
Helicopter mode ultimate load factor	4.50
Airplane mode ultimate load factor	6.75
Engine (1)	J52-P-8A
Fixed specification weights:	
Furnishings and equipment	1, 200 lb
Avionics	900 lb
Armor protection 100 lb/crew member 50 lb/engine	250 lb
Auxiliary power unit	150 lb
Payload	3, 000 lb
Fuel	3, 000 lb

NAME_____ PAGE_____
DATE_____ MODEL_____
REPORT_____

DETAIL WEIGHT STATEMENT
ROTORCRAFT ONLY
ESTIMATED—

(Cross out those not applicable)

CONTRACT DA 44-177-AMC-336 (T)
ROTORCRAFT, GOVERNMENT NUMBER_____
ROTORCRAFT, CONTRACTOR NUMBER_____
MANUFACTURED BY Hughes Tool Company - Aircraft Division

		Main	Auxiliary
Engine	Manufactured by	Pratt & Whitney	
	Model	J52-P-8A	
	Number		
Propeller	Manufactured by		
	Model		
	Number		

NAME_____ ROTORCRAFT PAGE_____
DATE_____ SUMMARY WEIGHT STATEMENT MODEL_____
WEIGHT EMPTY REPORT_____

1							
2	ROTOR Wing Group						2,753
3	BLADE ASSEMBLY					700	
4	HUB - Wing					2,053	
5	HINGE AND BLADE RETENTION						
6		FLAP	PING				
7		LEAD	LAG				
8		PITC	H				
9		FOLD	ING				
10	WING GROUP						
11	WING PANELS—BASIC STRUCTURE						
12	CENTER SECTION—BASIC STRUCTURE						
13	INTERMEDIATE PANEL—BASIC STRUCTURE						
14	OUTER PANEL—BASIC STRUCTURE—INCL TIPS			LBS			
15	SECONDARY STRUC—INCL FOLD MECH			LBS			
16	AILERONS—INCL BALANCE WTS			LBS			
17	FLAPS						
18	—TRAILING EDGE						
19	—LEADING EDGE						
20	SLATS						
21	SPOILERS						
22							
23	TAIL GROUP						704
24	TAIL ROTOR						
25	—BLADES Yaw Fan					22	
26	—HUB Yaw Fan					12	
27	STABILIZER—BASIC STRUCTURE					240	
28	FINS—BASIC STRUCTURE—INCL DORSAL			LBS			
29	SECONDARY STRUCTURE—STABILIZER AND FINS						
30	Elevon —INCL BALANCE WEIGHT			LBS		304	
31	RUDDER—INCL BALANCE WEIGHT			LBS		56	
32							
33	BODY GROUP						2,098
34	FUSELAGE OR HULL—BASIC STRUCTURE					1,692	
35	BOOMS—BASIC STRUCTURE						
36	SECONDARY STRUCTURE—FUSELAGE OR HULL					207	
37	—BOOMS						
38	—DOORS, PANELS & MISC					199	
39							
40							
41	ALIGHTING GEAR—LAND Tricycle TYPE						600
42	LOCATION *	ROLLING ASSEMBLY	STRUCT	CONTROLS			
43							
44	Main	156	300	17		473	
45	Nose	37	75	15		127	
46							
47							
48							
49							
50	ALIGHTING GEAR GROUP—WATER TYPE						
51	LOCATION	FLOATS	STRUTS	CONTROLS			
52							
53							
54							
55							
56							
57							

* Wheels, Brakes, Tires, Tubes and Air.

NAME _____ ROTORCRAFT PAGE _____
DATE _____ SUMMARY WEIGHT STATEMENT MODEL _____
WEIGHT EMPTY—Continued REPORT _____

1							
2	FLIGHT CONTROLS GROUP						729
3	COCKPIT CONTROLS					50	
4	AUTOMATIC STABILIZATION						
5	SYSTEM CONTROLS—ROTOR NON ROTATING					370	
6	ROTATING					105	
7	Tail Section					81	
8	- Yaw Non-Rotating					22	
9	- Yaw Rotating					5	
10	ENGINE SECTION						240
11	INBOARD						
12	Engine Mounts					40	
13	Structure					171	
14	DOORS, PANELS AND MISC					29	
15							
16	PROPULSION GROUP						3,545
17			X AUXILIARY X		X MAIN X		
18	ENGINE INSTALLATION						
19	ENGINE					2,118	
20	TIP BURNERS						
21	LOAD COMPRESSOR						
22	REDUCTION GEAR BOX, ETC						
23	ACCESSORY GEAR BOXES AND DRIVES					57	
24	SUPERCHARGER--FOR TURBOS						
25	AIR INDUCTION SYSTEM					100	
26	EXHAUST SYSTEM					210	
27	COOLING SYSTEM						
28	LUBRICATING SYSTEM					44	
29	TANKS						
30	BACKING BD, TANK SUP & PADDING						
31	COOLING INSTALLATION						
32	PLUMBING, ETC						
33	FUEL SYSTEM					204	
34	TANKS—UNPROTECTED				53		
35	—PROTECTED						
36	BACKING BD, TANK SUP & PADDING				131		
37	PLUMBING, ETC				80		
38	WATER INJECTION SYSTEM						
39	ENGINE CONTROLS					25	
40	STARTING SYSTEM					30	
41	PROPELLER INSTALLATION						
42	DRIVE SYSTEM						
43	GEAR BOXES Yaw Fan					23	
44	LUBE SYSTEM						
45	CLUTCH AND MISC						
46	TRANSMISSION DRIVE Yaw Fan					26	
47	ROTOR SHAFT						
48	JET DRIVE					562	
49							
50							
51							
52	AUXILIARY POWER PLANT GROUP						150*
53							
54							
55							
56							
57							

*This weight fixed by the statement of work.

NAME_____ ROTORCRAFT PAGE_____
DATE_____ SUMMARY WEIGHT STATEMENT MODEL_____
WEIGHT EMPTY—Continued REPORT_____

1								
2								
3								
4	INSTRUMENT AND NAVIGATIONAL EQUIPMENT GROUP						120	*
5	INSTRUMENTS							
6	NAVIGATIONAL EQUIPMENT							
7								
8								
9	HYDRAULIC AND PNEUMATIC GROUP						205	*
10	HYDRAULIC					205		
11	PNEUMATIC							
12								
13								
14	ELECTRICAL GROUP						300	*
15	A C SYSTEM							
16	D C SYSTEM					300		
17								
18								
19	ELECTRONICS GROUP						900	**
20	EQUIPMENT					58		
21	INSTALLATION					20		
22	Undefined Weight					822		
23								
24	ARMAMENT GROUP—INCL GUNFIRE PROTECTION				LBS		250	**
25								
26	FURNISHINGS AND EQUIPMENT GROUP						527	*
27	ACCOMMODATIONS FOR PERSONNEL					230		
28	MISCELLANEOUS EQUIPMENT	X INCL		LBS	BALLASTX	25		
29	FURNISHINGS					42		
30	EMERGENCY EQUIPMENT					65		
31	Undefined Weight					115		
32								
33								
34	AIR CONDITIONING AND ANTI-ICING EQUIPMENT						40	*
35	AIR CONDITIONING							
36	ANTI-ICING							
37								
38								
39	PHOTOGRAPHIC GROUP							
40	EQUIPMENT							
41	INSTALLATION							
42								
43	AUXILIARY GEAR GROUP						8	*
44	AIRCRAFT HANDLING GEAR							
45	LOAD HANDLING GEAR							
46	ATO GEAR							
47								
48								
49								
50								
51								
52								
53								
54	MANUFACTURING VARIATION							
55								
56								
57	TOTAL—WEIGHT EMPTY—PAGES 2, 3 AND 4						13,169	

*Statement of work allows a total of 1,200 lb. for these items.
**These weights fixed by statement of work.

4

NAME _____ SUMMARY WEIGHT STATEMENT PAGE _____
DATE _____ USEFUL LOAD GROSS WEIGHT MODEL _____
REPORT _____

1	LOAD CONDITION							
2								
3	CREW—NO. 2							400
4	PASSENGERS—NO.							
5	FUEL	LOCATION	TYPE	GALS				3,030
6	UNUSABLE						30	
7	INTERNAL	2 Cells	JP-4	462			3,000	
8								
9								
10								
11	EXTERNAL							
12								
13								
14								
15	BOMB BAY							
16								
17								
18								
19	OIL							
20	UNUSABLE							
21	ENGINE			4.8				36
22								
23								
24								
25	BAGGAGE							
26	CARGO							3,000
27								
28	ARMAMENT							
29	GUNS—LOCATION	TYPE**	QUANTITY	CALIBER				
30								
31								
32								
33								
34	AMM							
35								
36								
37								
38	BOMB INSTL*							
39	BOMBS							
40								
41	TORPEDO INSTL*							
42	TORPEDOES							
43								
44	ROCKET INSTL*							
45	ROCKETS							
46								
47	EQUIPMENT—PYROTECHNICS							
48	—PHOTOGRAPHIC							
49								
50	—*OXYGEN							
51								
52	—MISCELLANEOUS							
53								
54								
55	USEFUL LOAD							6,466
56								
57	GROSS WEIGHTS—PAGES 2-6							19,635

* If not specified as Weight Empty.

** Fixed, Flexible, etc.

SUMMARY WEIGHT STATEMENT — PAGE
NAME — DIMENSIONAL STRUCTURAL DATA — MODEL
DATE — ROTORCRAFT — REPORT

1	LENGTH—OVERALL FT 70.8			X BLADES FOLDED. FT			
2	GENERAL DATA			BOOM	FUS	NAC	CABIN
3	LENGTH—MAXIMUM FEET				70.8	20.5	26.2
4	DEPTH —MAXIMUM FEET				7.2	3.6	6.0
5	WIDTH —MAXIMUM FEET				6.7	6.3	5.5
6	WETTED AREA TOTAL Sq. Ft.				1,669	328	
7	WETTED AREA GLASS Sq. Ft.				55.7		
8	WING, TAIL & FLOOR DATA			WING	H TAIL	V TAIL	FLOOR
9	GROSS AREA—SQUARE FEET			591	158	130	144
10	WEIGHT/GROSS AREA—POUNDS PER SQUARE FEET			4.7	2.3	2.4	0.9
11	SPAN—FEET			45.3	27.8	15.5	
12	FOLDED SPAN—FEET						
13	*THEORETICAL ROOT CHORD—INCHES			190	90	131	
14	MAXIMUM THICKNESS—INCHES			26	12	21	
15	CHORD AT PLANFORM BREAK—INCHES			265	86	131	
16	MAXIMUM THICKNESS—INCHES			26	12	21	
17	THEORETICAL TIP CHORD—INCHES						
18	MAXIMUM THICKNESS—INCHES						
19	DORSAL AREA INCLUDED IN FUSELAGE			SQ FT	TAIL		SQ FT
20	TAIL LENGTH 25% MAC WING TO 25% MAC HORIZONTAL TAIL				32.5	FEET	
21	AREA—SQ FT PER ROTORCRAFT	FLAPS		AILERONS		SPOILERS	
22		SLATS		WING LE		WING TE	
23	**ROTOR DATA—TYPE	X ARTICULATING—FLAPPING—TEETERING—RIGID - Tail Rotor X					
24		X MAIN ROTOR-Rigid X			X Yaw TAIL ROTOR Fan X		
25	FROM CL ROTATION—INCHES	165	ROOT	TIP 300		ROOT 11	28 TIP
26	CHORD—INCHES		80	30		6.2	6.2
27	THICKNESS—INCHES		17	7		1.7	1.7
28					MAIN—FWD	MAIN—AFT	TAIL
29	BLADE RADIUS—FEET				25.0		2.35
30	NUMBER BLADES				3		6
31	BLADE AREA—TOTAL—OUTBOARD (R/W)/YF 165 11 INCHES RADIUS				182.7	Sq. Ft.	4.4
32	DISC AREA—TOTAL SWEPT 1964 SQ FT - OVERLAP						
33	TIP SPEED AT DESIGN LIMIT ROTOR—SPEED—POWER—FT/SEC *****				720		720
34	DESIGN FACTOR USED BY CONTRACTOR				1.12		1.12
35	LOCATION FROM HORIZONTAL REF DATUM INCHES				600		964
36	PRESSURE JET % BLADE SECTION AREA FOR DUCT						
37	TIP JET THRUST						GEAR***
38	POWER TRANSMISSION DATA			lbs	Thrust	RPM	RATIO
39	MAX POWER—TAKE-OFF				9,300		
40	ALIGHT GEAR TYPE TRICYCLE					OUTRGR MAIN—AFT	AUX—FWD
41	GEAR LENGTH—OLEO EXTND CL AXLE TO CL TRUNNION					113.8	36.5
42	OLEO TRAVEL—FULL EXTENDED TO COMPRESSED INCHES					10	10
43	WHEEL SIZE AND NUMBER REQUIRED X Main 11.00-12, 2 ea. X				X Aux	18.00-4 4	2eaX
44	FUEL AND OIL SYSTEM		LOCATION	NO. TANKS	****GALS UNPRTCTD	NO. TANKS	****GALS PROTECTD
45							
46	FUEL—BUILT IN		Fuselage	2	460		
47	FUEL—EXTERNAL						
48	LUBRICATING SYSTEM						
49	HYDRAULIC SYSTEM						
50	STRUCTURAL DATA—CONDITION			FUEL IN	DESIGN	STRESS	
51				WINGS—LB	GROSS WT	GROSS WT	ULT LF
52	FLIGHT					19,635	6.75
53	LANDING						
54	% DESIGN LOAD WING %			FWD RTR %		AFT RTR %	
55	175 Pounds			Per	Square	Foot	
56	**TYPE OF POWER TRANSMISSION—GEARED—PRESSURE JET—RAM JET						
57							

* Parallel to CL @ CL Rotorcraft.
** Cross out non-applicable type.
*** Gear ratio-eng to rotor.
**** Total usable capacity.
***** Refer MIL-S-8698, pg. 22, for definition limit and design maximum rotor speeds.

The requirements of MIL-S-8698 (ASG) govern the helicopter flight structural criteria; MIL-A-8861 (ASG) and MIL-A-8865 (ASG) govern the airplane mode. MIL-S-8698 (ASG) applies to landing and ground handling.

Weight loadings are summarized in Table VIII.

TABLE VIII. SUMMARY OF WEIGHT LOADINGS

Item	Weight (lb)
Weight empty	13,169
Crew (2)	400
Oil	36
Unusable fuel	30
Minimum flying weight	13,635
Payload	3,000
Zero fuel weight	16,635
Fuel	3,000
Gross weight	19,635

Weight and balance calculations for the CRA are contained in the following group of tables and illustrations. Figure 35 shows the reference data planes for the CRA. The center-of-gravity envelope is shown graphically in Figure 36. Cargo compartment weight and balance calculations, including permissible cargo loading limits, are shown in Figures 37 and 38.

SUBSTANTIATION OF ESTIMATED WEIGHTS

It is of particular significance that the weight estimate for the Composite Research Aircraft is more conservative than that which was forecast for the prototype OH-6A. No significant extrapolation or unusual mechanical innovations have been used in the Composite Research Aircraft.

Table IX presents a comparison of the CRA group weights with those of other helicopters and of airplanes.

The weight empty for the CRA was determined by using actual weight data, where available, and from specific design analysis, comparative analysis, and parametric analysis, as applicable for each case.

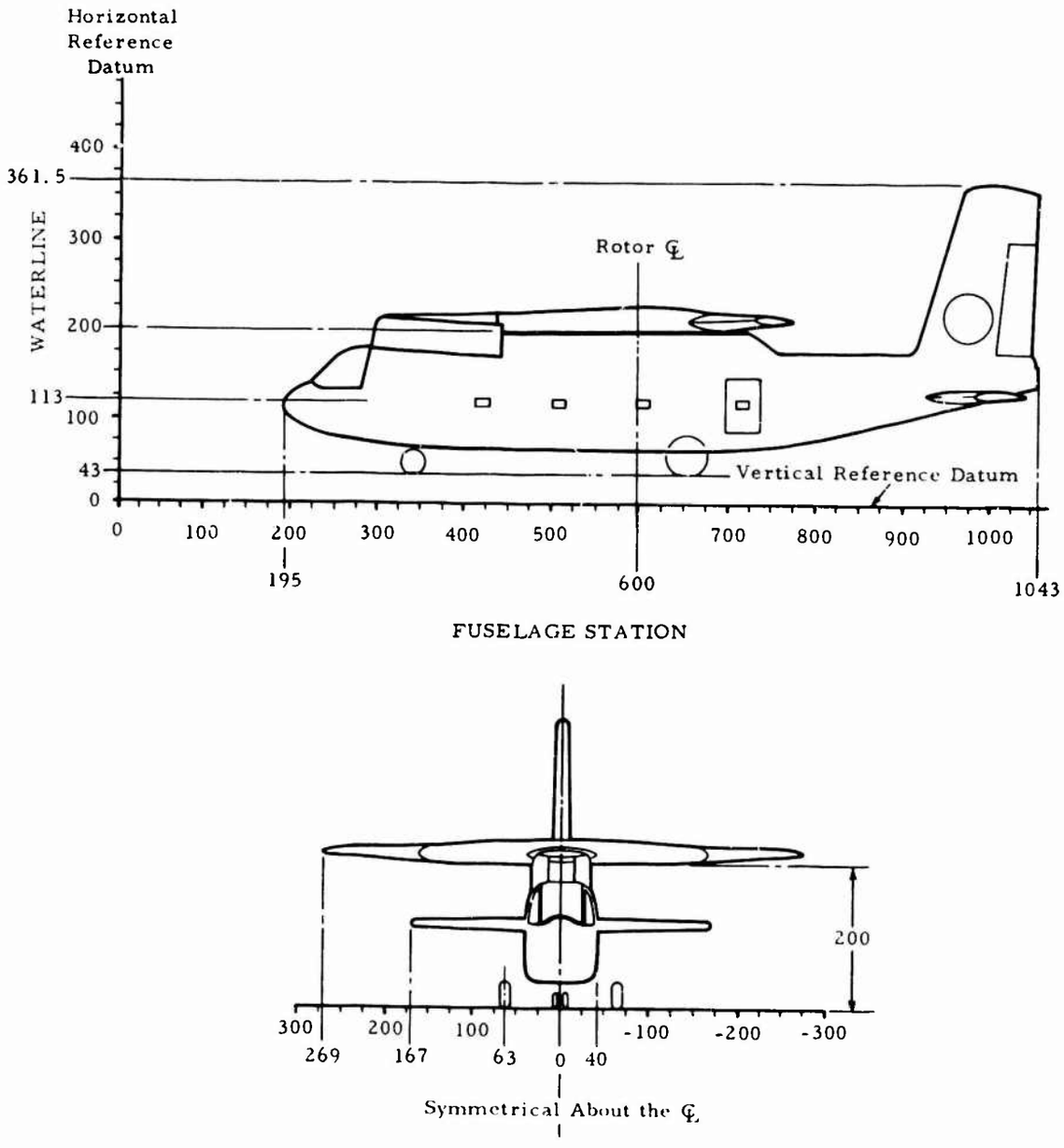

Figure 35. Reference Data Planes.

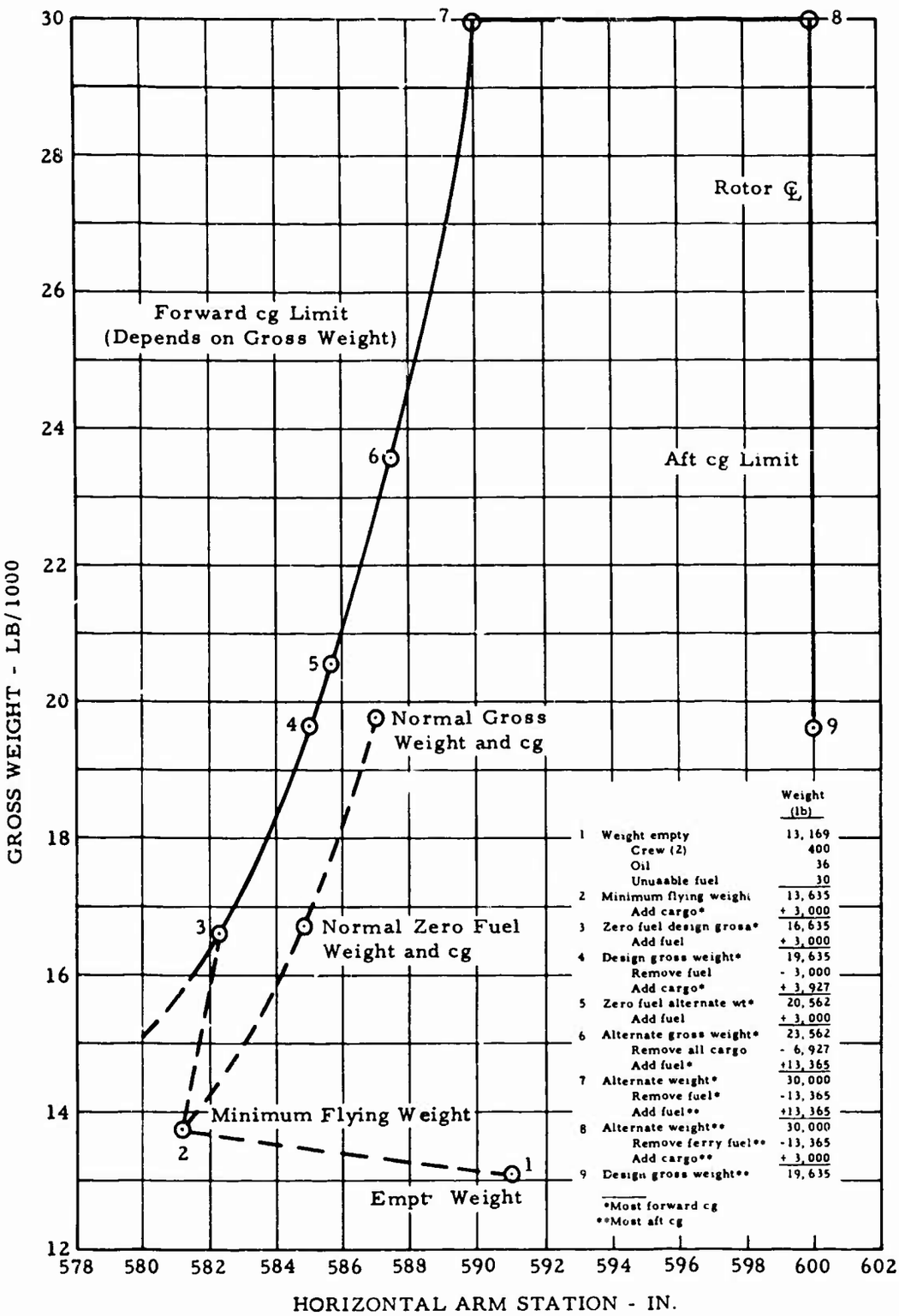

Figure 36. Center-of-Gravity Envelope - All Flight Modes.

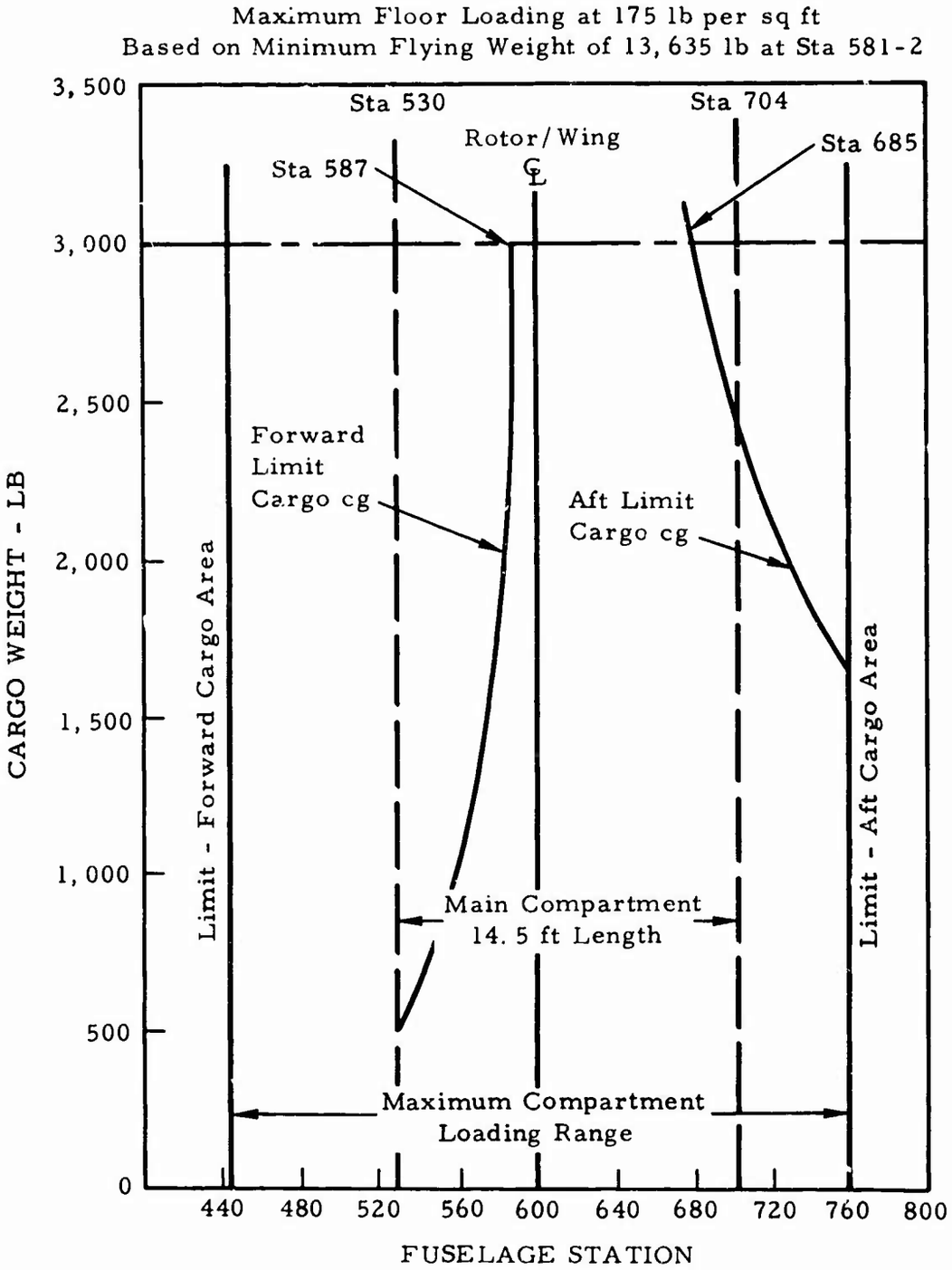

Figure 37. Permissible Cargo Loading Limits.

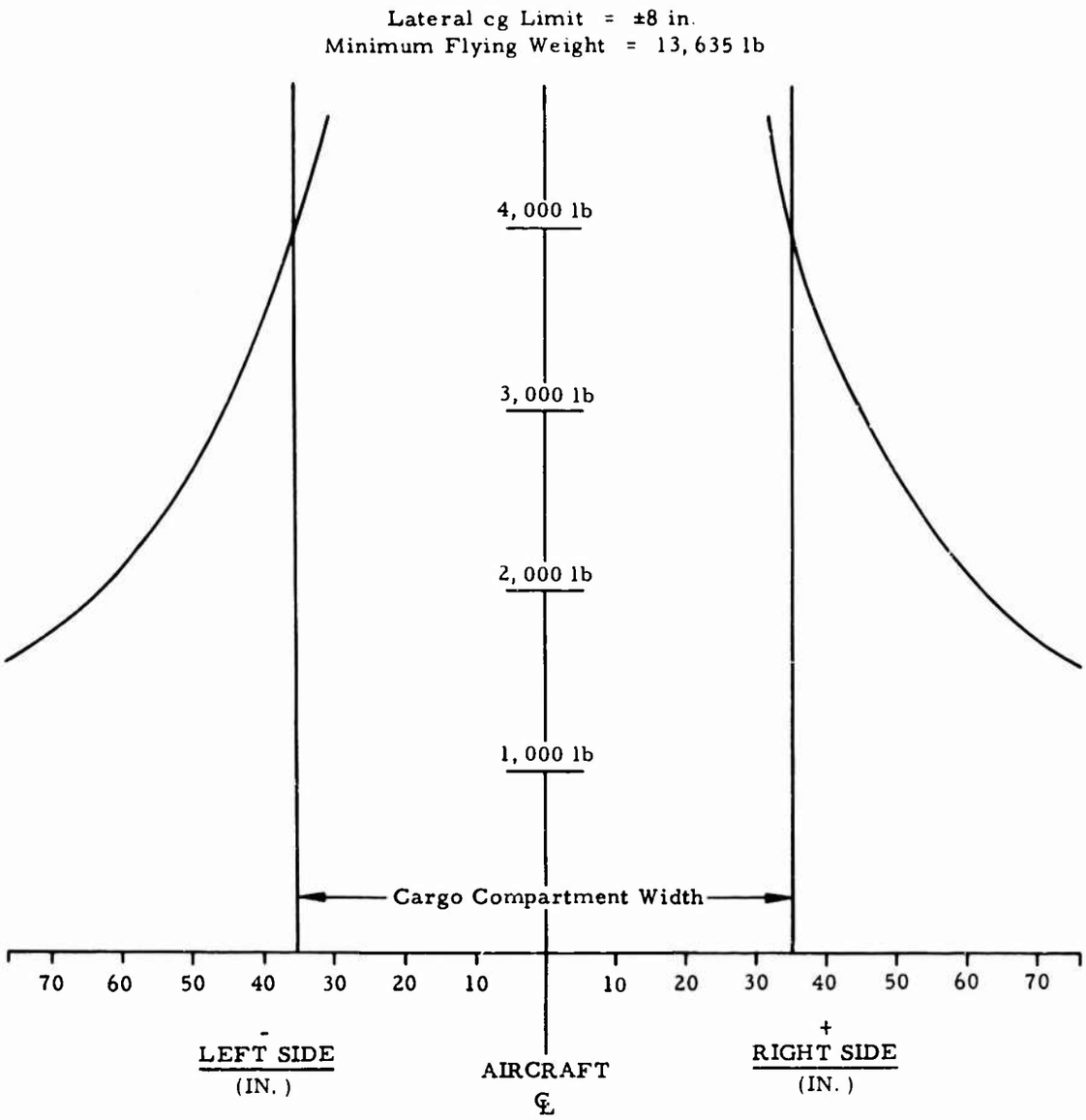

Figure 38. Permissible Lateral Center of Gravity Loading.

The fixed weights specified in the Statement of Work total 2,500 pounds, which, together with the fixed weight of the engine, amounts to 35 percent of the weight empty. Of the remaining 65 percent of the CRA weight empty, 85 percent was calculated by analysis of the design. The remaining 15 percent of the CRA weight empty was verified by comparative analysis and validated by statistical and parametric study. In addition, nearly all weights derived by design analysis were verified and validated against statistical data.

TABLE IX. GROUP WEIGHT COMPARISON

Group	CRA		XV-9A*	S-61	OH-6A	Buffalo	Sabre-Liner	A-4E
	(lb)	Percent Gross Weight						
Rotor/Wing	2,753	14.0	12.0	11.1	7.4	10.9	9.4	10.5
Empennage	704	3.6	0.7	0.8	0.8	2.5	1.8	4.0
Fuselage	2,098	10.7	5.3	12.7	9.5	11.8	10.0	9.3
Landing gear	600	3.1	3.0	4.1	2.2	4.6	3	5.3
Flight controls	729	3.7	3.3	3.3	2.8	1.4	1.0	3.7
Propulsion group	3,785	19.3	14.7	14.6	14.2	17.6	9.2	18.7
Equipment group	1,600	8.2	2.7	7.9	6.3	7.3	13.8	7.3
Electronics	900	4.6	-	6.8	4.4	0.9	2.6	2.7
Weight empty	13,169	67.1	41.7	61.3	47.7	57.0	52.1	61.5
Useful load	6,466	32.9	58.3	38.7	52.3	53.0	47.9	38.5
Gross weight	19,635	100.0	19,500**	17,813	2,400	38,000	17,760	15,500
Ultimate flight load factor	6.75	-	3.75	3.75	3.83	6.00	6.00	8.50

*Group weights have been adjusted to remove weight compromises documented in USAAVLABS Technical Report 65-29, in addition to the following:

1. Hot gas duct system transferred from rotor to propulsion group
2. Engine support stubs included in body group
3. Landing gear weight increased for higher gross weight
4. Yaw system transferred from flight controls to propulsion group

**Based on performance using current production T-64 engines rather than derated YT-64 engines.

Method of Analysis

The following paragraphs present a brief review of the methods employed in estimating the various component weights. Included also are tables, charts, and graphs used to derive or to validate the weight estimates.

Rotor/Wing Group

Rotor/Wing weights shown in Table X were derived by calculating the major structural elements and supplementing these weights with estimated allowances for minor elements. (See Figure 39.)

TABLE X. ROTOR/WING WEIGHT BREAKDOWN

Item	Component Weight (lb)	Total Weight (lb)
Blade Assemblies (3)		700
Spars	204	
Interspar panels	66	
Leading edge panels	48	
Trailing edge panels	57	
Ribs and stiffening	109	
Torque tube and attachment	165	
Balance weights	51	
Wing Assembly		2,053
Box beam structure	352	
Structural skin panels	245	
Structural ribs	516	
Blade retention system	280	
Hub structure and bearings	418	
Leading-trailing edge fairings	221	
Blade lock system	20	
Total Rotor/Wing Group		2,753

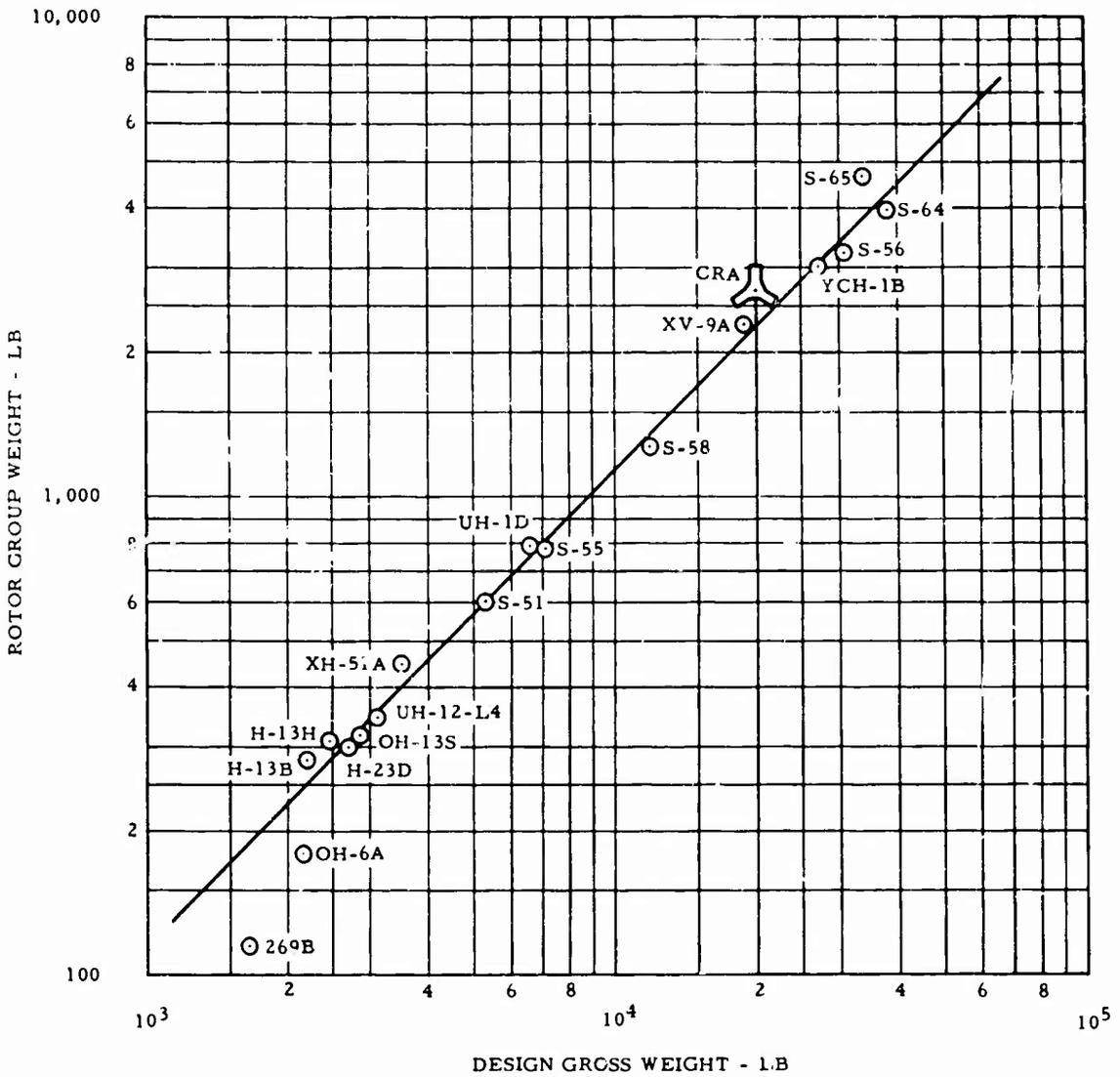

Figure 39. Main Rotor Group Weight Versus Design Gross Weight.

Tail Group

The tail group comprises the yaw fan assembly, the yaw fan doors, the vertical stabilizer including the rudder, and the all-movable horizontal surfaces that function as elevons.

Yaw Fan

The CRA yaw fan has six blades, each a scaled-up version of the light-weight blades used on the U. S. Army OH-6A light observation helicopter. The similarity of the blade size, power requirements, and construction

of the two aircraft permits a meaningful comparison of weights derived by design analysis with known data from the OH-6A design. The weights of the OH-6A components and the resulting yaw fan weights are summarized in Table XI.

TABLE XI. COMPARISON OF CRA AND OH-6A TAIL BLADE ASSEMBLY

Item	OH-6A	CRA
Unit blade weight, lb/blade	2.25	3.70
Total blade weight, lb/rotor	4.50	22.20
Hub weight, lb	2.80	12.00
Total yaw fan assembly weight, lb	7.30	34.20

Tail Surfaces Group

The basic dimensions and weights of the vertical and horizontal (elevon) surfaces are shown in Table XII.

TABLE XII. BASIC DIMENSIONS OF TAIL GROUP SURFACES

Item	Vertical Tail	Elevons (Total)
Span, in.	186	334
Area, sq ft (exposed)	130	158
Tip chord, in.	81	69
Root chord, in.	131	90
Aspect ratio	1.75	4.20
Leading edge sweep angle, deg	17	18
Airfoil section root	NACA 64_2 A016	NACA 64_2 A015
Airfoil section tip	NACA 64_2 A012	NACA 64_2 A010
Tail length to rotor, ft	30.1	29.5
Rudder hinge line (% chord)	80	-
Rudder span, in.	123	-
Weight, lb	306	364

Figure 40 presents the results of a parametric analysis of tail group unit weights taken from a group of representative aircraft. The correlation of the data derived by structural analysis with the historical data is good,

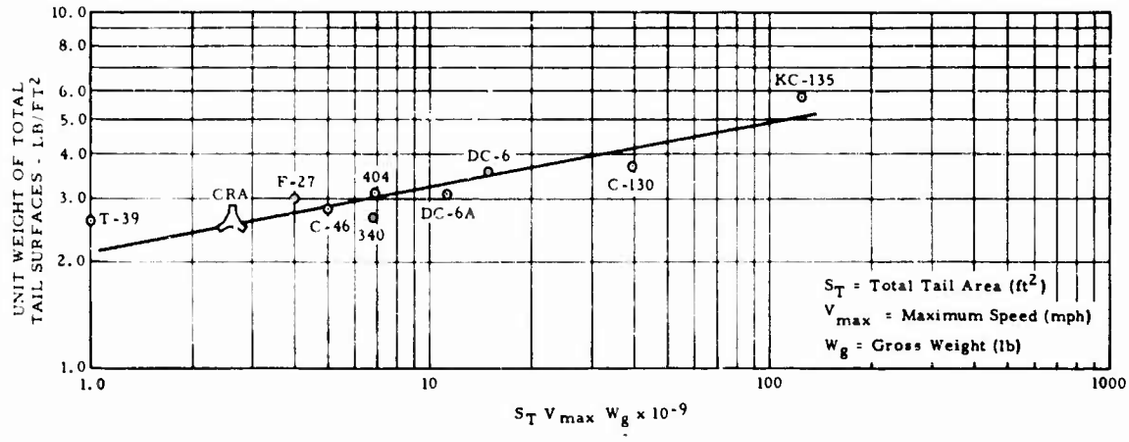

Figure 40. Tail Group Weight Comparison.

and the computed unit weight of the CRA tail surface compares favorably with the curve.

Body Group

The CRA fuselage weighs 2,098 pounds. A study of unpressurized aircraft fuselage weights (W_B) (Figure 41) shows an excellent correlation between weights and parameters containing the following variables:

1. Ultimate load factor (n)
2. Design gross weight (W_g), lb
3. Fuselage length (L), ft
4. Fuselage width (w), ft
5. Fuselage height (h), ft

The weight equation derived is as follows:

$$W_B = 117.7 n^{0.50} \left[\frac{W_g L(w+h)}{10^6} \right]^{0.651}$$

This curve clearly substantiates the CRA body group weight calculation based upon the structural analysis.

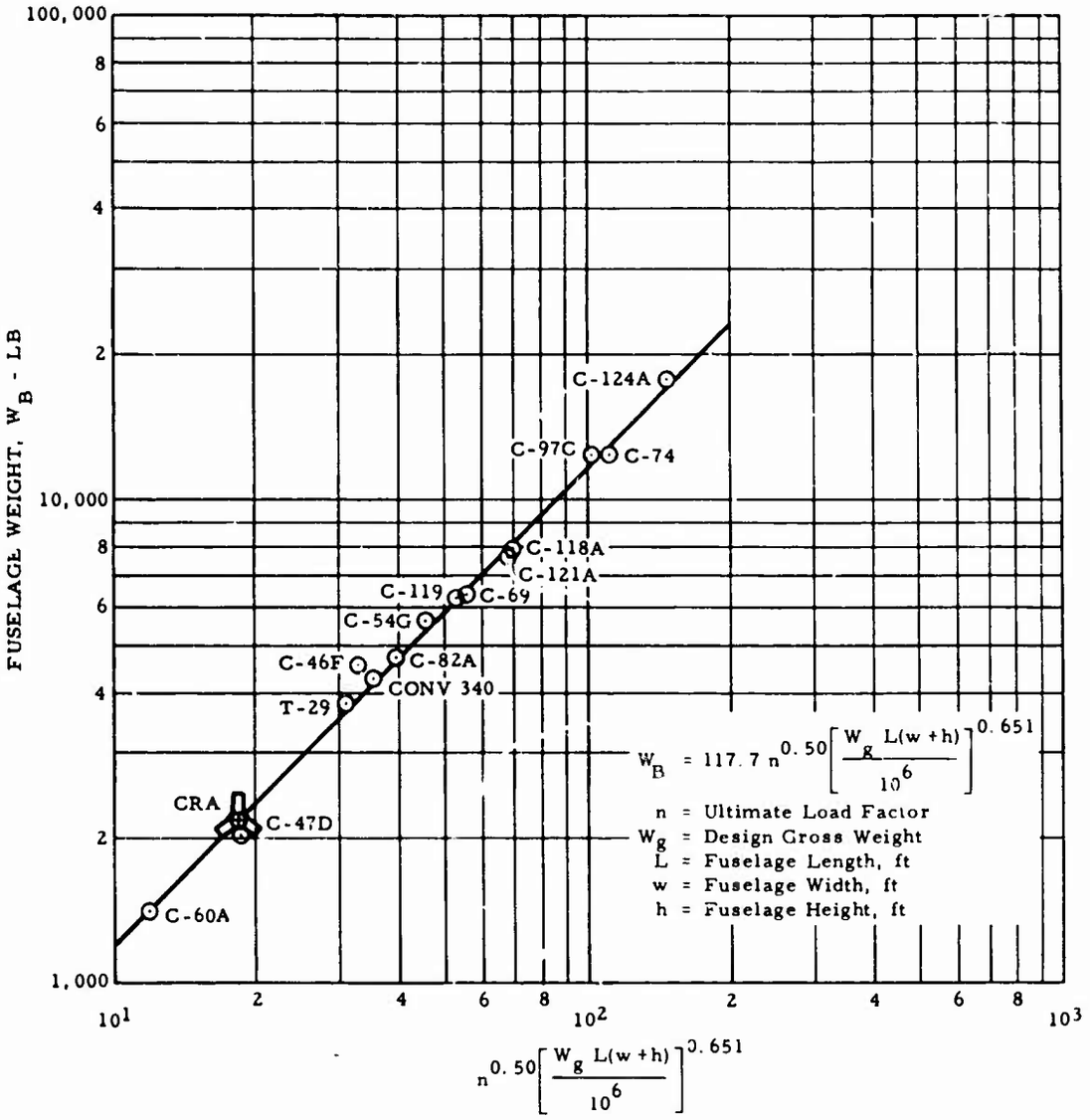

Figure 41. Fuselage Weight Comparison.

Landing Gear Group

The weight of the CRA landing gear is based on the analytical weight estimating procedures outlined in SAWE Technical Paper No. 210, "Rolling Type Alighting Gear Weight Estimation," dated 18 May 1959. The landing gear is designed for a vertical sink rate of 8 fps at the design gross weight. The weight breakdown for the landing gear is given in Table XIII.

TABLE XIII. LANDING GEAR WEIGHT BREAKDOWN

Item	Weight (lb)	Total (lb)
Main Gear		456
Wheels (11.0 - 12)	44	
Tires (32.2 x 11.20 Type III)	80	
Brakes	32	
Mechanism, oleo, actuators	260	
Support structure - body	40	
Nose Gear		112
Wheels (4.4 - 10)	16	
Tires (18 x 44 Type VII)	21	
Mechanism, oleo, actuators	65	
Support structure - body	10	
Gear Controls		32
Total alighting gear group		600

Flight Controls Group

The flight controls group as defined in this report consists of the following system controls:

1. Rotor/Wing blade controls (longitudinal, lateral, and vertical)
2. Rotor/Wing brake lock
3. Yaw fan and rudder controls (directional)
4. Elevon controls (longitudinal and lateral)
5. Yaw fan doors
6. Aerodynamic trim (artificial load feel)
7. Deactivating system (mode conversion)

The flight controls group weight has been estimated to be 729 pounds, based upon data obtained from layouts and structural analysis. Of the 729 pounds of total weight, 128 pounds is for controls, including actuators not usually associated with pure helicopter functions:

		Weight (lb)
1.	Elevon controls	60
2.	Deactivating system	13
3.	Aerodynamic load feed system	10
4.	Rotor/Wing brake-lock system	25
5.	Rudder controls	20
	Total aircraft mode controls	128

Figure 42 presents the results of a study of the variation of helicopter control systems weights with gross weight. The weight of 601 pounds for the conventional helicopter control systems correlates well with the curve.

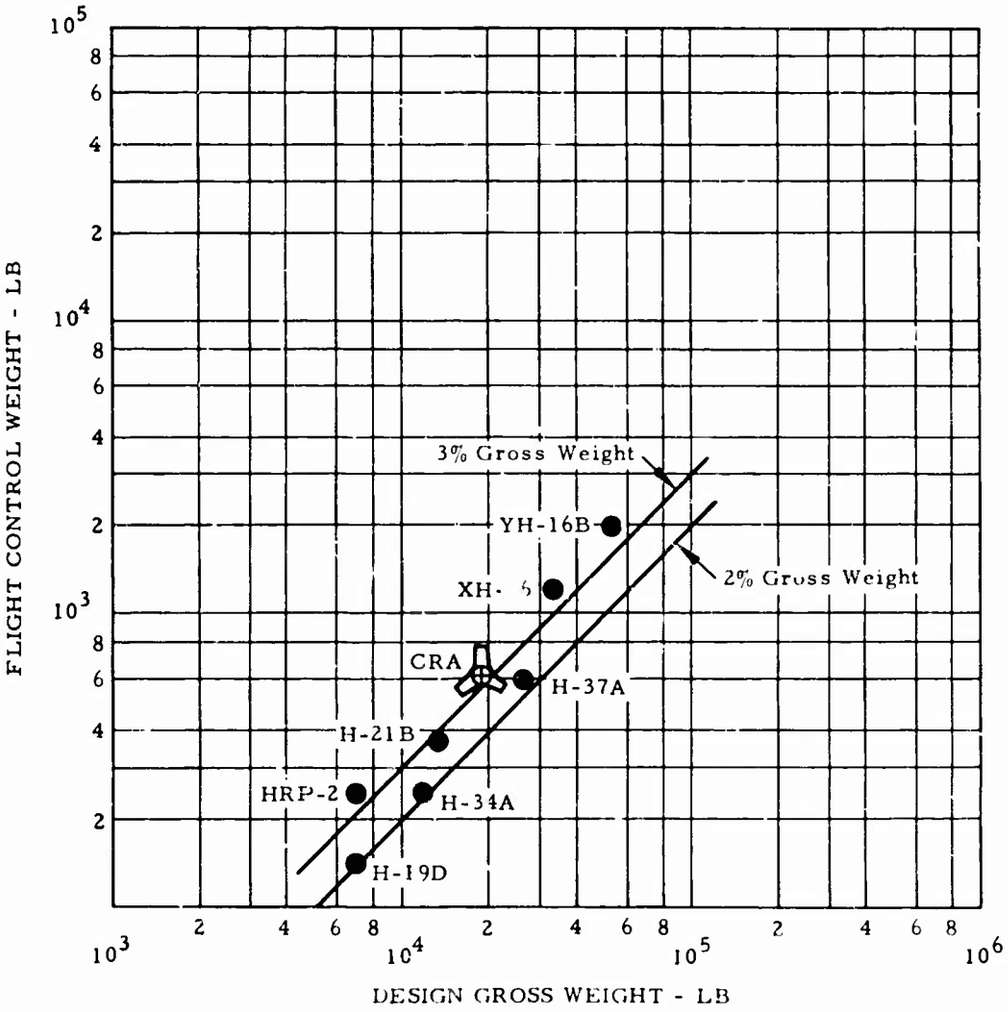

Figure 42. Flight Control System Weight Comparison.

Engine and Nacelle Section

This section consists of the engine mounts, fire walls, and fixed and removable panels enclosing the engine, diverter, and tail pipe sections. The combined weight of this group, including engine mounts, is calculated to be 211 pounds.

Propulsion Group

The various systems comprising the propulsion group of the Hot Cycle Rotor/Wing Composite Research Aircraft consist of the following:

1. Engine
2. Air induction system
3. Exhaust system
4. Accessory gearbox
5. Lubrication system (Rotor/Wing)
6. Fuel system
7. Engine controls
8. Starting system
9. Rotor/Wing jet drive system
10. Yaw fan drive system

Engine

The Pratt and Whitney J-52-P-8A engine weighs 2, 118 pounds.

Air Induction System

The weight of the air induction system is 181 pounds and includes the retraction system for the inlet duct assembly.

Exhaust System

The weight breakdown of this system is shown in Table XIV.

Accessory Gearbox

The weight of the accessory gearbox is 57 pounds and is based on the following design criteria:

1. High-speed rpm = 5, 000
2. Low-speed rpm = 275
3. Gear ratio ($\overline{GR}$) = 18. 2
4. High-speed torque = 105 ft-lb (weighted average)
5. Low-speed torque (Q) = 1, 908 ft-lb (weighted average)

TABLE XIV. EXHAUST SYSTEM WEIGHT BREAKDOWN	
Item	Weight (lb)
Exhaust duct	107
Thermal insulation	21
Seals, bellows, clamps, and connectors	38
Tail pipe ejector	20
Supports and miscellaneous	25
Total exhaust system weight	211

The calculated weight of the gearbox plotted on Figure 43 is within 4 per cent of the statistically derived curves.

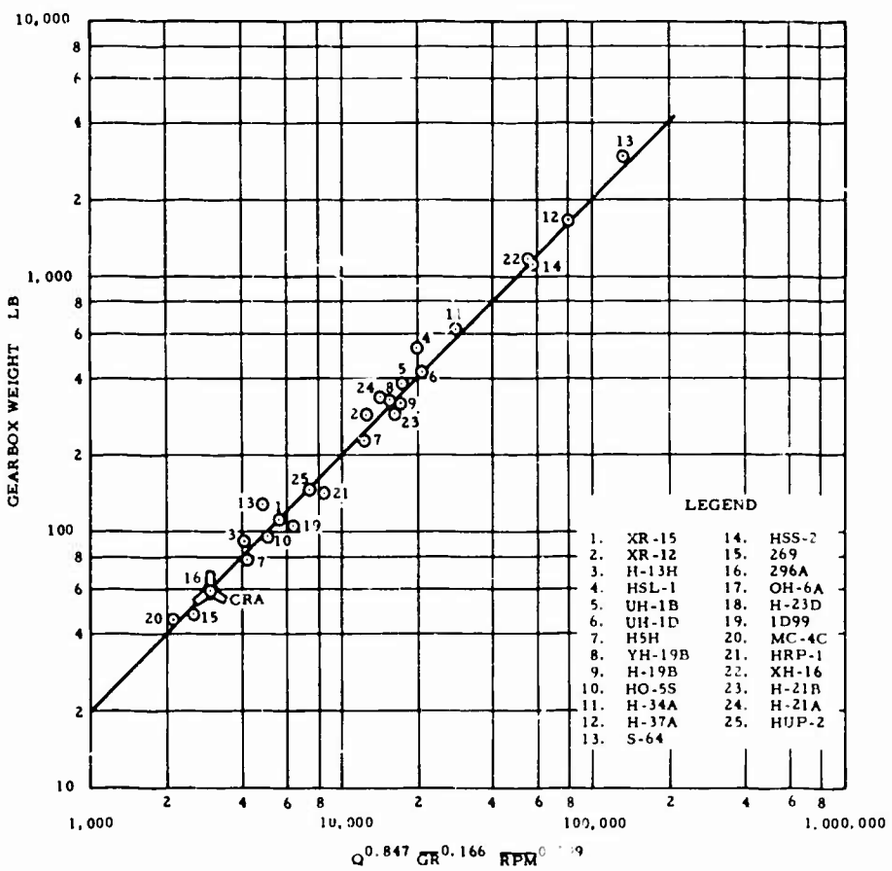

Figure 43. Gearbox Weight Comparison.

Lubrication System

The lubrication system weight of 39 pounds includes the elements required to supply circulating oil to the Rotor/Wing hub bearings and accessory gearbox.

Fuel System

The fuel system consists of two lightweight bladder-type fuel cells having a capacity of 1,500 pounds of fuel per cell. A system weight of 264 pounds was derived by comparative analysis with a similar XV-9A aircraft installation. Table XV presents a weight comparison of the CRA and the XV-9A fuel systems.

TABLE XV. FUEL SYSTEM WEIGHT BREAKDOWN

Item	CRA (lb)	XV-9A (lb)
Fuel cell installation	184	182
Pumps	32	16
Valves and plumbing	48	62
Total	264	260

Engine Controls

The engine control system consists of linkages, cables, and levers connecting the fuel control power lever on the engine to the control devices in the cockpit. On the basis of design analysis, the weight of the system has been established at 25 pounds.

Starting System

The engine is started using an engine-mounted impulse-type air turbine unit that operates from compressed air delivered by an M1-A1 gas-turbine cart. The starter rotates the rear compressor of the engine to a speed high enough to permit light-off. The on-board start system consists of the weight items listed in Table XVI.

TABLE XVI. STARTING SYSTEM WEIGHT BREAKDOWN	
Item	Weight (lb)
Starter (Bendix Model 36-E83 x 60A)	24.5
Air supply duct system	2.0
Air control valve	3.5
Total engine starting system	30.0

Rotor/Wing Jet Drive System

The CRA Hot Cycle Rotor/Wing jet drive installation consists of the diverter valve and the duct system required to direct the high-energy gas to the rotor blade tips for driving the Rotor/Wing. The weight estimate of 128 pounds for the CRA diverter valve has been obtained by a comparative sizing from the J-85 diverter valve, which weighs 85 pounds. A weight of 55 pounds has been estimated for the nonrotating portion of duct, stationary seal, and valve supports.

The rotating section of the jet-drive system begins at the rotating seal located on the lower end of the gas distributor duct manifold and terminates at the Rotor/Wing blade tip nozzles. The weight of this portion of the jet-drive system is 337 pounds; the total jet-drive system, including the diverter valve installation, weighs 520 pounds.

Yaw Fan Drive System

The yaw fan drive system consists of two gearboxes and a drive shaft system with weight estimated at 49 pounds.

Miscellaneous Fixed Equipment and Furnishing

In accordance with the requirements outlined in the Statement of Work, the empty weight includes allowance for the following equipment weights:

1. Auxiliary power unit - 150 pounds (including a 20-kva alternator)

2. Furnishings and equipment - 1,200 pounds to include the following:

   a. Instruments and navigation group
   b. Hydraulic and pneumatic group
   c. Electrical group

d. Crew accommodations group
e. Air-conditioning and anti-icing group
f. Auxiliary gear group (ground handling or hoisting)

3. Avionics - 900 pounds

4. Armor - 250 pounds (100 pounds per crew member plus 50 pounds per engine)

The weights of the APU, the armor, and the avionics are listed under their proper entries in the Detail Weight Statement. The 1,200-pound allowance for furnishings and equipment has been distributed among the listed groups based on weight estimates of proposed group systems.

Instruments and Navigation Group

Forty-eight instruments and indicators will be used, and the estimated weight of the instrument and navigation equipment installation is 120 pounds.

Hydraulic and Pneumatic Group

The hydraulic and pneumatic group consists of the components that make up the central power system. This group includes pumps, drives, reservoirs, accumulators, regulators, valves, controls, plumbing, fluid, supports, and other items. It does not include actuating cylinders and associated components, which are properly allocated to their respective functional group. The CRA hydraulic system has been estimated at 205 pounds. Figure 44 is presented to validate the estimated weight of the hydraulic system.

Electrical Group

A 28-vdc electrical power system with a 400-ampere generator is used to provide primary power for the CRA. The weight of the electrical group installation has been estimated at 300 pounds, based on the system requirements. Figure 45 presents the results of a study showing the relationship between helicopter electrical group weights and gross weight. A plot of the CRA electrical group on this graph shows that the weight is reasonable.

Furnishings and Equipment Group (Crew Accommodations)

The furnishings and equipment group consists of the crew accommodation items and miscellaneous pieces of equipment. A total weight of 420 pounds has been estimated for this group.

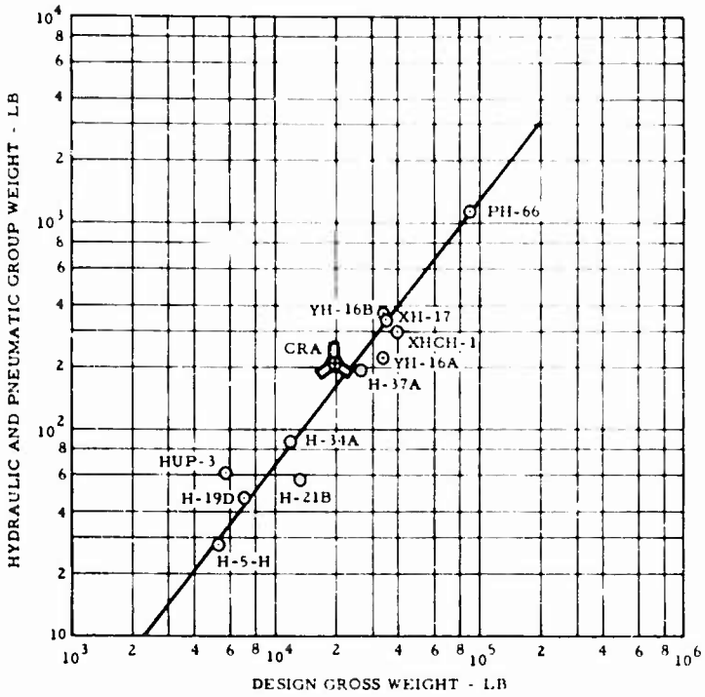

Figure 44. Hydraulic System Weight Comparison.

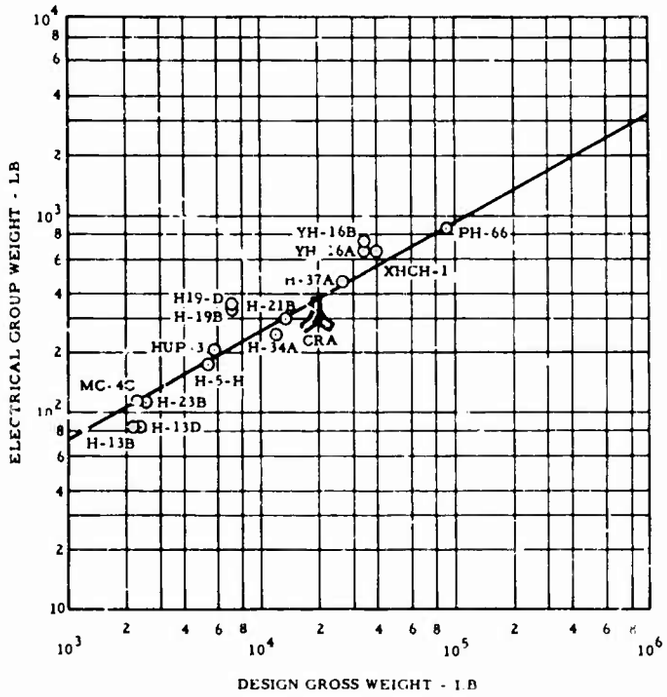

Figure 45. Electrical Group Weight Comparison.

Air-Conditioning and Anti-Icing Group

The cockpit air-conditioning system consists of a lightweight air-cycle turbine fan assembly that operates from engine bleed air. The weight breakdown of the system is as shown in Table XVII.

TABLE XVII. AIR CONDITIONING AND ANTI-ICING GROUP WEIGHT BREAKDOWN

Item	Weight (lb)
Conditioning unit (Hamilton Standard, P/N HS 570839-5)	18
Ram-air fan	4
Valves	6
Ducts, plumbing, and fittings	12
Total air-conditioning system weight	40

Auxiliary Gear Group

The auxiliary gear group consists of aircraft and cargo load-handling gear. A weight of 8 pounds has been allotted to this group.

Avionics Group

In accordance with the Statement of Work, an allowance of 900 pounds of avionics equipment has been included in the weight empty of the CRA. The weight of the HTC-AD-installed avionics equipment, however, has been estimated at 78 pounds.

STABILITY, CONTROL, AND FLYING QUALITIES

The stability and control characteristics of the helicopter, autogyro, conversion, and airplane flight modes of the Hot Cycle Rotor/Wing Composite Research Aircraft have been investigated. It was found that satisfactory flying qualities are achieved in all flight regimes. MIL-H-8501A and MIL-F-8785 (ASG) have been followed to assure satisfactory flying qualities in helicopter and airplane modes. In general, the handling qualities are superior to those required by military specification.

The extensive wind tunnel model data obtained during the Rotor/Wing model research program conducted under the sponsorship of the Office of Naval Research (References 4 and 7) and the Hughes-sponsored model test program (Reference 8) form a reliable basis for the stability and control analysis. During the Rotor/Wing research program, the major area of investigation has been directed toward developing the technique for conversion flight between the rotating and the stopped-rotor modes, to demonstrate that the Rotor/Wing could be successfully stopped and started in flight. Successful conversions were repeatedly accomplished in the wind tunnel from the running-rotor to the stopped-rotor mode and back again. The conversion procedure is simple and straightforward such that a pilot can perform conversion manually and have a large margin of control. An analysis of the vibratory acceleration at the pilot station during the time that the Rotor/Wing is starting or stopping in flight shows that this is less than 50 percent of the allowable limit in accordance with MIL-H-8501A.

Adequate control margins exist for all flight conditions from 40 knots rearward to the limit dive speed. The summary curves presented in Figures 46, 47, and 48 show the required control positions for trimmed level flight in the helicopter, autogyro, and airplane flight modes. It can be seen that there are no large control position changes during conversion from one flight mode to another.

In the helicopter and autogyro flight modes, the Rotor/Wing configuration provides angular response and damping in both pitch and roll, superior to that required by MIL-H-8501A. The yaw fan provides satisfactory handling characteristics in yaw. For the higher helicopter and autogyro flight speeds, the elevon and rudder surfaces become effective, and additional pitch, roll, and directional control is available.

The airplane flight neutral point of 68-percent wing mean aerodynamic chord (MAC) and the maneuver point of 74-percent wing MAC are well aft of the recommended aft cg of 36.6-percent wing MAC, demonstrating

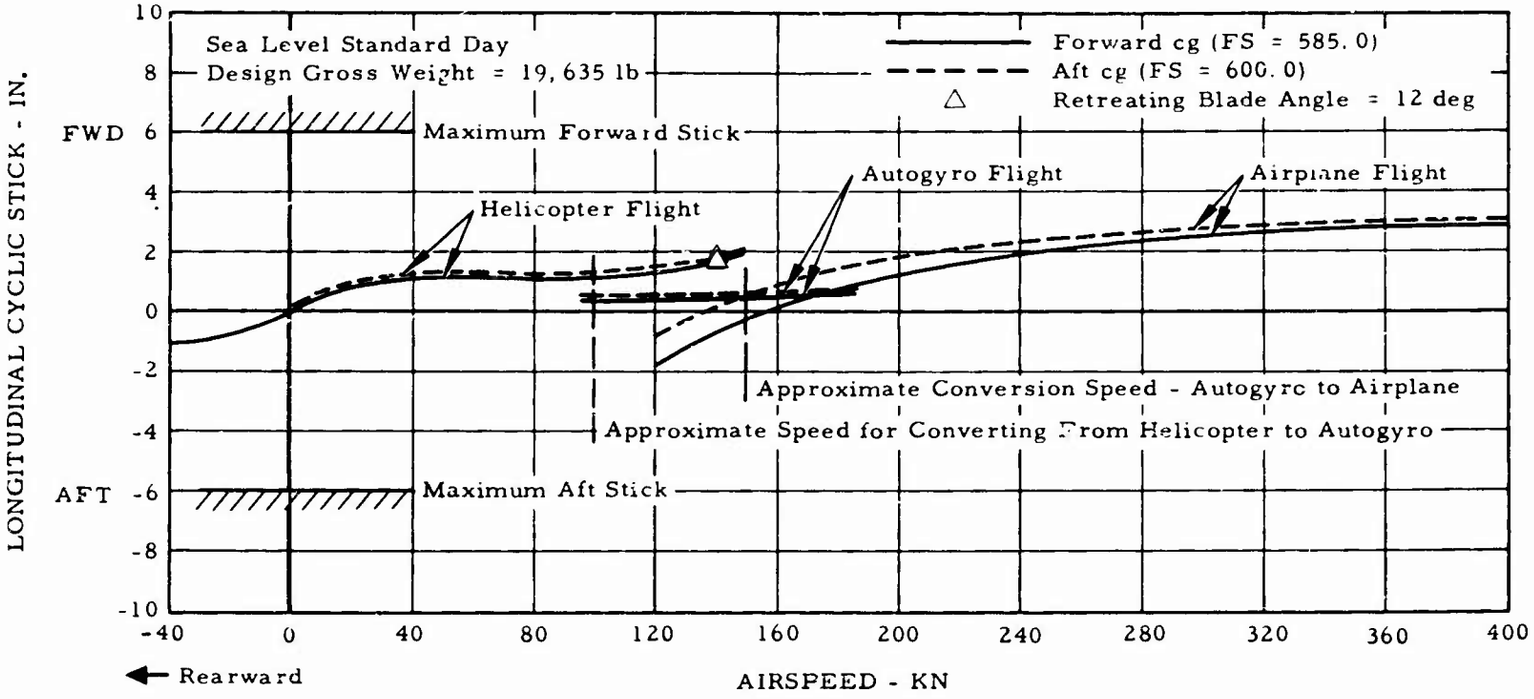

Figure 46. Longitudinal Stick Positions for Trimmed Level Flight.

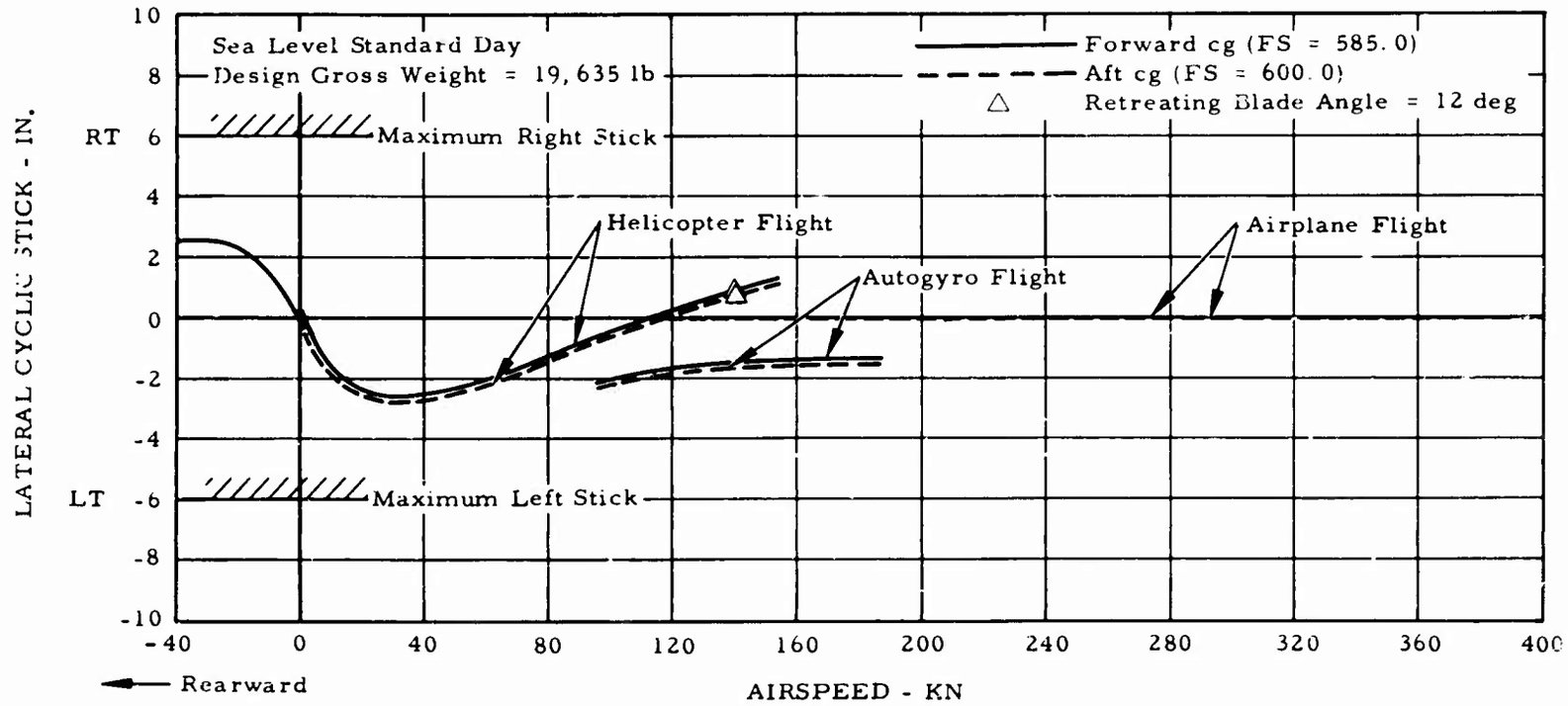

Figure 47. Lateral Stick Positions for Trimmed Level Flight.

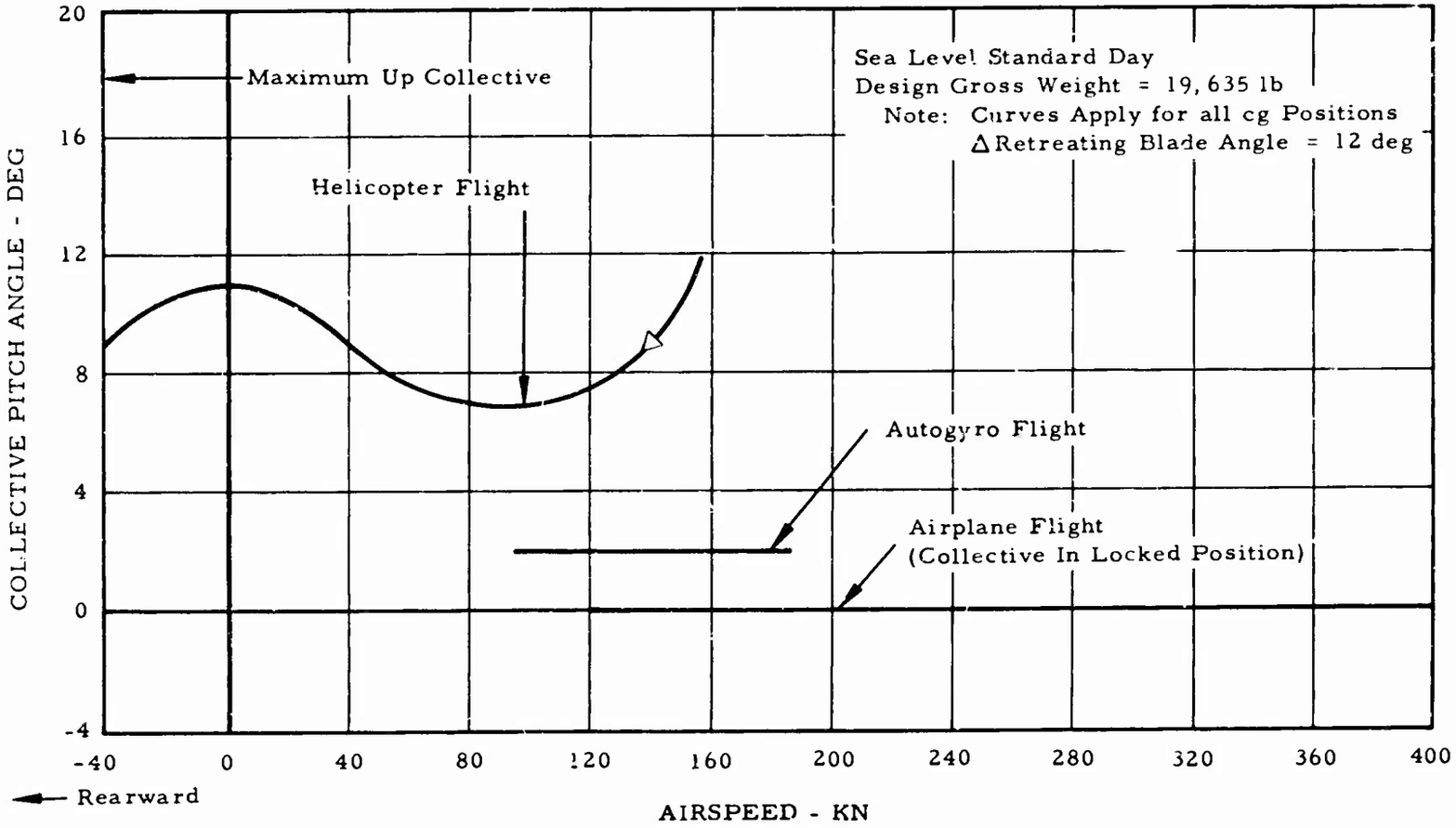

Figure 48. Collective Pitch Angle for Trimmed Level Flight.

adequate margin in accordance with MIL-F-8785 (ASG). This large static margin will provide good longitudinal dynamic stability characteristics for the Rotor/Wing aircraft.

The differential deflection of the elevons provides the roll control needed to meet the rolling requirements of MIL-F-8785 (ASG) in airplane flight. The normal adverse yaw characteristic experienced by the wing-aileron type of roll control is eliminated by the elevon roll control system. In fact, model test data show a favorable yawing moment with elevon deflection. Analysis shows that the damping of the lateral-directional oscillations of the aircraft is in compliance with MIL-F-8785 (ASG) requirements, and thus the aircraft will have satisfactory lateral dynamic characteristics.

The vertical tail provides positive directional stability for all flight modes. The tail was sized to provide satisfactory directional stability in helicopter flight mode. The tail area sized for this condition also satisfies the directional stability requirements for airplane flight in accordance with MIL-F-8785 (ASG). The rudder was sized to provide steady-state sideslip angle of at least 10 degrees during landing at 1.1 V_{S_L} (MIL-F-8785 (ASG)).

All flight control systems incorporate irreversible, hydraulically powered, tandem actuators with artificial feel systems. Satisfactory longitudinal cyclic stick forces are provided by the combination of a conventional q bellows-spring artificial feel system. At low speeds, the spring provides the desired level of stick force per inch. At high airplane flight speeds, the q spring provides the desired level of stick force per g. The system incorporates an electric actuator to trim feel forces to zero. The lateral and directional feel forces are provided by simple spring artificial feel systems that incorporate electric trim force actuators.

Discussion of the stability and control characteristics of the CRA and the conformation with requirements for each flight mode is presented in the subsequent paragraphs.

HELICOPTER FLIGHT

Hover

To study the hover control response of the CRA, a six-degree-of-freedom system of analysis was formulated. The effects of the flexibility of the rigidly attached Rotor/Wing-to-hub system are calculated with the rotor blades, wing, and pylon-fuselage combination represented by a series of concentrated mass-spring systems. The equations of motion were

programmed for the IBM 7094 computer to obtain the hover control response time histories for the CRA.

Figures 49 and 50 present the hover control response time histories in pitch and roll. Also shown for comparison purposes are the control response characteristics of an articulated rotor with 3-percent hinge offset. The results show that the pitch and roll rates of the Rotor/Wing aircraft develop much more rapidly than those of the articulated rotor system, resulting in excellent control response.

Table XVIII presents a summary of the angular response characteristics of the CRA in pitch and roll and compares them with the minimum angular response requirements of MIL-H-8501A for visual flight. As can be seen, the angular response in both pitch and roll is much superior to that required by MIL-H-8501A.

TABLE XVIII. ANGULAR RESPONSE IN HOVER - PITCH AND ROLL

Item	CRA	Minimum Requirements per MIL-H-8501A
	Angular Displacement in Degrees	
Pitch		
Response to 1-inch control (t = 1 sec)	12.6	1.6
Response to full control (t = 1 sec)	75.6	6.7
Roll		
Response to 1-inch control (t = 1/2 sec)	6.5	1.0
Response to full control (t = 1/2 sec)	39.0	3.0
Design gross weight = 19,635 lb		

Table XIX presents the angular velocity damping in both pitch and roll and compares it with the damping requirements of MIL-H-8501A. As can be seen, the damping of the CRA is approximately 12 times the minimum

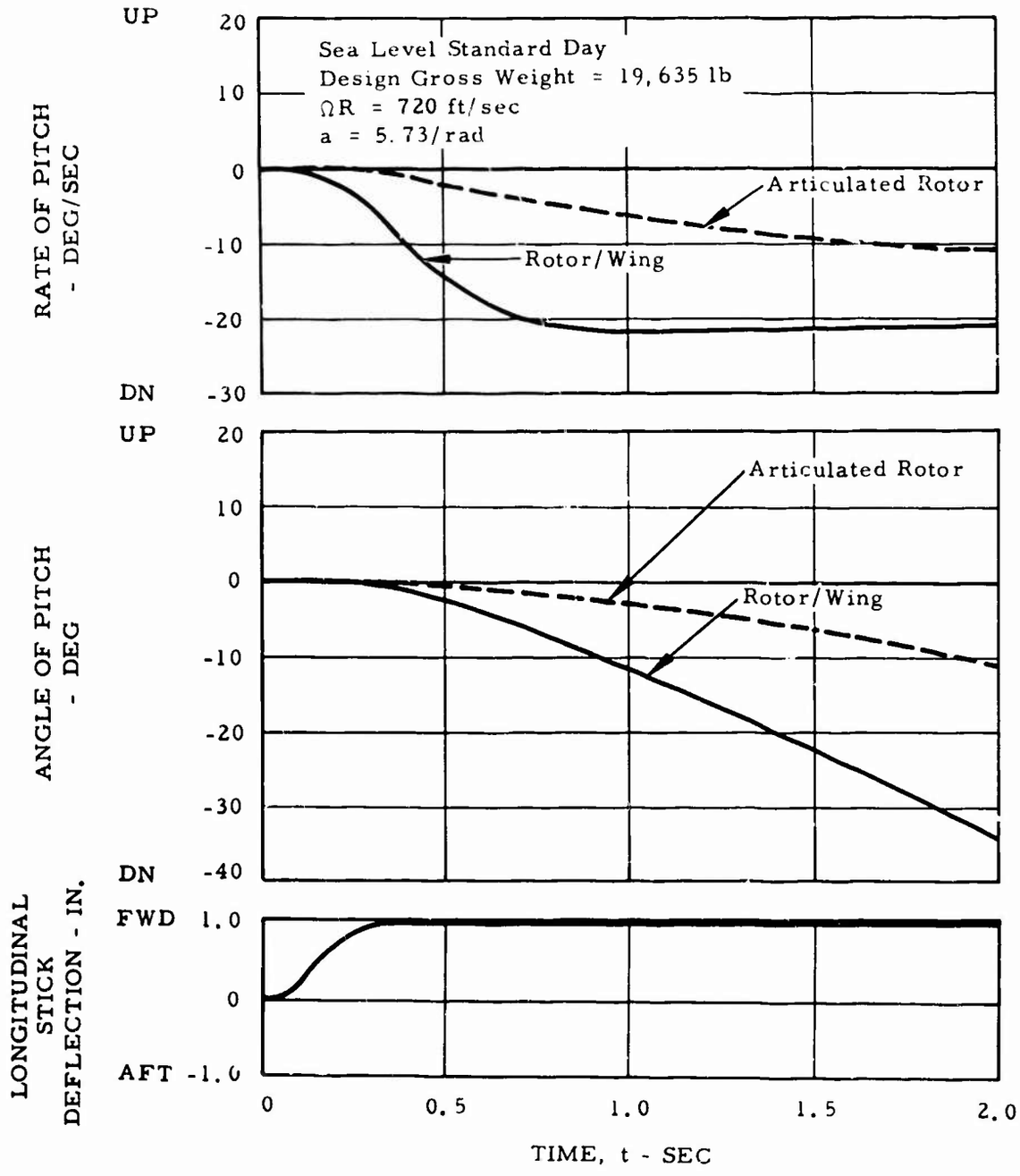

Figure 49. Aircraft Response in Hover to a Forward Longitudinal Control Input.

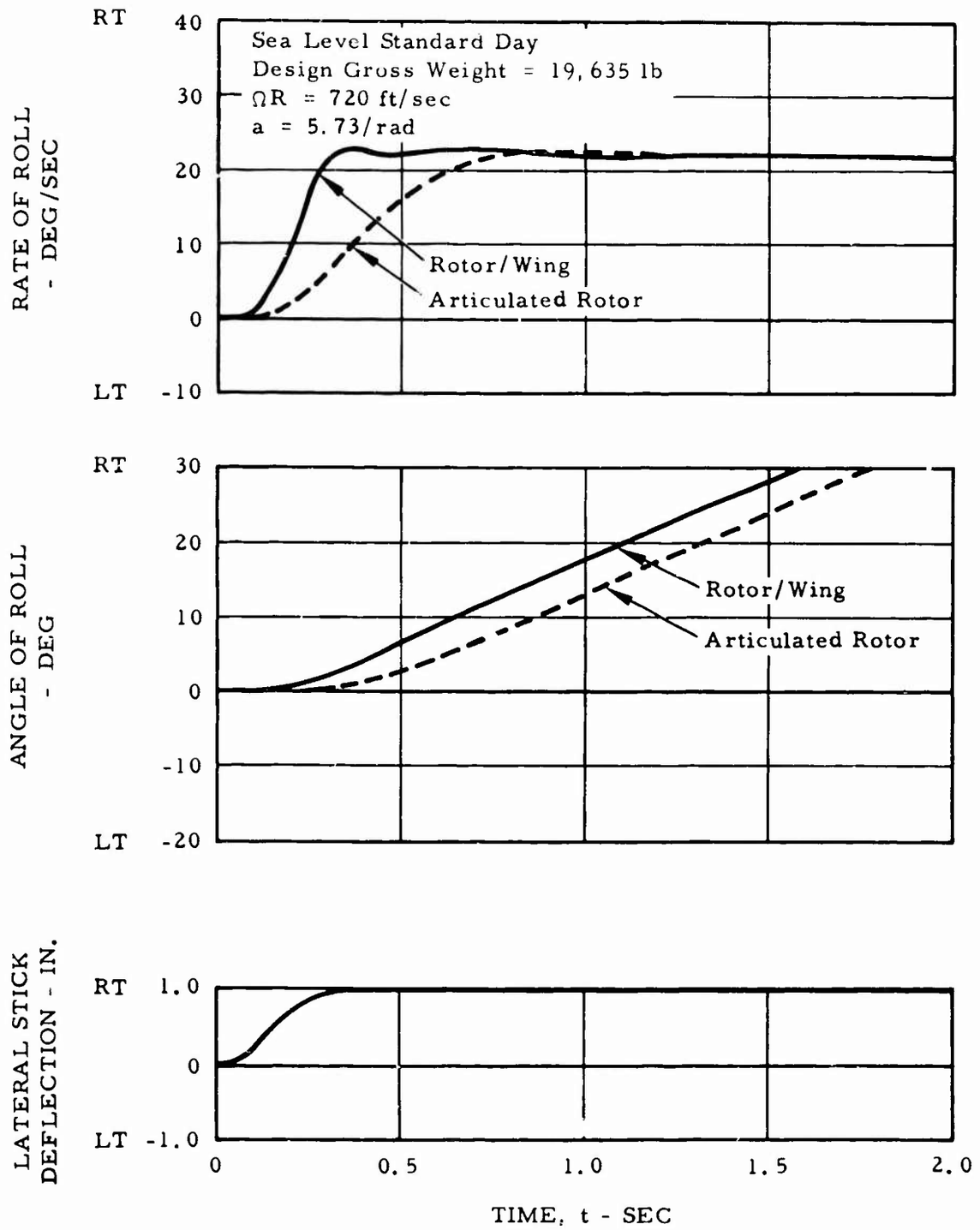

Figure 50. Aircraft Response in Hover to a Right Lateral Control Input.

damping in pitch and 23 times the damping in roll required by MIL-H-8501A. The high damping and high control power that are characteristic of the rigidly attached rotor-to-hub system will provide the CRA with excellent handling characteristics.

TABLE XIX. DAMPING IN HOVER

Axis	Angular Velocity Damping (Ft-Lb/Rad/Sec)	
	CRA	Per MIL-H-8501A
Pitch	372,000	29,700
Roll	372,000	15,372
Design gross weight = 19,635 lb		

Figure 50 shows that the roll rate is slightly greater than the maximum 20 degrees per second per inch of stick specified by MIL-H-8501A. If this condition is achieved by the full-scale aircraft, the lateral rotor cyclic pitch travel could simply be reduced, since adequate lateral pitch range exists for all flight conditions.

The directional angular response of the CRA presented in Table XX for hover and for a 35-knot side wind is expected to provide satisfactory handling characteristics in yaw for the tip-driven Rotor/Wing aircraft. Although the control responses are less than those required by MIL-H-8501A, it is felt that the response requirements of MIL-H-8501A are primarily for shaft-driven helicopters, which require large tail rotors to counteract the torque reaction of the main rotor and, in addition, to provide directional control. These large tail rotors are much more sensitive to gusts, and they require greater directional control response. Thus, it is felt that the directional control requirements of MIL-H-8501A are considerably greater than those necessary for the tip-jet-driven CRA. At normal helicopter flight speeds, the rudder surface becomes effective, and additional directional control is provided.

Forward Flight

Using the data and method of the analysis described in the preceding section, the helicopter forward flight trim control positions are shown in

Figure 51. The control positions are presented for both the forward and aft cg conditions at the design gross weight of 19,635 pounds for sea level standard day.

TABLE XX. ANGULAR RESPONSE IN HOVER YAW

Item	CRA	Requirements per MIL-H-8501A
	Angular Displacement in Degrees	
Yaw		
Response to 1-in. pedal (t = 1 sec)	2.2	4.0
Response to full pedal (t = 1 sec)	7.3	12.0
Response to full pedal in 35-kn side wind (t = 1 sec)	3.5	4.0
Design gross weight = 19,635 lb		

The results show the stick position variation with speed throughout the flight range from 40 knots rearward to maximum forward speed. The maximum helicopter forward speed as limited by a retreating blade angle of 12 degrees occurs at approximately 140 knots. This maximum forward speed provides more than the desired speed overlap of 20 knots between the helicopter mode and the low-speed end of the autogyro mode, for converting from the helicopter mode to the autogyro mode. This can be seen from the summary curves of Figure 46; in Figure 51, it can be seen that there is adequate stick margin, both longitudinal and lateral, throughout the helicopter mode speed range.

Figure 52 presents the results of the angle of attack stability calculations. Reference 9 shows that some instability with angle of attack, M_α, may be allowed, depending on the stabilizing effect of the pitch damping. The results presented in Table XIX show that the rotor of the CRA has approximately 12 times the damping in pitch required by MIL-H-8501A. In addition, the damping contribution from the large horizontal tail in forward

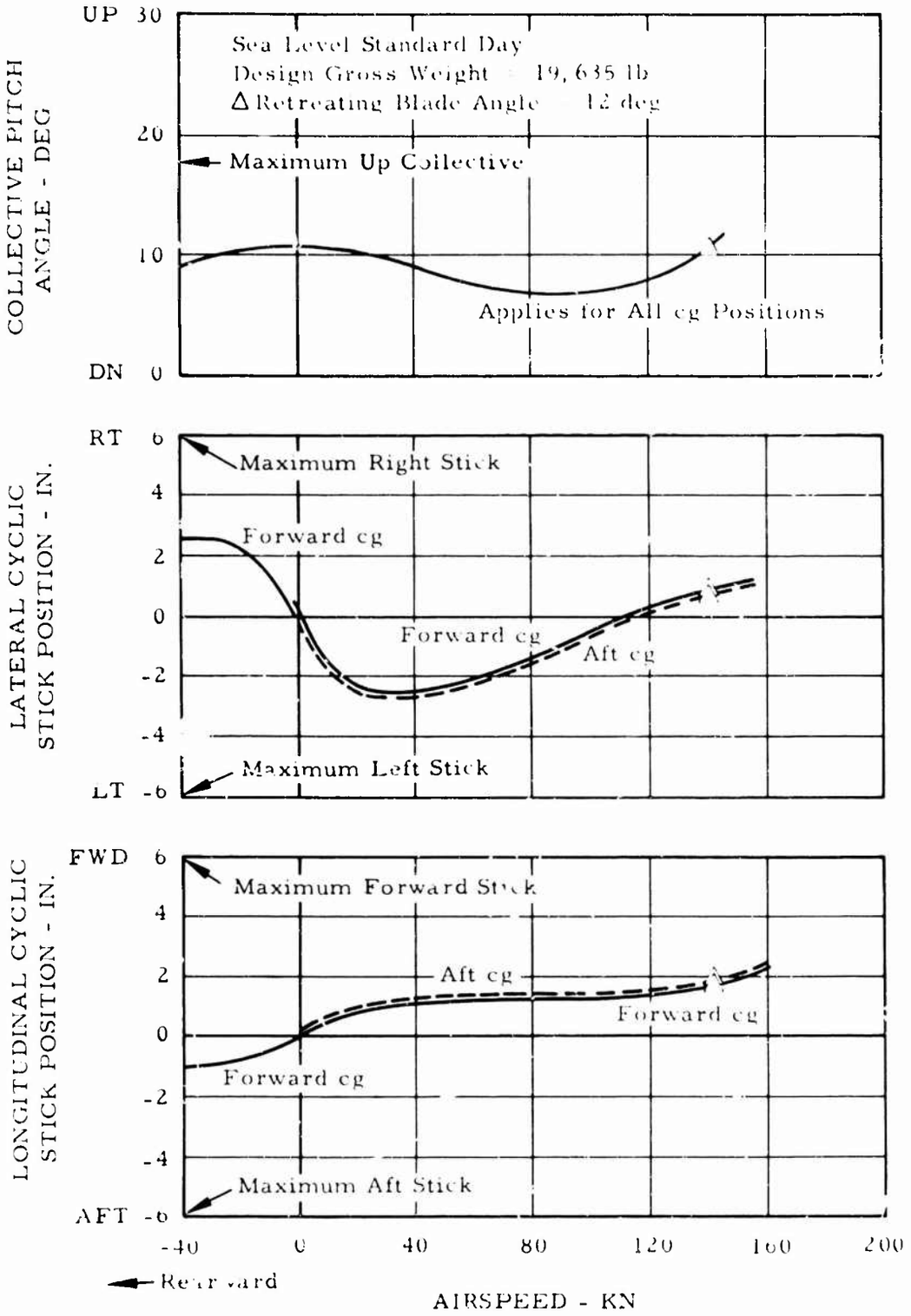

Figure 51. Control Positions for Trim Helicopter Level Flight.

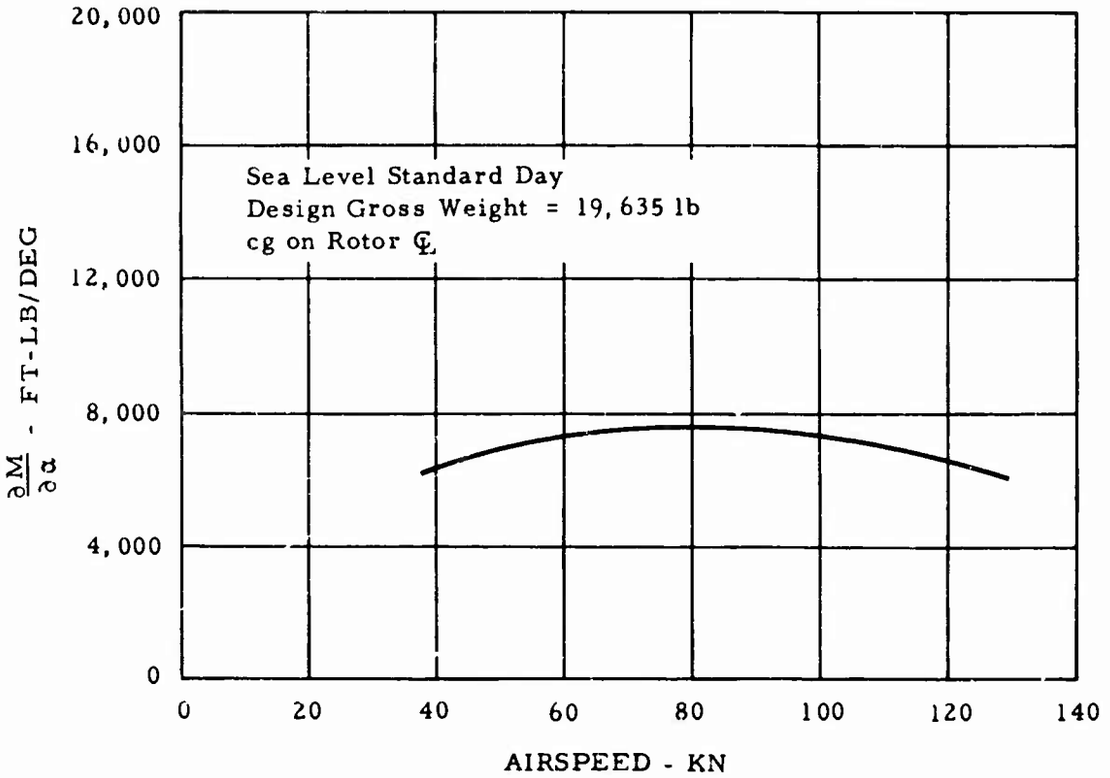

Figure 52. Helicopter Flight Angle-of-Attack Stability.

flight results in an aircraft with high pitch damping. Thus the CRA has good maneuver characteristics.

Figure 53 presents the directional stability characteristics in forward flight. The results show positive directional stability throughout the helicopter speed range. The CRA also possesses good directional control characteristics from the combination of the yaw fan and rudder.

The CRA has positive effective dihedral throughout the helicopter flight mode. This can be seen from the results presented in Figure 54. The aircraft also possesses good lateral control characteristics from the rotor control in conjunction with the differential elevons.

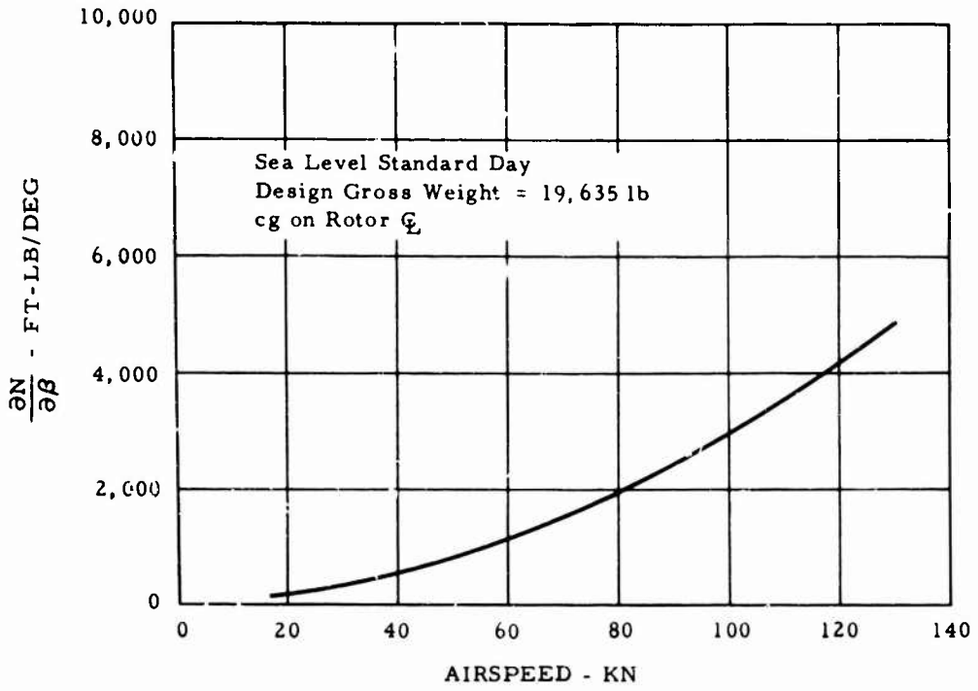

Figure 53. Helicopter Flight Directional Stability.

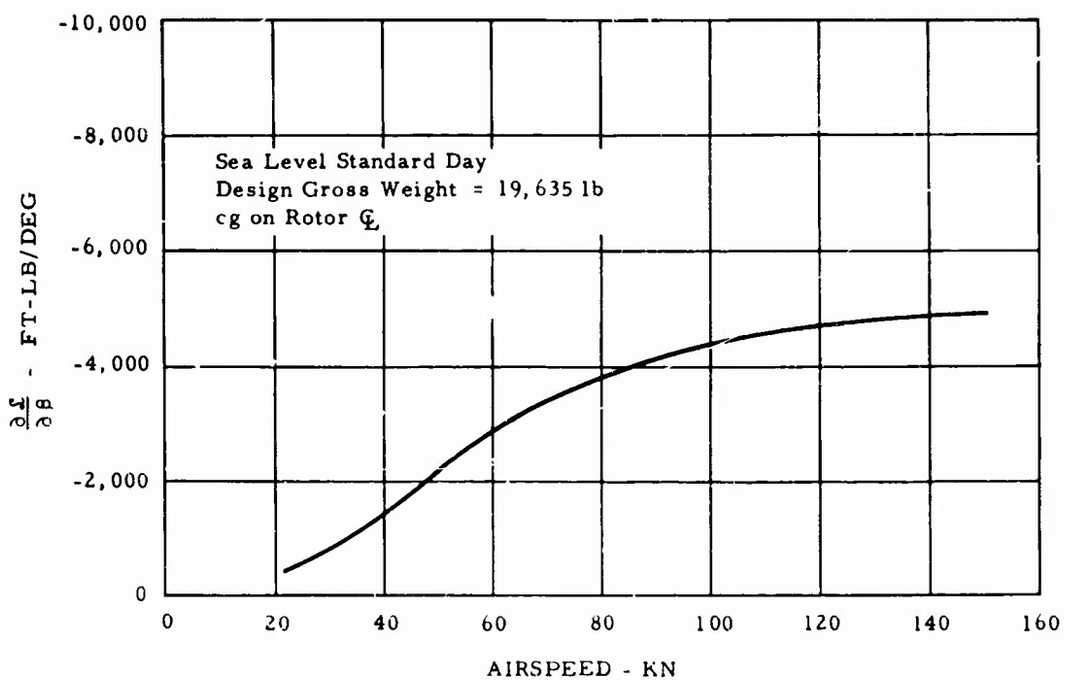

Figure 54. Helicopter Flight Effective Dihedral.

AUTOGYRO FLIGHT

Autogyro flight is an extension of the helicopter flight mode, where the rotor autorotates and the engine functions as a conventional turbojet; control is primarily from the cyclic pitch, augmented by the elevons.

The flight control characteristics required for level autogyro flight are presented in Figure 55 for the forward and aft cg conditions. The curves are based on the data and method of the analysis. The various power effects of tail pipe thrust on the control analysis are considered.

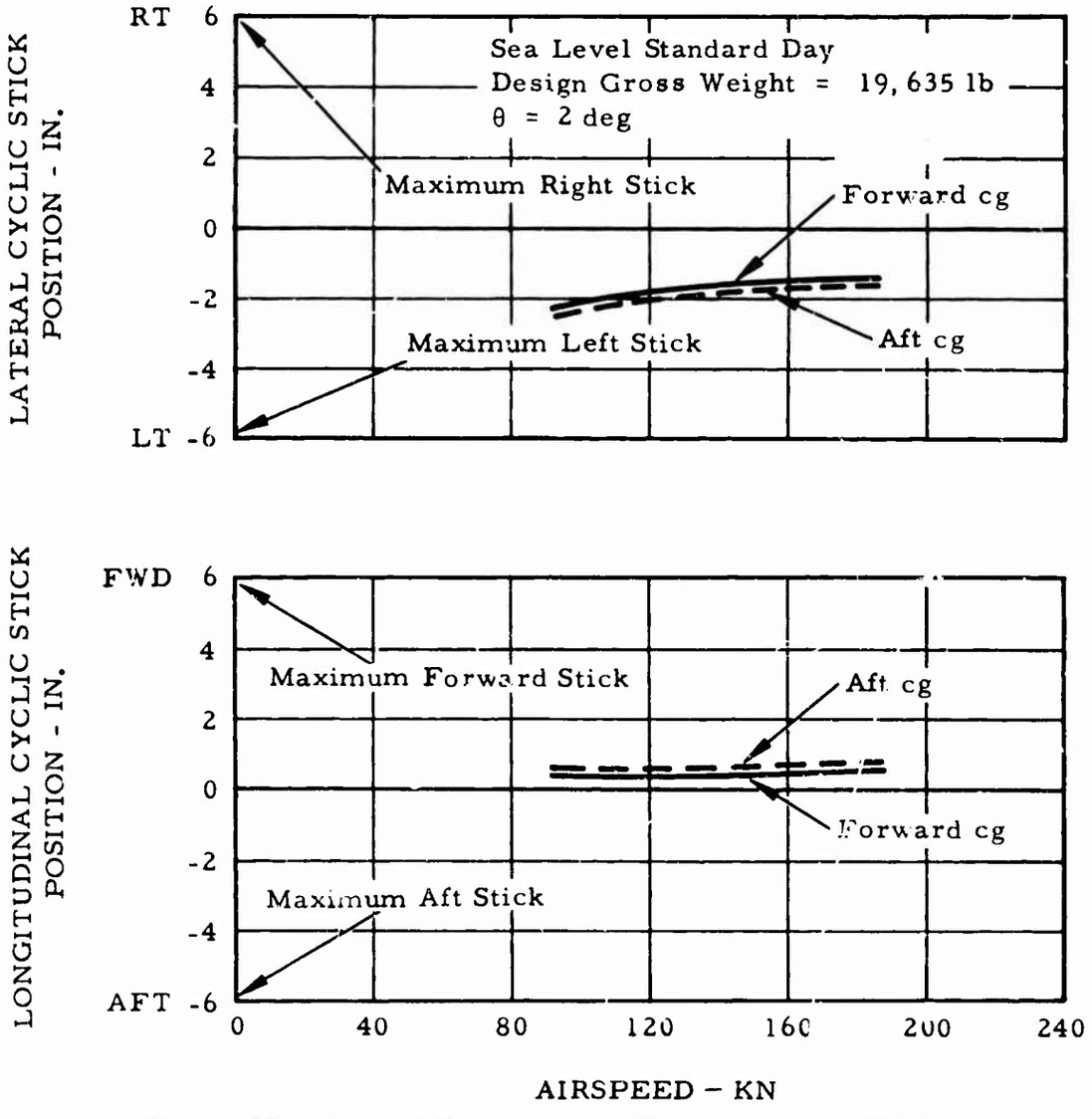

Figure 55. Control Positions for Trim Autogyro Flight.

The longitudinal cyclic-stick position with speed for both the forward and aft cg is fairly flat. However, with the q-bellows spring artificial-feel system, the increased force required to attain higher speed results in satisfactory flying characteristics. As can be seen, there is adequate control margin throughout the autogyro mode.

To simplify the flight control procedure for the pilot in the autogyro mode, flight is performed at a constant collective pitch setting. The setting is such as to produce an initial autorotating rotor rpm of 247 (90 percent) when going from helicopter to autogyro flight. The setting, of course, is dependent upon the weight and altitude conditions. A typical curve of rotor rpm versus airspeed is presented in Figure 56 for an up collective pitch setting of 2.0 degrees. This setting corresponds to the design gross weight of 19,635 pounds at sea-level standard conditions. In the initial return phase of the autogyro mode (V = 150 knots), the collective pitch is set to produce approximately 91 percent of full rotor rpm. This collective pitch then results in the proper rotor rpm for minimum power at the point of converting from autogyro back to helicopter flight.

The directional and effective dihedral characteristics of the CRA in the autogyro mode are very similar to the stable characteristics that the aircraft possesses in the helicopter configuration.

CONVERSION FLIGHT

During the Rotor/Wing model research program, the major area of investigation was directed toward establishing the technique for conversion between the rotating and stopped-rotor modes. These model tests have demonstrated repeated successful conversions in the wind tunnel from the rotating-rotor to the stopped-rotor mode and back again. The extensive model data accumulated during these tests are used as the basis for analyzing the conversion flight characteristics of the CRA. The results are presented and discussed herein in two parts: first, the conversion from autogyro flight to airplane; second, the reconversion from airplane back to autogyro.

Autogyro Flight to Airplane Flight

The longitudinal and lateral cyclic stick positions, collective pitch angles, and fuselage attitude required for conversion from the autogyro mode at 90-percent rotor speed to the stopped mode at a typical conversion speed of 150 knots are presented in Figures 57 and 58 for the forward and aft cg conditions. As can be seen, adequate longitudinal and lateral cyclic control is available throughout the conversion mode.

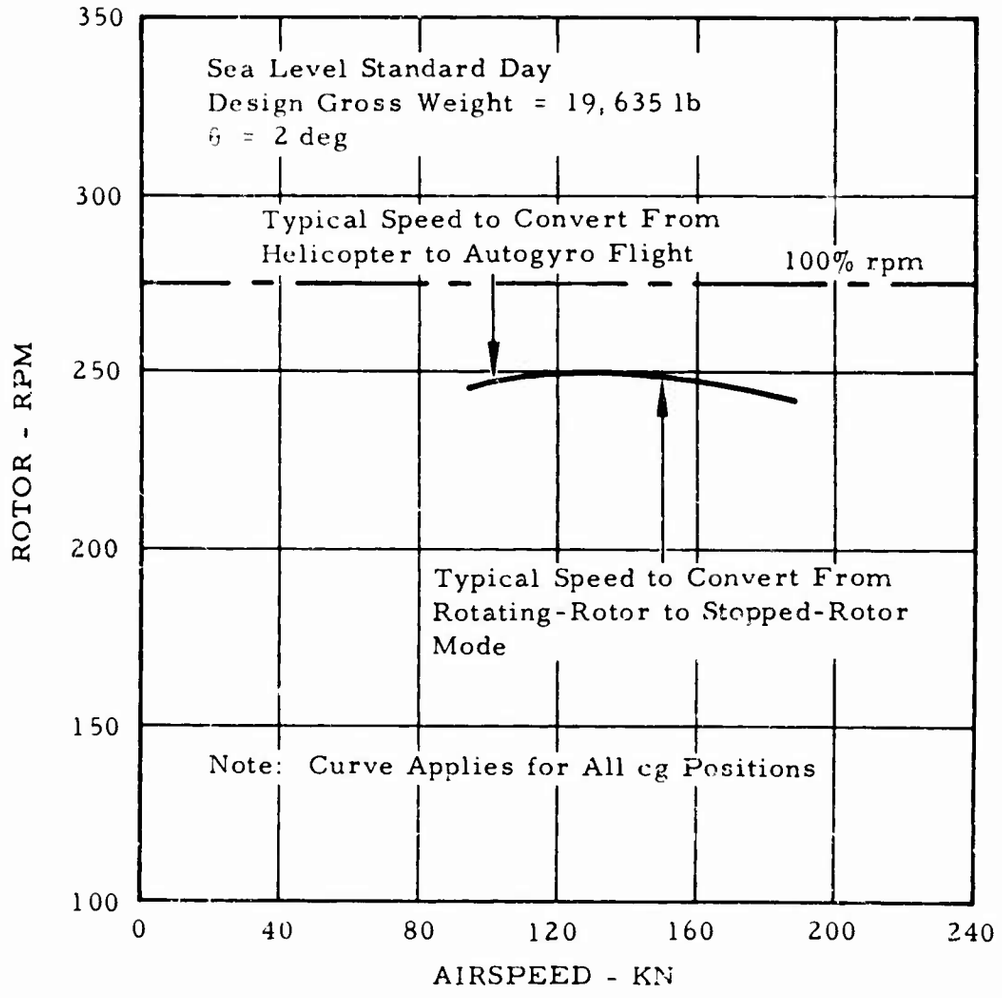

Figure 56. Autogyro Flight - Rotor RPM Versus Airspeed.

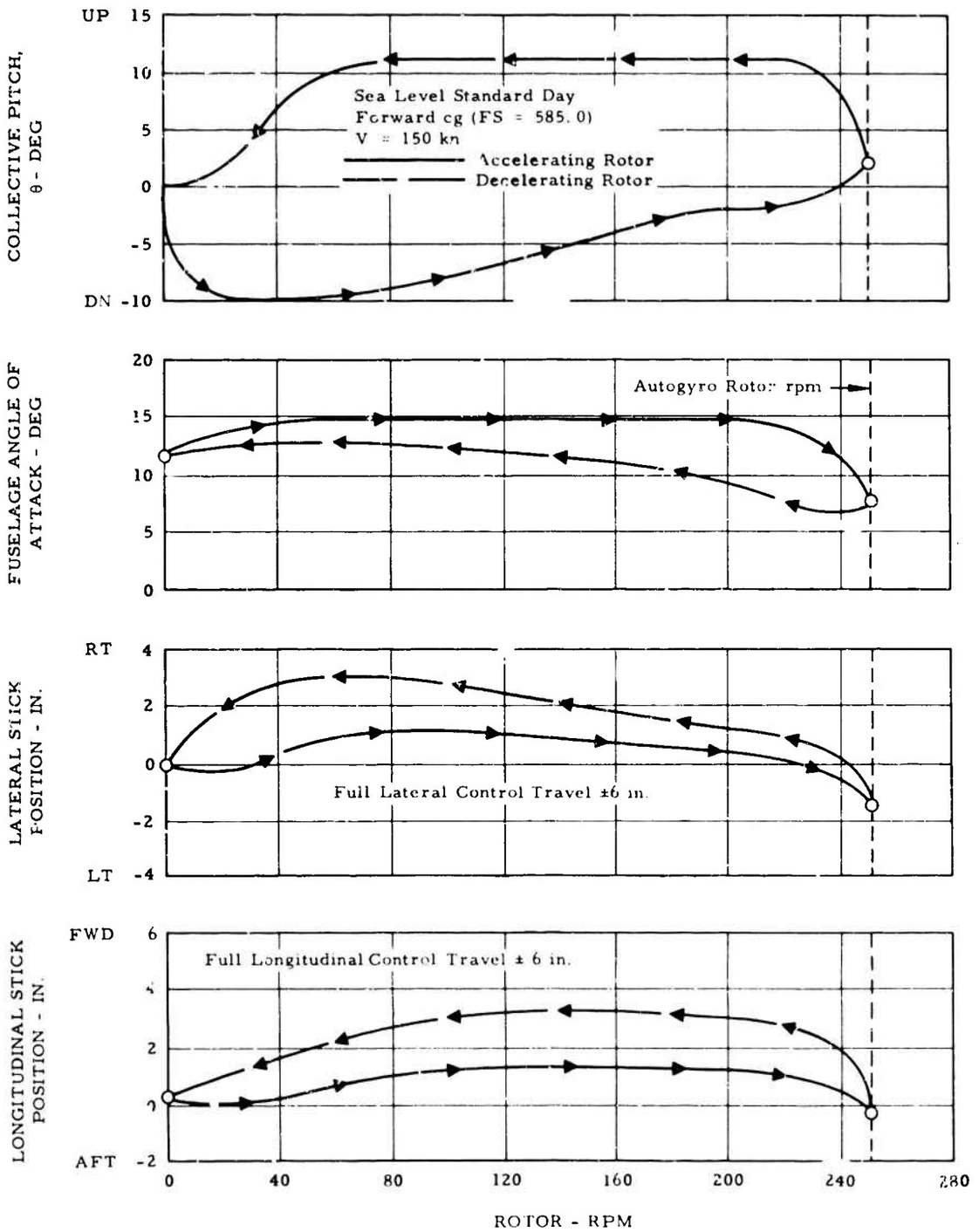

Figure 57. Control Characteristics During Conversion, Forward CG.

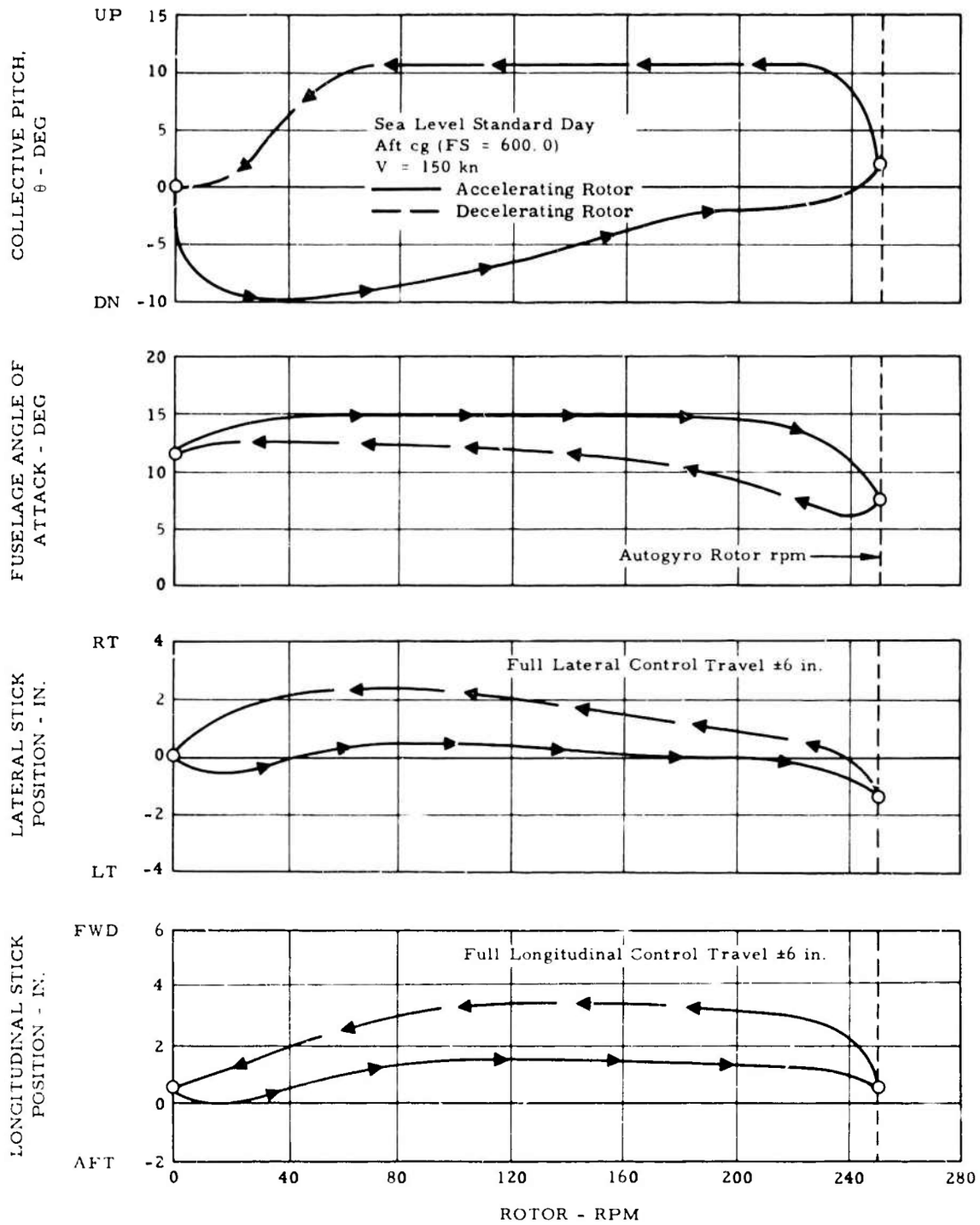

Figure 58. Control Characteristics During Conversion, Aft CG.

The collective pitch angles and fuselage attitudes shown during the level flight conversion are based on the model test results. The angles are considered to be typical of the angles expected during actual in-flight conversion. However, depending on pilot technique, these angles may vary somewhat. As can be seen from the test conversion map in Figure 59, there is a large latitude in the allowable combinations of fuselage attitudes and control positions that can decelerate the rotor in flight (outside of $C_Q = 0$ boundary) and yet maintain balanced 1-g flight.

Again, looking at Figures 57 and 58, when the pilot starts to decelerate the Rotor/Wing by applying up collective pitch ($\theta = 10°$), he will also move the cyclic stick forward and to the right to trim out the resulting rolling and pitching moments. At approximately 40-percent rotor speed, the pilot begins to apply brake pressure with the toe pedals to further decelerate the Rotor/Wing, gradually lowering the collective stick toward zero blade pitch until the Rotor/Wing reaches approximately 5 rpm. Upon reaching 5 rpm, the Rotor/Wing locator mechanism automatically raises and engages the locking pin. After the Rotor/Wing is locked, a deactivating mechanism automatically disengages the rotor cyclic and collective pitch control and locks the blades in zero-incidence position. The yaw fan doors close. The aircraft is then in airplane flight and is flown with normal airplane controls; namely, stick and rudder pedals.

A typical conversion time history is shown in Figure 60. The time required to aerodynamically decelerate the Rotor/Wing from autogyro rotational speed (90-percent) to 40-percent speed is calculated to be approximately 10 seconds, based on model test data (Reference 4) corrected to the full-scale Rotor/Wing configuration. Time to decelerate the Rotor/Wing from 40-percent rpm to 5 rpm using the Rotor/Wing brake is calculated to be between 3 and 5 seconds, depending on the rate of application of the toe pedal brake in conjunction with the use of rudder pedals to react the resulting torque. As the Rotor/Wing slows down to very low rpm's, the aircraft, for a brief period (1 to 2 seconds) until the Rotor/Wing is stopped, is subjected to the typical 3-per-rev rotor pitching and rolling moment amplitudes shown in Figure 61 measured during an initial startup of the Rotor/Wing (also applicable to the Rotor/Wing slowdown condition). Converting the moments into angular motion for the CRA, the maximum aircraft angular motion, based on the conservative assumption of zero damping, (as shown in Figure 62), is approximately ±3 degrees in roll and less than ±0.5 degree in pitch and occurs at approximately 5-percent rotor speed. At lower rpm, the combined characteristics of the low rpm and the collective pitch reduction remove the 3-per-rev moments. A more detailed discussion and presentation of data appears in Reference 4.

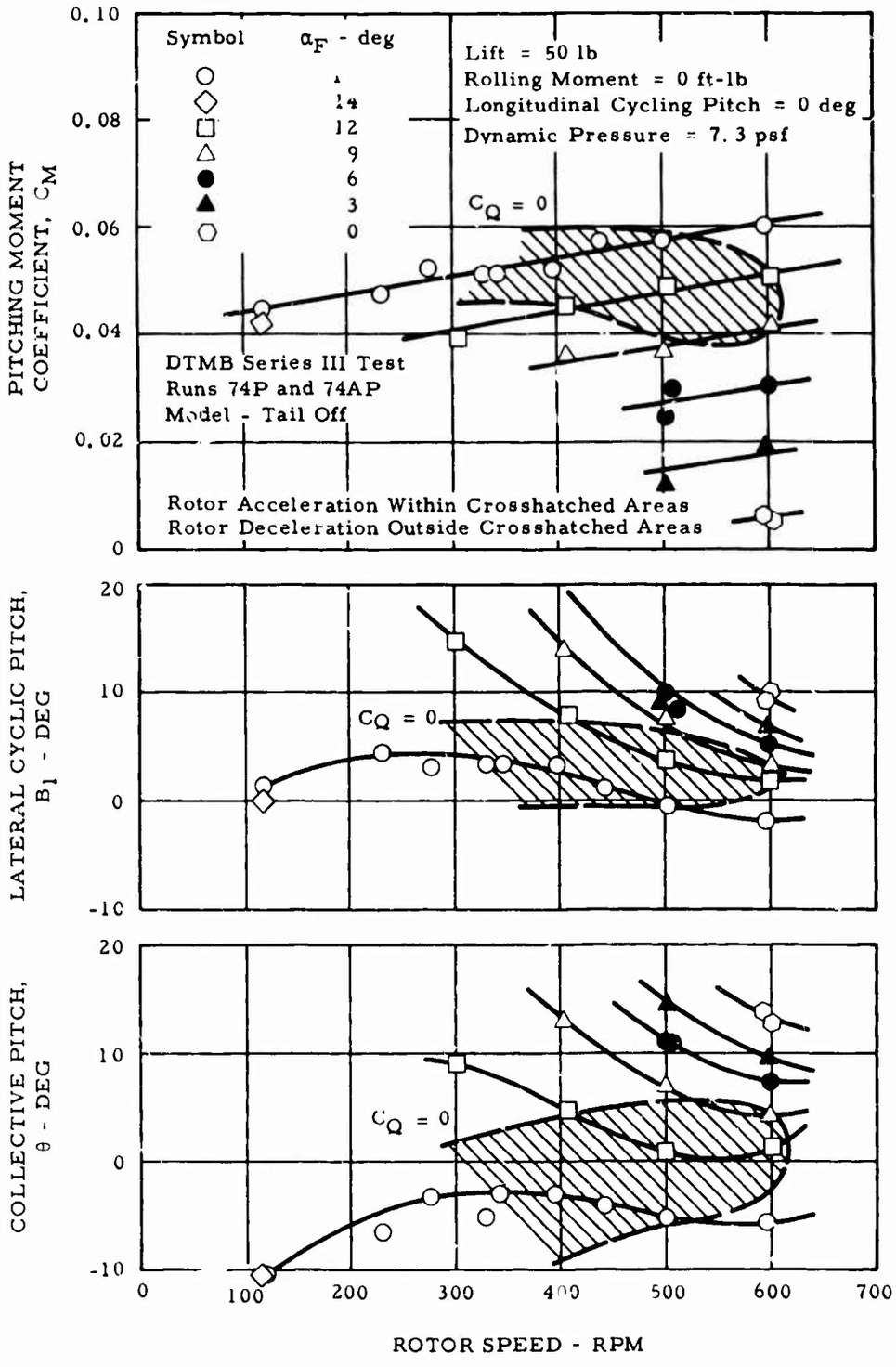

Figure 59. Conversion Test.

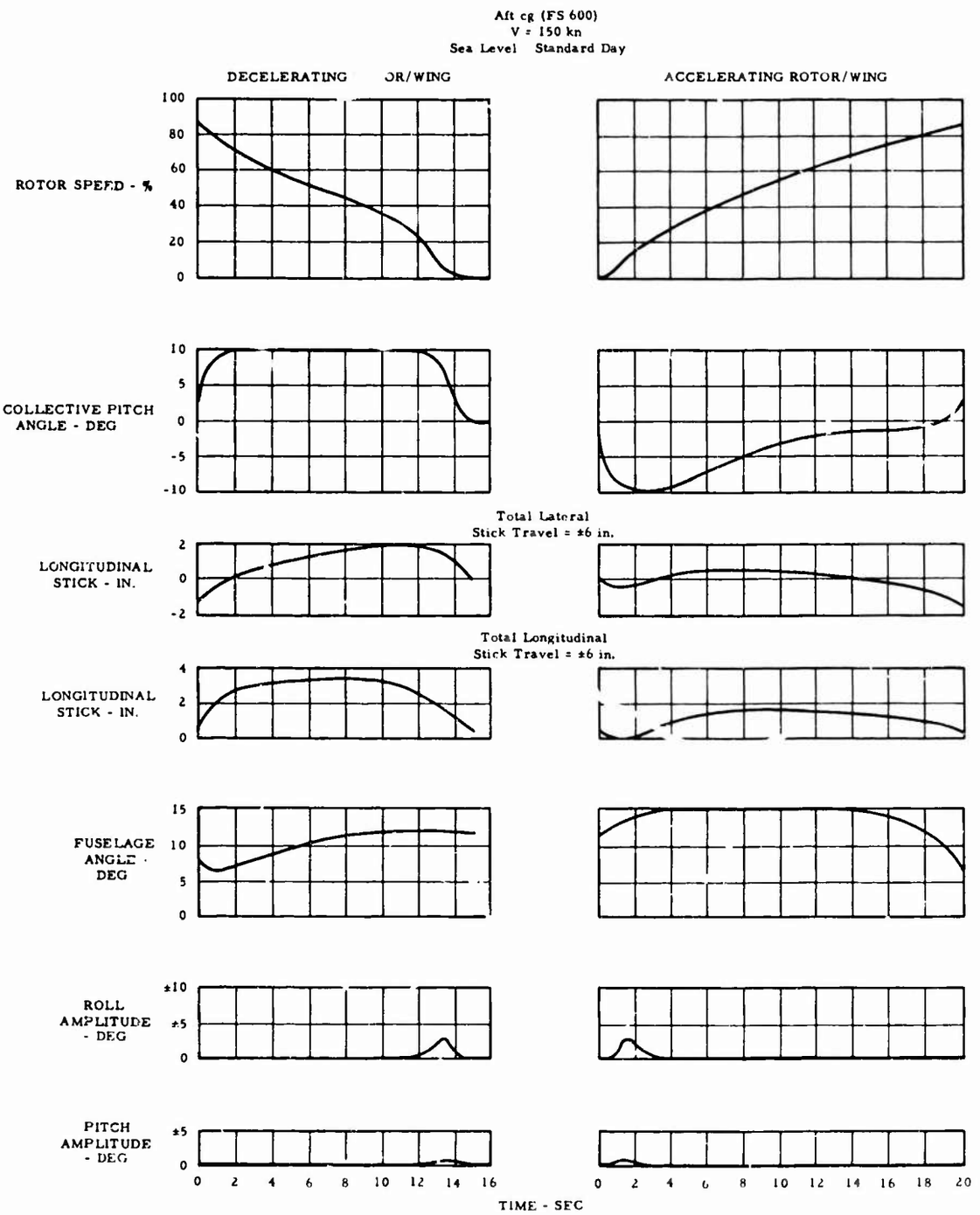

Figure 60. Conversion Time History.

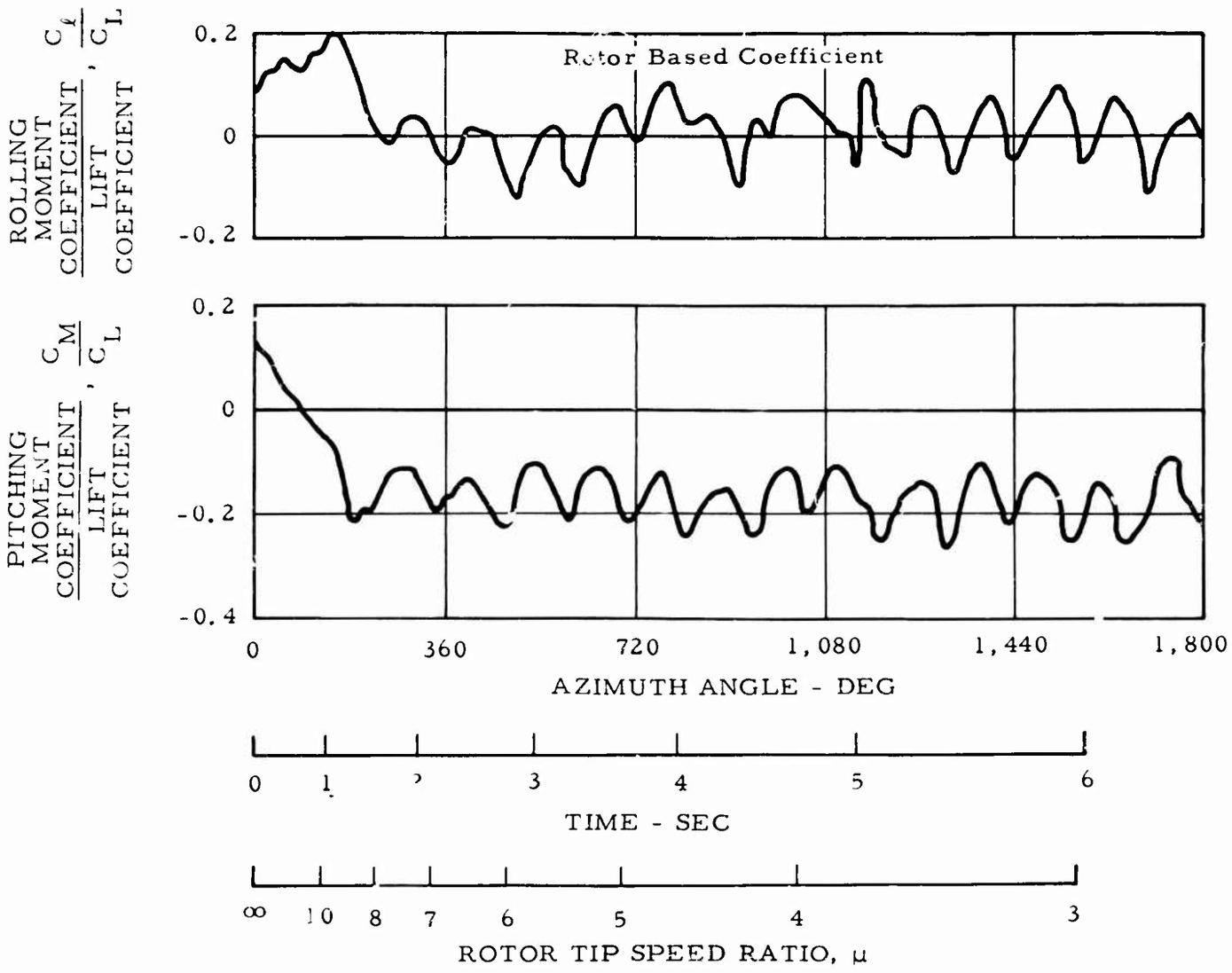

Figure 61. Time History - Rotor Shaft Bending Moments Rotor Acceleration During Conversion - Low RPM.

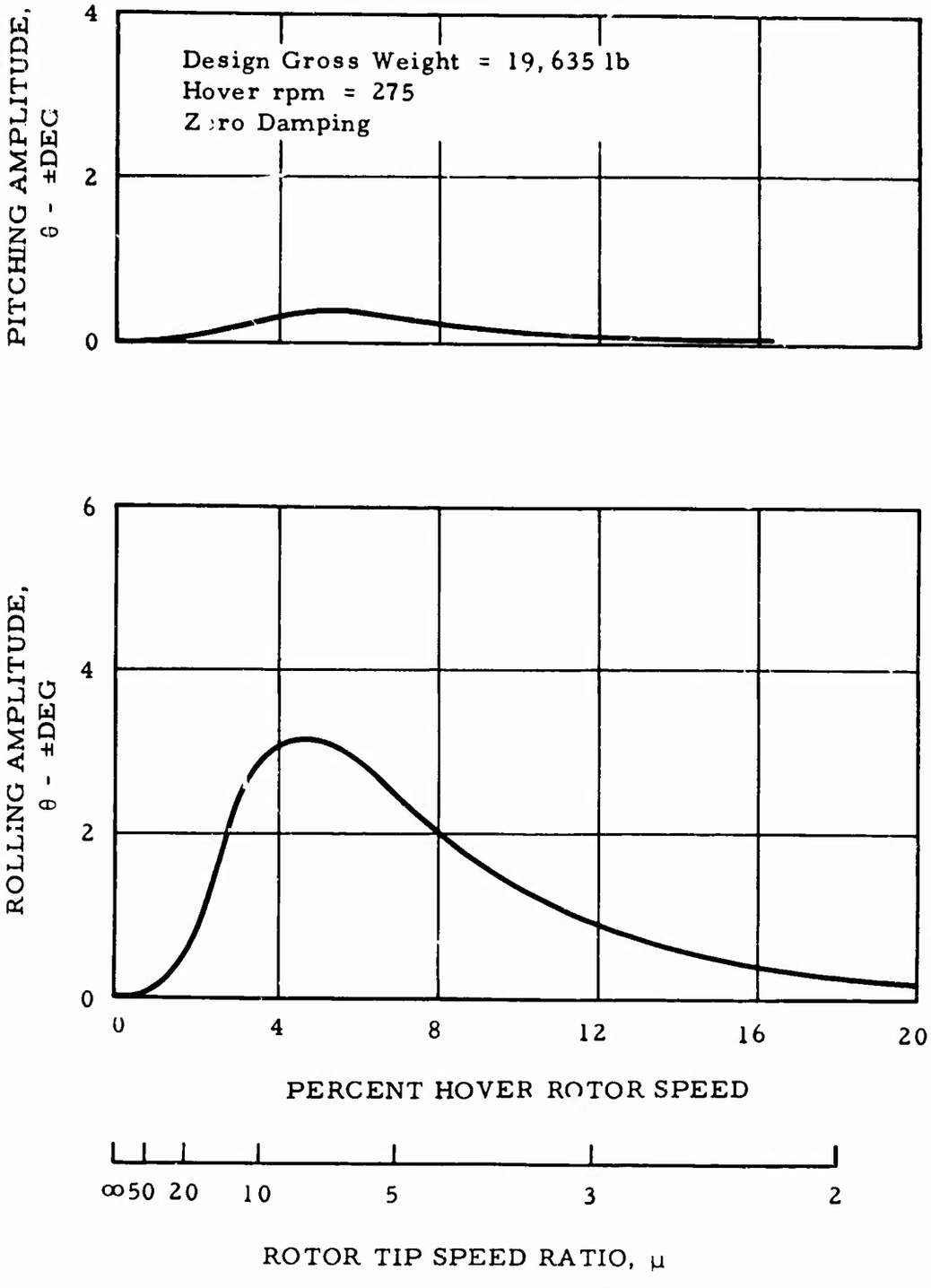

Figure 62. Aircraft Rolling and Pitching Amplitudes During Conversion.

These amplitudes of angular motion are considered to be sufficiently small that they should not cause any discomfort to the pilot. This is substantiated by calculating the vibratory acceleration at the pilot station based on the measured 3-per-rev moment amplitude of Figure 61, and by comparing the results with the maximum allowable vibratory acceleration of MIL-H-8501A. The results are presented in Table XXI. As can be seen, the vibratory acceleration at the pilot's station for the CRA during conversion is approximately 50 percent less than the allowable limit in accordance with MIL-H-8501A.

Thus, during the conversion, the vibratory acceleration at the pilot's station is very similar to that of current helicopters in transition flight.

TABLE XXI. VIBRATION CHARACTERISTICS AT PILOT STATION DURING CONVERSION

Direction	Vibratory Acceleration at Pilot Station	
	CRA (g)	Maximum Allowable per MIL-H-8501A, para 3.7.1 (c) (g)
Vertical	0.162	0.30
Lateral (at pilot's head)	0.106	0.30

Airplane Flight to Autogyro Flight

Figures 57 and 58 also present the longitudinal and lateral cyclic stick positions, collective pitch angles, and fuselage attitudes required to accelerate the Rotor/Wing from zero speed to full rotor speed using only aerodynamic forces and maintaining balanced 1-g flight. Based on the results of model test data extrapolated to full scale, the time required to accelerate the Rotor/Wing during 1-g flight from zero to 50-percent rpm is calculated to be approximately 9 seconds; from zero to 100-percent rpm, the time is calculated to be approximately 20 seconds. Detailed analysis of the time to accelerate the Rotor/Wing is presented in the section titled Performance Data. If the pilot desires to accelerate the Rotor/Wing much faster than the normal 1-g procedure presented here, he can pull the cyclic stick aft and flare the aircraft, which results in rotor

acceleration similar to that experienced by conventional helicopters during autorotational landing flares.

The reconversion procedure from airplane to autogyro flight is just a reverse procedure of the autogyro-to-airplane flight discussed previously, and it is not reiterated here.

During the accelerating rotor sequence, as in the decelerating rotor sequence, the Rotor/Wing has the capability of maintaining balanced 1-g flight throughout the rotor rpm range. As shown on Figures 57 and 58, for both forward and aft cg conditions, there is a generous margin of longitudinal and lateral cyclic control throughout the reconversion from airplane to autogyro flight.

Based on the positive longitudinal and directional stability and effective dihedral characteristics available in the airplane and helicopter flight modes, the stability characteristics during conversion are satisfactory.

Structural dynamic studies of the CRA during conversion show that the aircraft is free of aeroelastic divergence and control system flutter. Detail analyses of these studies are presented in the section titled Structures.

AIRPLANE FLIGHT

Longitudinal

Based on data and method of the analysis, the power-off neutral point was determined for several values of C_L and is presented in Figure 63. The results show that the power-off neutral point for the CRA is independent of C_L. The neutral point of 68-percent wing MAC is well aft of the recommended aft cg of 36.6-percent wing MAC. This, therefore, demonstrates adequate margin in accordance with MIL-F-8785 (ASG) and will result in good dynamic stability characteristics of the aircraft. As discussed previously, the large margin is due to the large horizontal tail, which was sized to provide satisfactory longitudinal stability characteristics in the helicopter and autogyro flight regimes.

Power effects on the neutral point were investigated and found to be small. The location of the jet exhaust exit aft of the horizontal tail and the close proximity of the thrust axis to the aircraft cg minimize the power effect on the aircraft neutral point. Thus, for all practical purposes, the power-on neutral point is equal to the power-off case. The maneuver point is calculated based on the method presented in Reference 10. The additional

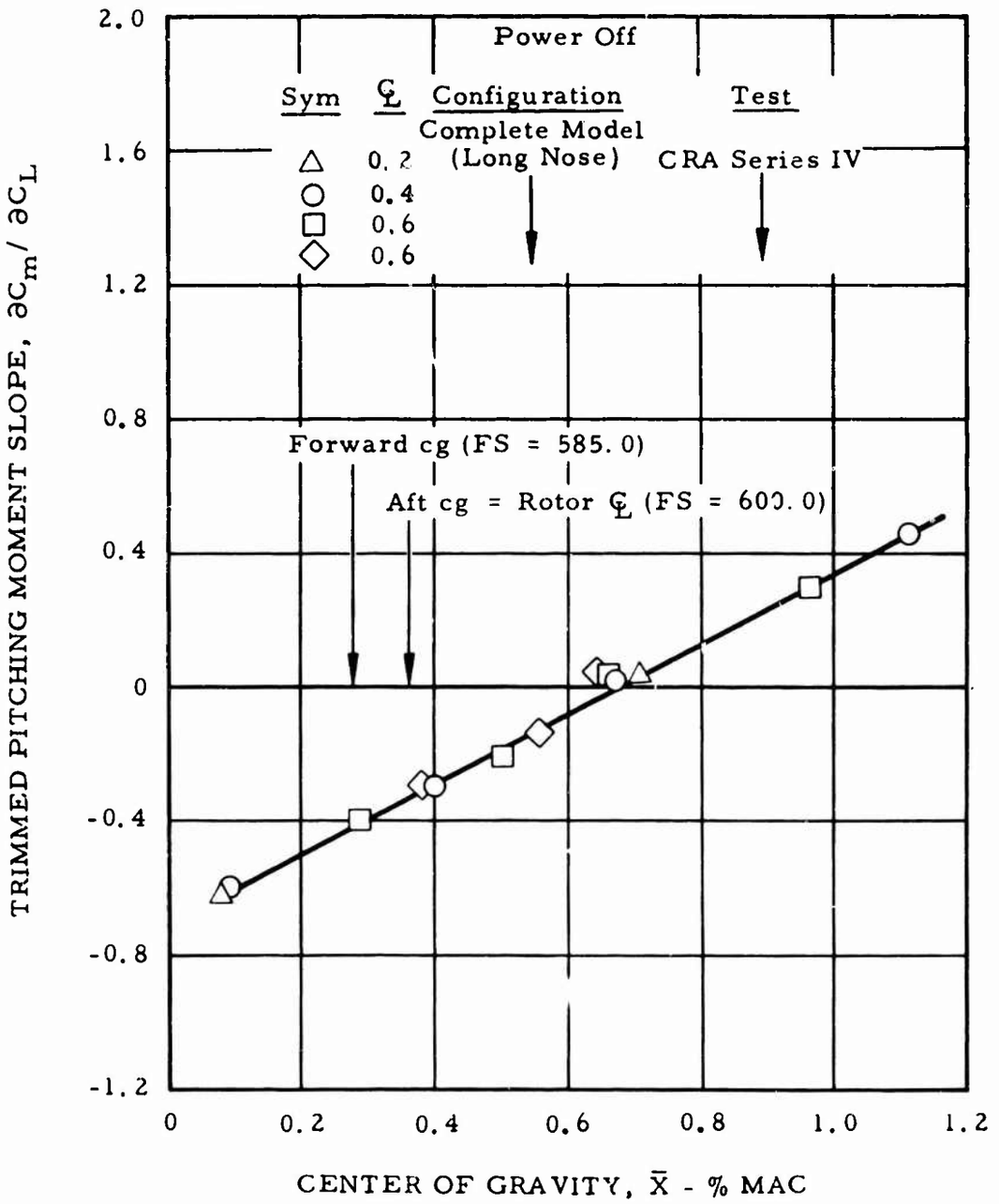

Figure 63. Determination of Stick-Fixed Neutral Point.

stability, $\Delta (dC_M/dC_L)$, during maneuvers due to damping in pitch from the large tail places the maneuver point approximately 6 percent aft of the neutral point, or at 74-percent wing MAC.

Figure 64 presents the elevon angle required for trim level flight versus airspeed for the design gross weight at sea level standard day. Curves are presented for both the forward and aft cg conditions. Since the elevon is directly geared to the cyclic stick, the corresponding stick positions can be obtained from the gearing curve presented in Figure 65.

Figure 66 presents the elevon angle required for trimmed flight as a function of wing C_L for the forward and aft cg. As can be seen, there is adequate longitudinal control power to trim out the aircraft at the most demanding condition of $C_{L\,max}$ during landing in ground effect. The elevon required for landing in ground effect was calculated based on Reference 11 in conjunction with the measured downwash angle presented in Figure 67. The elevon angle required for pull-up maneuvers versus wing C_L is presented in Figure 68 for 1-g and 4.5-g conditions.

The onset of initial drag divergence, which is discussed in the section titled Performance Data, is expected to occur at approximately M = 0.75. This is well above the maximum-speed sea-level Mach number of M = 0.6 (400 KEAS) used in the stability and control analysis. Qualitative investigation indicates that the compressibility effect on the stability and control characteristics at M = 0.6 should be small (Reference 12). The use of the all-moving tail instead of elevators will minimize the Mach number effect on the control effectiveness at higher speeds.

Preliminary test data from a recently completed transonic-speed wind tunnel test of the CRA model show good agreement with the above prediction of the compressibility effects on the aircraft. These test results show that between M = 0.4 and M = 0.8, there is little change in trim flight control position and neutral point location.

Satisfactory longitudinal control forces will be obtained in the airplane flight mode with a spring-assisted q-bellows artificial feel system that incorporates an electric actuator to trim forces to zero. This system provides the desired level of stick force per g in steady maneuvers. In addition, it incorporates a damper that provides good feel during transient maneuvers.

Lateral-Directional

The CRA will possess positive effective dihedral and stable directional stability characteristics throughout the airplane flight regime based on

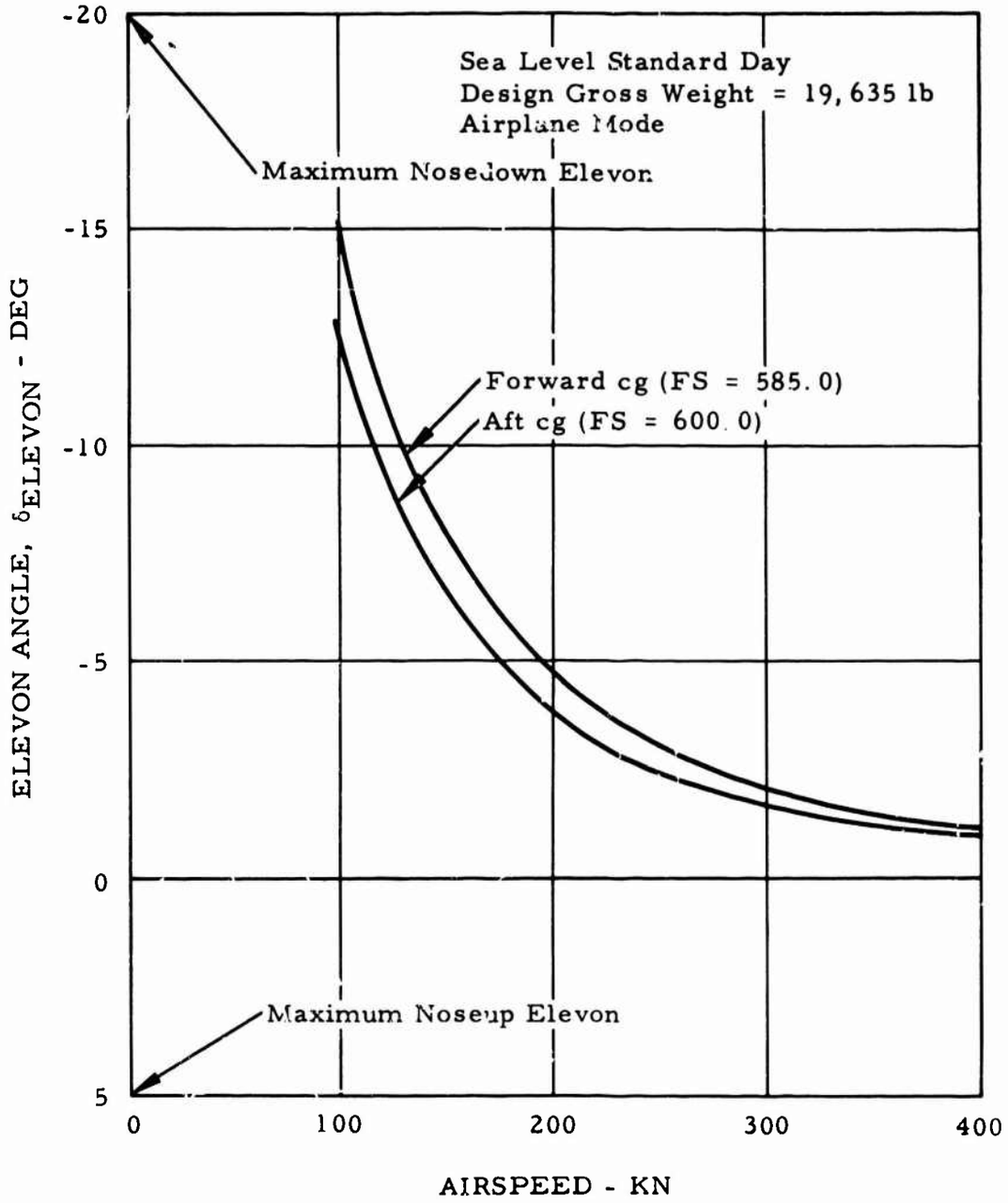

Figure 64. Elevon Angle Versus Airspeed for Trimmed Level Flight.

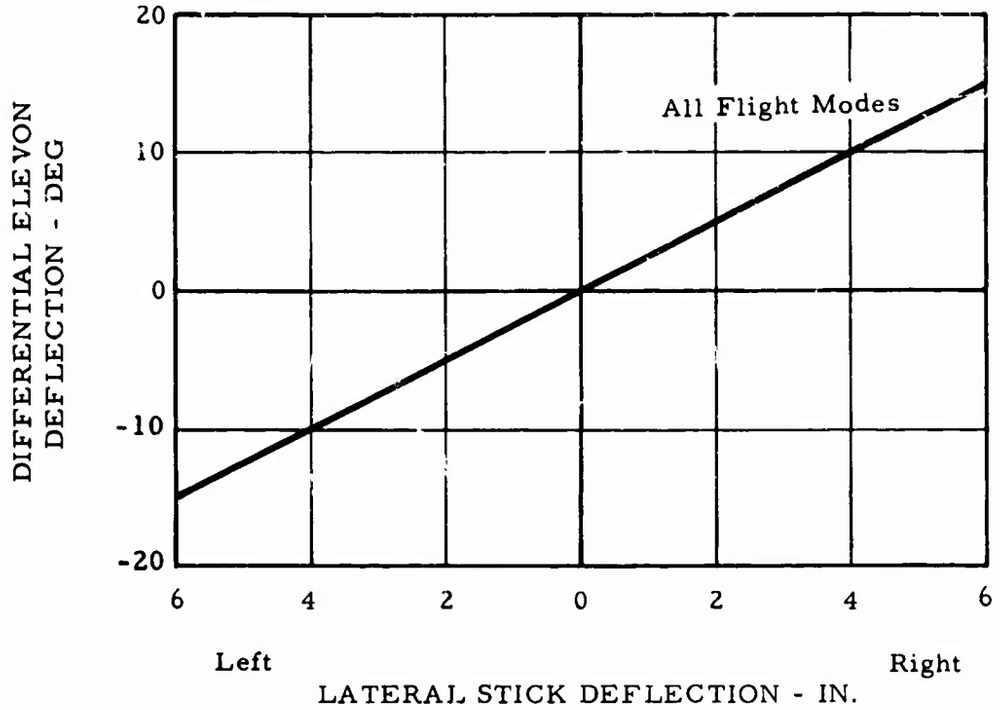

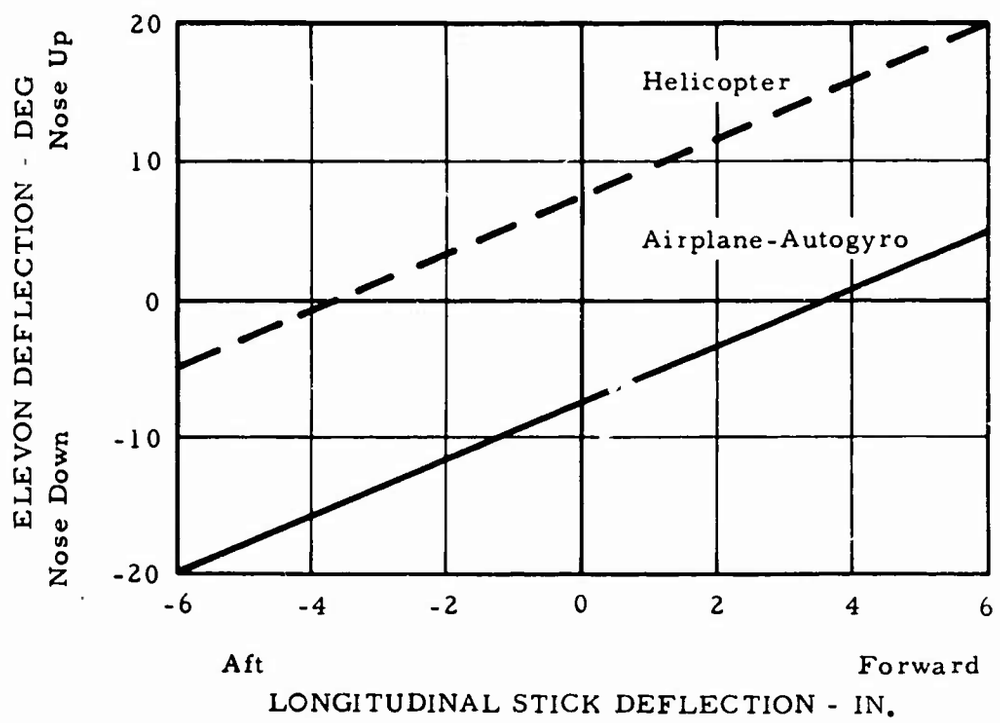

Figure 65. Stick - Elevon Gearing.

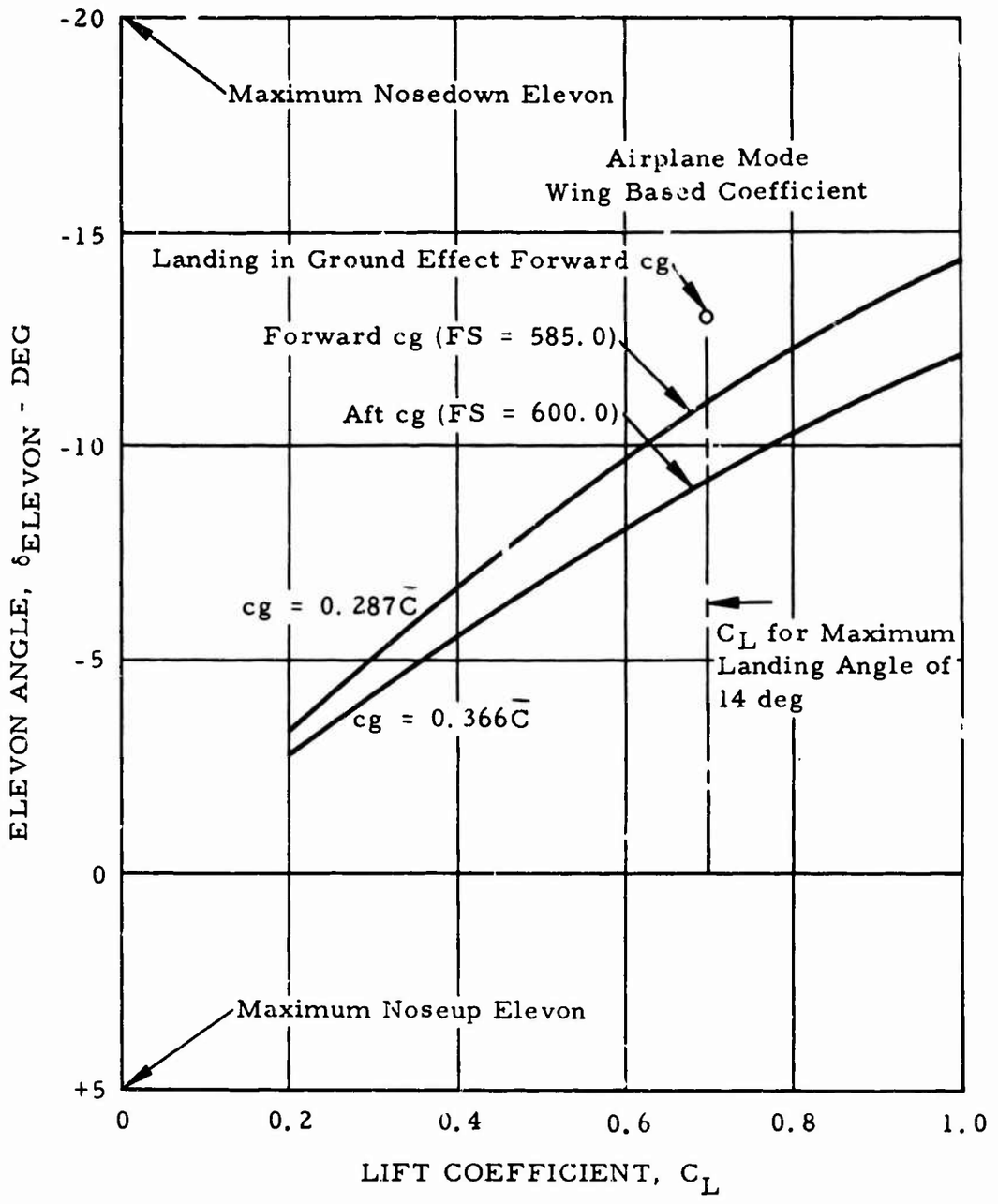

Figure 66. Elevon Angle Versus C_L for Trimmed Level Flight.

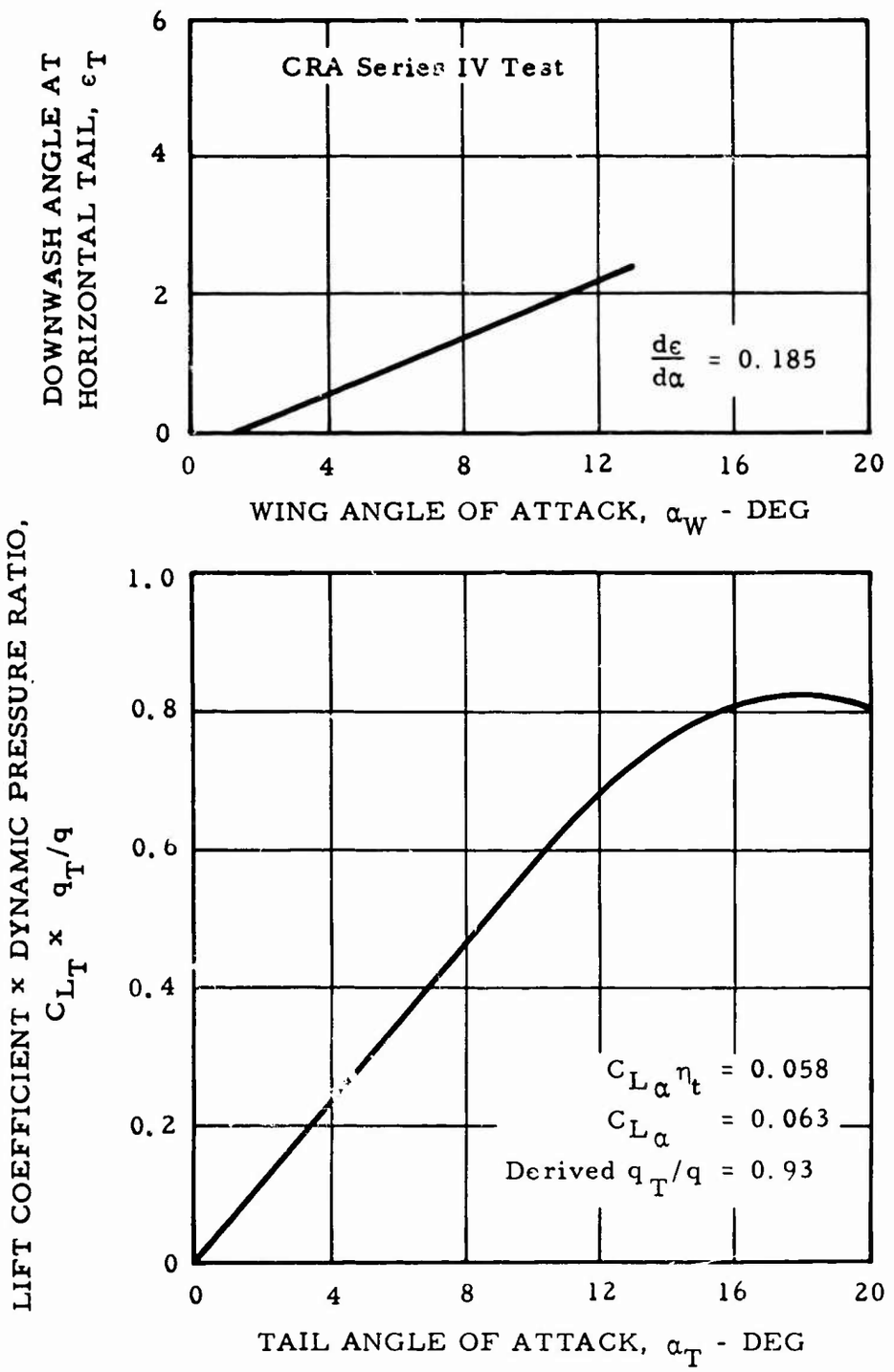

Figure 67. Horizontal Tail Contribution - Airplane Flight.

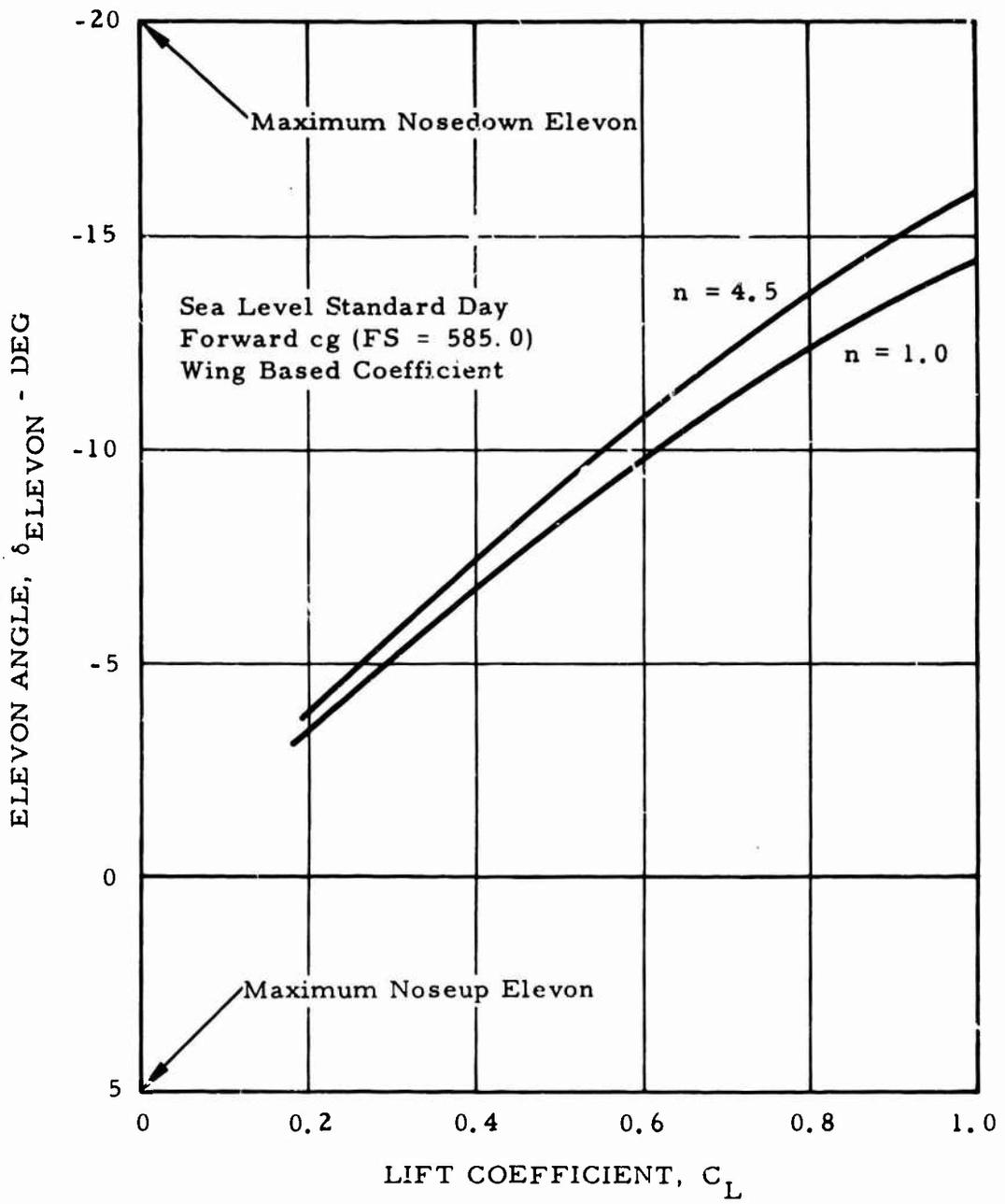

Figure 68. Elevon Angle Versus C_L in Pull-Up Maneuvers.

the results of model test and theoretical calculations. The vertical tail was sized to provide satisfactory directional stability in the helicopter flight mode. The vertical tail area sized for this condition also satisfies the requirement to provide a steady-state sideslip capability of at least 10 degrees with full rudder deflection (MIL-F-8785 (ASG) at 1.1 V_{S_L}), and not to exceed 15 degrees to prevent flow separation.

Based on measured wind tunnel test roll control power from the differential elevon deflections and the theoretical calculation of the aircraft's roll damping (Table XXII), the resulting roll characteristics of the Rotor/Wing are as shown in Figure 69. It can be seen that there is adequate roll control to meet the rolling requirements of $pb/2V = 0.07$ at 300 knots in accordance with MIL-F-8785 (ASG) for Class II aircraft. In order to prevent the possibility of the aircraft's exceeding its structural limitation at equivalent airspeeds in excess of 260 knots, a q-feel device, similar to that on the longitudinal control system, will be incorporated in the lateral artificial feel system. The device will limit the aircraft's roll rate by increasing the lateral control force gradient. The dashed lines of Figure 69 show the reduction in roll rate due to such a device. Aeroelastic effects on roll control response were considered but were found to be small, since the air loads on the differential elevons are acting near the hinge line.

The normal adverse yaw characteristic produced by the wing aileron-type roll controls is eliminated in the CRA differential elevon roll control system. This can be seen from the roll control power test presented in Figure 70. In fact, the model data show favorable yawing and differential elevon deflections.

The curve of $1/(C)_{1/2}$ versus $|\phi/V_e|$ showing Dutch-roll dynamic stability characteristics is presented in Figure 71. The stability derivatives used to calculate the above parameters are presented in Table XXII. As can be seen, the CRA meets the requirements of MIL-F-8785 (ASG) and thus has satisfactory lateral-directional dynamic characteristics. The basic reasons for the stable Dutch-roll characteristic for the CRA are due to the relatively large vertical fin surface and zero wing incidence setting with respect to the fuselage waterline. This latter design parameter, being dictated by helicopter requirements, produces a favorable product of inertia, which contributes to the stable Dutch-roll characteristics.

The rudder control power with a 30-percent-chord, 67-percent-span rudder is adequate to meet the MIL-F-8785 (ASG) requirement of developing at least 10 degrees of steady sideslip during landing at 1.1 V_{S_L}.

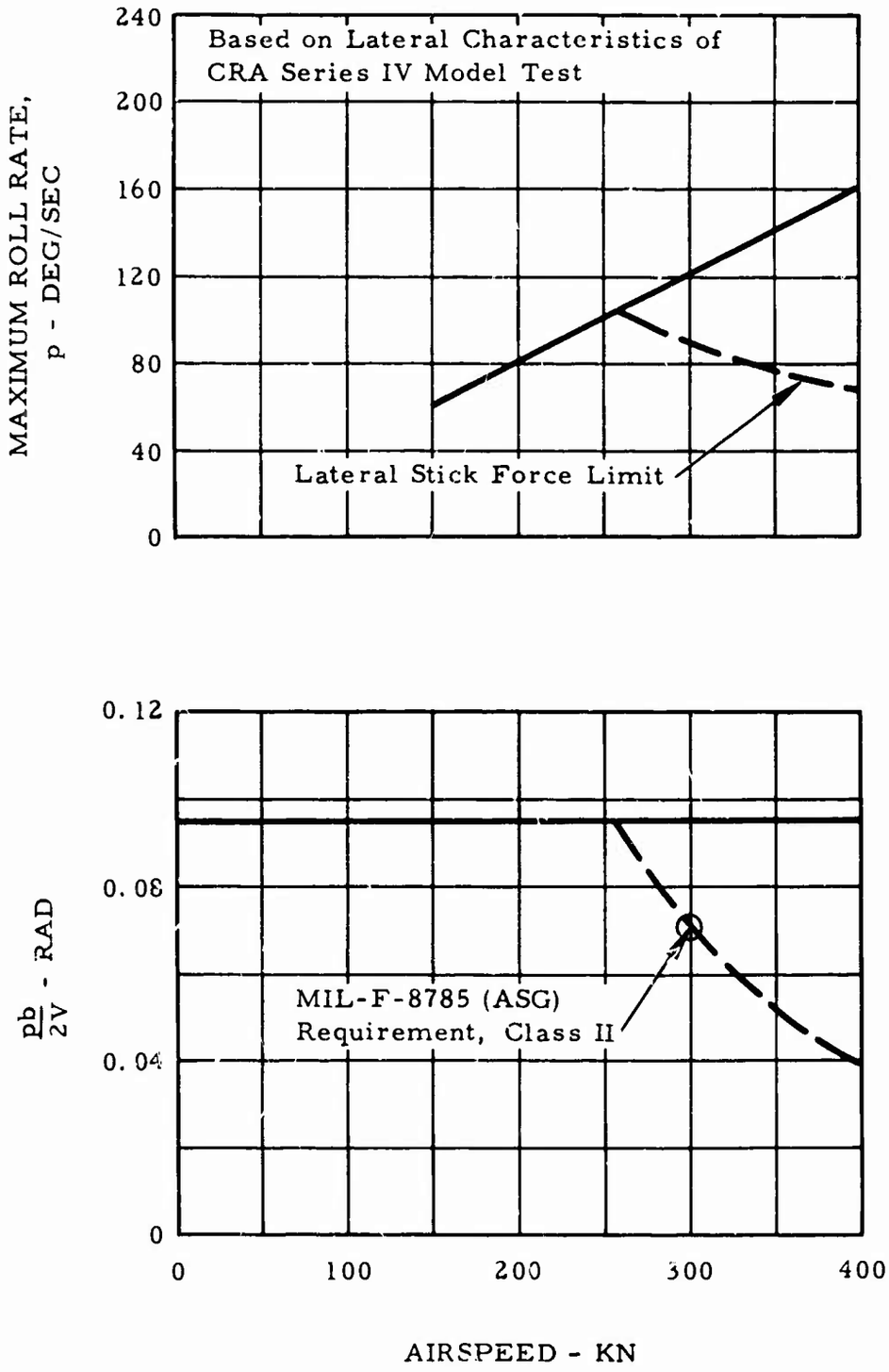

Figure 69. Roll Performance.

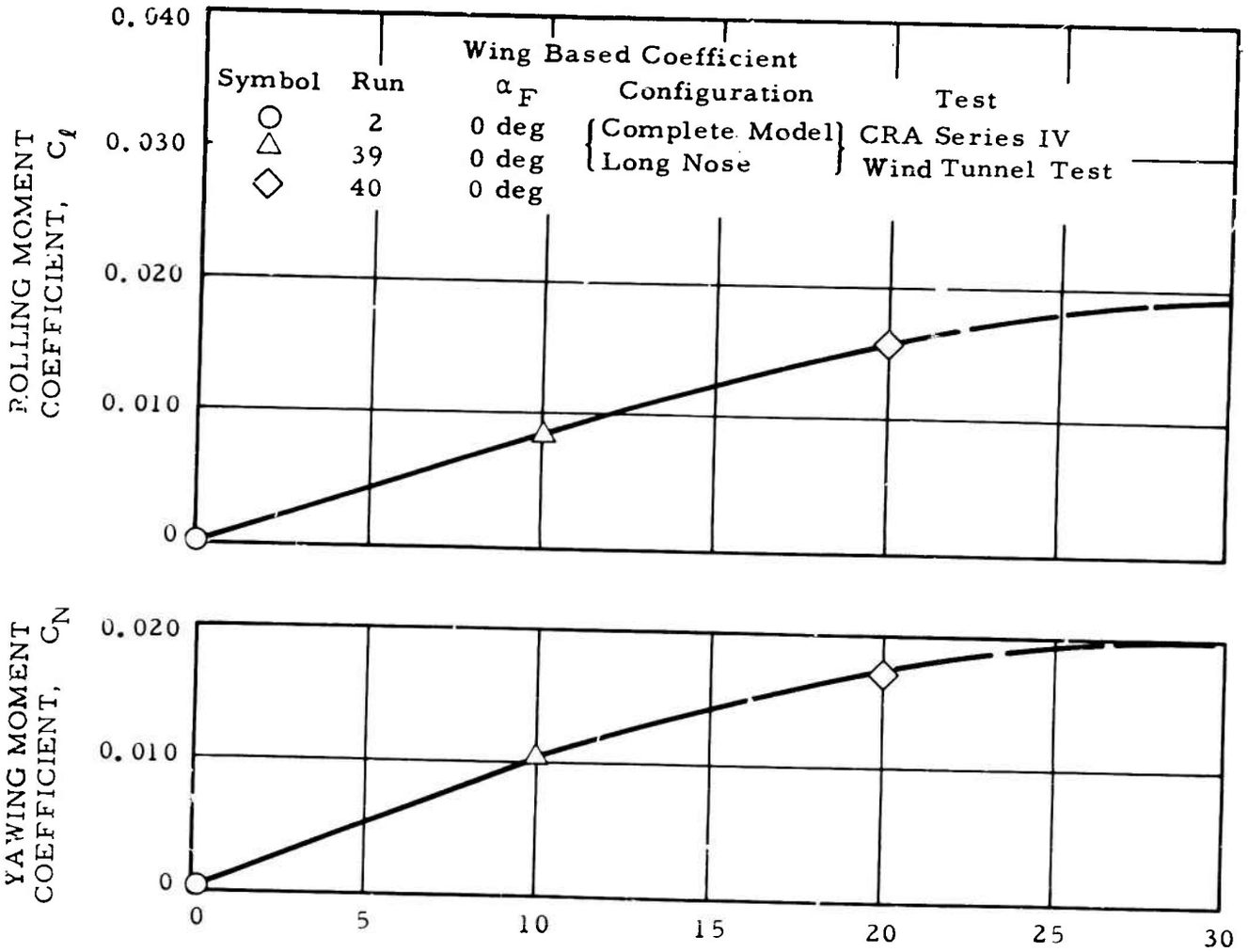

Figure 70. Lateral Control Power.

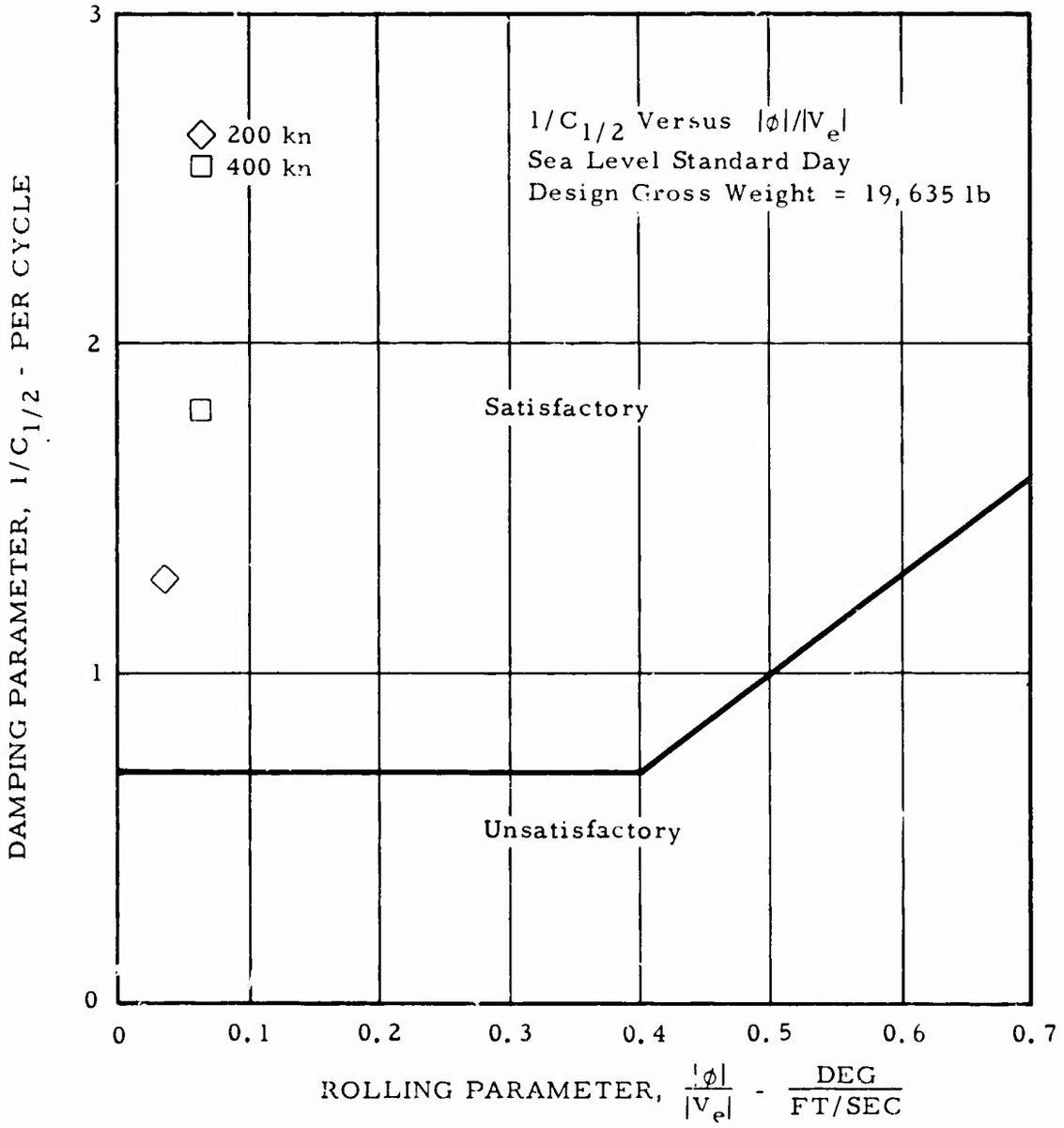

Figure 71. Lateral-Directional Dynamic Stability Parameter.

The lateral feel force is provided for the CRA by a simple spring artificial feel system and incorporates an electric actuator to trim forces to zero. As discussed previously, a q-feel device similar to the longitudinal control feel system will be incorporated in the lateral feel force system.

The directional feel force is also provided by a simple spring artificial feel system and is trimmed out by means of an electric actuator.

TABLE XXII. LATERAL STABILITY DERIVATIVES

(All derivatives are per radian)

Item	Value
C_{l_p}	-0.2075
C_{l_r}	$0.325\ C_L + 0.17243$
C_{N_p}	$-0.2200\ C_L$
C_{N_r}	-0.62572
$C_{Y_{\dot{\beta}}}$	-1.0583
C_{Y_p}	$0.8000\ C_L - 0.2636$
C_{Y_r}	0.9534
C_{l_β}	-0.1673
C_{N_β}	0.2349

STRUCTURES

This section of the preliminary design study covers structural design approach, principal structural features, design criteria, basic loads, structural analysis, and aeroelastic properties to indicate design solutions for the major structural areas. Criteria for treatment of fatigue and thermal stresses, and for the structural materials used and the corresponding allowable stresses, are included.

The preliminary structural analysis includes the data and the results for the major areas of interest and concern in the primary structure of the vehicle. Unconventional structural features are explained and analyzed. Important features are indicated by sketches or illustrations throughout the report.

The significant structural features of the Hughes Composite Research Aircraft are:

1. Simplicity - short direct load paths with a minimum of discontinuities or splices.

2. Light weight - due to use of well-proven advanced structural design and materials technology.

3. Reliability gains and weight savings - due to the Hot Cycle ducted pneumatic propulsion system as compared with a conventional drive through multiple dynamic elements.

4. Single main lifting surface - Rotor/Wing provides entire lift for both helicopter and fixed-wing airplane modes of operation.

5. Large aeroelastic margins - Rotor/Wing provides optimum strength and rigidity for high-speed fixed-wing flight.

6. Minimum vibration - helicopter vibratory accelerations and forces are minimized by use of both first and second harmonic main rotor pitch control.

7. Nonrotating hub type support - eliminates rotating-beam fatigue loads.

8. Fail-safe structural features - for improved level of safety.

9. Crashworthiness - provided by a combination of adequate crash load factors and energy-absorbing structure.

10. No antitorque rotor - tip-jet drive eliminates torque reaction on fuselage. The small yaw fan is used only for helicopter mode maneuvers.

11. Simple fan drive mechanism - yaw fan is driven through hypercritical shafting with minimum of dynamic elements (an extension of the supercritical shaft designs pioneered by HTC-AD on Model 269 and OH-6A helicopters).

12. Thermal safety design - insulation, isolation, and shielding employed for minimization of thermal stresses for both the hot and the cold structures, but providing a fail-safe installation even in the extremely unlikely case of puncture or leakage.

13. Avoidance of ground resonance problems - by use of the rigid Rotor/Wing.

14. Long fatigue life - through minimization of fatigue loadings and elimination of unnecessary discontinuities and stress concentrations, coupled with conservative application of advanced materials and processing technology.

15. Minimum vibration and fatigue loading in cruise flight - jet airplane smoothness obtained during major portion of flight through elimination of propellers and stopping of rotor.

16. Fixed-wing capability - structural provision for landing or takeoff as a fixed-wing aircraft.

17. Uncomplicated loading - comparatively indiscriminate loading of cargo, passengers, and fuel, as all major useful load items are centered near the vehicle center of gravity.

18. Structurally simple conversion - from helicopter mode to autogyro mode of operation; simple full-time flight controls; no rotor folding, retracting, or stowing; and a minimum of sequential actuating devices during conversion.

19. Aerodynamically clean structure - single lifting surface, submerged yaw fan, and adequately stiffened external aerodynamic skin surfaces provide low-drag fixed-wing aircraft aerodynamic characteristics up to transonic speeds.

PRINCIPAL STRUCTURAL FEATURES

The Hot Cycle propulsion system represents an advancement in safety, reliability, and low maintenance with long service life over current rotary-wing aircraft.

The outstanding attributes of the Hot Cycle rotor system are its simplicity, due to the elimination of the many moving parts required by other propulsion systems, and the light weight that results, not only in the propulsion system itself, but also throughout the entire vehicle as a result of the lightweight propulsion system. The reliability advantage obtained through the elimination of the many dynamic components is an equally outstanding feature of the Hot Cycle system.

Isolation of both thermal and structural strains is provided in the design of the hot gas ducting system through proper design of mounts, reinforcements, and flexible joints. In the event of a puncture or leak in the hot gas system from any unforeseen cause, the surrounding primary structure of the vehicle is both shielded and designed to provide continued safe flight and landing even after exposure to massive quantities of the hot gases.

In addition to the isolation of both hot and cold components from a structural viewpoint, judicious use is made of insulation, cooling airflow, and lightweight shielding to eliminate any detrimental effects from the interaction of the hot and cold components. Further, the differential expansion of the materials used in the primary structure, where slightly elevated temperatures may exist, is minimized either by using materials of similar expansion rates or by designing to permit a certain amount of differential expansion to be accommodated in the structure. Transient thermal effects are minimized within the hot gas system by detail design to assure uniform heat-up and cool-down of the components. The materials used in the hot components are standard production materials having wide usage in the jet-engine industry. They are used successfully on the XV-9A Hot Cycle Research Aircraft, and require no new technology development for application to the CRA.

Fail-safe structural and mechanical design philosophy is incorporated in the proposed aircraft. Design service life objectives for all important primary structural and mechanical components have been established at 4,000 hours to assure excellent initial safety and reliability of the research vehicles with minimum operational problems. The rigid Rotor/Wing is considered the optimum for the fixed-wing mode of operation, providing maximum bending and torsional rigidity and simplest conversion from the structural and mechanical standpoints.

The design approach to crashworthiness for the CRA continues along principles established and proven on the Model 269 and OH-6A helicopters. Heavyweight items that could inflict serious injury in the event of a minor crash are designed for crash load factors. In addition, impact energy absorption capability is designed into the structure, where appropriate, to provide an even greater level of crash safety.

Light Weight

The Hughes design approach has been to eliminate all possible deadweight not required for safety, reliability, and long life of the structure. This has been done by careful attention in design and analysis toward an optimum structure; by using modern, currently available materials and processes; by incorporation of detail design features to maximize the fatigue strength of the structure; by structural provisions to achieve the desired aeroelastic characteristics; and by choosing the simplest, most compact configuration to meet the mission requirements. The preliminary stress analysis substantiates all important structural areas for both the static and the fatigue loading requirements.

The fuselage, landing gear, and empennage are all representative of lightweight conventional subsonic fixed-wing aircraft components. Much statistical information is available on the weight of structures of this type; however, the adequacy of the weights presented for the proposed CRA design is further substantiated by the preliminary stress analysis for all the important structural sections. The component weights presented for this vehicle are substantiated by using only current state-of-the-art design, materials, processes, fabrication, and assembly practices.

Simplicity

Articulation joints, folding hinges, retraction mechanism, rotor stowage, tilting or fairing provisions. and main rotor mechanical drive system components are absent in the proposed design. The control system eliminates duplicate control systems and disconnection devices. Elimination of the need for such systems reduces weight and complexity while enhancing safety and reliability.

Major structure in the rotor blade and wing consists of a central box beam in the blade and two parallel box beams in the wing. Leading and trailing edge structures are of aluminum alloy honeycomb or truss-core sandwich material in both cases. Major frames or ribs occur only at the root transition structure from the blade to the pitch shaft in the blades, and at the two pitch bearing support points at the outboard ends of the Rotor/Wing primary structure. There is no rotating drive shaft for the main rotor;

instead, a nonrotating space-frame pylon structure provides support for the main rotor bearings inside the Rotor/Wing hub itself. The pylon, in turn, is supported by the fuselage at the four points where the rugged main frames and the upper main longerons intersect.

The fuselage is a very simple structural arrangement, consisting of a semimonocoque structure composed of four main longerons plus skin, stiffened by transverse frames and formers. The semimonocoque horizontal tail surfaces are all-movable elevons providing control of both pitch and roll in the aircraft mode. The vertical surface consists of a chordwise stiffened semimonocoque two-spar construction that supports the rudder and houses the yaw fan. The tail surfaces are supported in the fuselage by light but rigid truss-type bulkheads. The center fuselage contains an uninterrupted rectangular-box passenger/cargo compartment, centered directly below the Rotor/Wing and at the vehicle center of gravity. The fuel is contained in two tanks that are also centered about the vehicle center of gravity, one forward and one aft of the passenger-cargo compartment.

The retractable tricycle-type landing gear represents the simplest possible arrangement, being mounted at the intersections of rugged frames and longerons in the fuselage.

The all-jet Hot Cycle propulsion system follows the simple arrangement already proven in the XV-9A Hot Cycle Research Aircraft.

Structural Materials

Currently available materials are used throughout the structure of the Hughes Hot Cycle Rotor/Wing CRA. Where primarily static loads are critical and the intensity of loading is relatively low, aluminum alloys are used. Where aerodynamic smoothness and maximum fatigue strength are essential and yet loading intensity is low, adhesive-bonded honeycomb or truss-core sandwich-type material is utilized; for example, at the leading and trailing edges of the Rotor/Wing and of the rotor blades. Machined, integrally stiffened aluminum alloy box-beam covers are used for the Rotor/Wing primary structure. For the fuselage and tail surfaces, adequately stiffened conventional semimonocoque aluminum alloy aircraft-type structure is provided. Aluminum alloy materials are not used where long-time operating temperatures may exceed 200°F.

Where static loads are critical and the intensity of loading is relatively high, high-strength low-alloy or maraging steels are used. Where maximum fatigue strength is desired and possible exposure to temperatures

of approximately 350°F may exist, either a maraging stainless steel or a titanium alloy is used. In areas of moderate static loading intensities, one of the titanium alloys is utilized. The high-strength low-alloy steel used in the landing gear structure likewise reflects current practice throughout the aircraft industry.

In the preliminary stress analysis presented in this report, there are many instances where the structural weight differences resulting from using a titanium alloy or the maraging stainless steel are so slight that computations have been shown for both materials, and other factors such as availability and fabricability would govern.

For the hot components of the Hot Cycle ducted propulsion system, Inconel 718 nickel alloy is an overall optimum choice for the anticipated duct-wall temperatures. This material received wide and very successful usage in the XV-9A Hot Cycle Research Aircraft, where its comparative simplicity of fabrication and processing was also noteworthy.

Fatigue Considerations

Preliminary fatigue test data presented in this report, plus other published and unpublished research information, have been utilized in choosing the structural materials that have been considered for use in the Rotor/Wing and blade structures. Elimination of the many usual joints and splices in the proposed Rotor/Wing and blade designs constitutes a major factor in obtaining maximum fatigue resistance of the proposed structure. Adhesive bonding is utilized in many secondary structural areas to provide maximum fatigue strength, particularly where aluminum alloys are used. Where mechanical joints are unavoidable for fabrication or assembly purposes, such currently available and proven techniques as shot peening or expansion prestressing of holes and reduction of stress concentrations by such design techniques as scalloping or integrally machined reinforcements are used. There is ample evidence to prove that these techniques materially increase the fatigue strength of the proposed Rotor/Wing and rotor blade structure. Detail design to minimize such deleterious effects as fretting is in keeping with proven past practice developed for the TH-55A, OH-6A, and XV-9A helicopters. Optimum pretensioning of all fasteners is another factor employed. Careful detail attention to the provision of ample fillet radii and minimum discontinuity of cross sections is likewise provided. Materials subject to stress-corrosion cracking are either avoided in the design or given special heat-treat or mechanical processing to prevent this problem. In the fatigue-loaded areas, the materials chosen are those that provide minimum notch sensitivity and lowest crack propagation rates established by test data (see Figure 72).

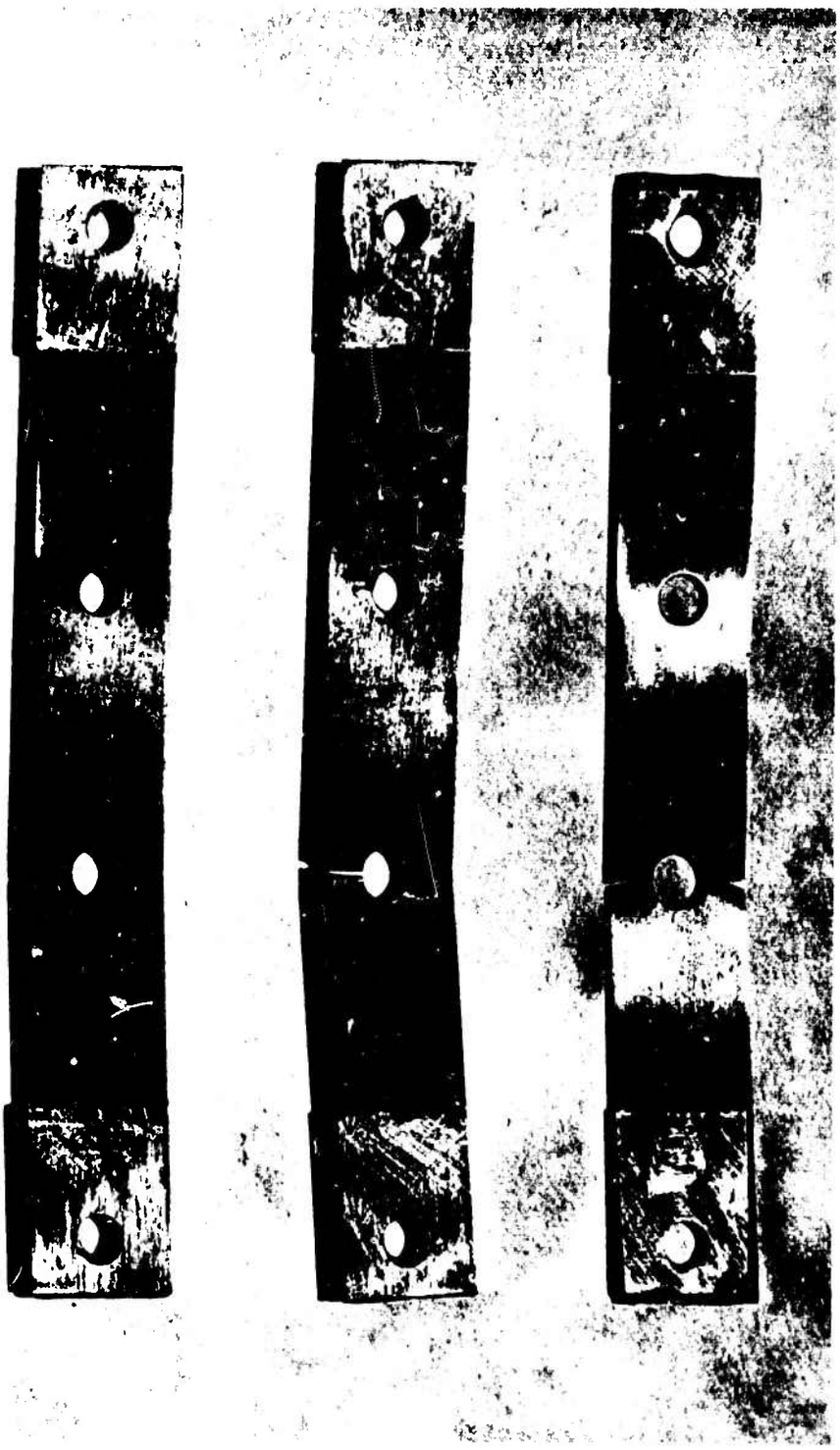

Figure 72. Partially Failed Notched Fatigue Specimens, Carpenter 455 Maraging Steel.

DESCRIPTION OF MAJOR STRUCTURAL COMPONENTS

Rotor/Wing Blades

The Rotor/Wing blade, shown in Figure 73, is a low-aspect-ratio, rigidly retained type for maximum simplicity of structure and ducting and for ease of in-flight conversion between helicopter and fixed-wing modes of operation. The blade centrifugal force is transmitted through a laminated tension/torsion member to a retainer at the rotor hub that is common to all three blades. The laminated strap member permits both collective and cyclic feathering in the helicopter mode. Steady and cyclic shears and bending moments at the roots of the blades are transmitted through two sets of angular-contact ball bearings into the tip ribs of the Rotor/Wing structure. Each of these bearing sets is supported by a rugged transverse frame attached rigidly to the Rotor/Wing primary beam structure. The rotor blade structure in the area of the feathering bearings and the blade root consists of a tubular pitch shaft that permits the propulsion duct to be located coaxially on the feathering axis. Immediately outboard of the feathering bearings, the tubular shaft tapers into a two-spar box that constitutes the primary bending and centrifugal load-carrying structure of the blade. The propulsion ducting in this transition section of the blade splits into two ducts of smaller diameter in order to stay within the airfoil contour. The hot gas ducting reacts all gas pressure loadings independently, and it is interconnected flexibly and mounted to the blade structure to isolate both thermal and structural deflections. The primary bending structural material chosen for both the tubular pitch shaft and the box beam is titanium alloy; however, a maraging stainless steel may be used alternatively within the allotted weight. The hot gas ducting is insulated and shielded from the surrounding primary structure so that the maximum structural temperatures will not exceed approximately 300°F in the hottest spots. Cooling airflow is provided to the extent necessary to maintain the desired temperatures. In the event of a puncture of the hot gas ducting, the adjacent primary structure is capable of operating at the resulting higher temperatures until a safe landing can be effected. The blade box-beam structure is designed to provide maximum fatigue strength by elimination of splices and other discontinuities and by use of scalloped edges, expansion prestressing, and/or shot peening of the attachment holes. These techniques for maximizing the fatigue strength of fabricated assemblies of this type are readily accomplished within the current advanced state of the art. The allowable fatigue stresses that have been used in the analysis section of this report allow conservatively for statistical scatter, to assure high probability of no failure. The leading and trailing edge structures support the local air loads on those portions of the blade; in addition, they are utilized for torsional strength and rigidity of the blade.

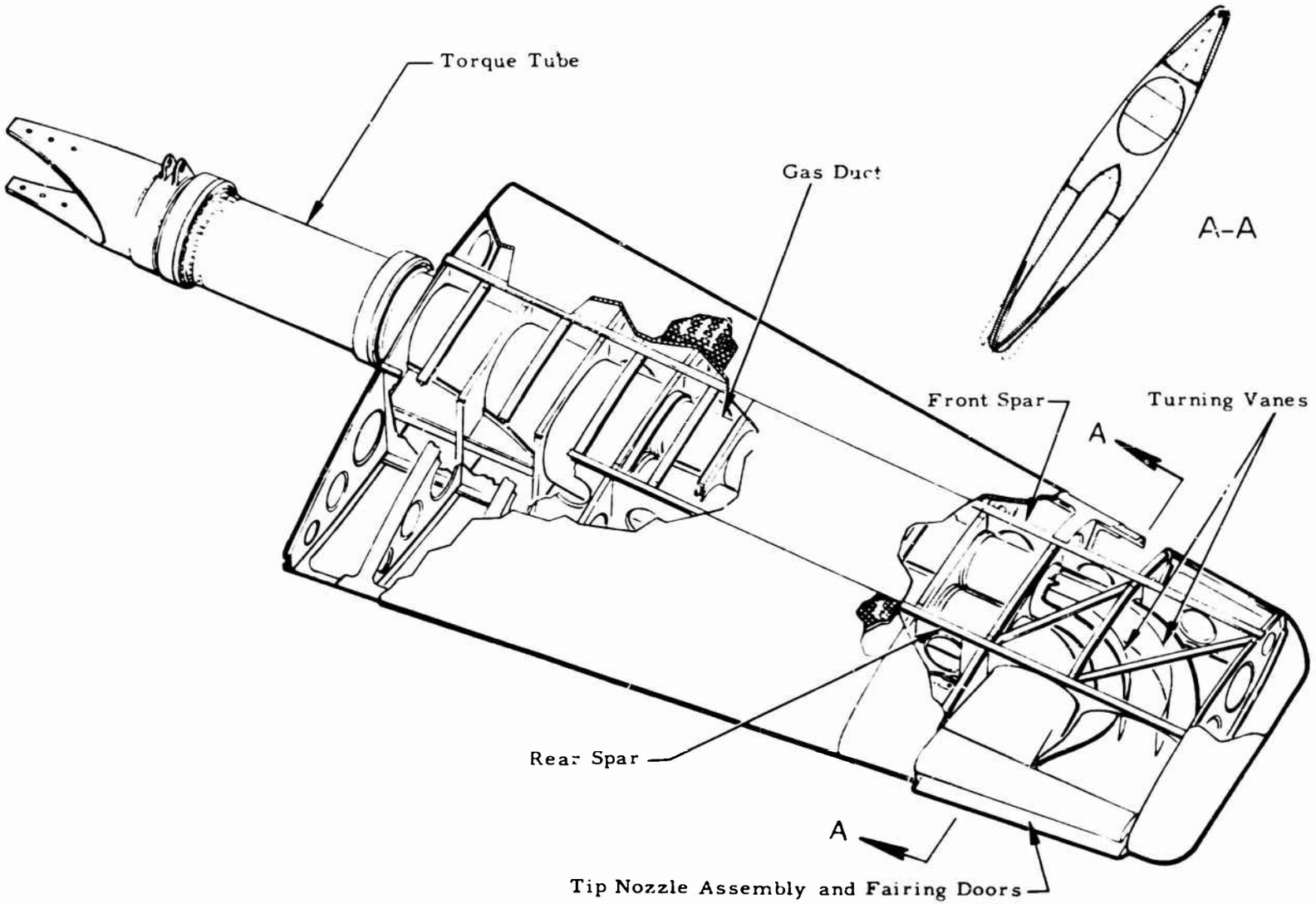

Figure 73. Rotor/Wing Blade.

This secondary structure is not subjected to significant heating from the propulsion system and, thus, may be fabricated as an adhesive-bonded aluminum alloy honeycomb sandwich-type structure. This construction provides maximum buckling stability and fatigue strength versus weight for these comparatively lightly loaded portions of the blade. The blade tip is removable, providing easy inspection and removal or replacement of all propulsion components. The removable blade tip section also houses the nozzle that provides the rotor tip thrust of the propulsion system.

Wing

The wing, shown in Figure 74, provides two main functions; namely, support of the rotor blades during helicopter mode of operation and provision of fixed-wing lift in the airplane mode. As in the case of the blade structure, the helicopter mode of operation produces the maximum design loads, from both the static and the fatigue viewpoints. Centrifugal loads from the blade, as previously mentioned, are supported independently of the primary wing structure, thus reducing the steady tension stresses in the wing beams. Rotor blade shear and bending loads imposed at the bearing support ribs in the wing tips are transmitted inboard to the main central hub bearing attachment by a double box-beam structure located on both sides of each set of propulsion ducts. Again, those portions of the primary structure immediately adjacent to the hot gas ducting are fabricated of either stainless steel or titanium alloy to withstand the anticipated maximum long-time elevated temperature of approximately 300°F. These same materials will also withstand short-time emergency loadings at the higher temperatures that might be encountered if a hot gas duct were punctured. The remaining portion of the primary box-beam structures consists of tapered, uniformly stressed, aluminum alloy, integrally machined beam caps that run uninterrupted, with no splices, from one wing tip to the opposite wing tip. The double box-beam construction is used to permit removal of the top center cover material in the region of the ducting, bearings, and controls for ease of inspection. The sculptured aluminum alloy beam caps not only eliminate all major splices across the wing but also permit local reinforcements in an optimum manner to counteract such stress raisers as rivet or bolt holes. Temperatures in the area of these primary wing beam caps are not expected to exceed 200°F during operation -- well within the long-time allowable temperature for aluminum alloy. As in the case of the rotor blades, all hot gas ducting is insulated and shielded from the primary structure, and cooling airflow is metered to maintain the desired temperatures. The thrust load, radial load, and the pitching and rolling moments that must be transmitted from the wing through the main rotor bearings to the fuselage are provided for in the Hughes CRA design by a rugged triangular rib-frame hub structure in the

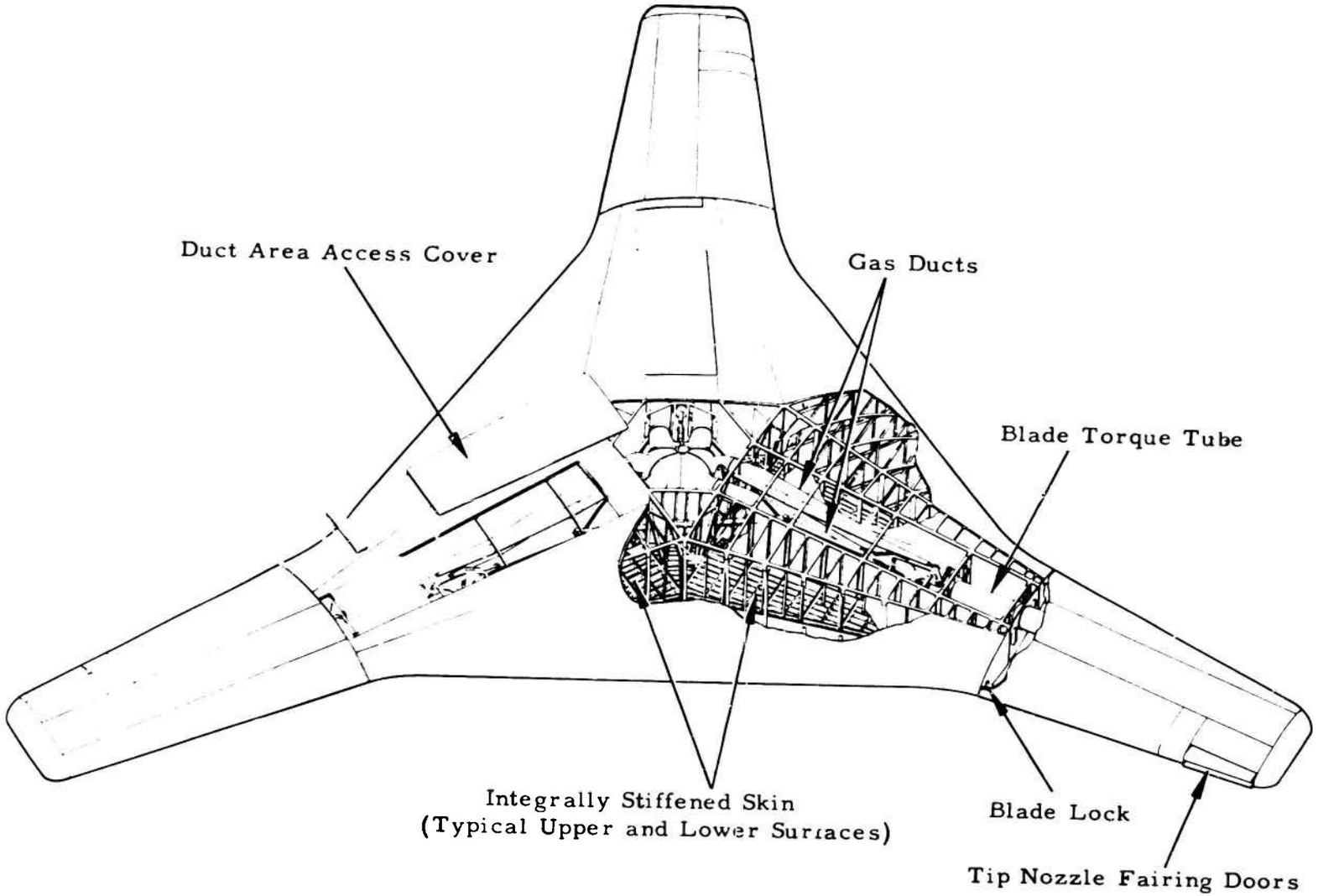

Figure 74. Rotor/Wing Assembly.

wing. In addition, three intercostal ribs are included to attach the hub at six uniformly spaced locations around the outer bearing housing. This structure provides the most direct load paths from the wing to the main rotor bearing with a minimum disruption of wing and bearing housing structure. The bearing attachments are made in such a manner that distortion of the bearing due to wing bending deformation is minimized, while the triangular rib frame tends to maintain a true plane at all times. This type of support provides the most uniform loading of the bearings. The remaining leading and trailing edges of the wing structure are of aluminum-alloy adhesive-bonded honeycomb-sandwich construction to provide optimum airfoil smoothness, to withstand local air loadings, and to add torsional stiffness to the overall Rotor/Wing structure. Light intermediate ribs at approximately 20-inch spacing support the local air loads and stabilize the overall wing structure.

THERMAL CONSIDERATIONS

The hot portions of the propulsion system for the Composite Research Aircraft are designed for temperatures and pressures very similar to those of the XV-9A Hot Cycle Research Aircraft. Design experience as applied to the CRA is listed below:

1. Safety and reliability - additional 1.33 limit factor of safety on all pressure-loaded hot gas components.

2. Long service life - all hot ducting components designed to a 0.2-percent creep deformation life of 4,000 hours for the vehicle.

3. Simplicity - circular sections used to the greatest possible extent for hot gas ducting. A minimum of secondary stiffeners required; easy fabrication.

4. Light weight - pressure loads carried as hoop tension stresses for maximum strength/weight; circular shapes provide minimum duct wall surface area versus cross-sectional area.

5. Optimum material choice - hot gas components are fabricated of Inconel 718 nickel alloy. This material has excellent short- and long-time strength at operating temperatures, is easy to fabricate and process, and resists crack propagation.

6. Isolation of hot and cold components - undesired restraints that would otherwise induce locked-in stresses due to differential thermal expansion are eliminated. Structural strains are also isolated from the hot gas components.

7. Insulation, shielding, and cooling - the strength and service life of the primary structure adjacent to the hot gas ducting are increased by the use of insulation, shielding, and cooling. Differential temperature strains within the adjacent primary structure are reduced to insignificant levels. Primary structure is protected against direct hot gas impingement in case of a puncture in the ducting.

8. Fail-safe design - primary structural elements adjacent to the hot gas ducting are designed for safe short-time operation at the elevated temperatures that might be encountered even in the very unlikely event of a massive hot gas duct leakage.

9. Uniform heating of hot gas components - stiffening and supporting elements of hot gas components are designed to operate as close as possible to the duct wall temperatures in order to minimize thermal stresses, particularly during transient operating conditions such as start-up or shutdown.

10. Overall system - no dynamic elements; jet aircraft reliability of hot components.

The CRA employs the exhaust gases of a J52-P-8A turbojet engine for flight propulsion in both the helicopter and airplane modes. In the helicopter mode of operation, the hot gases are directed from the diverter valve through the ducting in the hub, the wing, and the blades. The gases are exhausted at the blade tips through nozzles that supply the driving torque to the Rotor/Wing. In the airplane mode, the diverter valve shuts off the flow to the Rotor/Wing and allows the hot gases to flow through the engine exhaust tail pipe. In this mode, propulsion is the same as in a conventional jet aircraft.

The typical ducting cross section is circular. This results in the lightest weight system, since all the pressure loads are carried by hoop tension stresses and since duct surface area versus cross-sectional area is optimum (that is, minimum). Any additional weight that otherwise results from stiffening is held to a minimum and occurs only in those areas where there is a departure from the circular cross section, such as at the tip nozzles.

The required duct wall thicknesses for either peak or long-time stress conditions are thinner than the minimum gages required for fabrication, which are held to 0.007 inch for the Rotor/Wing system ducting and 0.012 inch for the engine exhaust tail pipe, hot gas distributor, and diverter

valve. Thus, very conservative operating duct wall stresses are indicated, providing exceptional reliability and safety.

MATERIALS AND ALLOWABLE STRESSES

Materials to be used for the structure of the CRA have been selected on the basis of the greatest strength-to-density ratio suitable for the temperature environment and the fatigue and static loads expected to be encountered. The design conditions are very similar to the temperature and static and fatigue conditions previously encountered on the XV-9A Hot Cycle Research Aircraft. Design and material selection experience as applied to the CRA is listed below:

1. Safety and reliability - titanium and steel are used in areas of 300° to 400°F maximum temperature environments. These materials have good short-time properties up to approximately 1,000°F for an assumed emergency, such as the puncture of a hot gas duct.

2. Optimum materials - aluminum alloy has the greatest strength-to-density ratio up to 200°F for structure that is designed to buckling stability requirements. Titanium alloys or maraging stainless steels have the greatest fatigue strength-to-density ratio for use at temperatures of 300° to 400° F and are also superior for maximum static tensile loading. Inconel 718 nickel alloy has superior strength-to-density ratio for the hot gas ducting components (René 41 cobalt alloy shows no significant advantage at the expected duct wall temperatures, and would be more difficult to fabricate).

3. Maximum fatigue strength - the safe, conservative, fatigue allowables that have been used are based on test data, reduced by factors to allow for statistical scatter, size effects, and finish tolerance.

4. Minimum designed-in stress concentrations - scalloping, reinforcement, and prestressing or shot peening are used to minimize the effects of stress raisers where fatigue loadings are expected.

5. Stress corrosion - temperatures and stress levels are held well below the limiting levels (for both aluminum and titanium alloys).

6. Growth possibilities - René 41 cobalt alloy offers excellent potential for further increase in Hot Cycle gas temperatures for more

advanced propulsion systems without any advance in the existing materials state of the art.

Basis of Material Selection

Materials proposed for the structure of the CRA are based on the selection of the currently available materials with the greatest strength-to-density ratios for the temperature environment and static and fatigue loadings expected to be encountered during vehicle operation. The selection of the material on the basis of strength-to-density ratio is demonstrated by Figures 75 through 77.

Special attention is given to eliminating fretting and its detrimental effect on fatigue life. High clamp-up loads are used in attachments subject to cyclic loads to eliminate relative movements of the attached parts that would otherwise lead to fretting. An example of this type of attachment is the bolted connection of the Rotor/Wing to the shaft. Where high clamp-up loads are not used, shrink-fit bushings are used. The bushings provide a prestress in the material around the bolt hole to minimize the stress cycling under fatigue loads. Adhesives plus fasteners are also used in many structural areas where fretting must be prevented. Such a case is in the blade retention strap assembly, where the laminates are bonded together in the attachment area to prevent relative movement. Adhesive bond in this case is not relied on to transfer load, which is carried entirely by the clamp-up bolt attachment.

Surface coatings such as zinc chromate, epoxy, and so forth, are used to prevent fretting where the relative movement of parts due to deflection cannot be eliminated.

Aluminum Alloy

Aluminum alloy is used for all structural parts where the design is dictated primarily by the buckling stability of the structure rather than by a fatigue strength requirement, and where the temperature does not exceed approximately 200°F. Figure 75 shows that aluminum alloy is lighter than steel or titanium alloy in an application of this type, such as for panels under edge compression on the compression side of the wing and for fuselage longerons and skin panels.

In all statically loaded and fatigue loaded structure that is critical in tension, 2024 alloy is used instead of 7075 alloy, which has a higher static strength but which also has a higher notch sensitivity.

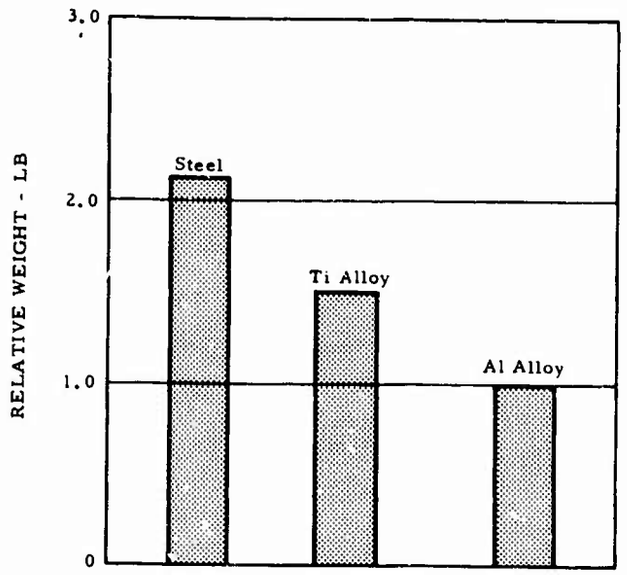

Figure 75. Relative Weights of Equivalent Load-Carrying Panels Where Buckling Instability Governs.

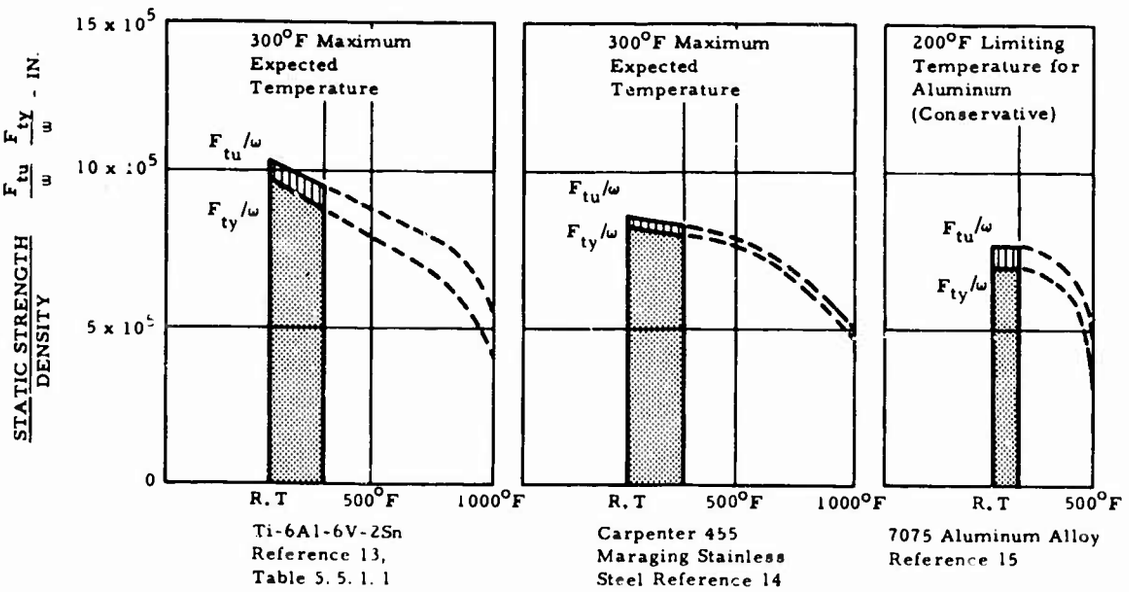

Figure 76. Static Strength-to-Density Ratio Versus Temperature for Titanium Alloy, Steel, and Aluminum Alloy.

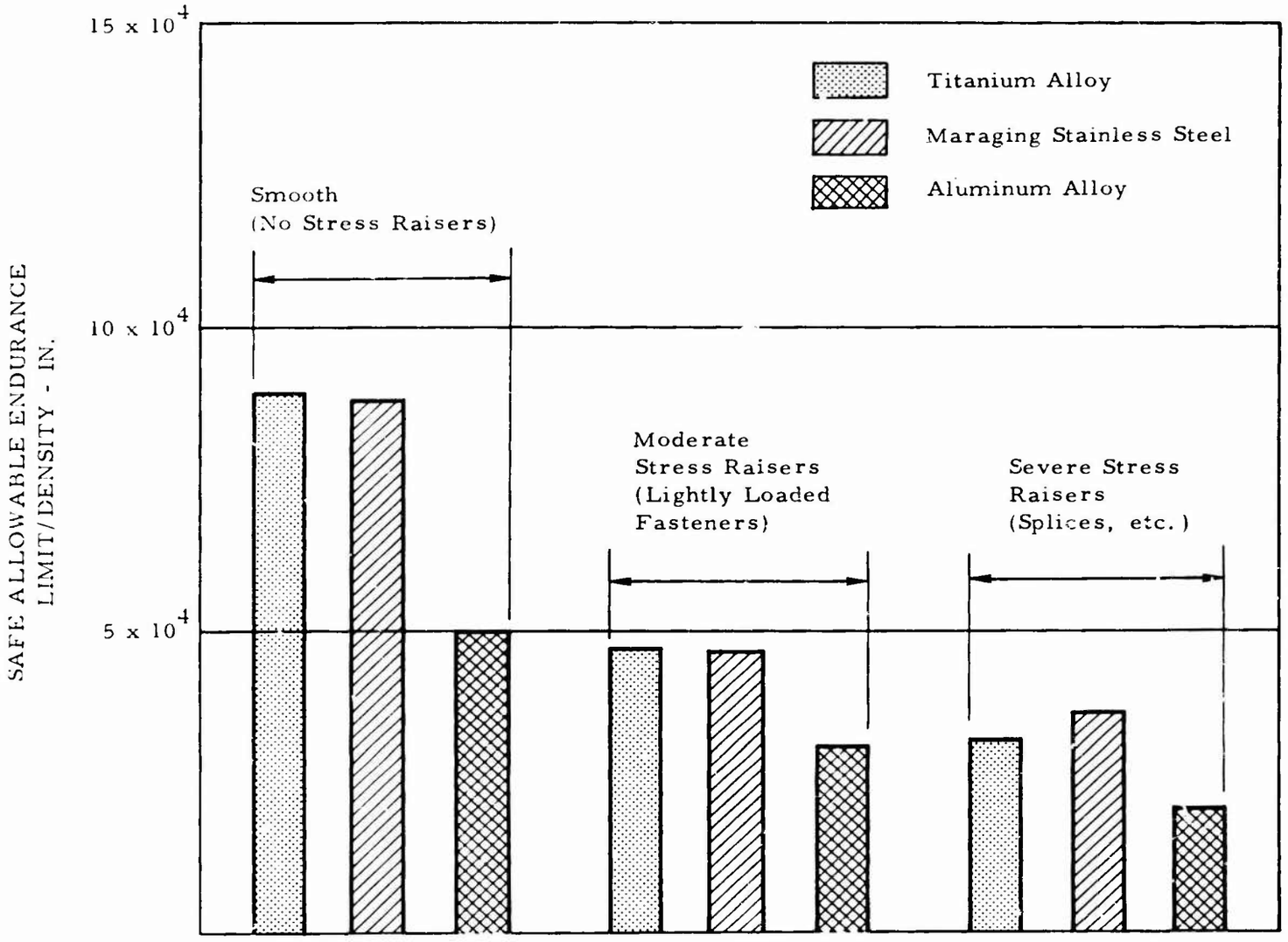

Figure 77. Safe Allowable Endurance Limits, Design Cyclic Stress Versus Density.

A typical endurance limit value for cyclic testing on smooth aluminum alloy specimens ($K_t = 1$) is ±19,000 psi. The maximum allowable value used for design in areas free of stress raisers has been reduced arbitrarily to ±5,000 psi to allow for statistical scatter, size effects, and finish tolerances. This is an accepted, reliable, and proven value which has been used widely by the helicopter industry.

The Al 7000 series alloys are used only where advantageous for compressive loadings or for structure where fatigue and stress corrosion problems are not a significant consideration.

Adhesive bonding is used to the fullest extent in lieu of the conventional rivet or bolt attachments in order to provide excellent fatigue strength.

The design of the aircraft also takes full advantage of scalloping, local reinforcement and prestressing or shot peening to reduce the effect of the unavoidable stress raisers for fatigue loadings. Scalloping has been used by jet engine manufacturers to reduce the adverse effects of stress concentrations at holes. Also, generous transition radii are used to reduce stress concentrations. Another form of scalloping which has been used by the aircraft engine industry is the undercutting of studs and bolts.

Prestressing or shot peening is used on such stress raisers as holes. The prestressing consists of passing a slightly oversized metal ball or mandrel through the hole, leaving favorable residual compressive stresses around the hole and thus improving the fatigue strength.

As a result of all the design provisions for relieving the adverse effects of stress raisers, an allowable design endurance limit fatigue stress of ±3,000 psi is justified for those structures using lightly loaded bolt or rivet attachments. It has been proven by tests that the fatigue improvement techniques mentioned above will actually force any fatigue crack that may occur during testing to initiate outside the bolt or rivet holes. Detrimental effects due to fretting are eliminated in such areas of mechanical attachments by detail attention to surface coatings and to fastener preloads during fabrication. In areas where mechanical splices are unavoidable for assembly or other reasons and the bolts and rivets are more highly loaded, the safe endurance limit fatigue allowable is further reduced to ±2,000 psi.

Steels

Figure 76 shows that Carpenter 455 maraging steel has a higher static strength-to-density ratio than 7075 aluminum alloy and a slightly lower

ratio than 6AL-6V-2Sn titanium alloy. High static loading is encountered on such structures as the rotor strap retention.

Figure 77 shows that this steel has a higher fatigue strength-to-density ratio than aluminum alloys and is comparable with the best titanium alloys. It shows only a slight drop-off in strength due to temperature at the expected 300° to 500°F environment where aluminum alloys cannot be used. It also performs satisfactorily for short-time temperature conditions up to 1,000°F. For fatigue applications, this steel is considered as one of the best all-around materials tested to date, showing exceptionally consistent static and fatigue test properties for both smooth specimens and those with holes, and for both sheet and bar as well as for longitudinal and transverse grain directions.

After precipitation hardening to the high strength level, Carpenter 455 maraging steel exhibits good toughness and excellent notch ductility. Fatigue tests on notched specimens (hole in specimen) exhibited yielding and necking down of the specimen rather than the brittle-type failure that is typical of the usual fatigue failure (see Figure 72). Crack propagation is slow. A fatigue testing program on Carpenter 455 maraging steel conducted by Hughes Tool Company showed that cracks in notched specimens were usually found by visual inspection before they were propagated sufficiently to cause rupture or a decrease in test load. This maraging stainless steel requires no corrosion protection or plating for resisting normal atmospheric corrosion and salt-water atmospheres. Tests in 5-percent and 20-percent salt spray at 95°F demonstrated excellent resistance to rusting and pitting; no rusting was apparent after 14 days in 5-percent salt spray at 95°F. Stress corrosion cracking tests in (a) 20-percent salt spray at 95°F and (b) boiling 6-percent sodium chloride plus 1-1/2-percent sodium dichromate showed that this alloy resists stress corrosion cracking at considerably higher stress levels than any other precipitation hardening stainless steel. It also shows excellent resistance to elevated temperature oxidation up to approximately 1,200°F.

Carpenter 455 is readily formed, machined, or welded in the annealed state and its cold work-hardening rate is low -- an advantage in forming parts. Another advantage of the material is that during age hardening its dimensional change is only 1/10 percent, thus permitting close machining and forming in the annealed state followed by the simple aging heat treatment.

Carpenter 455 maraging stainless steel can be used readily in combination with titanium alloys at moderately elevated temperatures without developing detrimental thermal stresses, since the coefficient of linear

expansion of this steel is only slightly higher than that for the titanium alloys (6.0×10^{-6} in. /in. /°F versus 5.0×10^{-6} in. /in. /°F).

Fatigue tests showed an endurance limit at a maximum stress of 145,000 psi (equivalent to 80,000 ±65,000) at $K_t = 1$ and R = 0.1. The test data show a very narrow scatter band. The safe endurance limit fatigue value used for design has conservatively been reduced to ±25,000 psi for areas free of stress raisers to allow for scatter, size effects, and finish tolerances. Fatigue testing of notched specimens (holes), without prestressing or shot peening treatments, showed an endurance limit of 68,000 psi maximum stress (R = 0.1), which is equivalent to 37,500 ±30,500 psi.

For the fatigue-loaded parts of the aircraft, full advantage is taken of scalloping, reinforcements, and prestressing or shot peening to improve the fatigue strength in those areas where stress raisers, such as bolt holes, cannot be avoided. In view of this attention given to relieving the adverse effect of stress raisers, the safe allowable design endurance limit (fatigue stress of ±13,000 psi) is used in areas of lightly loaded mechanical fasteners. At the few unavoidable splices with more heavily loaded fasteners, a further reduction in the safe allowable endurance limit fatigue stress to ±10,000 psi is conservatively assumed.

Titanium Alloys

Titanium alloys may also be used for those structural parts subject to a slightly elevated temperature environment of 300° to 400°F (maximum), and in applications where high static and high fatigue strength-to-density ratios are desired. Such applications are in the rotor mast, rotor bearing housing, blade spars, and ribs.

Two titanium alloys are considered to be most suitable for the aircraft -- Ti-6AL-6V-2Sn and B-120-VCA.

Ti-6AL-6V-2Sn is similar in many respects to Ti-6AL-4V but has somewhat higher strength and greater depth hardenability for the heat-treated condition. Considerably higher toughness with some sacrifice in static strength is attained by restricting the oxygen content to 0.12 percent maximum.

B-120-VCA titanium is an all-beta alloy and is supplied in the solution heat-treated condition. The most desirable feature of this alloy is that after machining, only aging is required to obtain the desired strength level. This alloy is superior to the other titanium alloys in bending and cold-forming operations. For fatigue applications, there is no significant

penalty for using the proven Ti-6AL-4V alloy based on many data sources, including data for specimens with holes and burrs.

The possibility of stress corrosion in titanium alloys has also been investigated, and there should be no problem in the proposed applications. Stress corrosion has been a potential problem only at temperatures above 450°F and at steady stress levels above 45,000 psi. In the CRA applications, the temperatures and stress levels are both held well below these limits. Thus, no problem of this type is envisioned.

Test data for Ti-6Al-6V-2Sn show an endurance limit at a maximum stress of 95,000 psi at K_t = 1 and R = 0.1 (equivalent to 52,250 ±42,750 psi).

The safe endurance limit fatigue value used for design has conservatively been reduced to ±14,500 psi for structural areas having no stress raisers in order to allow for scatter in the test data, size effects and finish tolerances.

Fatigue test results of Ti-6AL-2Sn notched specimens (K_t = 3.5 and R = 0.1) indicate 40,000 psi maximum stress at endurance limit (equivalent to 22,000 ±18,000 psi). These properties were obtained on specimens in the same heat-treated condition that gives an ultimate tensile strength of 167 to 174 ksi along with 12 to 15 percent elongation and 32 to 47 percent reduction of area.

Fatigue testing of hole notched specimens at Hughes shows endurance limit for the same material of 35,000 psi maximum stress (equivalent to 19,200 ±15,750 psi). Where mechanical fasteners are used, scalloping, reinforcement, and prestressing or shot peening are used to assure maximum fatigue strength. Where the fasteners are lightly loaded, the safe endurance limit fatigue allowable stress is conservatively reduced to ±7,500 psi. At unavoidable splices with more heavily loaded fasteners, the safe fatigue allowable is further reduced to ±5,000 psi. Table XXIII presents a summary of safe design allowable stresses.

Hot Gas Ducting Material

Inconel 718 is used for all hot gas ducting systems in the CRA. It has superior short-time strength properties and elongation values up to 1,200°F (see Figure 78), which is above the peak temperature in this design.

Long-time rupture and creep properties of Inconel 718 are also superior to those of René 41 up to 1,150°F. This is above the expected peak temperature (see Figure 79).

TABLE XXIII. SUMMARY OF SAFE DESIGN ALLOWABLE STRESSES

Material	F_{tu} (psi)	F_{ty} or F_{cy} (psi)	Safe Endurance Limit Fatigue Allowables Mean ± Cyclic Stresses		
			Smooth Areas Normal Finish	Moderate Stress Raisers	Splices
2024 Aluminum	65,000	48,000	15,000 ± 5,000	12,000 ± 3,000	10,000 ± 2,000
7075 Aluminum (Compression only)	73,000	64,000	Zero/or ± 5,000 Steady Compression	Zero/or ± 3,000 Steady Compression	Zero/or ± 2,000 Steady Compression
Titanium	175,000	160,000	25,000 ± 14,500	25,000 ± 7,500	25,000 ± 5,000
Maraging Stainless Steel	250,000	245,000	50,000 ± 25,000	50,000 ± 13,000	50,000 ± 10,000

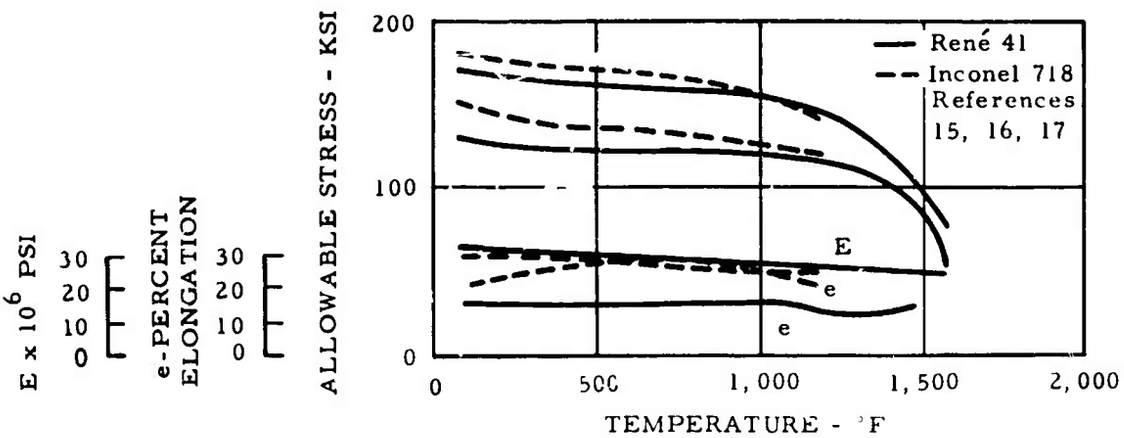

Figure 78. René 41 and Inconel 718 Static Properties Versus Temperature.

Inconel 718 has good forming qualities. Its slow response to age hardening allows it to be welded in either the annealed or the aged condition without spontaneous hardening during heating and cooling. It has good corrosion resistance to a wide variety of environments.

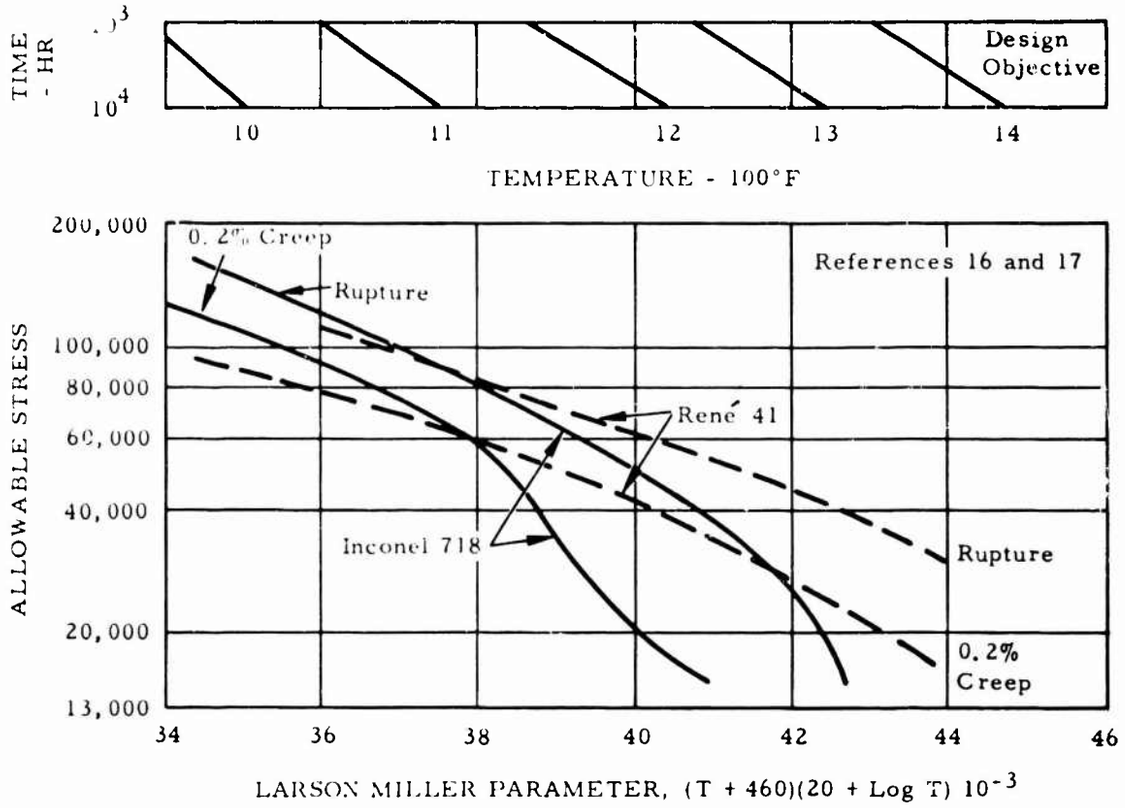

Figure 79. Two-Tenths Percent Creep and Creep Rupture Stress for High-Temperature Materials.

René 41 was also considered as a ducting material. It has excellent static strength and superior creep and rupture properties in the 1,200° to 1,400°F range (see Figures 78 and 79). It therefore offers excellent potential for further increase in Hot Cycle gas temperatures that may be encountered with more advanced engines in a future growth version without requiring any new advance in the materials state of the art.

René 41 is not as easily formed and fabricated as Inconel 718; therefore, it is not used in this aircraft. Both René 41 and Inconel 718 were very satisfactory when used as ducting materials on the XV-9A.

The Advanced Engine and Technology Department of General Electric Company is now developing a weldable nickel-base sheet alloy that has a yield strength of 150,000 psi and a stress rupture life of 1,000 hours at 75,000 psi, both at 1,400°F. These properties are comparable with those of René 41 at 1,400°F and provide another possible alloy for use in future growth versions of the CRA.

Comparison of strength versus density for Inconel 718 and René 41 at peak temperatures and for the calculated mean effective temperature for the 4,000-hour design aircraft operating life is shown in Table XXIV.

TABLE XXIV. COMPARISON OF STRUCTURAL MATERIALS FOR THE HOT GAS COMPONENTS

Material	Static Strength F_{tu}/w Peak duct wall temperature = 1090°F	Creep Strength F(0.2% creep)/w Duct wall temperature = 1063°F
René 41 w-0.278-lb/in.^{3}	523,500 in.	315,400 in.
Inconel 718 w-0.296-lb/in.^{3}	533,400 in.	405,400 in.

AEROELASTICITY AND DYNAMICS

Rotor/Wing Vibration and Flutter

Vibration and flutter calculations were made for both the helicopter and the airplane operating mode. The methods employed and the significant results for the final configuration are summarized below. The requirements of specifications MIL-A-8870 (ASG) and MIL-S-8698 (ASG) are met or exceeded for all components.

Method of Analysis

1. Helicopter Mode Structure

The dynamic model used for the helicopter mode represents one-third of the Rotor/Wing. It consists of a pair of beams with bending and torsional flexibility to represent the wing, and a single beam with bending and torsional flexibility to represent the blade. Concentrated masses and pitching inertias are located at twelve judiciously spaced stations. The model is connected to the fuselage in pitching and flapping by flexible pylon springs. The flexibility of the control system is introduced as a concentrated torsional spring between the blade and the wing.

Two different symmetry conditions were analyzed in the helicopter mode. In the first, called cyclic symmetry, the wing root was elastically restrained by the pylon springs in pitching and flapping, and vertical motion was rigidly restrained. In the second, called collective symmetry, the wing root was rigidly restrained in pitching and flapping; the vertical motion was restrained by a concentrated mass representing the fuselage.

2. Airplane Mode Structures

The left wing was analyzed in preference to the right wing in view of the adverse distribution of the center of gravity and elastic axis locations for the left wing.

The model consists of the same beams used in the model for the helicopter mode and an additional beam to represent the forward part of the wing. The Rotor/Wing is clamped in vertical translation to the fuselage at two locations. The Rotor/Wing is additionally connected to the fuselage at the hub by means of flexible pylon springs for pitch and roll and by a rigid link for vertical translation. The blade control system flexibility is locked out by a shear pin.

Three different symmetry conditions were analyzed in the airplane mode:

a. Clamped condition - all fuselage motions were rigidly restrained.
b. Symmetrical condition - fuselage was free in pitch and plunge but was rigidly restrained in roll; the right wing was assumed to be the mirror image of the left wing; the horizontal stabilizer was represented by a single elastic degree of freedom.
c. Antisymmetrical condition - fuselage was rigidly restrained in pitch and plunge but was free in roll; the right wing was assumed to be the mirror image of the left wing.

3. Aerodynamic Forces

Incompressible strip theory was used to represent aerodynamic forces at five spanwise stations. The center of pressure for each strip was assumed to be at the (local) quarter-chord position.

The formulas for aerodynamic forces in the hovering helicopter mode are built into the computer program used in the analysis. They include the effect of spanwise slope on the aerodynamic pitching velocity. The terms in the formulas for aerodynamic forces in the airplane mode were computed for an assumed sweepback angle equal to 30 degrees. They include the effect of spanwise slope on angle of attack. The effects of the Theodorsen lift deficiency function were treated in an approximate manner.

4. Helicopter Vibration Modes

Since the Rotor/Wing has three blades, the important resonances for cyclic modes are the second and fourth harmonics of rotor speed, and the important resonance for collective mode is the third harmonic of rotor speed.

From calculations, it can be seen that there are no resonances between vibration modes and these harmonics of rotor speed. For example, the second harmonic resonance of first cyclic flapping occurs at 60 percent of full rotor speed.

As a result of the absence of prominent resonance with the second, third, and fourth harmonics of rotor speed, the fuselage vibration level at the third harmonic rotor speed can be expected to be low.

The effect of fuselage response in pitch and roll on the lower Rotor/Wing vibration mode frequencies has been evaluated by the six-degree-of-freedom analysis. The frequencies of the vibration modes observed in the non-rotating coordinate system at full rotor speed are recorded in Table XXV. The absence of third harmonic resonance will be noted.

TABLE XXV. GYROSCOPICALLY COUPLED FUSELAGE-ROTOR VIBRATION

Mode	ω (rad/sec)	ω/Ω_o (cycles/rev)	Damping Ratio (Aerodynamic)
1	5.4	0.19	0.34
2	22.7	0.79	0.13
3	69.7	2.42	0.06
4	75.1	2.61	0.06
5	131.4	4.55	0.04

5. Flutter

Results of the hovering flutter analysis for cyclic and collective helicopter modes were presented in V-g curves (speed versus damping). A flutter speed margin of 40 percent above maximum operating speed is indicated in Figure 80 for the cyclic mode. Minor adjustments of the properties of the blade can be made to bring the collective mode flutter speed up to the

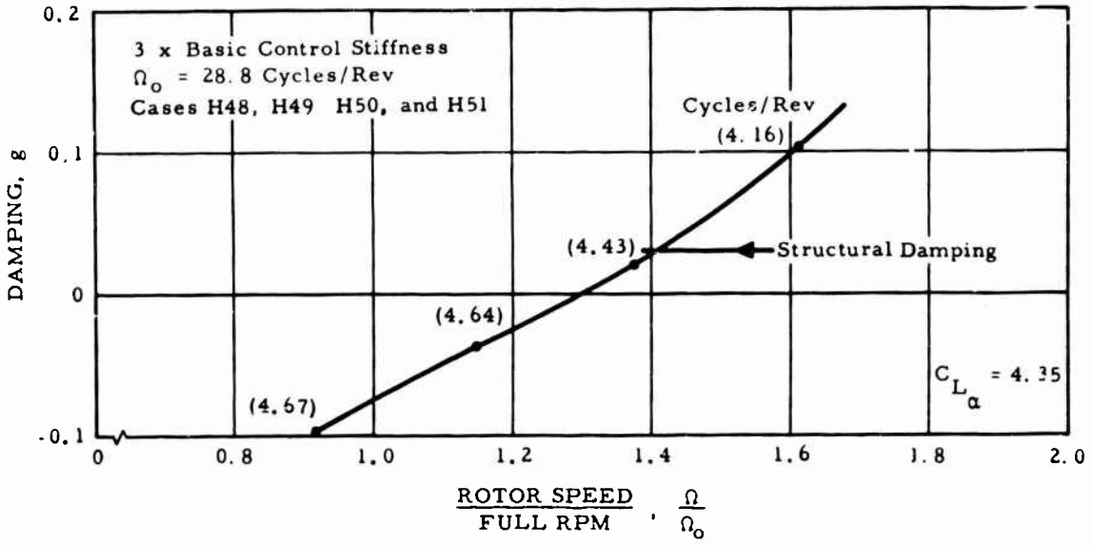

Figure 80. Helicopter Configuration Cyclic Symmetry, Critical Flutter Mode, 3 x Basic Control Stiffness.

same margin. In addition, it should be noted that test data presented in NACA TN 4005 indicate that no flutter will occur at a tip Mach number greater than 0.73. This tip Mach number is attained at less than the calculated (incompressible) flutter speed, indicating that no flutter should be encountered on this rotor. Dynamic model tests of full-scale Mach number are scheduled, and they are expected to confirm this conclusion.

The airplane flutter speed of 575 KIAS permits a V_L of 500 KIAS and a V_H of 450 KIAS in accordance with MIL-A-8860, paragraph 6.2.3.8. Thus, by means of a minor increase in load criteria, the 400 KIAS V_H value of the Rotor/Wing CRA could be raised to 450 KIAS.

The elastic axis and center of gravity of each blade are located near the midchord. This location is inherent in the Rotor/Wing concept in order to provide a reasonable symmetrical static aeroelastic configuration in the airplane mode. It also represents a compromise between flutter prevention requirements in the helicopter and airplane modes, since a location nearer the leading edge in the helicopter mode is nearer the trailing edge of the left wing in the airplane mode. For a conventional helicopter blade, or even for a conventional airplane wing, a midchord location of the center of gravity would be regarded as quite unfavorable from the flutter viewpoint. Its effects are mitigated for the Rotor/Wing configuration by the relatively thick airfoils, short movable blade span, and generally rugged construction.

The type of flutter that has been observed in the analyses of both operating modes is a simple binary flutter in which the frequency of the lowest torsion mode is depressed downward toward coalescence with the first bending mode. In the airplane configuration, sweepback accentuates the tendency toward flutter by increasing the frequency of the first bending mode with airspeed. This type of flutter is avoided in the helicopter mode by maintaining a sufficiently high stiffness in the control system. It is avoided in the airplane mode by maintaining midchord positions for the center of gravity and elastic axes on both wings and by providing sufficient torsional stiffness.

6. Divergence in the Autogyro Mode During Conversion

As the Rotor/Wing is slowed to zero rpm during conversion to the airplane mode, it becomes subject to static aeroelastic divergence. The most critical condition occurs for each blade when it is near the 240-degree-azimuth position. A calculation of divergence speed has been made using the two lowest cyclic modes (first flapping and first torsion) as degrees of freedom in a coupled analysis. The calculated divergence speed is 342 knots -- well above the operating forward speed range during conversion.

Tail Surface Flutter and Divergence Analysis

As seen in Table XXVI, the tail surfaces have flutter and divergence speeds substantially in excess of the margin required by MIL-A-8870 (ASG) (that is, 1.15 V_L).

TABLE XXVI. TAIL SURFACE FLUTTER AND DIVERGENCE.

Surface	U_F (kn)	$\frac{U_F}{V_L}$	U_D (kn)	$\frac{U_D}{V_L}$
Elevon	700	1.40	925	1.85
Vertical Fin	760	1.52	>760	>1.52

Note: V_L = 500 knots

Because of the conservatism in the calculation (neglect of structural damping and finite aspect ratio effects) and the more than adequate margin indicated, it is concluded that the straightforward, uncoupled analysis is sufficient substantiation of freedom from flutter and divergence of the tail surface.

SUMMARY OF THE PRELIMINARY STRUCTURAL ANALYSIS

A comprehensive preliminary structural analysis was conducted covering the primary structural components of the CRA. A general discussion of the major structural areas follows.

Rotor/Wing Blade

The arrangement of the Rotor/Wing blade structure is shown in Figure 81. The critical loading for the blade occurs in the helicopter mode of operation. The fatigue case designs most of the structure, and the 3-g helicopter maneuver gives more critical static loads than the 4.5-g airplane case. This is because the entire lift in the helicopter mode is centered outboard of the wing, entirely on the blades, while in the airplane mode the lift is applied almost entirely on the delta planform. The loading is given in Figures 82 through 85.

Aluminum alloy is used for the leading and trailing sections of the blade. Titanium alloy (alternate, maraging stainless steel) is used where temperature considerations preclude the use of aluminum and where fatigue strength is the prime consideration, as in the main spars and the feathering torque tube.

Wherever the analysis has shown fatigue strength to be a consideration, particular attention is to be given to the fabrication techniques employed. The intent is to improve fatigue strength by use of such techniques as: shot peening or prestressing of holes, adequate clamping preload of the fasteners, and use of adhesive bonding to prevent fretting. The resulting improvement in allowables will enhance service life and reliability.

Two pages showing a summary of stress levels in the blade follow the loading curves. These stress levels are in line with those in general use in the helicopter industry.

Wing

The critical loading for the wing occurs in the helicopter mode of operation. The fatigue case designs most of the structure, and the 3-g

helicopter maneuver gives more critical static loads than the 4.5-g airplane maneuver, because again the entire lift in the helicopter mode is centered on the blades outboard of the wing.

Design and analysis considerations are similar to those for the blades. The choice of materials, the design, and the fabrication techniques are such as to provide a maximum of safety, reliability, and service life.

A sketch of the primary wing structure is shown in Figure 81. This structure consists of three pairs of box beams that carry the shears, bending, and torsion loads to a central hub made up of three main ribs, which in turn transfer the loads to the Rotor/Wing mount. Preliminary structural analysis data for the wing is given in Appendix IV.

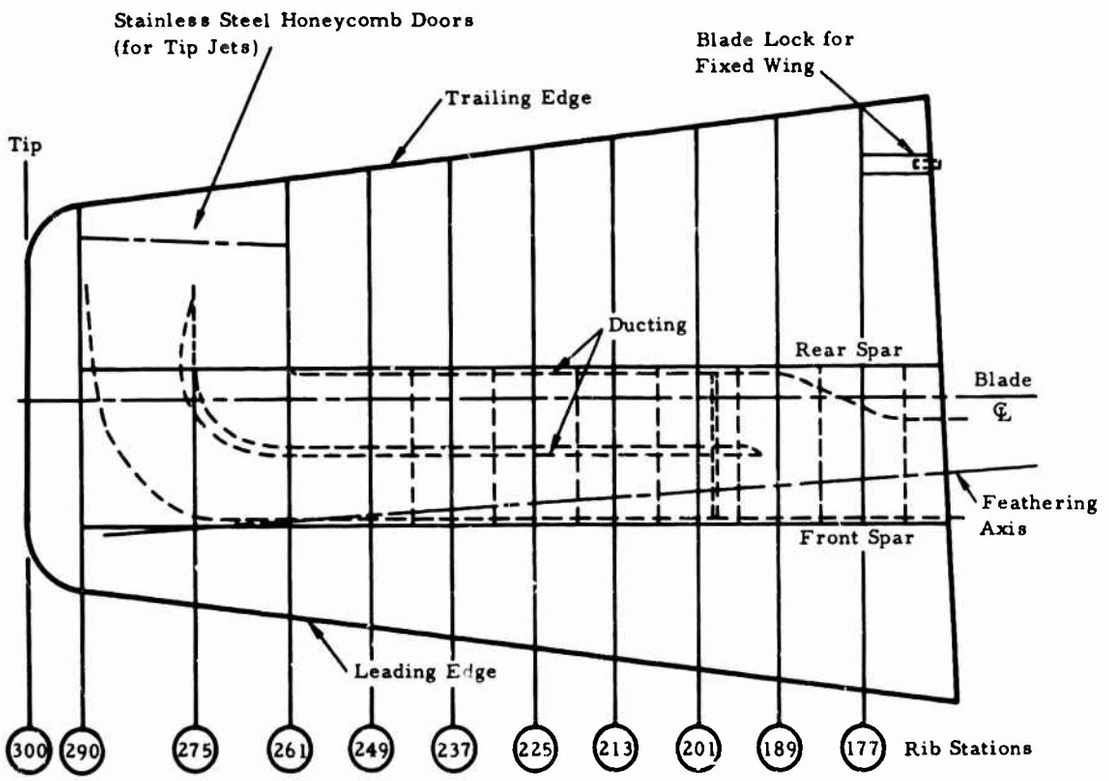

Figure 81. Rotor/Wing Blade Structure.

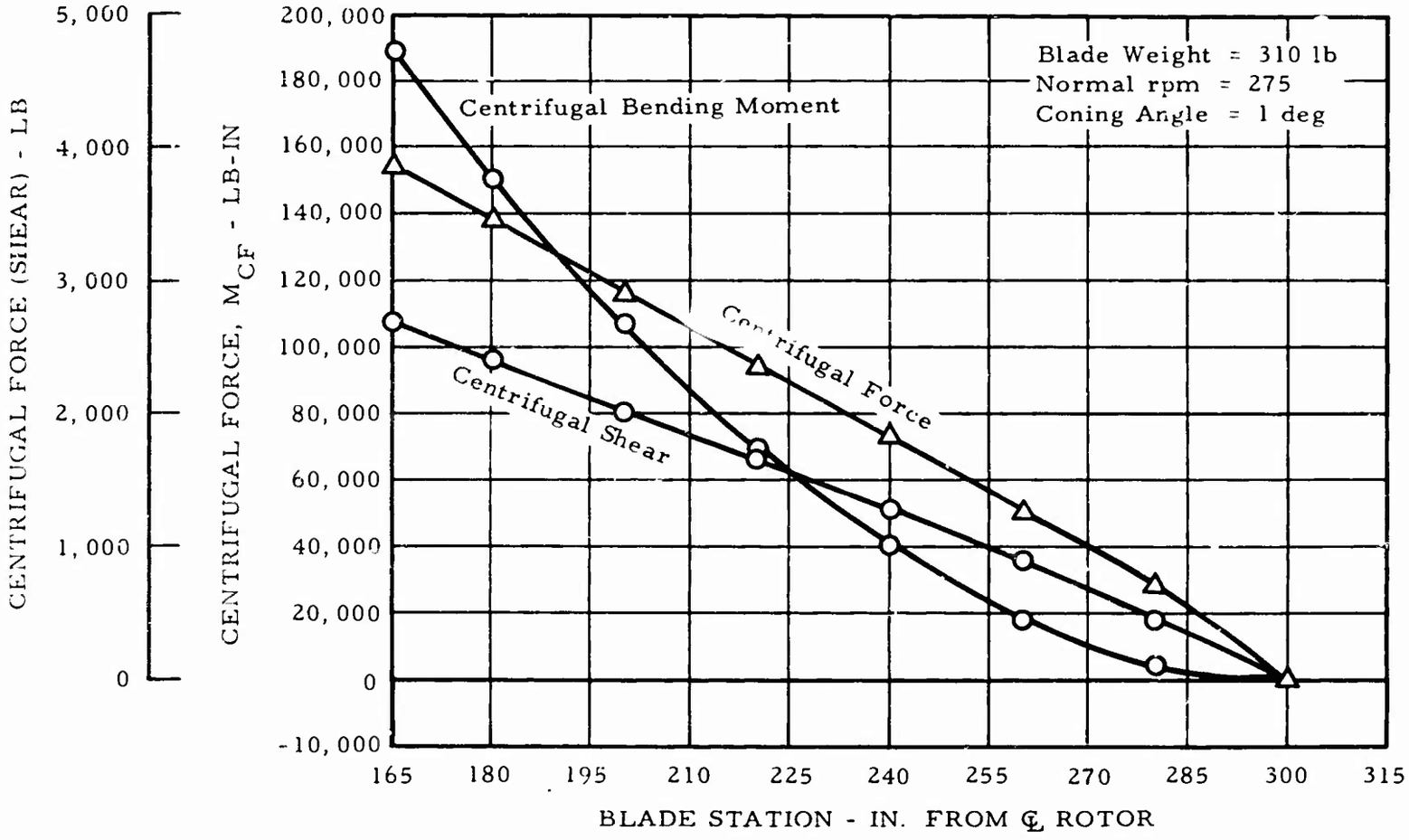

Figure 82. Blade Centrifugal Loading.

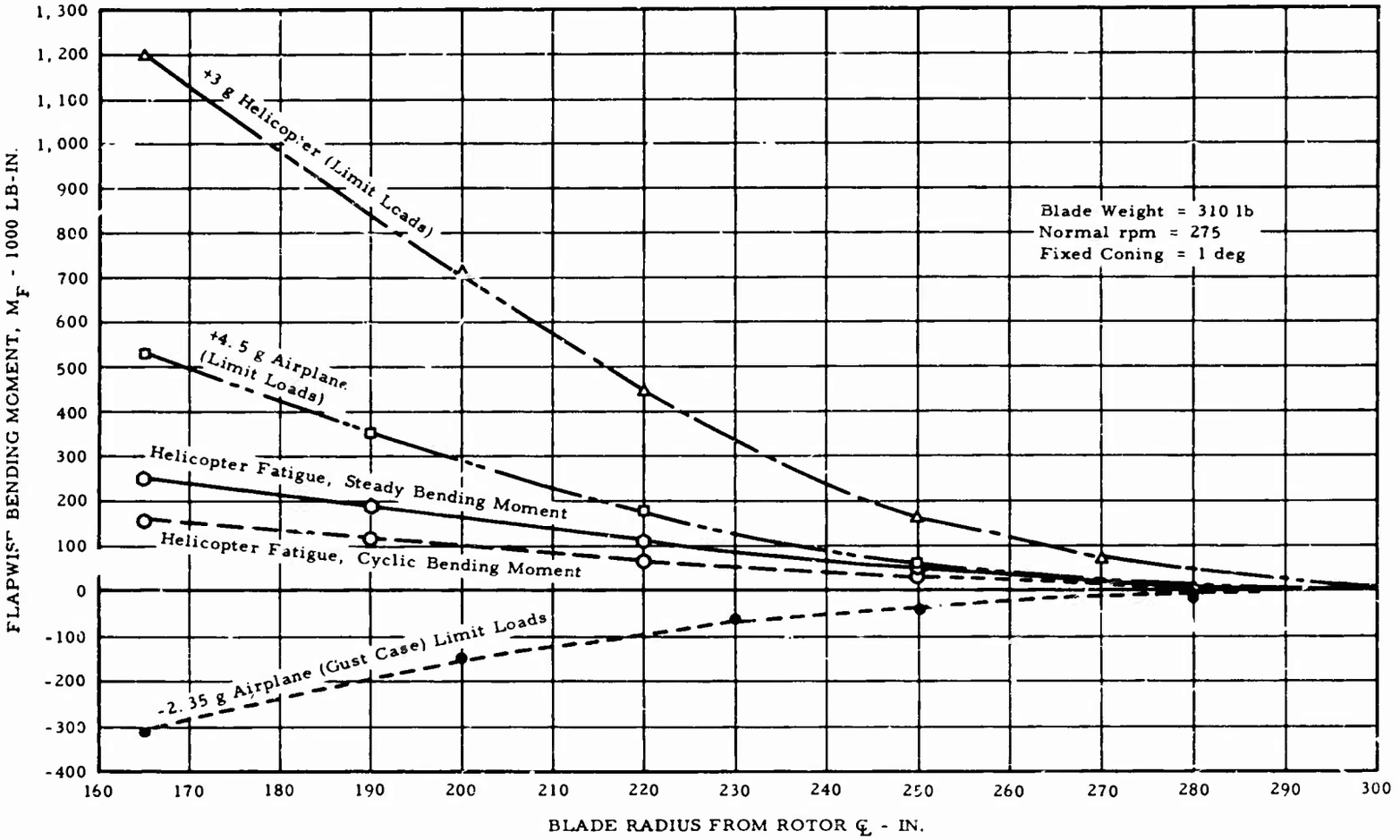

Figure 83. Blade Limit Loads, Flapwise Bending Moments.

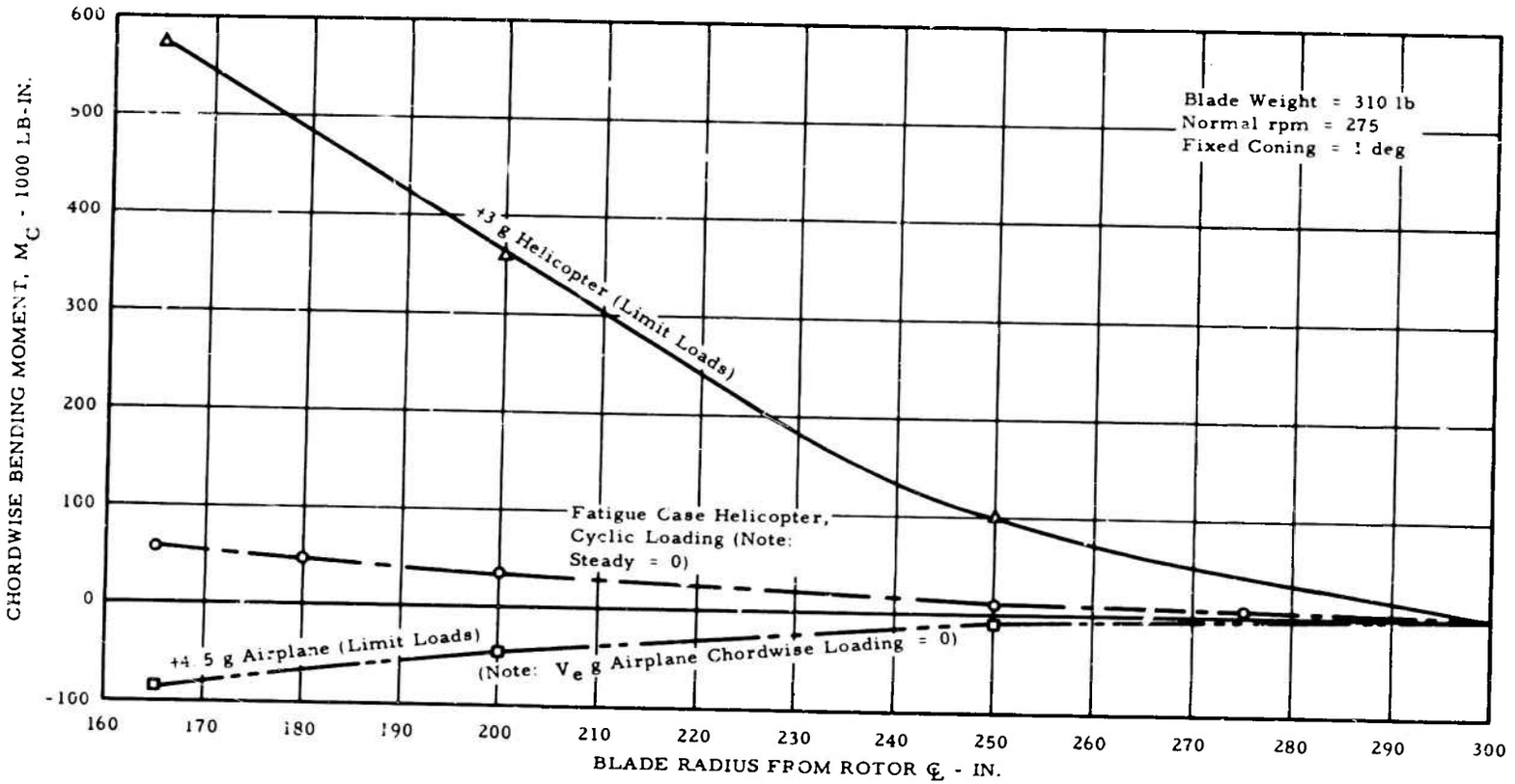

Figure 84. Blade Limit Loads, Chordwise Bending Moments.

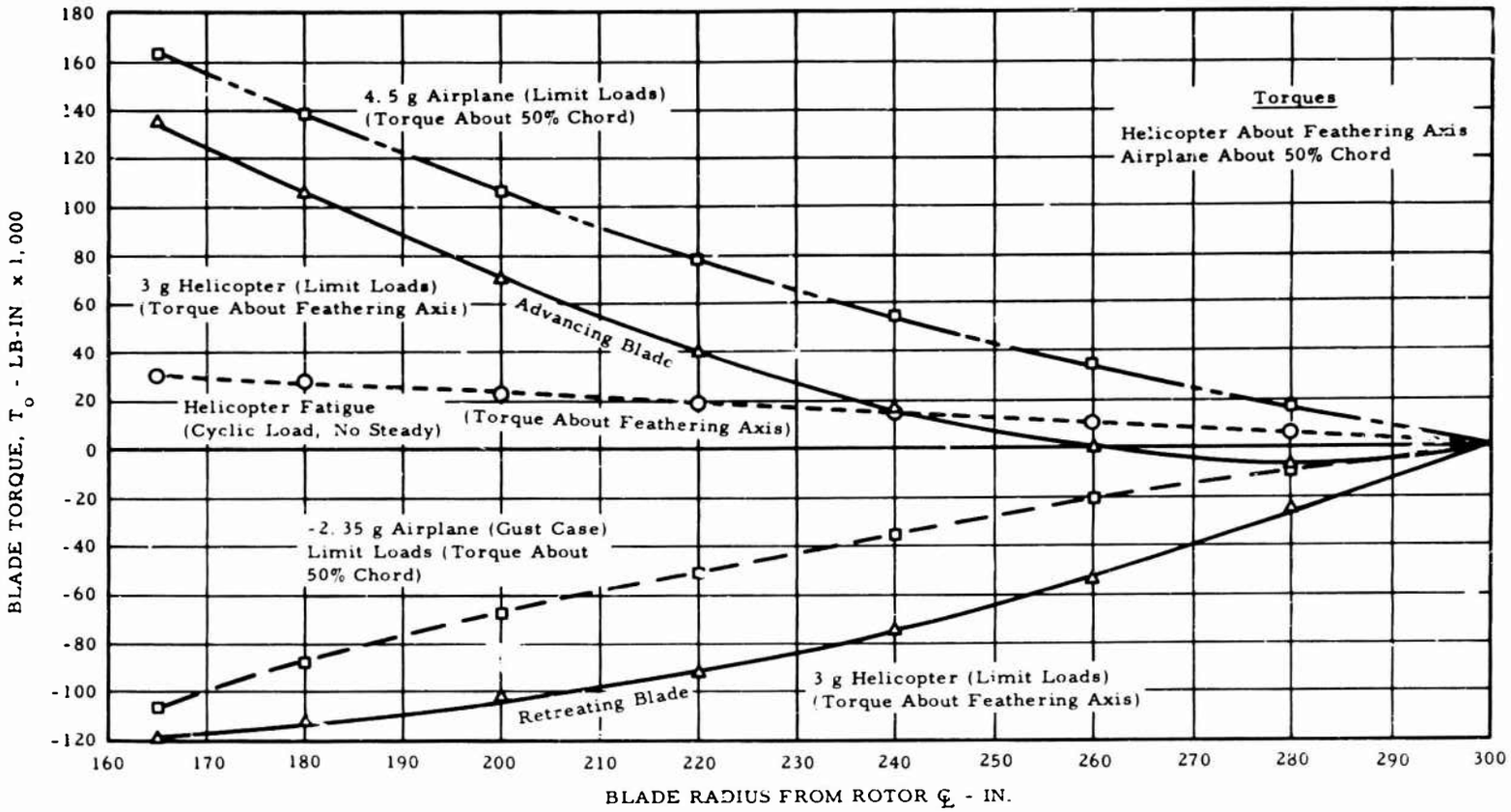

Figure 85. Blade Limit Loads, Torque Loads.

THERMAL STRESS ANALYSIS

The following paragraphs present more detailed information on the thermal stress analysis. Areas covered are as follows:

1. Ducting
2. Engine exhaust tail pipe
3. Diverter valve and hot gas distributor
4. Primary structure adjacent to the hot gas ducting
5. Insulation
6. Isolation of thermal strains and minimization for temperature differential stresses

Duct Calculations

The overall vehicle design service life objective for the Hot Cycle propulsion system and structural components used in the C-7A is 4,000 hours.

The ducting system used for the helicopter mode begins at the diverter valve exit and continues through the hub, wing, and blades. These hot gas components are conservatively designed for a minimum life of 1,000 hours, which permits 25 percent of the total aircraft life to be used in the helicopter mode, based on the following temperature and pressure conditions (Table XXVII).

TABLE XXVII. TEMPERATURE AND PRESSURE SPECTRUM FOR HUB, WING, AND BLADE HOT GAS DUCTING - HELICOPTER MODE

Item	Peak Values (for static strength check only)	1,000 Hour Military Power	Spectrum Normal Rated Power
Hours	-	400	600
Gas temperature, °F	1,190	1,190	1,070
Pressure, psig	29.4	26.5	22.8

The engine exhaust tail pipe used for the airplane mode is designed for a conservative minimum life of 3,500 hours or 87-1/2 percent of the total design vehicle life for the following temperature and pressure conditions (Table XXVIII).

TABLE XXVIII. TEMPERATURE AND PRESSURE SPECTRUM FOR ENGINE EXHAUST TAIL PIPE - AIRPLANE MODE

Item	Peak Values (for static strength check only)	Military Power	Normal Rated Power
Hours	-	100	3,400
Gas temperature, °F	1,190	1,190	1,070
Pressure, psig	50.0*	34.3	29.4

*Conservatively includes dive speed dynamic pressure increase.

Wing Ducting Calculations

Sample calculations for 9-1/2-inch-diameter wing ducting follow:

1. Material is Inconel 718 (see Materials and Allowable Stresses Section)

   Peak gas temperature = 1,190°F and pressure = 29.4 psig

   Duct wall temperature = 1,090°F

   F_{tu} at 1,090°F = 154,000 psi

   $$F_t = \frac{PR}{t}$$

   $$\therefore \quad t \text{ (duct wall thickness)} = \frac{(29.4 \text{ psig})(1.33)(1.5)(4.75 \text{ in.})}{154,000 \text{ psi}}$$

   $$= 0.00182 \text{ in.}$$

2. Long-time equivalent gas temperature (based on Larson-Miller curves included in the Materials and Allowable Stresses Section) = 1, 160°F and pressure = 26. 5 psig

Duct wall temperature = 1, 064°F

0. 2 percent creep allowable = 109, 000 psi

$$F_t = \frac{PR}{t}$$

$$\therefore \quad t \text{ (duct wall thickness)} = \frac{(26.5 \text{ psig})(4.75 \text{ in.})}{109,000 \text{ psi}}$$

$$= 0.00117 \text{ in.}$$

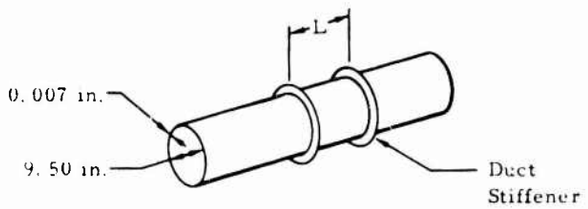

3. Sample calculation for wing duct stiffeners required for a 5-psi negative internal pressure due to autorotation:

$$f_c = \frac{PR}{t} = 3,400 \text{ psi}$$

$$F_{c_{cr}} = \frac{Ky^2 E}{12(1 - \nu_e^2)} \left(\frac{t}{L}\right)^2$$

where:

f_c	= compressive stress	P	= -5 psi
$F_{c_{cr}}$	= critical compressive stress	E	= 25 x 10^6psi at 1, 090°F
t	= 0. 007 in.	L	= stiffener spacing
R	= 4. 75 in.	Ky	= 16
ν_e	= 0. 3		

From this L = 2. 3 in. ; but L is increased to 3 inches to account for the fixity resulting from the continuity of the duct past the stiffener rings.

Ring stiffener at 3-in. spacing

$p' = 3 \text{ in.} \times (-5 \text{ psi}) = -15 \text{ lb/in.}$

$$p' = \frac{5EI}{R^3}$$

$I = 21.4 \times 10^{-6} \text{ in.}^4$ required

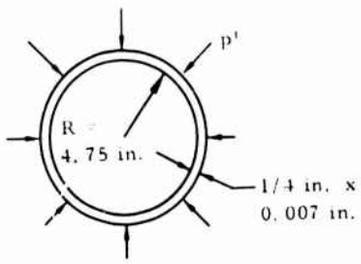

Engine Exhaust Tail Pipe Calculation

1. Material is Inconel 718 (see Materials and Allowable Stresses Section)

   Peak gas temperature = 1,190°F and pressure = 50.0 psig (Reference Table XXVIII) Note: Ram pressure adds during airplane mode.

   Duct wall temperature = 1,090°F

   F_{tu} at 1,090°F = 154,000 psi

   $$F_t = \frac{PR}{t}$$

   $$\therefore \quad t \text{ (duct wall thickness)} = \frac{(50.0 \text{ psig})(1.33)(1.5)(11.0 \text{ in.})}{154,000 \text{ psi}}$$

   $$= 0.0072 \text{ in.}$$

2. Long-time equivalent gas temperature (based on Larson-Miller curves included in Materials and Allowable Stresses Section) = 1,090°F and pressure = 34.3 psig

   Duct wall temperature = 999°F

   0.2 percent creep allowable = 120,000 psi

   $$F_t = \frac{PR}{t}$$

   $$\therefore \quad t \text{ (duct wall thickness)} = \frac{(34.3 \text{ psig})(11.0 \text{ in.})}{120,000 \text{ psi}}$$

   $$= 0.00315 \text{ in.}$$

Calculation for Diverter Valve and Hot Gas Distributor

Material is Inconel 718 (see Materials and Allowable Stresses Section).

1. Hoop tension in Rotor/Wing hot gas distributor. Peak gas temperature = 1,190°F and pressure = 29.4 psig

   Duct wall temperature = 1,090°F

   F_{tu} at 1,090°F = 154,000 psi

   t = Thickness required for hoop tension stresses

   a. Spherical end $F_t = \frac{PR}{2t}$

   $$\therefore \quad t \text{ (duct wall thickness)} = \frac{(29.4 \text{ psig})(1.33)(1.5)(19 \text{ in.})}{154{,}000 \text{ psi} \times 2}$$

   $$= 0.0036 \text{ in.}$$

   b. Cylinder $F_t = \frac{PR}{t}$

   $$\therefore \quad t \text{ (duct wall thickness)} = \frac{(29.4 \text{ psig})(1.33)(1.5)(12 \text{ in.})}{154{,}000 \text{ psi}}$$

   $$= 0.0046 \text{ in.}$$

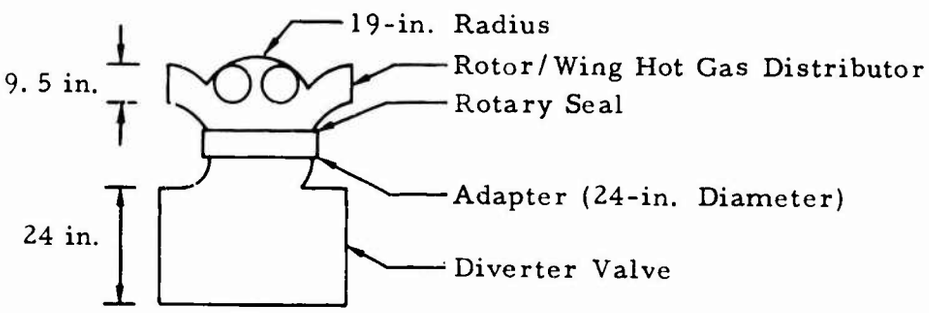

2. Hoop tension stress in diverter valve.

Peak gas temperature = 1,190°F = 50.0 psig
(Reference Table XXVII)

Diverter wall temperature = 1,090°F

$$F_t = \frac{PR}{t}$$

$$\therefore \text{ t (duct wall thickness)} = \frac{(50.0 \text{ psig})(1.33)(1.5)(12 \text{ in.})}{154,000 \text{ psi}}$$

$$= 0.0078 \text{ in.}$$

The long-time temperature and pressure condition does not design the duct thickness, as previously shown for the wing ducting.

Adjacent Primary Structure

The hot gas ducting system is routed through the fuselage, the hub, the wing, and the blade. This requires that the primary structure in these areas be adequately protected from the heat of the hot gas system, so that the structural materials do not suffer loss of strength, undesirable metallurgical changes, or detrimental thermal stresses. The routing of the hot gas system in the CRA is quite similar to the very satisfactory system in the XV-9A; therefore, it requires temperature protection for very similar conditions. The hot gas ducting system is isolated and separated from the primary structure, thus permitting insulation to reduce the temperature of the structure. In the fuselage, hub, wing, and blade, cooling air is also circulated to prevent local temperature buildup. In the blade and the wing, shielding is also employed to reduce heating of the primary structure by radiation. The shielding also prevents the impingement of any hot gas on the structure in the event of a gas leak. All expected temperatures are well within the tolerance limits of the titanium alloy and steel materials to be used for adjacent primary structures. The maximum temperature expected in areas of aluminum alloy structures is 200°F.

Sample Calculation of Rotor/Wing Blade Rib Thermal Stresses

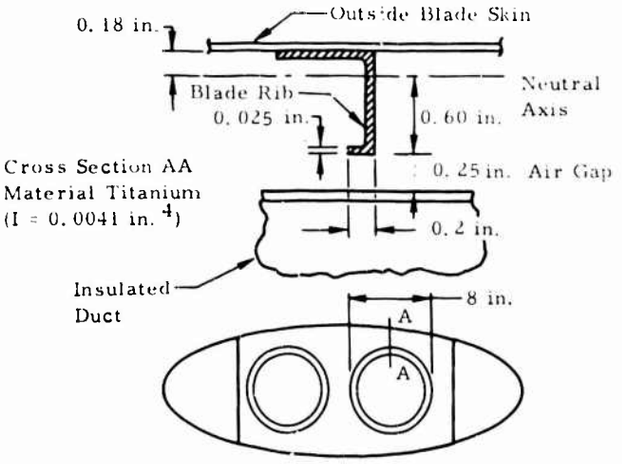

Typical Cross Section Through Rotor/Wing Blade

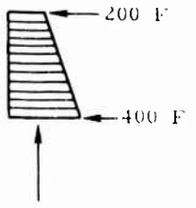

Expected Temperature Gradient for Uninsulated Rotor/Wing Blade Rib Based on XV-9A Test Data

Element	Dimensions (in.)	(Area) A (in.^{2})	Δt (° F)	α x 10^6 (in./in. ° F)	E x 10^6 (lb/in.^{2})	f = αΔtE (lb/in.^{2})	f x A (lb)	f (net psi)
1	0.175 x 0.025	0.0044	330	7.1	15.0	25250	110.00	-11100
2	0.75 x 0.025	0.0188	250	5.0	15.5	19400	365.0	- 5250
3	0.75 x 0.50	0.0375	130	4.9	16.0	10200	382.00	3950
		0.0607					858.00	
Therefore, $\frac{858.00}{0.0607}$ = 14,150 psi								

Rib Cross Section AA (thermal and air load bending stresses add at the center)

Air load = 3 psi

w = 3 psi x 6 in. Rib spacing x 1-1/2 = 27.0 lb/in.

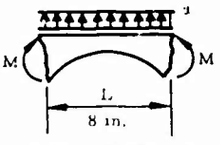

Rib at Duct Cutout

$$M = \frac{wL^2}{12} = \frac{27.0 \text{ lb/in. } (8 \text{ in.})^2}{12} = 149 \text{ in./lb}$$

$$f_b \text{ air load} = \frac{Mc}{I} = \frac{149 \text{ in./lb } (0.60 \text{ in.})}{0.0041 \text{ in.}^4} = 21,800 \text{ psi}$$

$$f_b \text{ air load} + f_{thermal} = -21,800 - 11,100 = 32,900 \text{ psi}$$

F_{cr} = 126,000 psi allowable; therefore, margin of safety = high.

Insulation

The complete ducting system is insulated to prevent excessive heating of the adjacent primary structure. The effectiveness of the duct insulation can be shown by the experience on the XV-9A, where the only elevated temperature protection of the fuselage from the yaw duct system was the duct insulation and some cooling air. The highest peak temperature measured on a fuselage frame where the duct passed through was 214°F. This is well within the allowable temperature for aluminum.

The diverter valve, hot gas distributor, wing and blade ducting, and tail pipe are insulated to reduce the heat flux.

Isolation of Thermal Strains

The hot gas system is structurally isolated from the aircraft structure in a manner similar to the conventional mounting of jet engines, as shown in the following sketch. This mounting allows the duct to grow as a result of elevated temperatures without restraint diametrically or longitudinally. This same mounting arrangement also isolates structural strains from the hot gas ducting system.

The flexible bellows that divide the ducting system into appropriate lengths likewise perform a dual function: they isolate the thermal strains from the primary structure and also prevent the structural strains from loading the hot gas system.

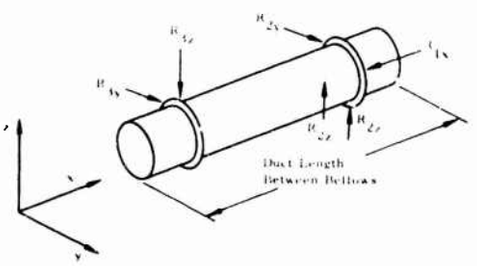

Typical Six-Component Duct Mounting

Minimization for Temperature Differential Stresses in the Hot Structure

The ducting is insulated in order to reduce both maximum and differential temperatures in the colder primary structure. Isolation of the hot ducting from the structure also aids in lowering the temperature differential in the cold structure, since almost no heat is then transferred by conduction. Also, cooling airflow is provided from the fuselage through the hub and on into the wing and blade. In the wing and blade, the top and bottom panels of

the bay containing the ducting are single-thickness skin panels. The areas of these skin panels are approximately equal to the circumferential area of the ducts, thus providing an efficient path for whatever heat passes through the duct insulation to escape to the outside, and reducing temperature buildup in the structure.

A light titanium shield is provided for the spar webs in both the blade and the wing, in order to prevent a high temperature gradient from developing between the center of the spar web and the outside of the wing or blade. Also, the structural materials are arranged so that the areas of highest temperature rise during operation are of a material (steel or titanium alloy) having the lowest coefficient of thermal expansion, and the areas of least temperature rise are of a material (aluminum alloy) having the highest coefficient of thermal expansion.

With the duct insulation and the shielding of the primary structure, detrimental thermal gradients in the primary structure are eliminated. The highest predicted temperature in the blade structure is 300°F; in the wing structure, 200°F.

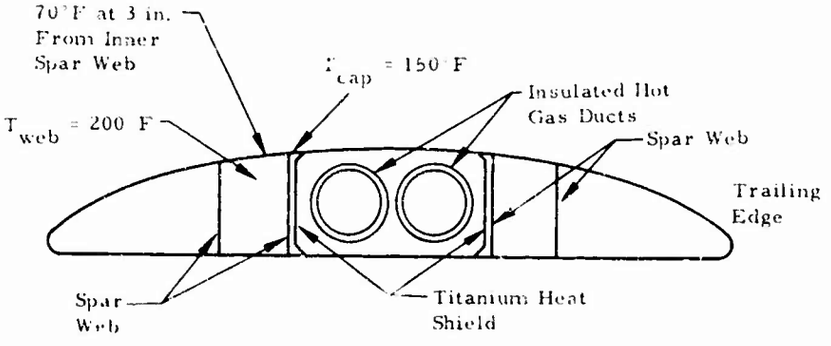

Typical Wing Cross Section

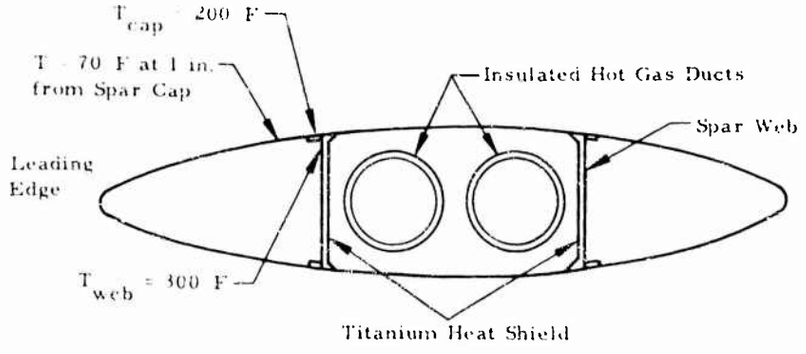

Typical Blade Cross Section

PROPULSION SYSTEM

The design of the propulsion system provides for operation of the Hot Cycle Rotor/Wing CRA as a high-speed VTOL airplane. Primary design emphasis is placed on simplicity, reliability, and safety in an easily maintainable single-engine installation. These factors are inherent in the Hot Cycle propulsion system and are used to their full advantage. During the autogyro and airplane modes, as depicted in Figure 2, the engine thrust is used in the normal manner. In the helicopter mode shown in Figure 2, high energy gas is diverted from the engine exhaust up through the hub to the tip of each blade, where it is exhausted to drive the Rotor/Wing.

DESIGN CHARACTERISTICS

The primary advantage of the Hot Cycle propulsion system is its simplicity, with the resulting advantages of light weight and reliability gained by the elimination of many heavy and complex dynamic components required by other types of propulsion systems. The weight savings obtained from this design concept are reflected not only in the propulsion system but throughout the aircraft. The increased reliability achieved is an equally outstanding feature of the Hot Cycle system. Materials and fabrication methods are fully understood and, in general, follow jet-engine technology.

ENGINE INSTALLATION

The J52-P-8A engine (Figure 86) is located below the wing and above the cargo compartment, just forward of the rotor centerline, and is mounted to the fuselage through truss members. The engine is readily accessible for inspection and maintenance from stowable platforms that attach to the side of the fuselage. The engine removal and installation procedure is shown in Figure 87.

AIR INDUCTION SYSTEM

The engine air induction system (see Figure 88) has been designed to give maximum pressure recovery and minimal flow distortion in all modes of flight. For helicopter operation, a bellmouth on the engine draws air directly from the area beneath the Rotor/Wing. This inlet location assures maximum protection from the recirculation of debris during operation in unprepared areas. For airplane flight, the inlet duct is raised to

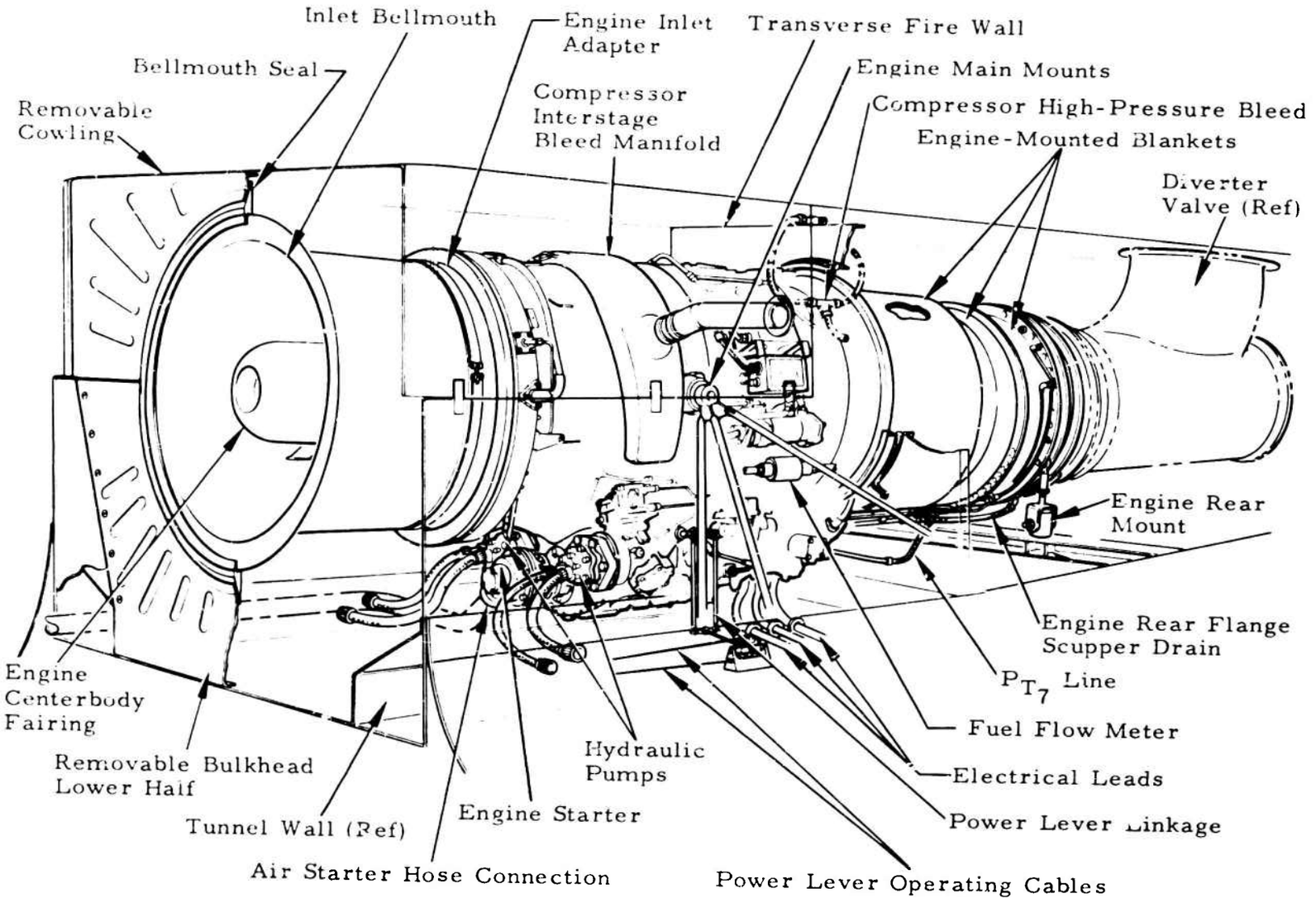

Figure 86. Engine Installed.

provide a smooth, gradual diffusion passage from the duct inlet above and behind the cockpit to the bellmouth entry on the engine. Conversion is made smoothly from one flight mode to another without detrimental effect on engine operation. The inlet duct also provides a smooth external aerodynamic fairing between the rotor and the fuselage.

HOT GAS DUCT SYSTEM

The knowledge and experience gained from the successful XV-9A Hot Cycle Program have been utilized in the design of the Rotor/Wing hot gas system. Additional factors of safety have been applied to the design of all pressurized hot gas ducting, and only materials having excellent corrosion resistance and crack-propagation resistance are used. Isolation of both thermal and structural strains is provided in the design of the hot gas ducting system, through proper design of mounts, reinforcements, and flexible joints. The surrounding primary structure of the vehicle is both shielded and designed to continue safe flight and landing even in the unlikely event of exposure to massive quantities of the hot gases. In addition to the isolation of both hot and cold components from a structural viewpoint, insulation, cooling airflow, and shielding minimize any possible detrimental effects from the interaction of the hot and cold components. Further, thermal differential expansion in the primary structure is minimized by using materials having similar thermal expansion rates. Transient thermal effects in the hot gas system are minimized by detail design to assure even heat-up and cool-down of the components. The materials used in the hot components are standard production materials that have wide usage in the jet engine industry and do not require the development of new technology.

The diverter valve located immediately aft of the engine directs the gas up through the rotor for helicopter operation or through the tail pipe and thrust nozzle for autogyro and airplane modes. A slip joint between the engine and diverter valve provides for sealing and thermal expansion. A seal above the diverter valve permits rotation between the stationary duct and its counterpart in the rotating system. As it emerges from the hub, the gas flows into three separate pairs of parallel ducts (separated to provide the necessary clearance for the blade retention straps) and then is routed through the wing to each blade. Each pair of ducts combines into one single duct in order to pass through the torque shaft into the blade. In the blade the gas is again routed through paired, separate ducts, turned 90 degrees, and ejected at the trailing edge of the blade. All the ducts are insulated to reduce heat flux; bellows are utilized to allow for thermal expansion; and seals at the blade root are installed to permit rotation for blade feathering.

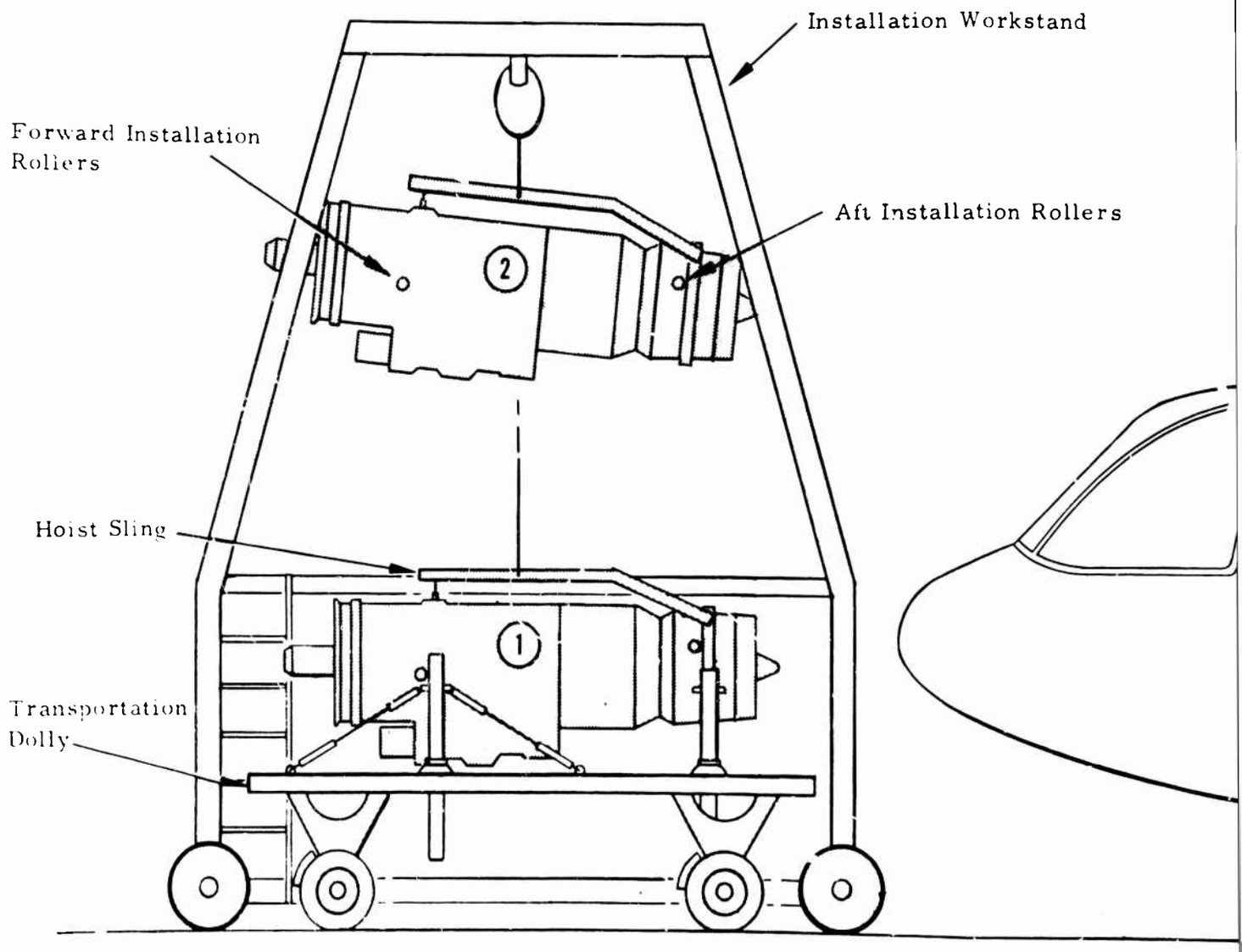

Figure 87. Engine Installation Procedure.

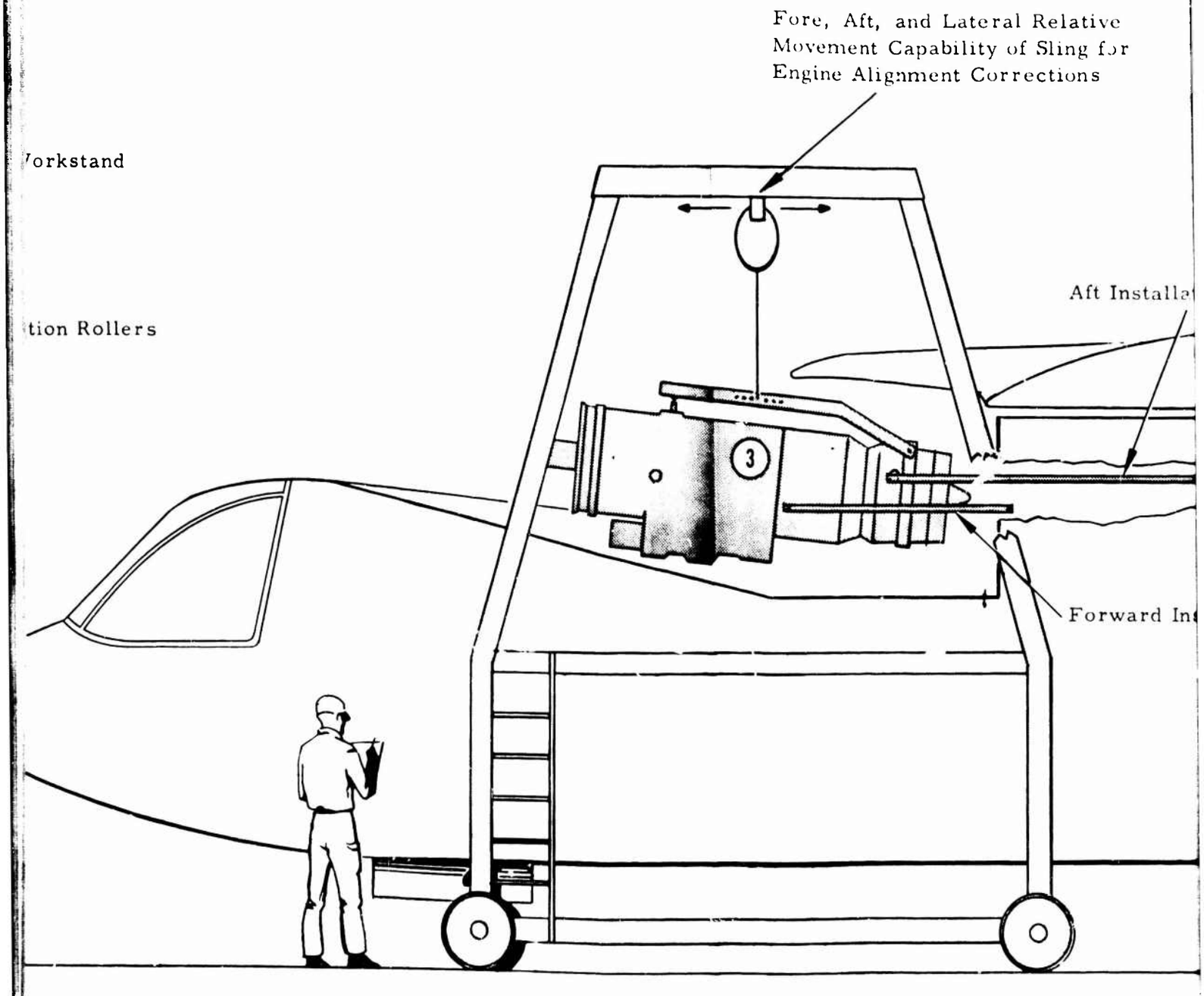

Workstand

tion Rollers

B

al Relative
of Sling for
rections

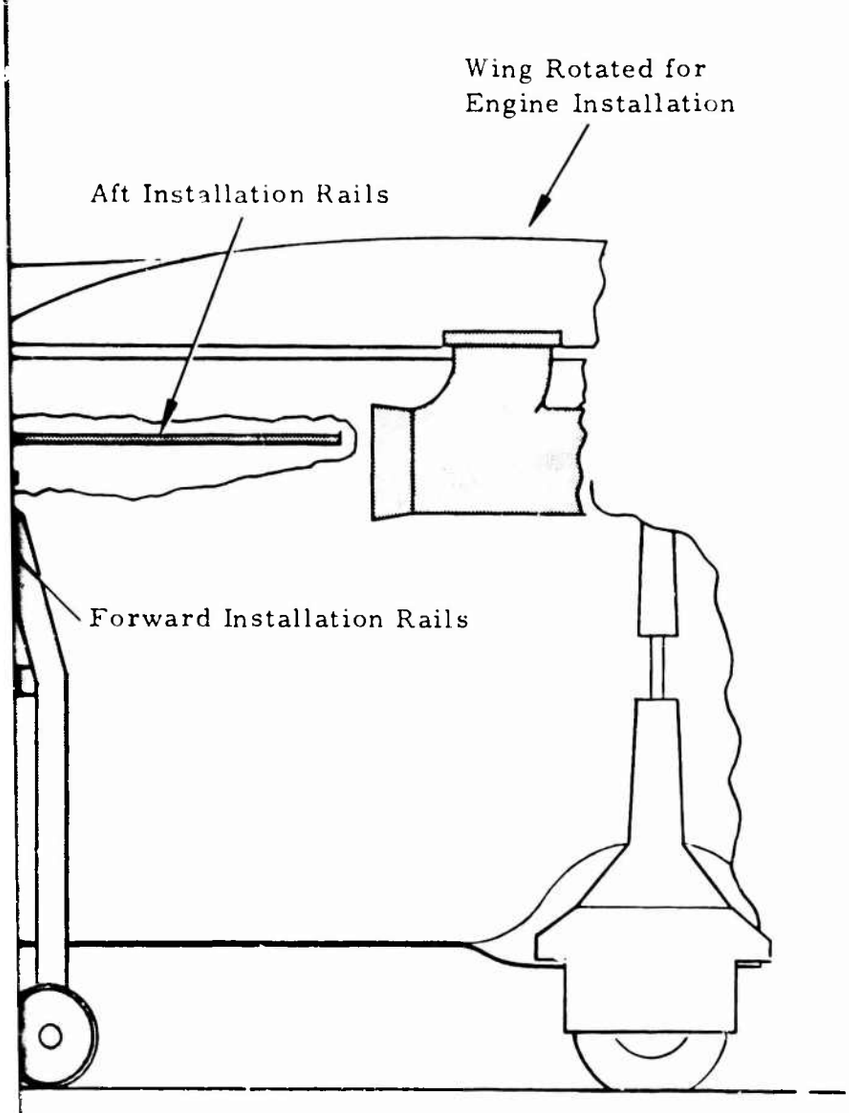

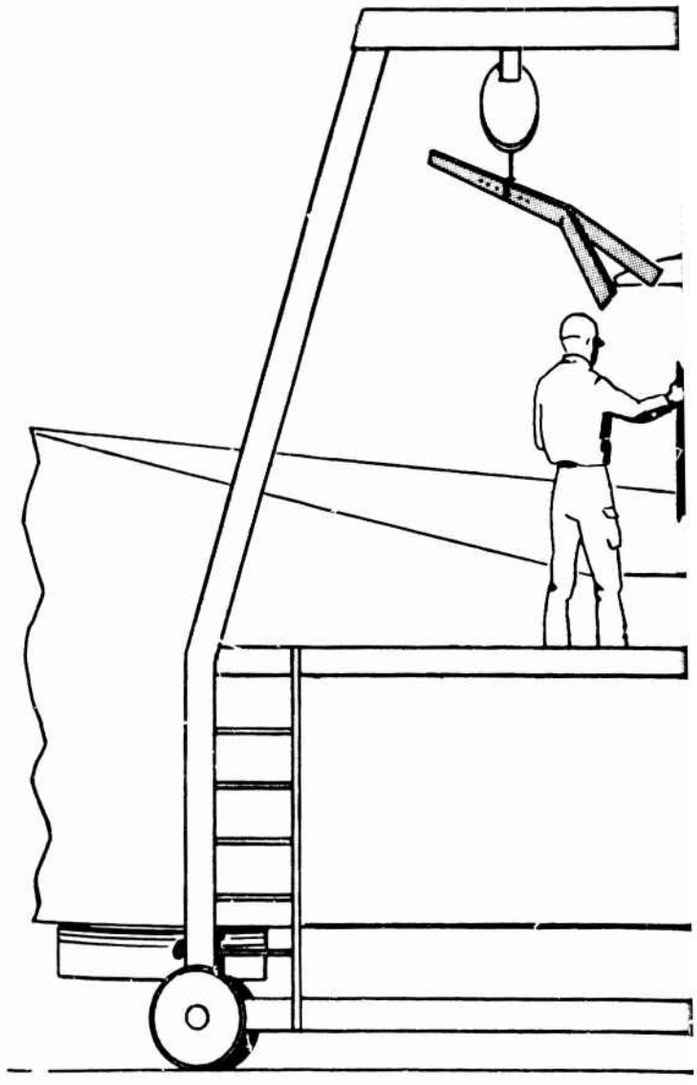

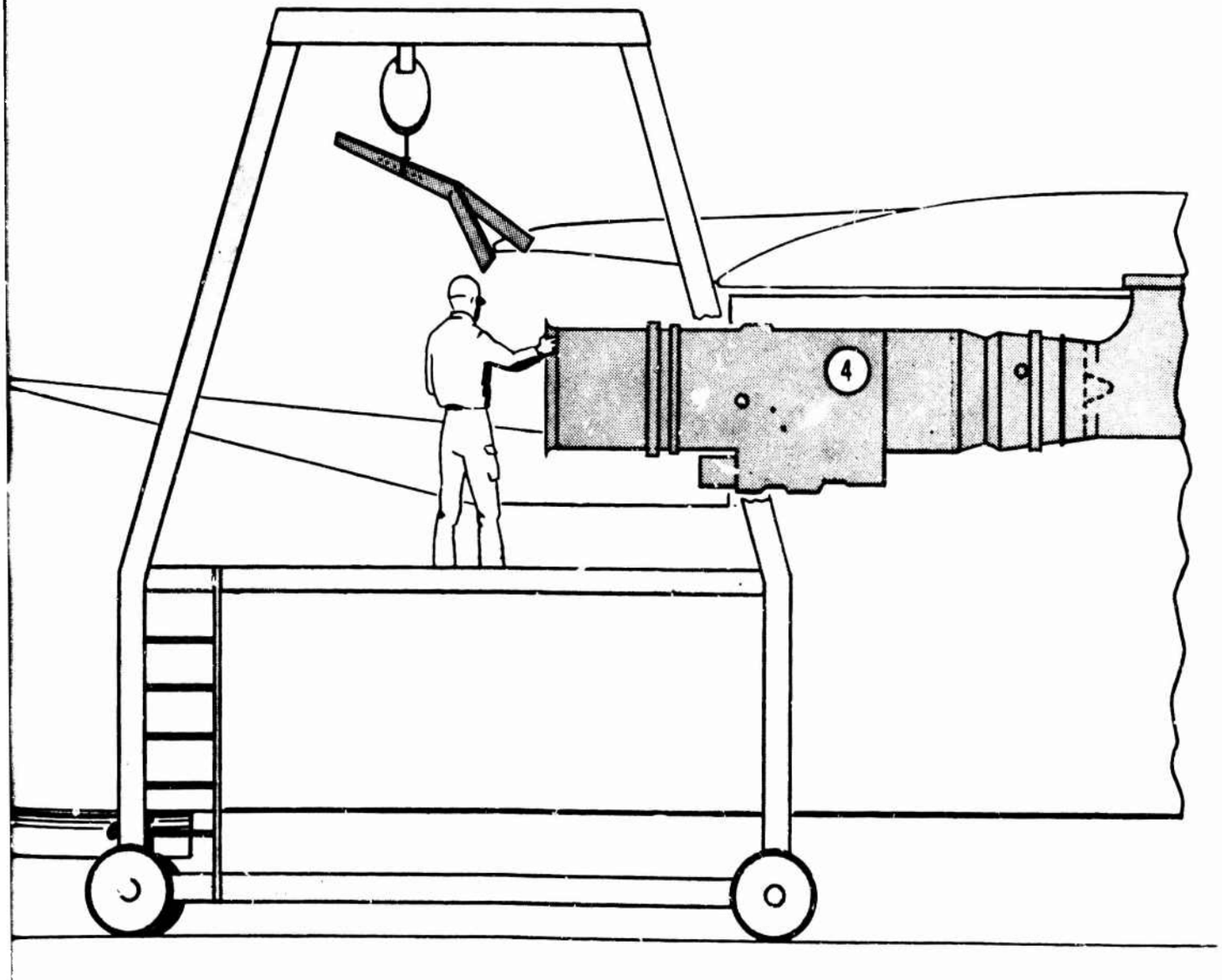

D

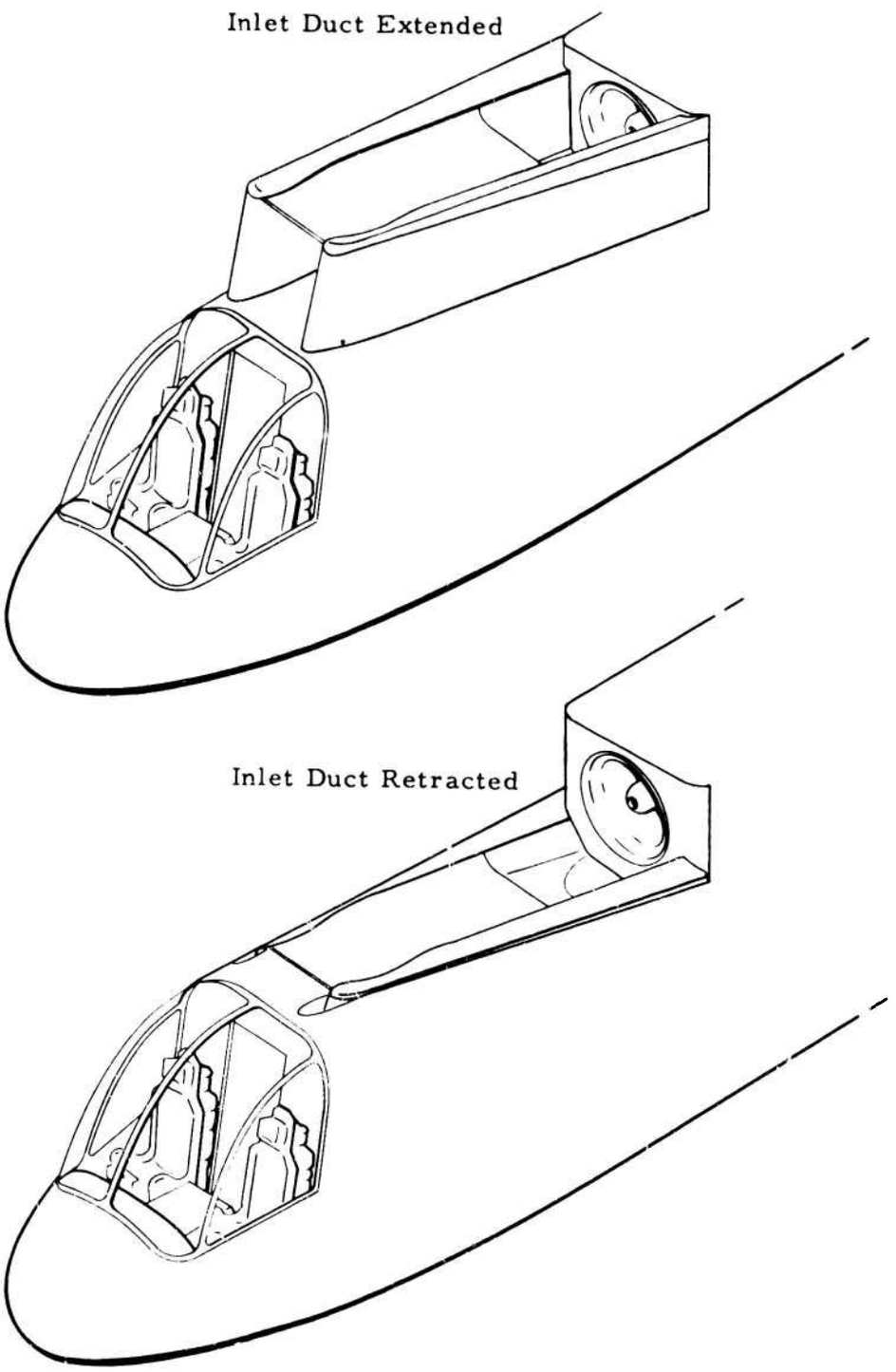

Figure 88. Engine Air Induction System.

Nozzle fairings are installed in the blade trailing edge in the form of upper and lower hinged doors, which are aerodynamically balanced and spring-loaded to the closed position. No actuators are necessary because gas pressure opens the fairings and holds them open during the helicopter operation. The spring-loaded fairings close and provide an uninterrupted faired trailing-leading edge on the blades when the gas flow is diverted to the tail pipe for autogyro and airplane flight.

FUEL SYSTEM

The fuel system (Figure 89) comprises the tanks, pumps, valves, filters, and attendant plumbing. Two tanks, each with a 1,500-pound usable fuel capacity, are used; one tank is mounted forward and one tank is mounted aft of the cargo compartment. Tanks are shaped to permit full utilization of the fuel. Each tank is equipped with two pumps installed in parallel, with check valves to prevent cross flow. This provides a system that is fail-safe, since any one pump has the capacity to supply the engine with the required fuel. Fuel management is effected through the use of pump sequencing. Normally, the engine is fed from both tanks, and levels remain relatively even. Therefore, only limited management is required. For fire protection, motor-driven shutoff valves are installed at the tanks and fire wall.

POWER CONTROL SYSTEM

Simplicity of operation, reliability, and safety were the prime considerations in the design of the power control system. This philosophy has resulted in a direct, uncomplicated system for controlling engine thrust to satisfy the requirements for helicopter flight, conversion, and operation as a fixed-wing aircraft.

The engine hydromechanical fuel control unit regulates the flow of fuel in accordance with the power setting selected by the pilot. The power control system consists of the linkages, levers, and cables connecting the fuel control unit to the cockpit controls (see Figure 90). Power settings may be changed either by the throttle quadrant or the twist grip on the collective stick, depending upon the flight mode.

The throttle quadrant is installed in the center console and provides a full range of control of the engine from OFF to MILITARY power settings. The throttle lever has full authority and is used to start, idle, conduct operational checks, and shut down the engine, as well as to control power in the

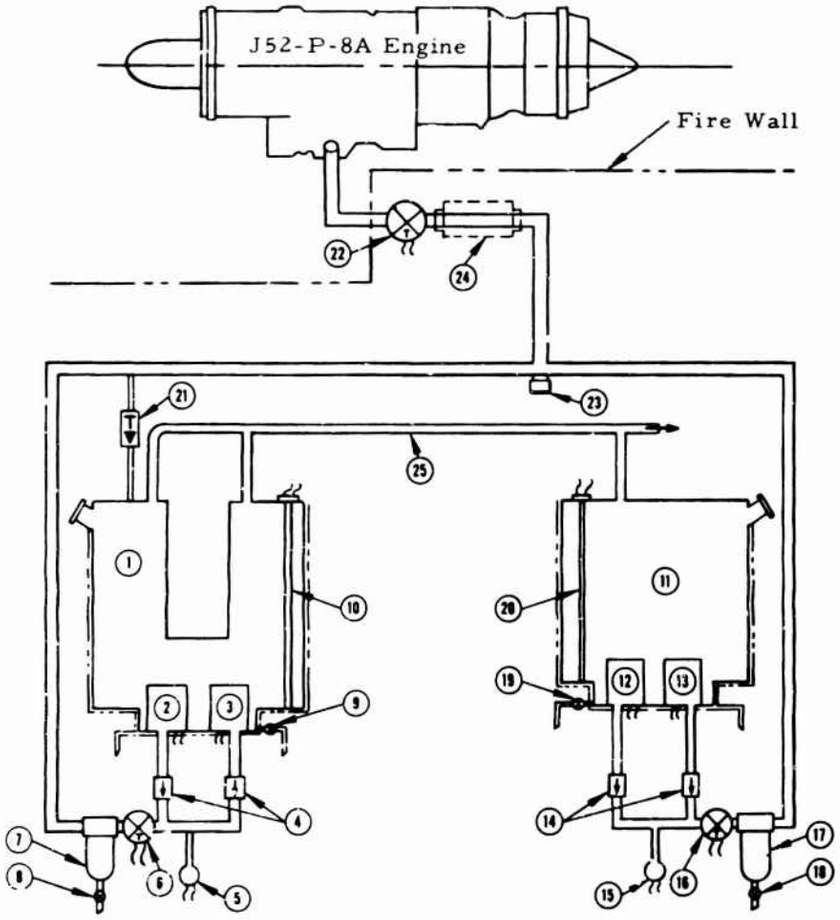

1. Forward Fuel Tank - 1,500-lb Capacity
2. Forward Tank Booster Pump - Normal
3. Forward Tank Booster Pump - Emergency
4. Check Valve
5. Fuel Boost Pressure Switch
6. Forward Tank Shutoff Valve (Thermal Relief)
7. Forward Fuel Filter
8. Filter Drain
9. Forward Tank Water Drain
10. Forward Tank Quantity Transmitter
11. Aft Fuel Tank - 1,500-lb Capacity
12. Aft Tank Booster Pump - Normal
13. Aft Tank Booster Pump - Emergency
14. Check Valve
15. Boost Pump Pressure Switch
16. Aft Tank Shutoff Valve (with Thermal Relief)
17. Aft Fuel Filter
18. Filter Drain
19. Aft Tank Water Drain
20. Aft Tank Quantity Transmitter
21. System Thermal Relief Valve
22. Fire Wall Shutoff Valve (with Thermal Relief)
23. Ferry Fuel Connection (Capped)
24. Hydraulic Oil/Fuel Cooler (Provisions for)
25. Vent Line

Figure 89. Fuel System - Normal Mission.

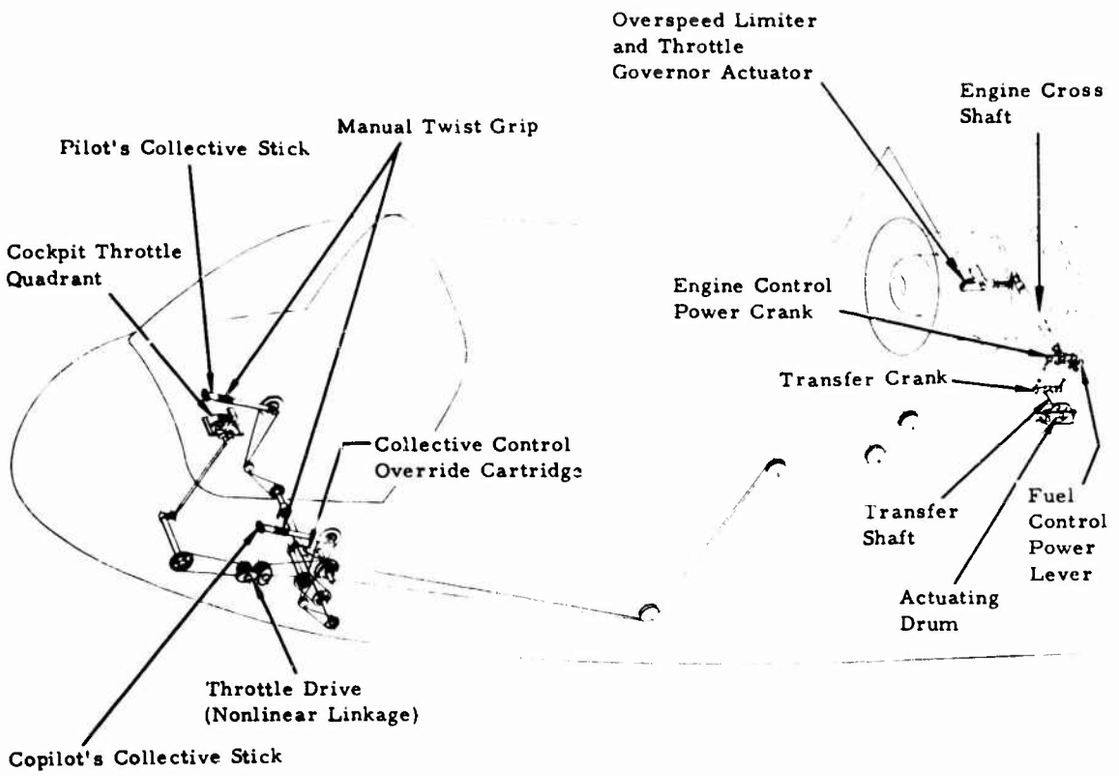

Figure 90. Engine Power Control System.

airplane mode. The lever is free to move in either direction to advance or retard power as required; but for safety, to prevent inadvertent engine shutdown by movement below IDLE, it is provided with a stop that must be lifted to move the lever below IDLE. Since the throttle lever is linked directly to the engine, it serves as an indicator of the true position of the fuel control power lever at all times.

When switching to the helicopter mode, the rotor speed sensing and governing system is energized. The governing system must be switched off for manual operation by twist grip if desired. The function of the rotor speed sensing and governing system is to provide:

1. Beep control of the throttle setting to provide desired rotor rpm within a limited range (96 to 100 percent N_R).

2. Automatic governing to maintain the rotor speed selected by the beep control.

3 Overspeed control to limit the rotor speed to 104 percent.

COOLING SYSTEMS

The cooling problem has been approached in a straightforward manner by using insulation to reduce the heat flux and heat rejection requirements and by providing the necessary cooling airflow. The main areas requiring cooling are those adjacent to the hot gas system and the engine, and the rotor lubrication system. For ground operation with the rotor stopped, cooling air is induced into the forward engine compartment by a pair of ejectors utilizing air from the engine compressor. The tail pipe exit functions as an ejector nozzle to induce cooling airflow into the aft engine compartment and along the tail pipe. In the helicopter mode, the forward engine compartment continues to be cooled by the ejectors, but centrifugal pumping of the rotor replaces the tail pipe ejector and draws cooling air into the aft engine compartment, up through the hub, and out the wing to the blade attachment, where it exhausts. Blade cooling air is taken in at the root of the blade, is centrifugally pumped by the rotor, and is ejected at the blade tip.

When switching to the airplane flight mode, ram air provides cooling of the forward engine compartment and the ejectors are shut off. In this mode, the tail pipe ejector once again induces cooling airflow into the aft engine compartment and along the tail pipe.

The rotor lubricating system utilizes circulating oil for bearing and accessory gearbox lubrication and cooling. Airflow past the rotor bearing housing and components maintains the oil temperature at a safe level. Provisions have been made to install an air-oil heat exchanger if it is required for additional cooling.

STARTING SYSTEM

The air turbine starting system, which was selected because of its light weight and simplicity, is designed for ground starting utilizing an MA-1A gas turbine compressor. Since the mission of this aircraft is research, on-board starting capability was considered to be inappropriate and was not provided. On-board starting capability for an operational aircraft can be installed readily for only 75 pounds of additional weight.

ENGINE LUBRICATION SYSTEM

The engine lubrication system is completely contained on the engine. Servicing and venting the system are accomplished by a pressure-filling system

utilizing easily accessible quick-disconnect fittings. The pressure oiler includes a continuity checker for determining filling requirements and chip detection.

FIRE PROTECTION

A primary consideration in the design of the Rotor/Wing aircraft has been the preclusion of fire hazards. Combustibles have been isolated from ignition sources by proper routing, draining, venting, and insulating. Every effort has been made to eliminate potential line failures by using conservative design practices such as generous radii provisions for relative movement and by using simple and short routing. Fire zones have been established to localize and contain hazards.

Fire and overheat detection systems have been incorporated as shown in Figure 91. The systems utilize heat-sensing elements to alert the pilot in case an overtemperature condition exists. A fire extinguishing system is installed for the forward engine compartment. Fire in the forward engine compartment is indicated by lights contained in the fire extinguisher pull handle. Pulling the handle will discharge the fire extinguisher agent. Bromotrifluoromethane has been selected as the extinguishing agent in view of its effectiveness, noncorrosiveness, and low toxicity.

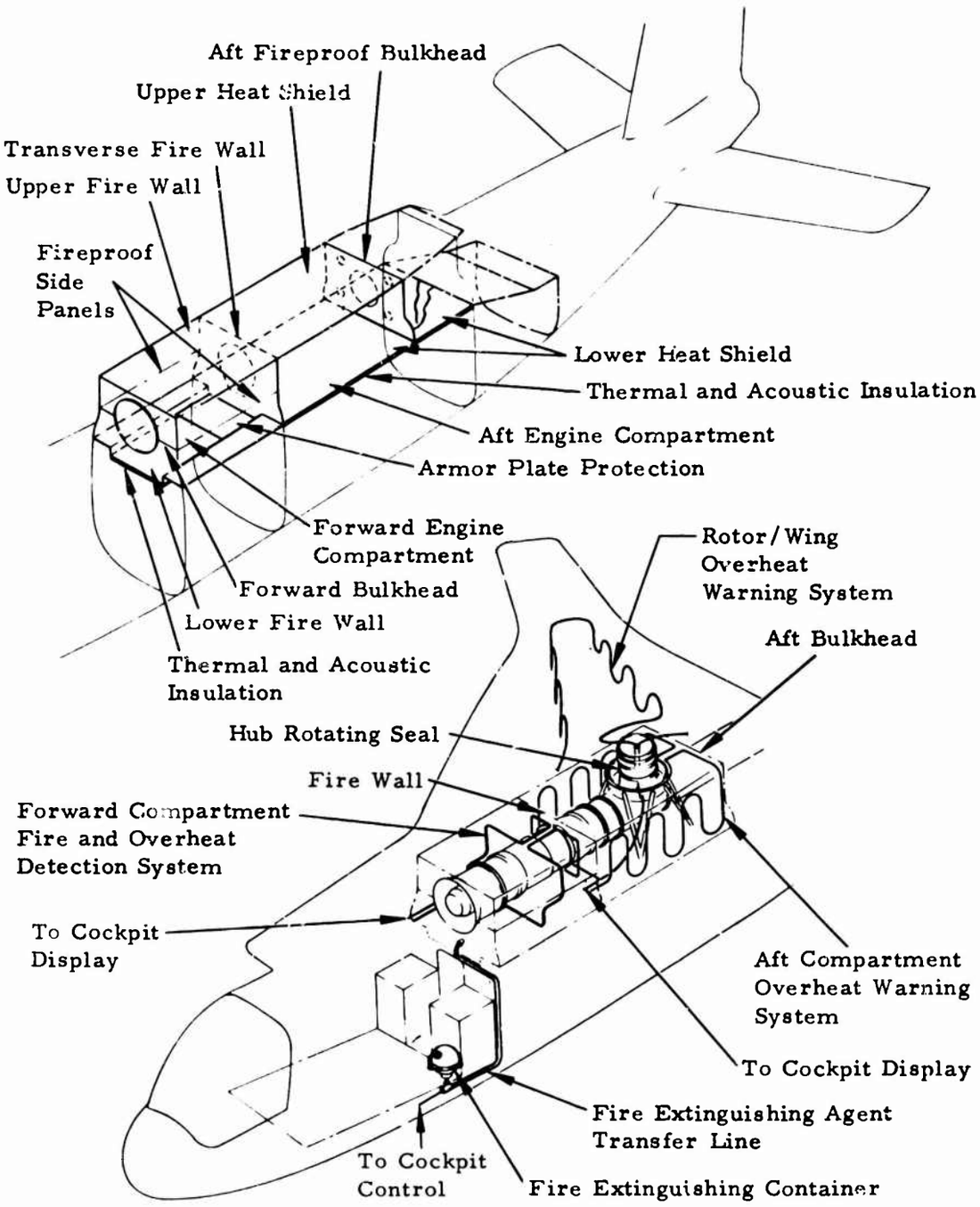

Figure 91. Fire and Overheat Protection.

ELECTRICAL, HYDRAULIC, AND MECHANICAL SYSTEMS

ELECTRICAL SYSTEM

The electrical system shown in Figure 92 is designed as simply as possible with the minimum number of components to ensure maximum reliability, lowest cost, and lightest weight. Experience has shown that the inclusion of automatic control devices such as current limiters does not provide the additional safety and convenience that might be expected. On the contrary, these auxiliary circuits often result in increased weight and cost, add significantly to service requirements, and are a potential source of electrical and mechanical failure. Therefore, the CRA design philosophy has been to eliminate all nonessential items and to keep the basic system as simple as possible.

The electrical system selected for the CRA consists of a 28-volt direct-current primary system and a secondary alternating-current system. The primary system derives power from a dc generator, and the secondary system employs static inverters that operate from the primary system. This selection results in a lightweight system that has excess generating capacity and operating margins to permit safe autorotational night landings and conversion from airplane to helicopter mode using battery power only. In the event of an engine failure, the low bus load allows 15 minutes for conversion to autogyro mode and provides for a safe autorotational night landing requiring only 75 percent residual battery energy.

Ground power may be supplied by any of the existing 28-volt military ground power units of a standard military aircraft battery of sufficient capacity. The design includes an interlock to prevent damage to the system by removing the on-board battery from the line when external power is connected.

The electrical system designed for the CRA is more than adequate to provide for the needs of a research aircraft; it is a conventional system using off-the-shelf components employed in the most direct and uncomplicated manner.

Instruments and Navigation Equipment

The primary mission of the Hot Cycle Rotor/Wing CRA is to perform as a research aircraft for evaluation; consequently, only limited adverse-weather or night operations are required or anticipated. Sufficient instrumentation is provided to ensure that the pilot can control and operate the

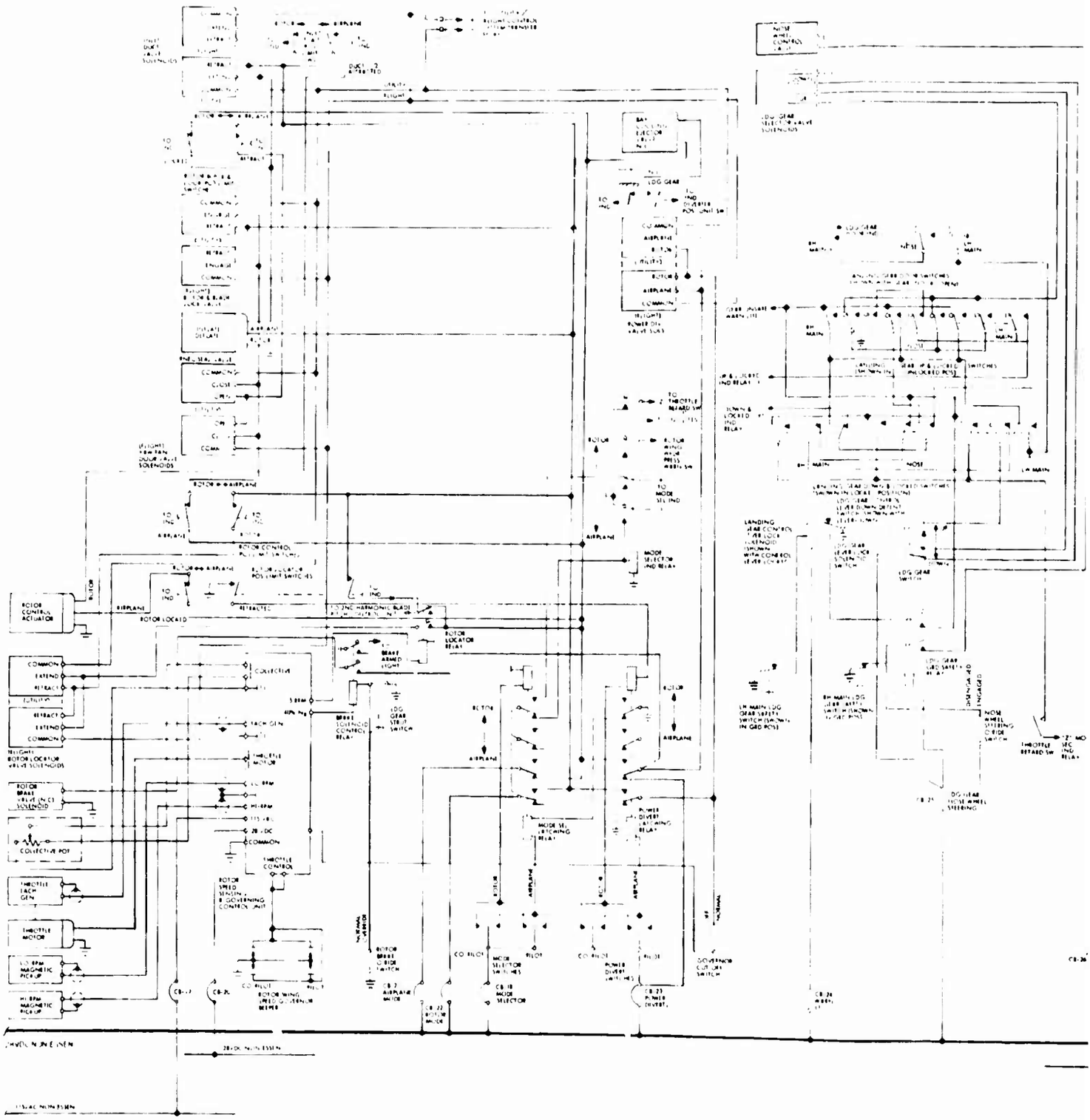

Figure 92. Electrical System Schematic Diagram (Sheet 1 of 2).

A

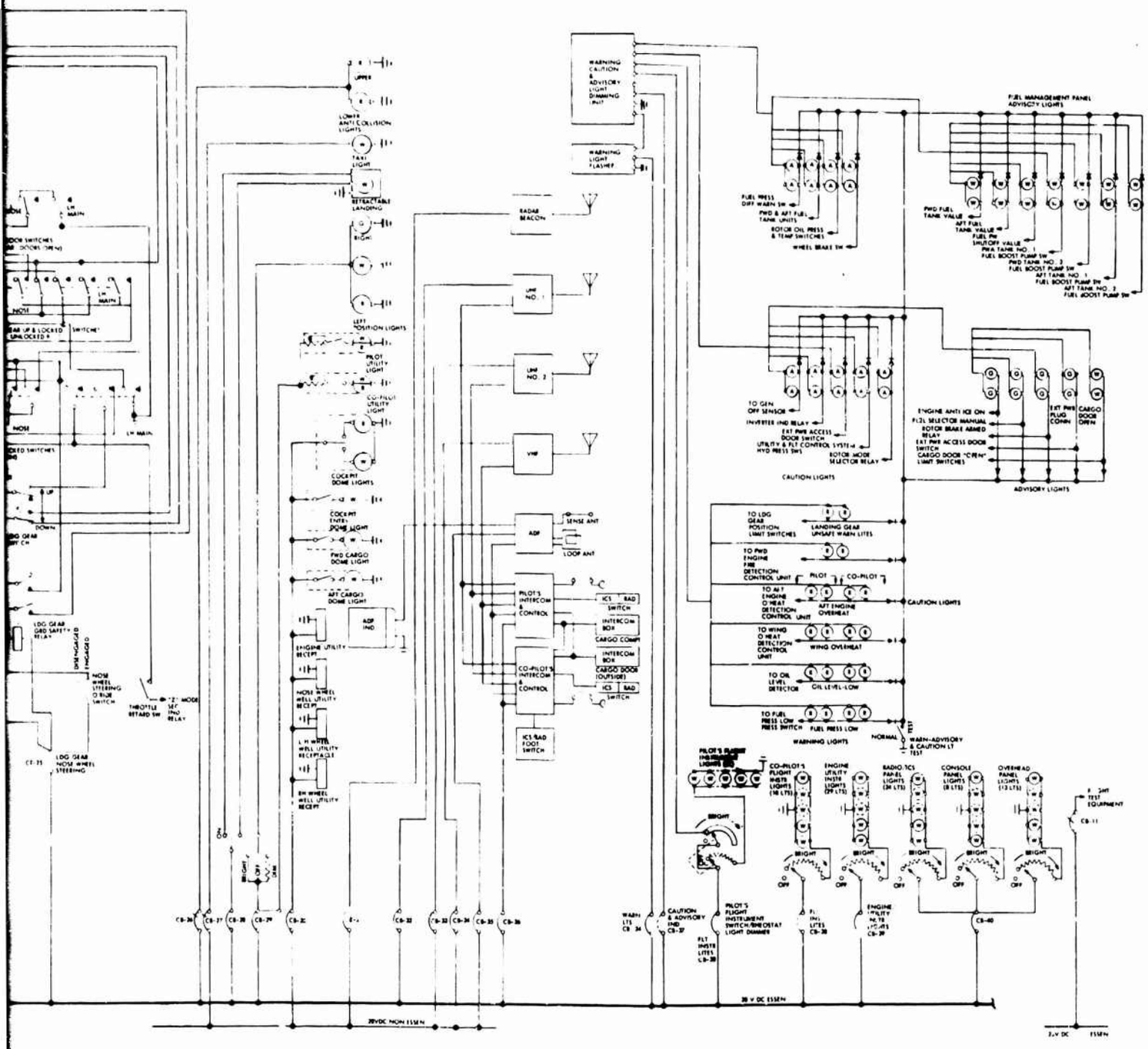
WARNING CAUTION & ADVISORY LIGHT DIMMING UNIT
WARNING LIGHT FLASHER
FUEL MANAGEMENT PANEL ADVISORY LIGHTS
CAUTION LIGHTS
ADVISORY LIGHTS
WARNING LIGHTS
RADAR BEACON
VHF
ADF
LOOP ANT
SENSE ANT
PILOT'S INTERCOM & CONTROL
CO-PILOT'S INTERCOM & CONTROL
ICS RAD FOOT SWITCH
ICS RAD SWITCH
INTERCOM BOX
CARGO COMPT
CARGO DOOR (OUTSIDE)
ADF IND
ENGINE UTILITY RECEPT
NOSE WHEEL WELL UTILITY RECEPTACLE
LH WHEEL WELL UTILITY RECEPTACLE
RH WHEEL WELL UTILITY RECEPT
LOWER ANTI COLLISION LIGHTS
TAXI LIGHT
RETRACTABLE LANDING
RIGHT
LEFT POSITION LIGHTS
PILOT UTILITY LIGHT
CO-PILOT UTILITY LIGHT
COCKPIT DOME LIGHTS
COCKPIT ENTRY DOME LIGHT
FWD CARGO DOME LIGHT
AFT CARGO DOME LIGHT
LDG GEAR GRD SAFETY RELAY
NOSE WHEEL STEERING ENGAGED
NOSE WHEEL STEERING ENGAGED SWITCH
THROTTLE RETARD SW
"Z" MODE SEL IND RELAY
LDG GEAR NOSE WHEEL STEERING
TO LDG GEAR POSITION LIMIT SWITCHES
LANDING GEAR UNSAFE WARN LITES
TO FWD ENGINE FIRE DETECTION CONTROL UNIT
PILOT
CO-PILOT
TO AFT ENGINE O'HEAT DETECTION CONTROL UNIT
AFT ENGINE OVERHEAT
TO WING O'HEAT DETECTION CONTROL UNIT
WING OVERHEAT
TO OIL LEVEL DETECTOR
OIL LEVEL-LOW
TO FUEL PRESS LOW PRESS SWITCH
FUEL PRESS LOW
TEST
NORMAL
WARN-ADVISORY & CAUTION LT TEST
FUEL PRESS DIFF WARN SW
FWD & AFT FUEL TANK UNITS
ROTOR OIL PRESS & TEMP SWITCHES
WHEEL BRAKE SW
FWD FUEL TANK VALVE
AFT FUEL TANK VALVE
FUEL PW SHUTOFF VALVE
FWD TANK NO. 1 FUEL BOOST PUMP SW
FWD TANK NO. 2 FUEL BOOST PUMP SW
AFT TANK NO. 1 FUEL BOOST PUMP SW
AFT TANK NO. 2 FUEL BOOST PUMP SW
TO GEN OFF SENSOR
INVERTER IND RELAY
EXT PWR ACCESS DOOR SWITCH
UTILITY & FLT CONTROL SYSTEM HYD PRESS SWS
ROTOR MODE SELECTOR RELAY
ENGINE ANTI ICE ON
FUEL SELECTOR MANUAL
ROTOR BRAKE ARMED RELAY
EXT PWR ACCESS DOOR SWITCH
CARGO DOOR "OPEN" LIMIT SWITCHES
EXT PWR PLUG CONN
CARGO DOOR OPEN
PILOT'S FLIGHT INSTRUMENT LIGHTS
CO-PILOT'S FLIGHT INSTR LIGHTS (16 LTS)
ENGINE UTILITY INSTR LIGHTS (29 LTS)
RADIO TCS PANEL LIGHTS (34 LTS)
CONSOLE PANEL LIGHTS (8 LTS)
OVERHEAD PANEL LIGHTS (13 LTS)
BRIGHT
OFF
PILOT'S FLIGHT INSTRUMENT SWITCH/RHEOSTAT LIGHT DIMMER
FLT INSTR LITES CB-38
ENGINE UTILITY INSTR LITES CB-39
CAUTION & ADVISORY IND CB-37
WARN LTS CB-34
CB-40
F. SHT TEST EQUIPMENT
CB-11
28 V DC ESSN
28VDC NON ESSN
28 V DC ESSN

B

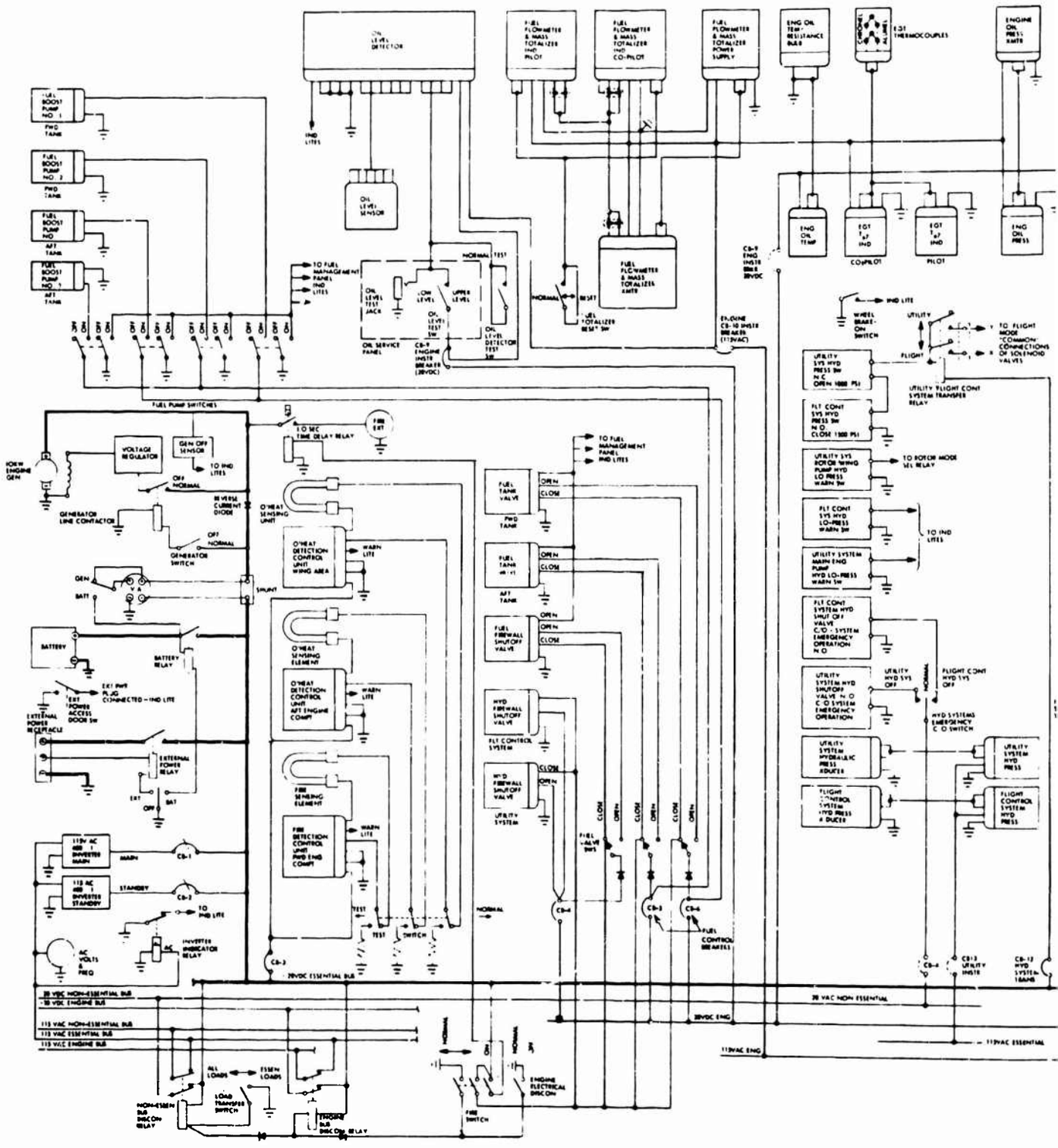

Figure 92. Electrical System Schematic Diagram (Sheet 2 of 2).

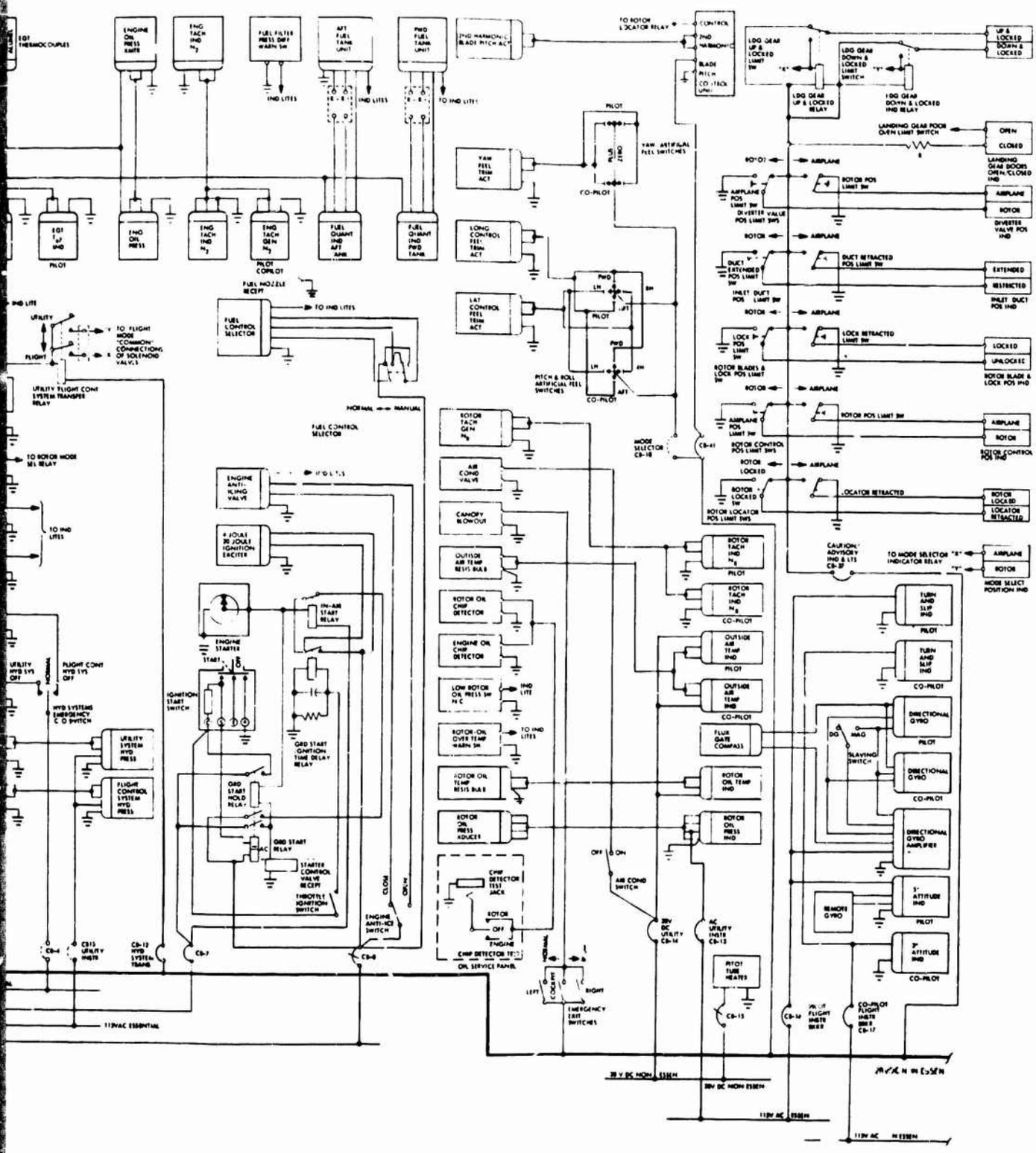

B

aircraft and perform test flight maneuvers and navigation within the limits of the CRA mission.

Instruments

The instrument panel has dual flight and engine instruments: one set for the pilot and one set for the copilot with utility instruments located in the center console. Flight instruments are arranged in the basic T-layout.

A flashing fire-warning indicator-switch combination is centered between the pilot and copilot at the top of the instrument panel. Other warning lights are located at the top and center of both the pilot's and copilot's panels. The caution and advisory lights are grouped on the center portion of the instrument panel.

The console contains switches, radio and navigation equipment controls, and landing gear and flight controls. An overhead panel contains circuit breakers, light switches, and various electrical controls. Both the console and overhead panel are readily accessible to both pilots.

Lights

A 600-watt retractable landing light is located on the underside of the aircraft forward of the nose wheel. For taxi purposes, a 450-watt light is mounted on the steerable nose wheel strut. Each of these lights may be controlled by either the pilot or the copilot (see Figure 93).

Red and green position lights for safe operation are located on the sides of the forward fuselage section. The white position light is located on the aft end of the fuselage tail cone. Two anticollision lights are provided. To provide maximum visibility, one anticollision light is located atop the vertical stabilizer and the other is located on the underside of the fuselage.

Complete cockpit illumination is included in the form of a dome light, utility lights, panel lights, console lights, radio control lights, and overhead panel lights. Variable switches are provided for the control of lighting intensity for each group on the instrument panel. Each group can be independently controlled. The cargo compartment and cockpit entryway are lighted by dome lights. A portable utility light with coiled cord is stowed on board for convenience illumination (see Figure 94).

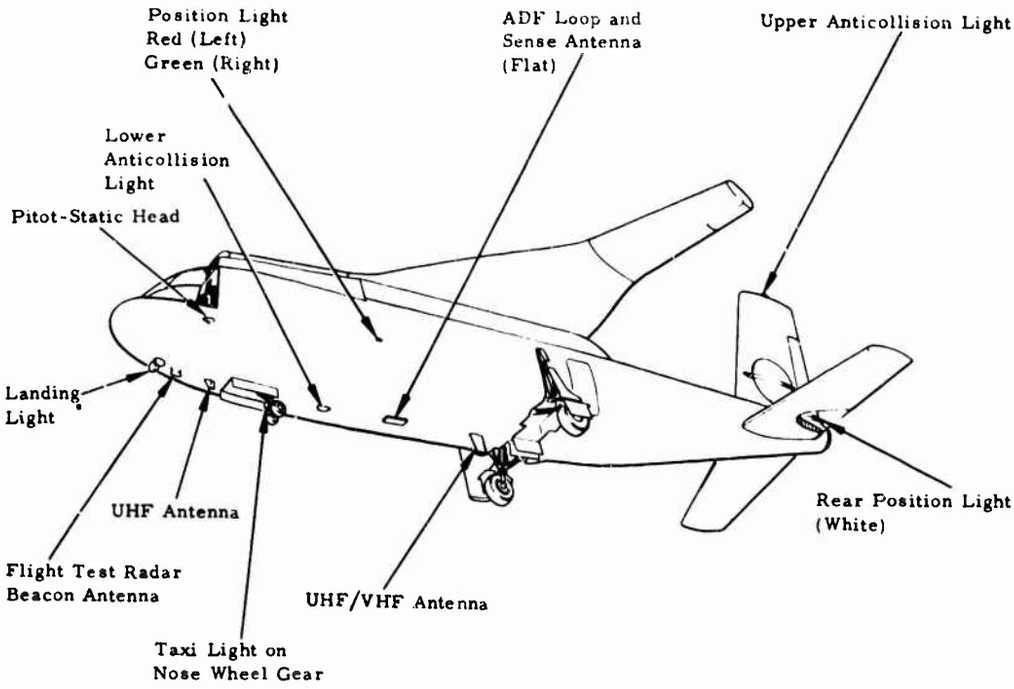

Figure 93. Exterior Lighting and Antenna.

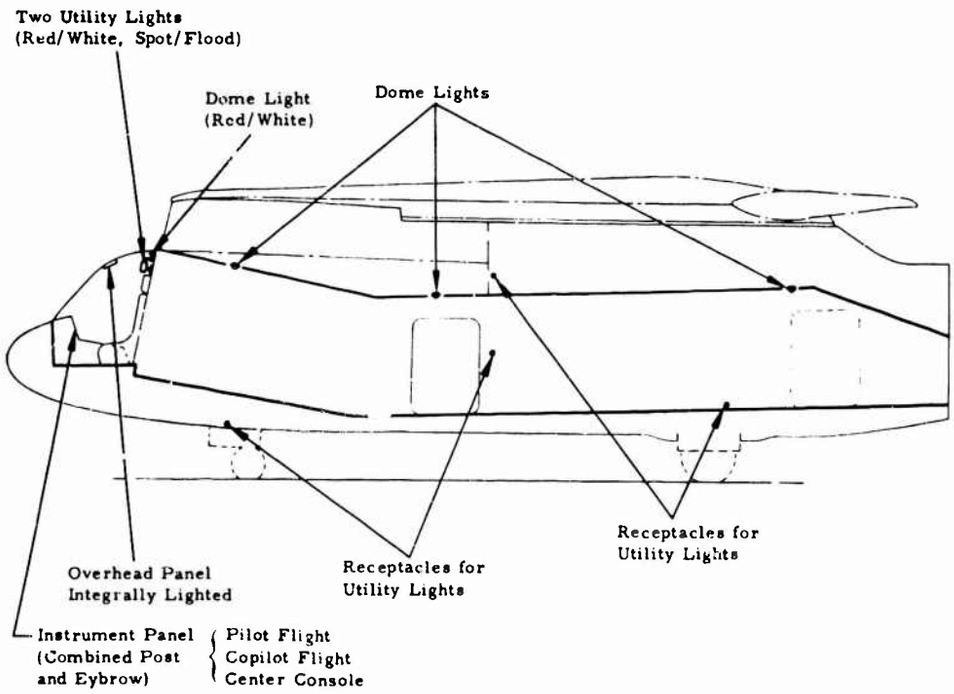

Figure 94. Interior Lighting.

AVIONICS SYSTEM

The radio communication and navigation equipment has been combined into a single integrated system to provide maximum usefulness (see Figure 95). This optimum system coordinates the radio mechanism with few controls and an indicator so that the pilot can quickly obtain information for flight control and effective mission performance. The overall simplicity has been maintained, and all components are readily accessible. The equipment selected for the CRA is from the LOH lightweight avionics package being developed for the U. S. Army. These compact units provide high output power with low input power and represent a major breakthrough in communication and navigation equipment. Below is a list of the units to be used.

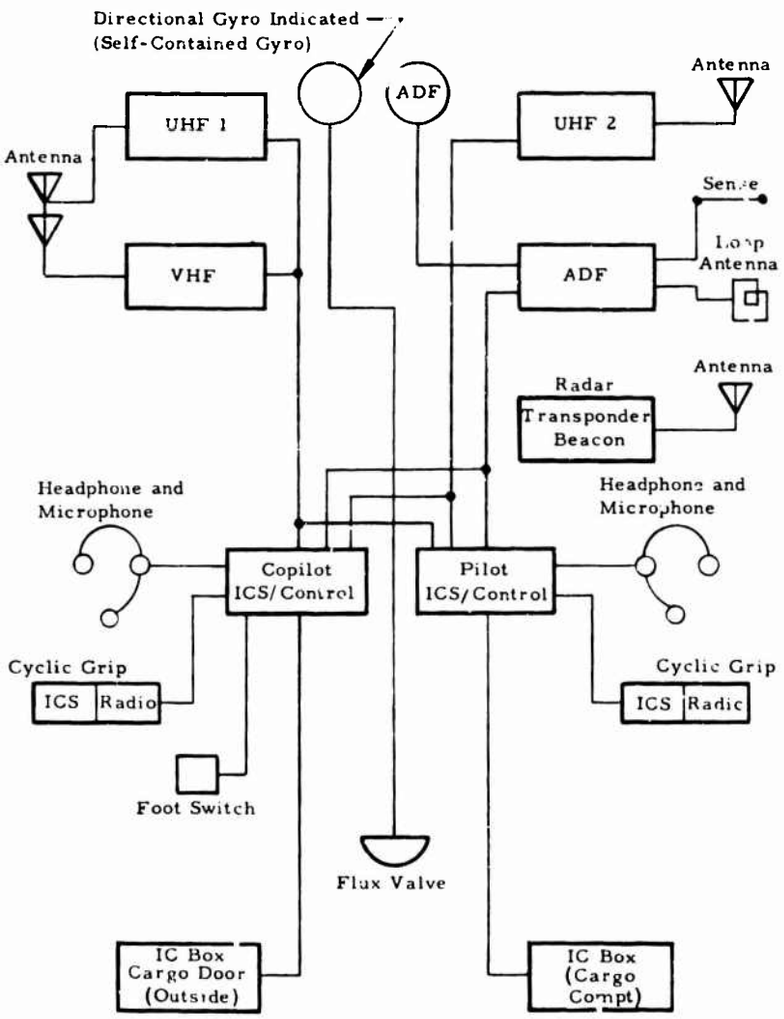

Figure 95. Avionics Block Diagram.

AN/ARC-116 UHF-AM Transceivers

Complete air-to-surface and air-to-air voice communications between military aircraft in the continental United States are provided by this equipment. It has 3,500-channel tuning on 50-kc separation in a frequency range of 225 to 399.95 mc; it can also be used for retransmission or for data transmission, or as a guard receiver.

AN/ARC-115 VHF-AM Transceiver

This equipment provides complete air-to-surface and air-to-air voice communication between military and commercial aircraft in the continental United States. It has 1,360 channels on 25-kc spacing in the frequency range of 116 to 149.975 mc. This transceiver can also be used for retransmission and data transmission.

AN/ARN - LF/MF Automatic Direction Finder

Automatic df, manual df, and a radio receiver provide capability for operation in the 100-kc to 3,000-kc range.

C-6533/ARC Intercom Panel (2 Units)

Interphone operation, audio level, and radio switching control are provided by this equipment. It is compatible with all the communication units used in the CRA.

H-101 Headset/Microphone Unit

Two headset/microphone units are included.

HYDRAULIC AND MECHANICAL SYSTEMS

The hydraulic and mechanical systems of the Hot Cycle Rotor/Wing Aircraft were designed with safety, reliability, simplicity, and light weight as primary objectives. State-of-the-art materials, parts, and processes were used.

Flight Controls

A conventional, irreversible, power-operated system is provided for the operation of the flight controls. Power is supplied by two independent hydraulic systems, with each system serving as a continuous backup for the other (see Figure 96). Conventional helicopter-type cyclic sticks,

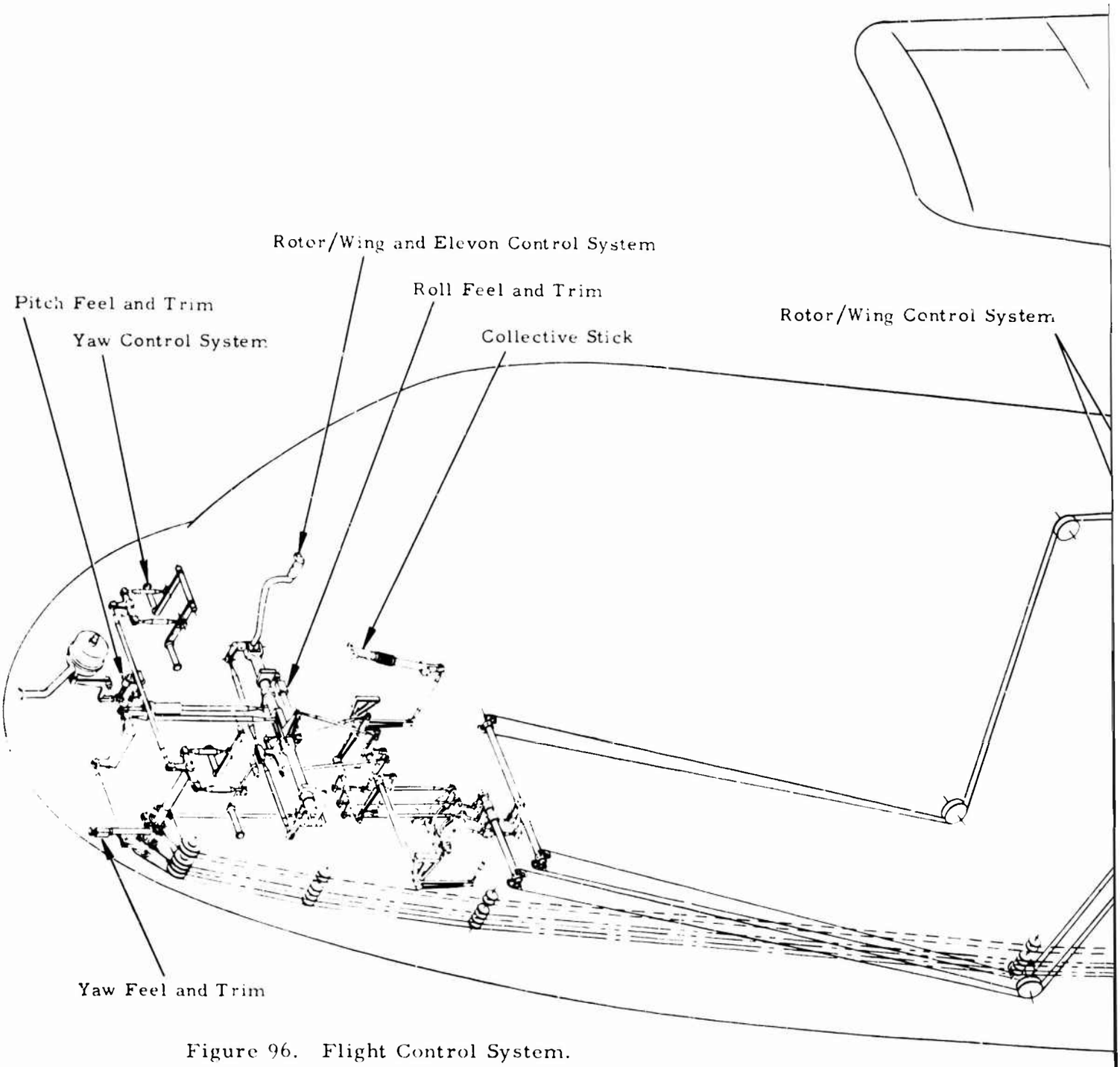

Figure 96. Flight Control System.

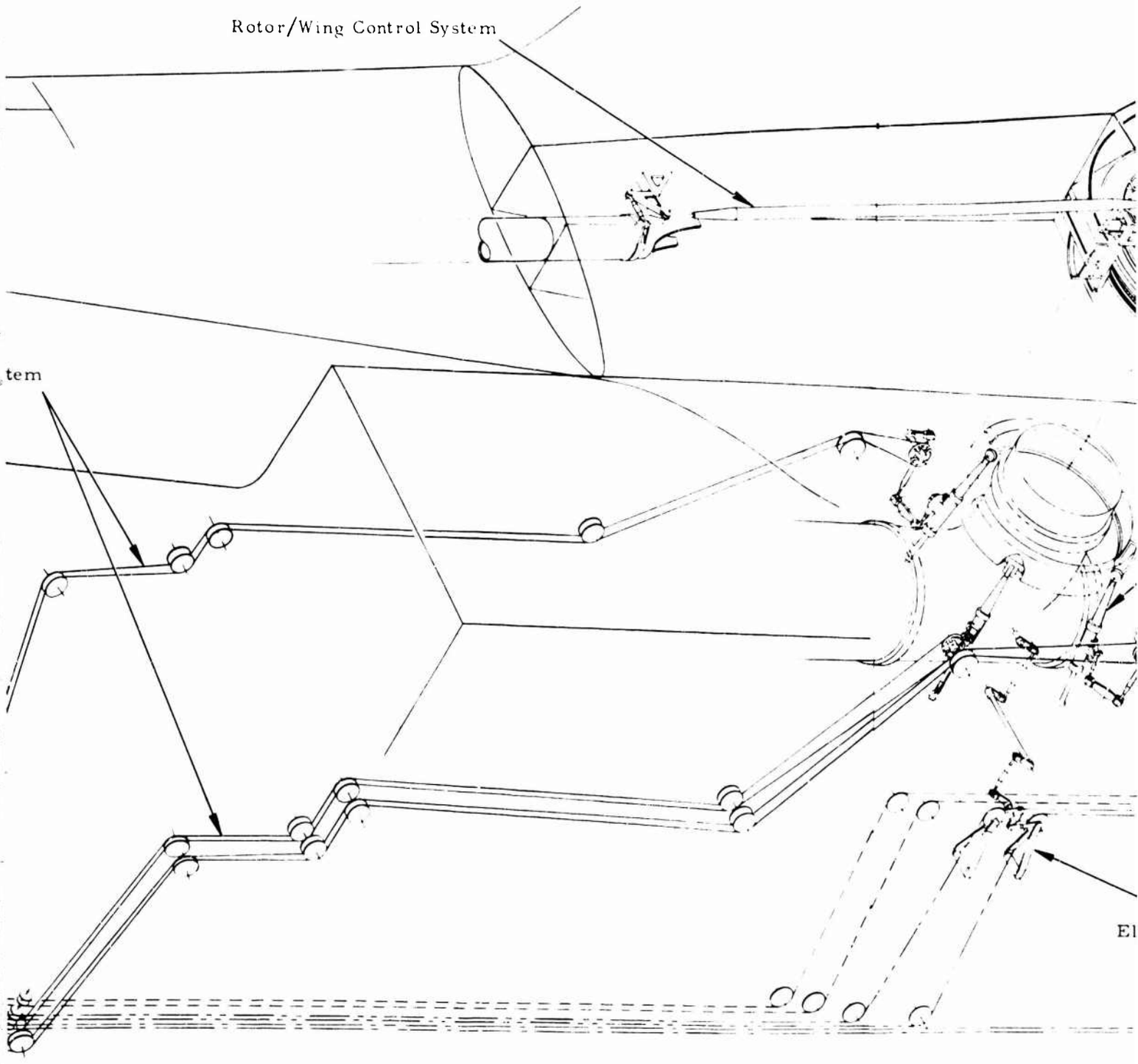
Rotor/Wing Control System
tem
El

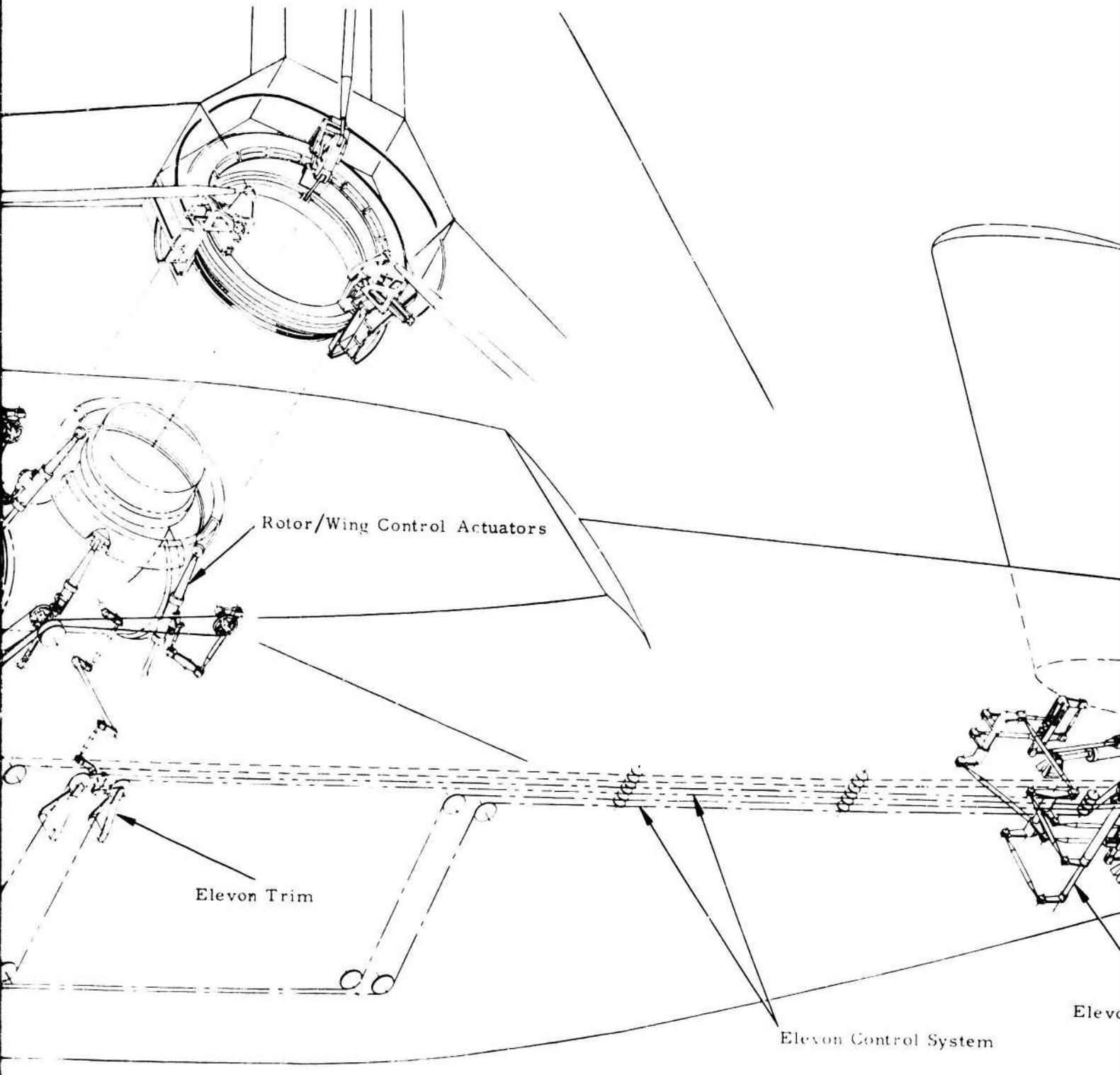
Rotor/Wing Control Actuators
Elevon Trim
Elevon Control System

C

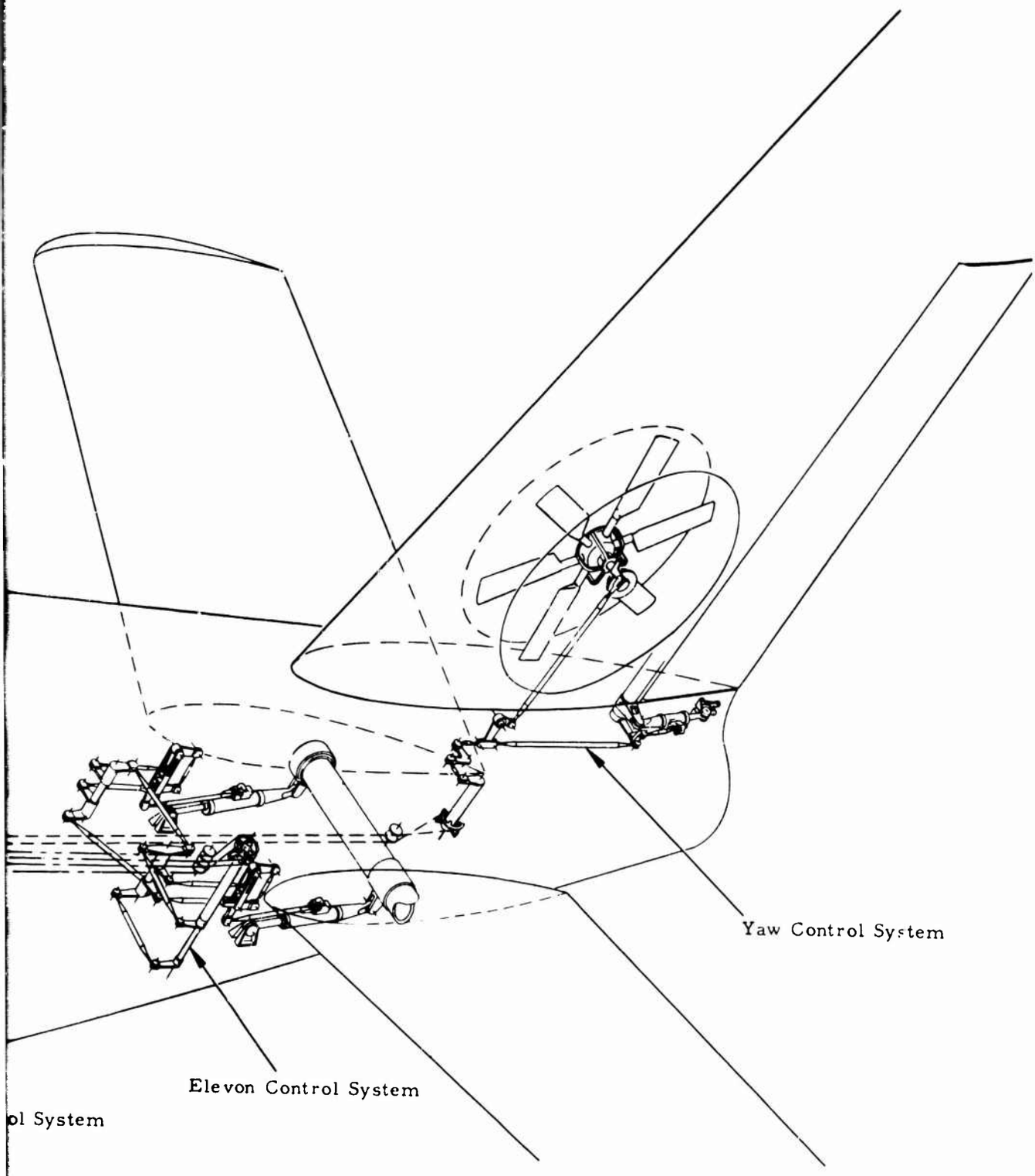

ol System

collective sticks, and rudder pedals are provided in the cockpit for the pilot and copilot, and are connected together through mechanical linkages and cables to dual-tandem hydraulic actuators that operate the control surfaces and rotor controls in helicopter flight, and the rudder and elevons in airplane flight. Pilot control motions are transmitted to the rotor area by cables that terminate at the mechanisms that control the servo valves on the swashplate actuators.

To reduce the oscillating bending moments that occur in the blades in high-speed helicopter flight and at the same time to reduce blade/rotor-induced fuselage vibration, an automatically adjustable mechanism has been incorporated to apply 2-per-rev cyclic pitch. The amplitude of the 2-per-rev input is automatically varied in helicopter and autogyro flight with airspeed. This mechanism has the effect of reducing the pitch of the blade over the forward and aft sectors of the rotor disc and increasing the pitch over the lateral sectors, thereby distributing the lift around the rotor more uniformly and reducing the oscillating blade-root bending moments.

For airplane flight, it is necessary to deactivate the rotor controls. This is accomplished by a simple mechanism between the mixer and servo valves (see Figure 97). No physical disconnection or declutching is used. The deactivation simply reorients the control linkage so that pilot control motions produce no movement at the servo valves. When deactivated, positive mechanical centering holds the Rotor/Wing blade pitch in the zero blade pitch position.

The cyclic stick is continuously connected to the elevons through tandem servo actuators for lateral and longitudinal control in the airplane mode. The two elevons move in unison with fore and aft cyclic stick motion for pitch control of the aircraft and move differentially with lateral stick motion for roll control. Rudder pedals are connected to the yaw fan blade pitch control and rudder through a tandem servo actuator for all modes of flight.

Directional control in helicopter mode is provided by the yaw fan. The yaw fan is driven by the rotor through an accessory gearbox, connecting shafting, and intermediate gearboxes. In airplane mode, doors close over the fan to reduce drag, and yaw control is achieved by conventional rudder displacement.

Artificial feel devices are incorporated in the lateral, longitudinal, and directional control systems to provide the pilot with the characteristics of an unpowered system. No automatic stabilization system is required in any flight mode.

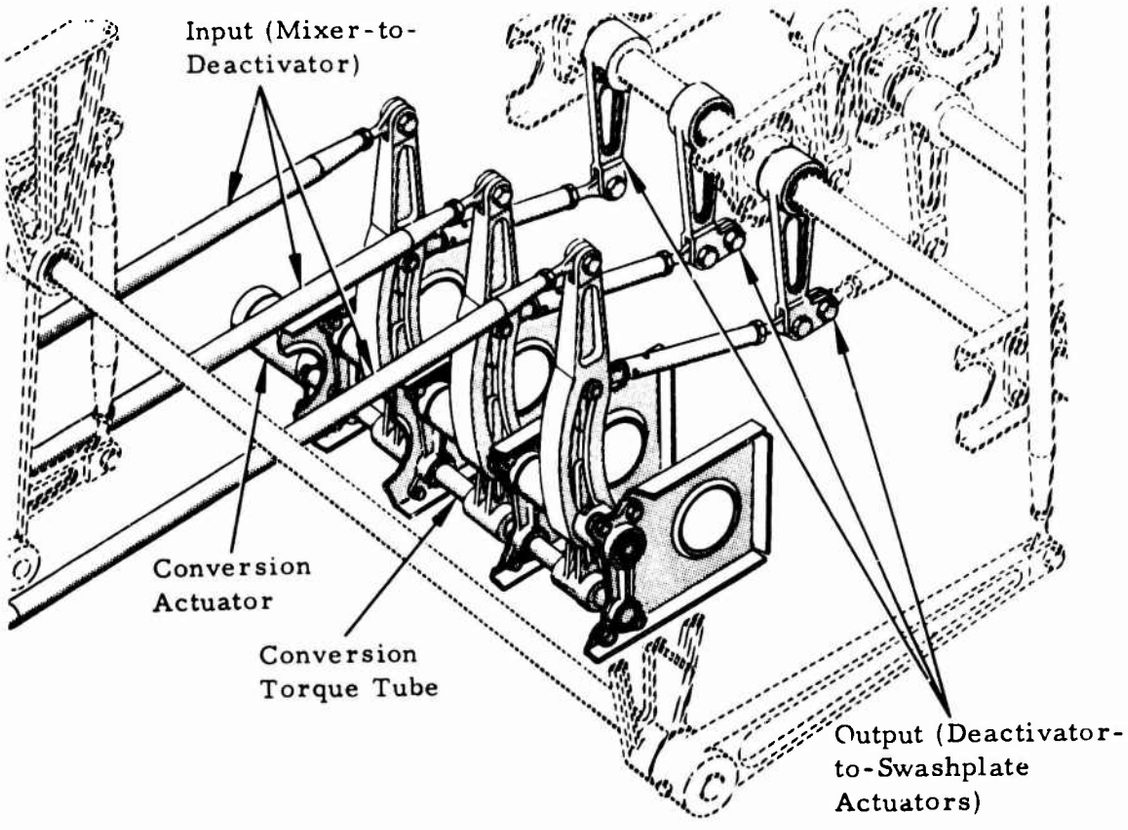

Figure 97. Rotor/Wing Control Deactivator.

Hydraulics

Hydraulic power is provided by two independent hydraulic systems, each with its own pumps, accumulators, filters, and valves (see Figure 98). The flight control system is normally powered by an engine-driven variable delivery pump, with a secondary power source provided by a ram-air turbine-driven variable delivery pump. The secondary or utility system power is supplied by an engine-driven variable-delivery pump, with its backup power source being a Rotor/Wing-driven pump. Both systems operate at the conventional and well-proven 3,000-psi pressure.

Hydraulic fail-safe capabilities are provided by the incorporation of the two independent systems. Through the use of dual tandem actuators, the output of both systems is used to power each of the primary flight control systems with one system providing a continuously operating backup for the other. Should one system fail, the other continues to supply power for uninterrupted flight control operation without requirement for pilot action. Actuation of the diverter valve, Rotor/Wing locks, and inlet duct assembly is accomplished by single-ended actuators, each incorporating two electric

1. Pump - Engine Driven, Flight Control and Utility
2. Pump - Rotor/Wing Driven
3. Pump - Ram-Air Turbine Driven
4. Reservoir, Flight Control and Utility
5. Accumulator
6. Actuator - Swashplate
7. Actuator - Elevon
8. Actuator - Rudder
9. Actuator - Rotor/Wing Locator
10. Actuator - Inlet Duct, Retractable
11. Actuator - Wing and Blade Locks
12. Actuator - Power Diverter Valve
13. Actuator - Yaw Fan Doors
14. Actuator - Main Landing Gear
15. Actuator - Nose Landing Gear
16. Actuator - Nose Wheel Steering
17. Actuator - Gear Up Lock
18. Valve - Power Brake
19. Valve - Landing Gear Selector
20. Valve - Nose Wheel Steering Control
21. Valve Shutoff Normally Closed, Rotor/Wing Brake and Nose Wheel Steering
22. Valve Shutoff Normally Open, Checkout of Systems Emergency Operations
23. Valve - Fire Wall Shutoff
24. Filter - Pressure Line
25. Filter - Return Line
26. Switch - Low Pressure
27. Switch - Pressure Normally Open
28. Switch - Pressure Normally Closed
29. Transmitter - Pressure
30. Gage - Pressure
31. Valve - Air Charging
32. Valve - Minicheck
33. Valve - Minicheck
34. Brake Assembly - Rotor/Wing
35. Brake Assembly - Main Wheel
36. Restrictor - One Way
37. Coupling - Ground Service, Return
38. Coupling - Ground Service, Pressure
39. Valve - Steer/Damper

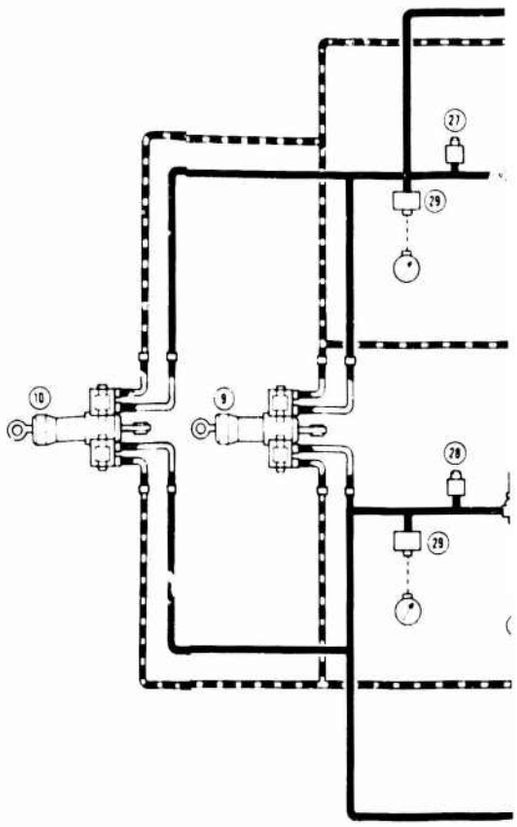

Figure 98. Hydraulic System Schematic Diagram.

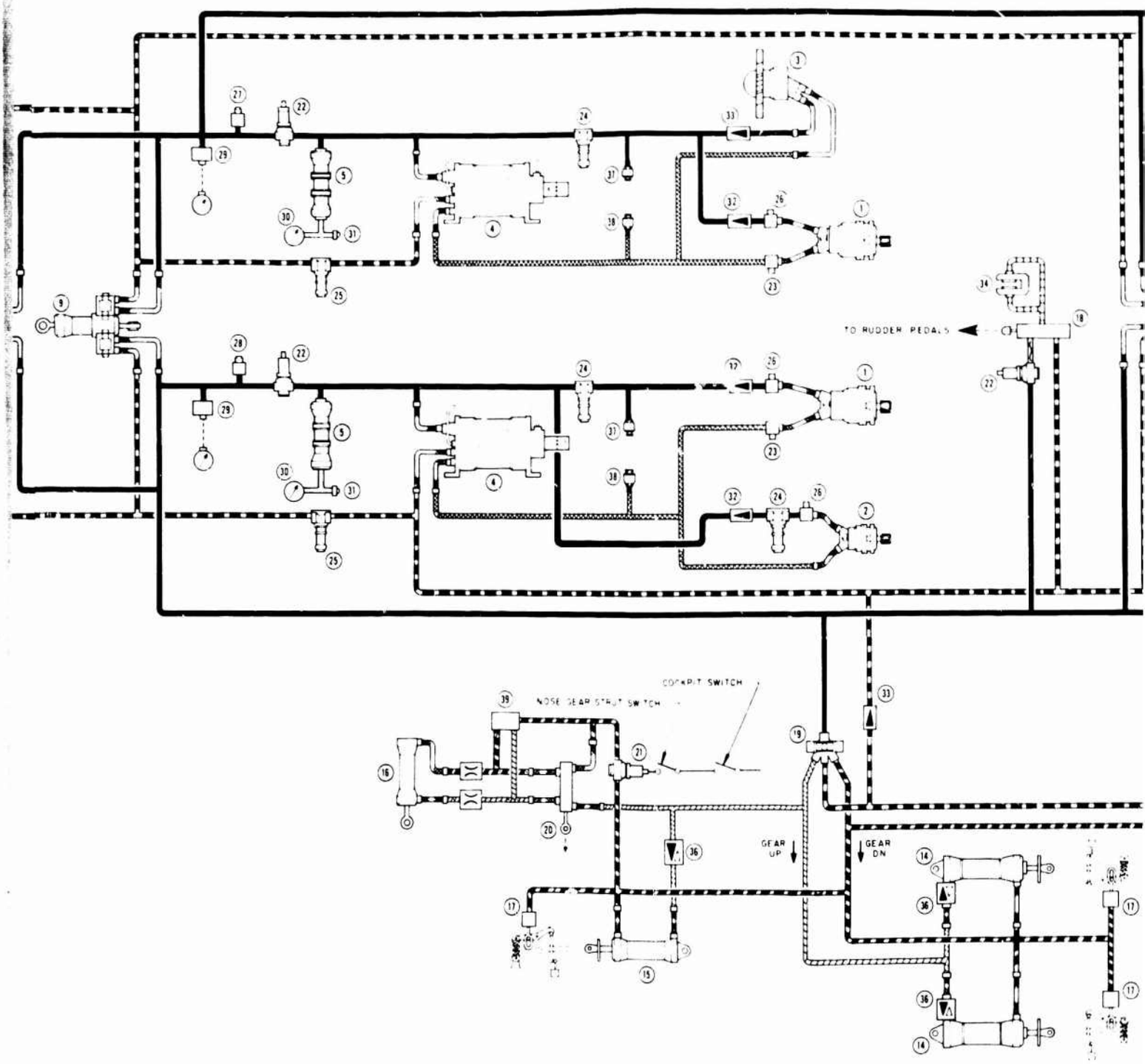
TO RUDDER PEDALS
COCKPIT SWITCH
NOSE GEAR STRUT SWITCH
GEAR UP
GEAR DN

B

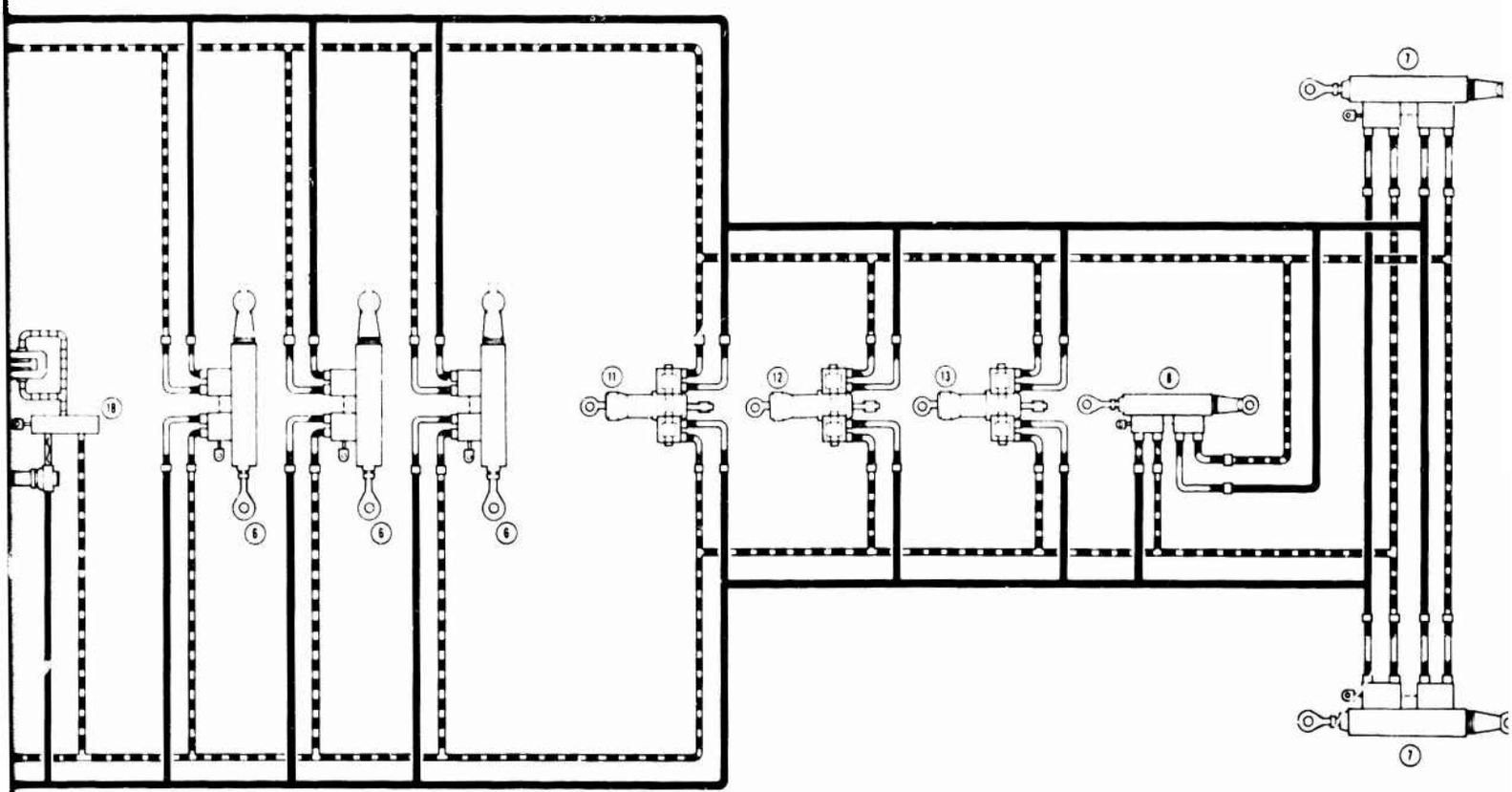
7
18
6
6
6
11
12
13
8
7

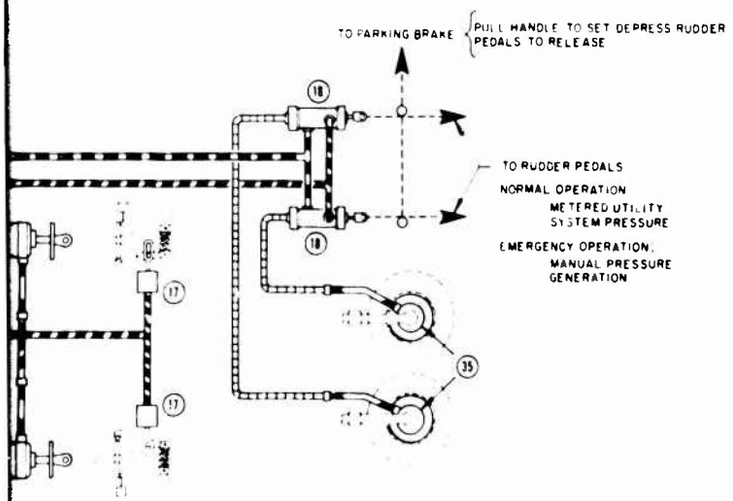
TO PARKING BRAKE
PULL HANDLE TO SET DEPRESS RUDDER PEDALS TO RELEASE
18
TO RUDDER PEDALS
NORMAL OPERATION
METERED UTILITY SYSTEM PRESSURE
EMERGENCY OPERATION, MANUAL PRESSURE GENERATION
18
17
17
35

solenoid-operated valves. One valve is connected to the flight control hydraulic system, and the other valve is connected to the utility system control valve. If the utility hydraulic system malfunctions, a differential pressure switch automatically diverts hydraulic power to the flight control system control valves.

Hydraulic power from the utility hydraulic system is provided for normal operation of the main and nose landing gears and their locks. The landing gear is controlled by an electrically operated directional valve. Limit switches in the uplocks deenergize the landing gear control valve when the gear is up and locked, thereby depressurizing the landing gear actuators. Hydraulic pressure is continually maintained on the actuators when the gear is down.

Landing Gear

The main landing gear (see Figures 99 and 100) is a single-tire laterally articulating configuration. The tire size is 11.00-12 Type III (tubeles Retraction is accomplished by shrinking the oleo leg and folding the axle fork; this folds the wheel into the bottom of the fuselage. A lock secures the gear in the retracted position. Free-fall emergency extension of the landing gear is accomplished by manual release and gear weight. Locking in the down position is accomplished by overcenter linkages aided by mechanical springs.

The nose landing gear (see Figure 101) is a dual corotating wheel attached to a cantilevered oleo. The tire size is 18 x 4.4 Type VII (tubeless). The gear retracts forward with a folding drag brace. The retraction system utilizes jury links to position the lower drag brace, which is arranged to lock the gear in both the up and the down position. In an emergency situation, the nose gear will free-fall to the down and locked position.

Nose wheel steering is accomplished through use of a hydraulic steering actuator. Hydraulic power for nose wheel steering is provided by the utility hydraulic system when the landing gear control valve is in the down position. Steering directional control is accomplished by operation of the rudder pedals, which are connected to the steering actuator control valve through mechanical linkage. Steering is automatically engaged when the aircraft weight is on the nose wheel. A switch is provided on the cyclic stick grip to deenergize the nose gear steering if desired.

Main wheel brakes are individually controlled by operation of brake control valves through mechanical linkage to the rudder toe pedals. The wheel brake system incorporates power brake control valves having both a normal and an emergency mode of operation. For normal operation of the

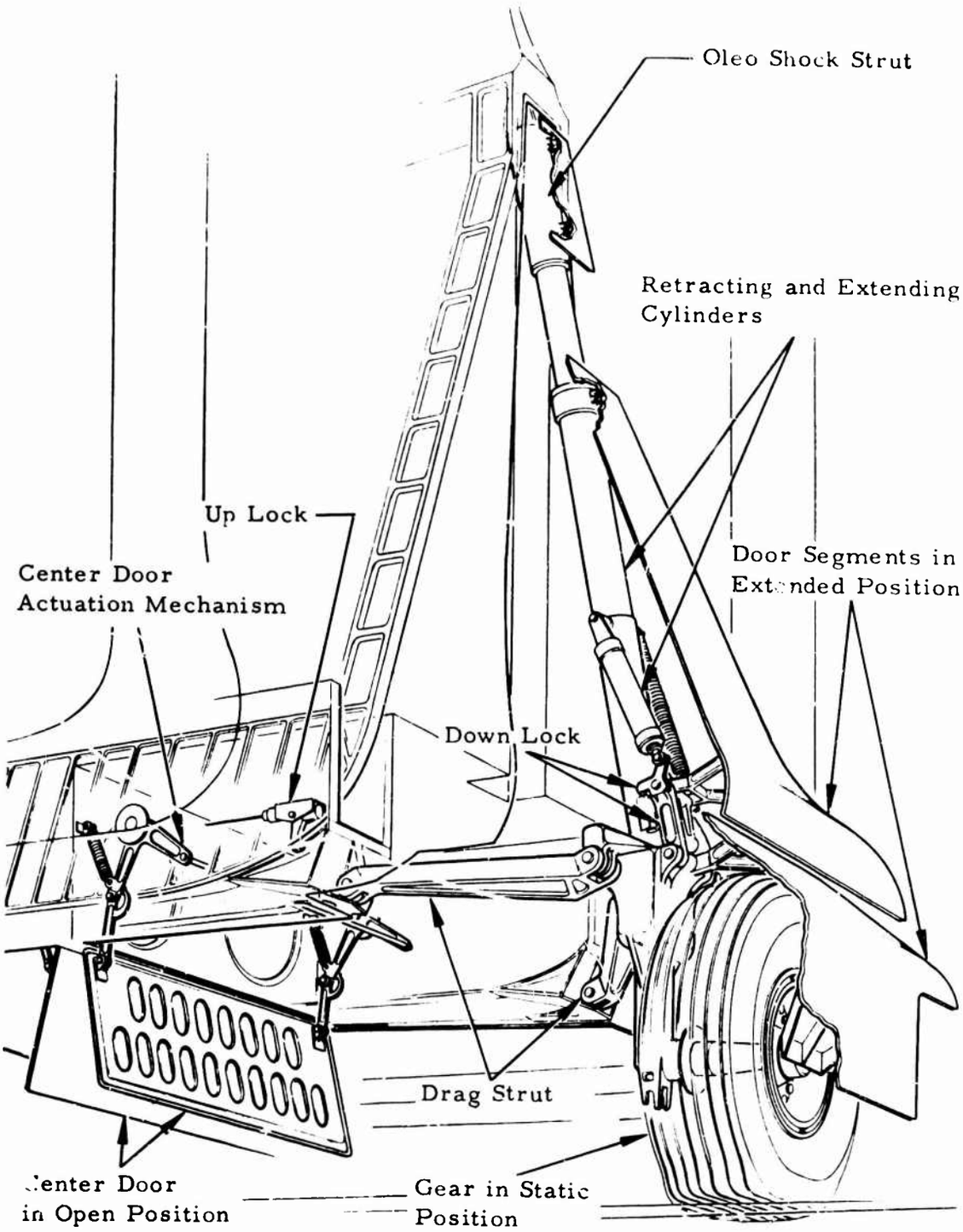

Figure 99. Main Landing Gear - Extended.

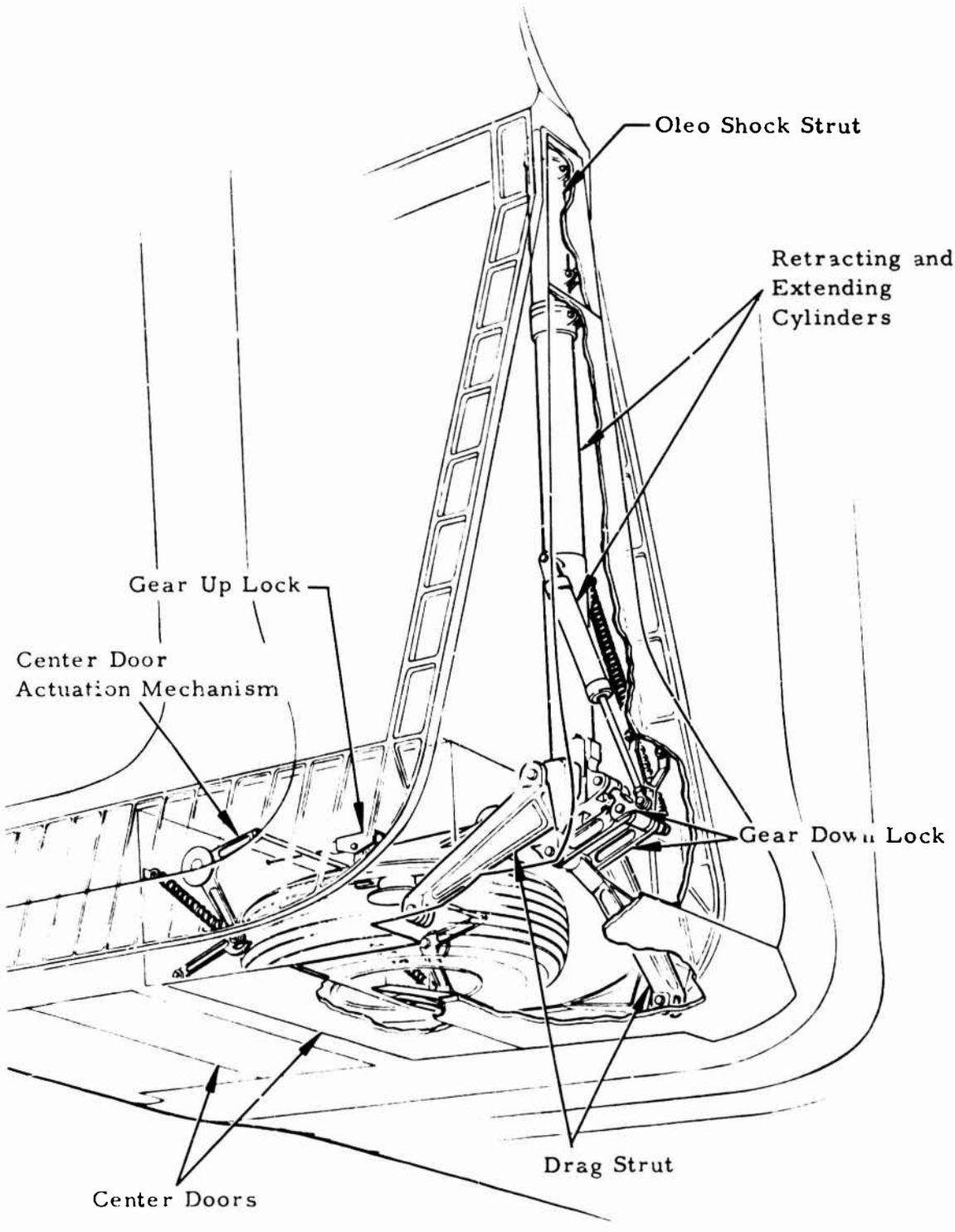

Figure 100. Main Landing Gear - Retracted.

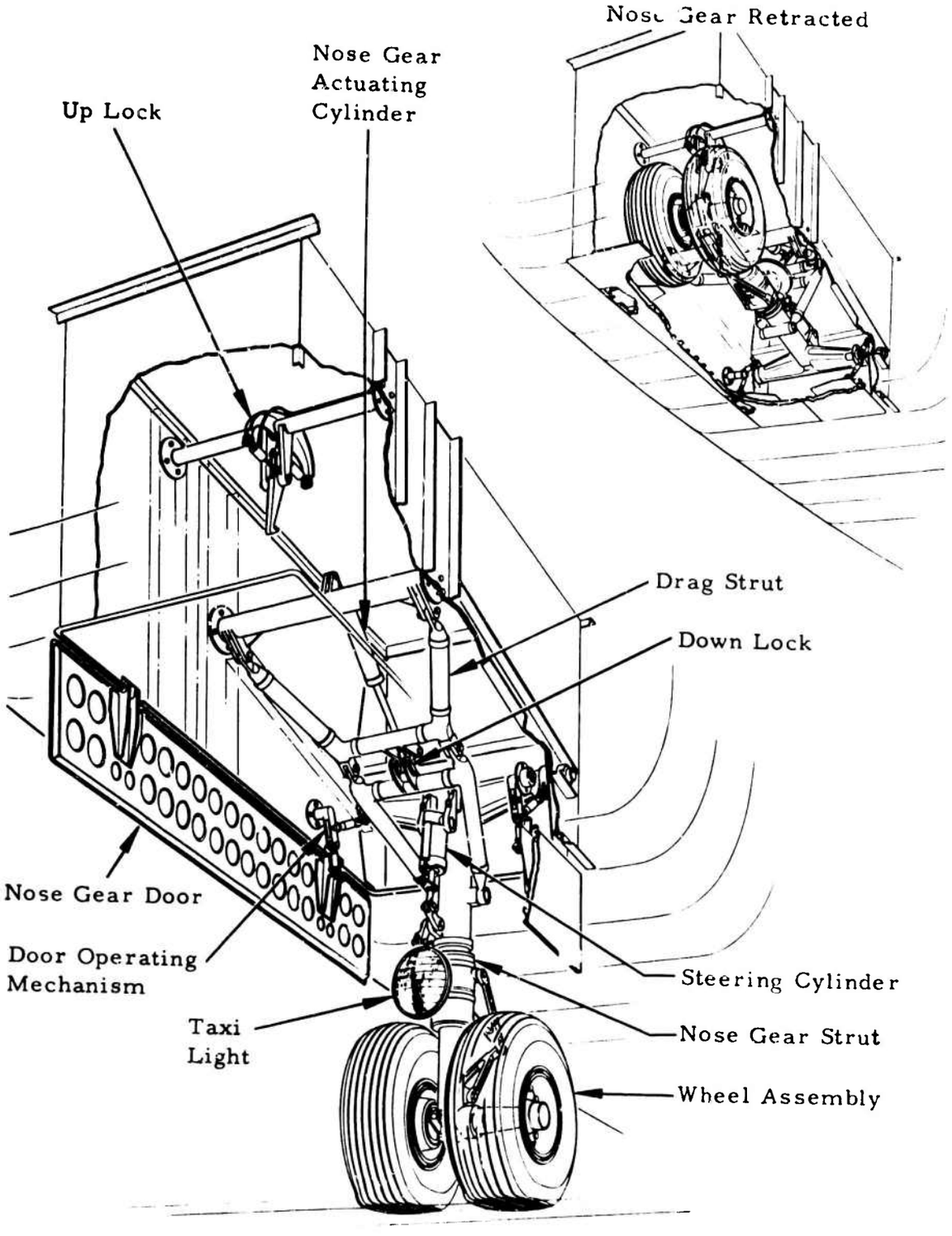

Figure 101. Nose Landing Gear.

wheel brakes, hydraulic pressure is supplied by the utility hydraulic system and metered to the wheel brakes by brake control valves. When the utility hydraulic system is not in operation, the power brake valves act as master cylinders to provide hydraulic pressure for the brake operation.

Rotor Brake

During the mode conversion from autogyro to airplane, the rotor brake in conjunction with collective pitch provides a decelerating torque to reduce the rotational speed in preparation for stopping the rotor and positioning the wing by the locator. Braking is accomplished by toe pressure on the rudder pedals, which are connected to the rotor brake control valve by mechanical lines. Either or both rudder toe pedals may be used to apply the brake. The utility hydraulic system supplies the power to the brake control valve through a shutoff valve that supplies pressure only below 40 percent rotor speed, thereby eliminating the possibility of inadvertent brake application. The brake is capable of reducing the rotor speed from 40 percent N_R to 5 rpm in 5 seconds without introducing undue yaw loads to the aircraft. In the event that utility system hydraulic power is lost, the brake control valve acts as a master cylinder to provide hydraulic pressure for manual operation.

Rotor/Wing Locator

The Rotor/Wing locator consists of a channel incorporating a spring-loaded ratchet and an air-oil shock absorber stop activated by a single-ended, dual-control valve hydraulic actuator (see Figure 102). When the rotor reaches a speed of 5 rpm on run-down, the hydraulic actuator is activated by the mode selector switch and, in sequence, raises the locator to engage the locator pin that is located on the underside of the Rotor/Wing. The pin passes over the spring-loaded ratchet and is decelerated to a stop upon engagement of the shock absorber. The air spring in the shock absorber then returns the rotor to the ratchet stop, where it is held.

Rotor Locks

After the Rotor/Wing has been brought to a stopped position by the locator, the rotor is then locked to the fuselage at three points. Two are located across the aircraft from each other at the centerline of the rotor to stiffen the wing-to-fuselage attachment in the rolling moment direction. The third wing-to-fuselage lock is located forward of the rotor centerline and engages the wing to stiffen the wing-to-fuselage attachment in a pitching moment direction (see Figure 103).

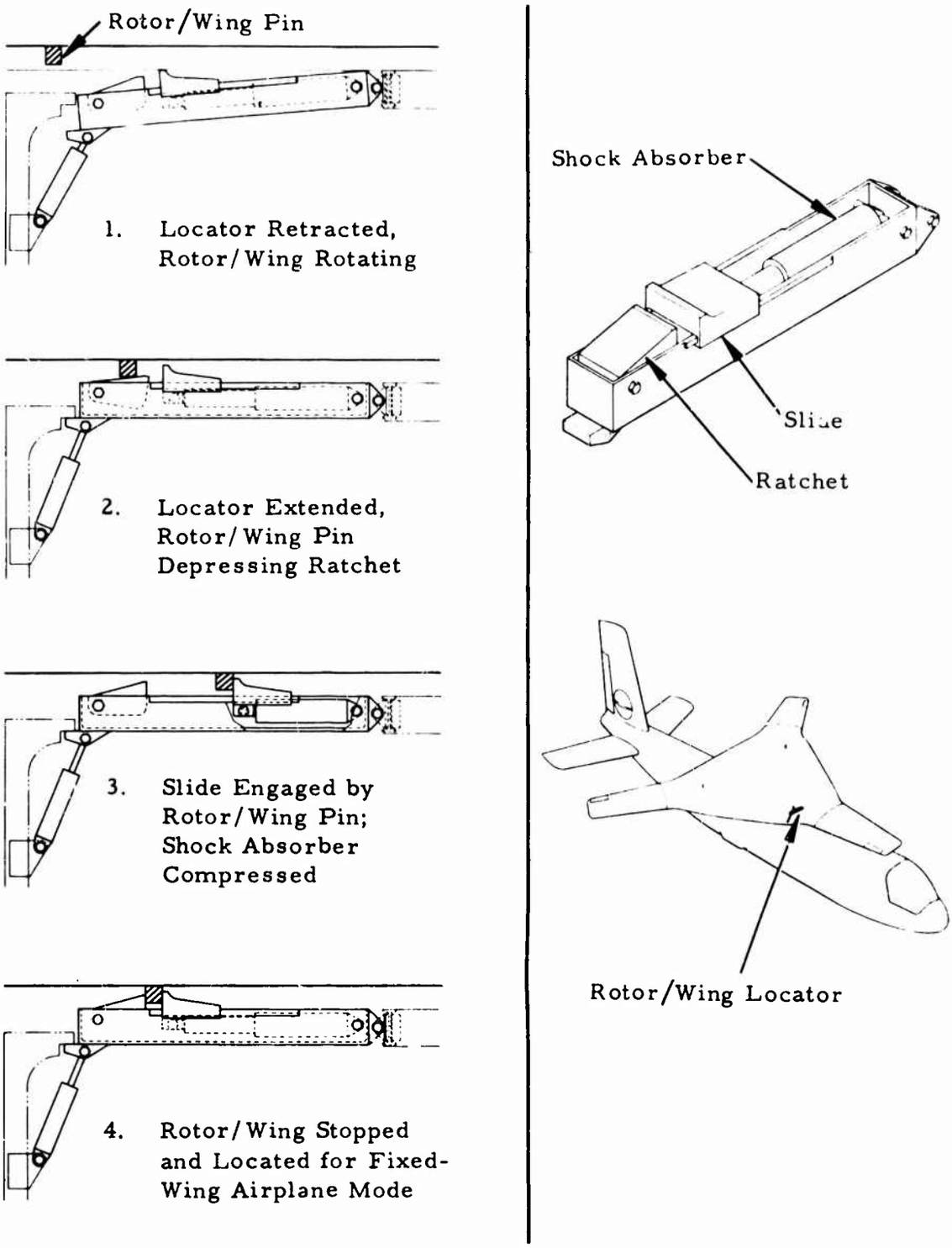

Figure 102. Rotor/Wing Locator.

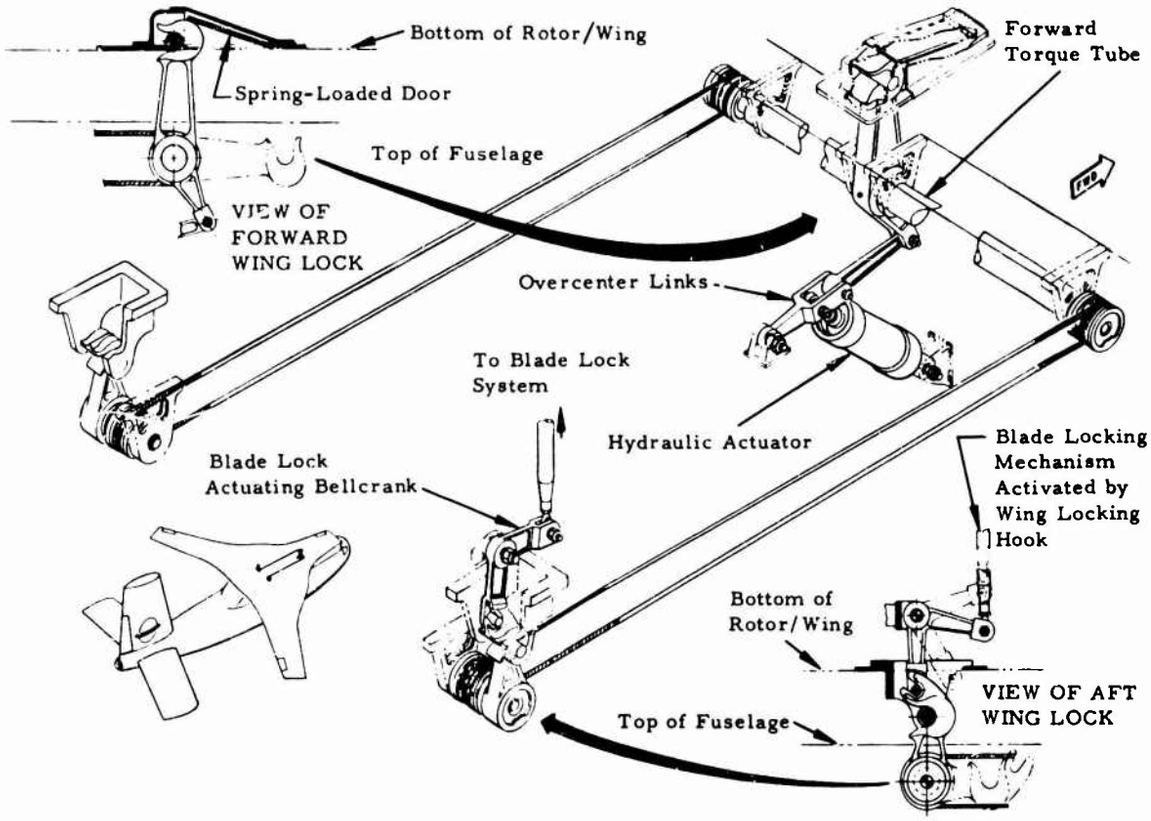

Figure 103. Wing Lock System.

Blade Locks

Blade-to-wing locks (see Figure 104) have been installed to fix the blade to the wing under torsion loads. These locks are engaged after the rotor has stopped. Engagement of the blade locks is accomplished by the action of locking the wing to the fuselage to preclude completely the possibility of blades being locked in the rotating rotor condition.

Engine Duct Assembly

To provide an aerodynamically efficient engine inlet in the airplane mode and to provide blade clearance for the rotor turning in the helicopter mode, the engine inlet assembly is made retractable; it extends upward to the underside of the forward blade in the airplane mode and retracts into the fuselage for the helicopter and autogyro modes. The assembly, extending from the canted cockpit bulkhead to the forward edge of the engine

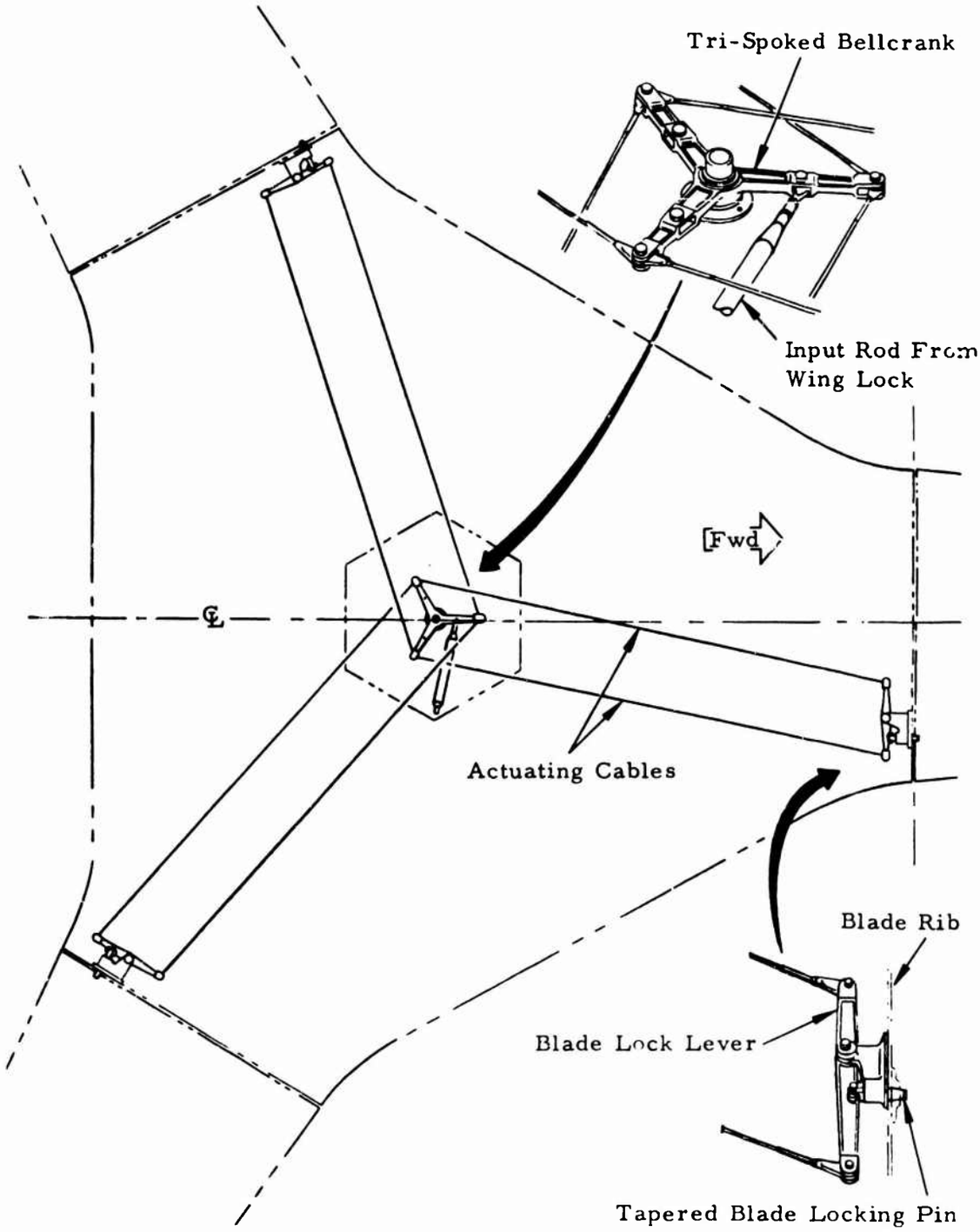

Figure 104. Wing and Blade Locks.

bellmouth, is an inverted U-section that seals against the underside of the forward blade (see Figure 105).

The inlet duct assembly mechanism consists of two sets of scissors on each side linked together with torque tubes. Centrally located bellcranks attached to each torque tube are operated by a single-ended, dual-control-valve hydraulic actuator that is controlled by the mode selector switch mounted on the collective control stick.

Rollers, incorporated with each scissor pickup fitting, traverse in the vertical tracks provided in the fixed fuselage structure.

Yaw Fan Drive System

A hypercritical-speed shaft design was chosen to provide maximum simplicity and reliability for the yaw fan drive system (see Figure 106). This type of system is a simple extension of the tail rotor drives proven so successfully on the HTC-AD 269A and OH-6A helicopters. It is admirably suitable for this type of application and has the added advantage of reducing the overall vibration level of the aircraft.

As shown in Figure 106, the yaw fan is driven by lightweight shafting, running from a power takeoff at the rotor accessory gearbox through intermediate gearboxes, to the yaw fan gearbox.

The shaft between the forward and aft intermediate gearboxes incorporates flexible couplings at each end that do not require lubrication and have high reliability and a long service life. Two supports are located to permit the operating speed to fall within the fifth and sixth critical speeds. This drive configuration and operating speed permit the torsional natural frequency to be maintained at between 5 and 6 cps to eliminate the possibility of excitation by the pilot The gearboxes are smaller and more lightly loaded as a result of the high rpm and low torque used in transmitting the required power.

The yaw fan is a 6-bladed configuration with a 4.7-foot diameter; it turns at a speed of 2,930 rpm and incorporates a blade pitch change of ±20 degrees. The yaw fan gearbox utilizes a conventional gear system of spiral bevel meshes and lightweight housing. A short shaft connects the yaw fan gearbox to the aft intermediate gearbox with flexible couplings at each end. The intermediate gearboxes utilize spiral bevel gears of 1:1 gear ratio. A self-contained lubrication system is used. A Rotor/Wing brake is provided on the forward intermediate gearbox output shaft.

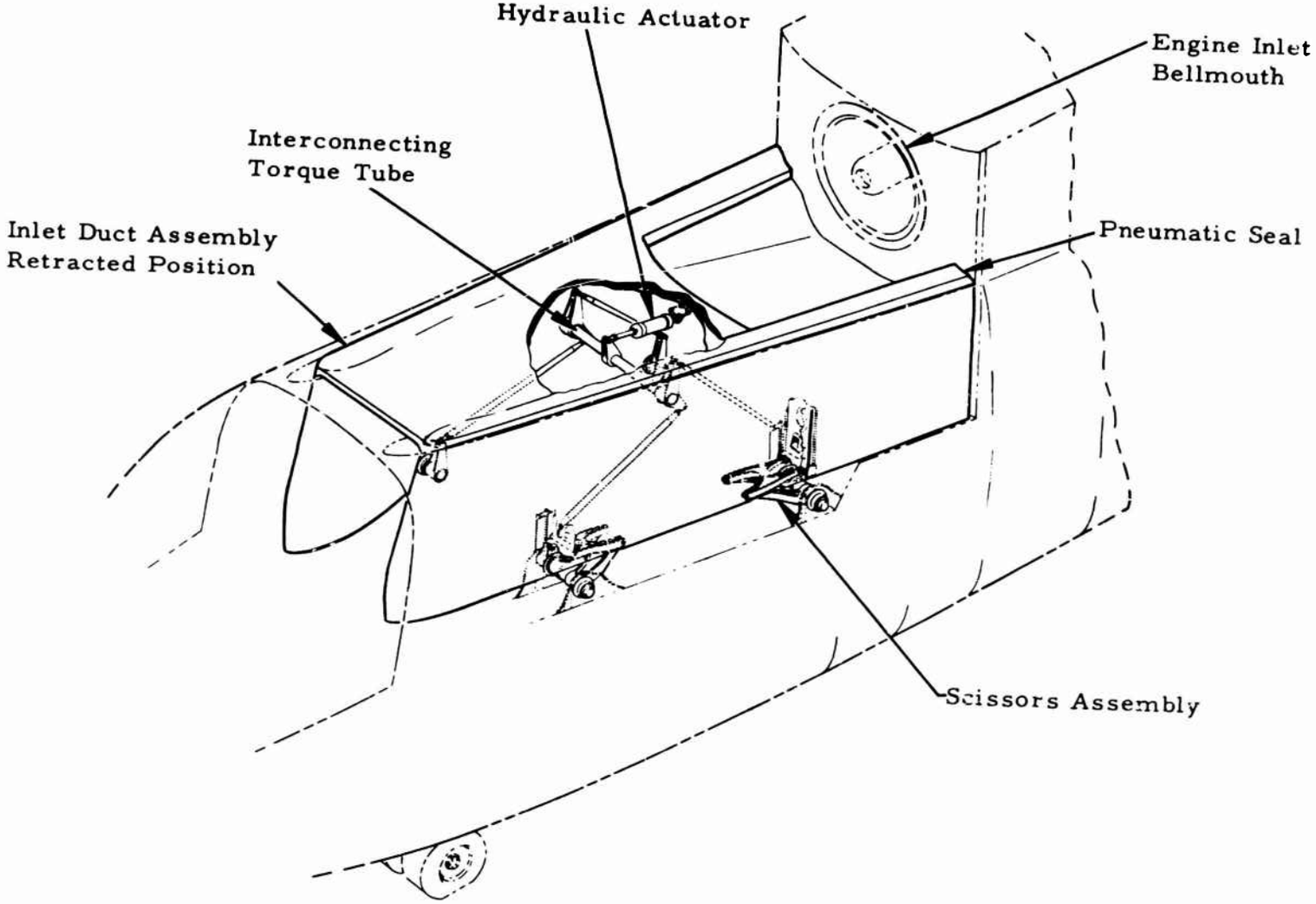

Figure 105. Retractable Inlet Duct.

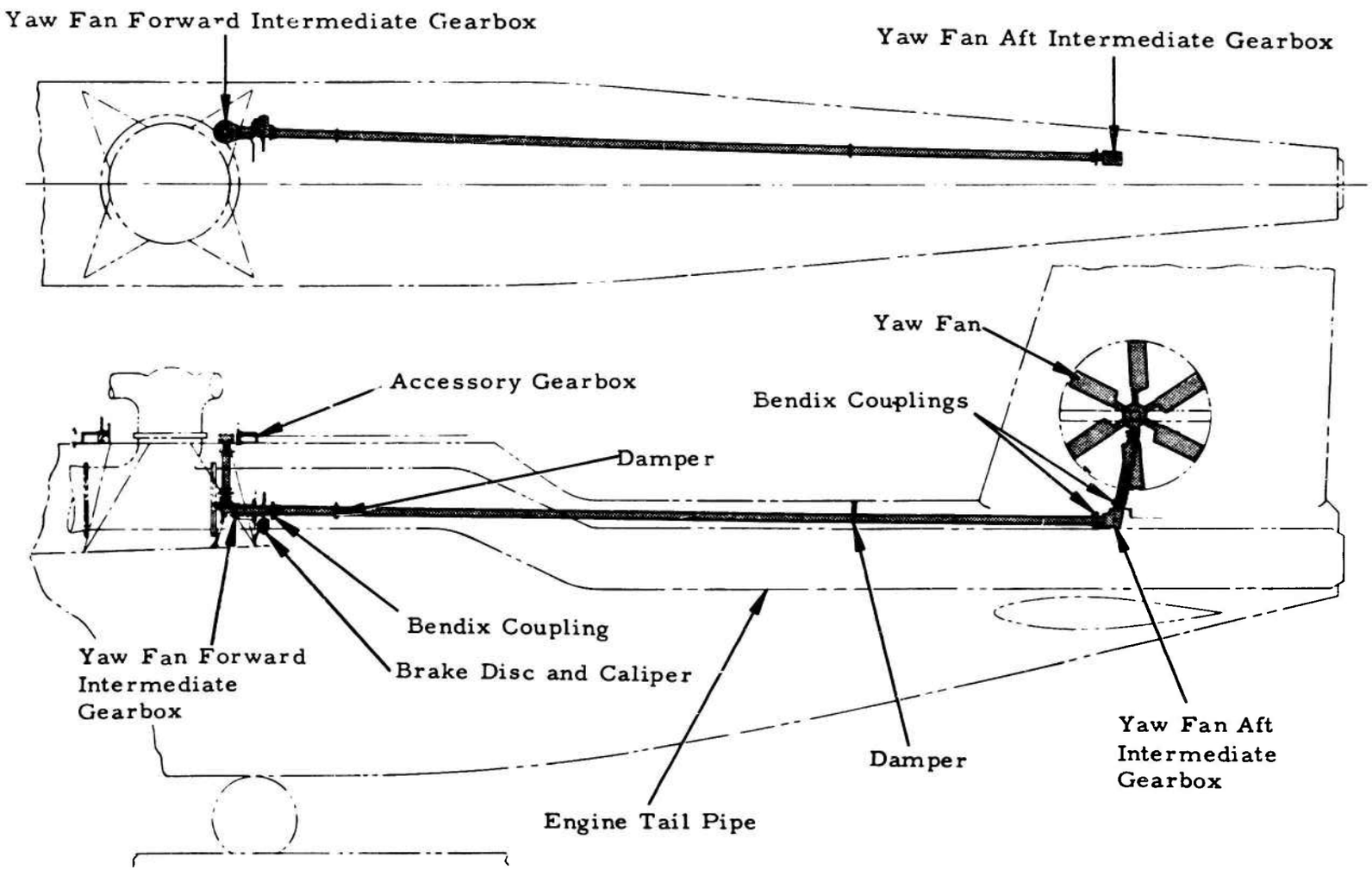

Figure 106. Yaw Fan Drive System.

Accessory Gearbox

The Rotor/Wing hub structure serves a dual purpose in that it accommodates the rotor hub main bearing assembly and accessory drive ring gear. The ring gear is attached to the rotating hub structure, which drives independent power takeoffs through conventional spur gearing for the yaw fan drive shaft, hydraulic pump, oil pressure/scavenger pump, and tachometer (see Figure 107).

The hydraulic pump, pressure/scavenge pump, and tachometer are bolted directly to the power takeoff pad on the underside of the accessory gearbox. The yaw fan drive power takeoff assembly is bolted to the underside of the accessory gearbox and consists of a conventional input spur gear with a short shaft connecting it to the forward intermediate gearbox.

The rotor lubrication system, shown in Figure 108, supplies circulating lubricating oil for the rotor main bearing and accessory gearbox. The system employs a dual pressure and scavenge pump driven from the accessory gearbox. Lubricating jets direct oil to the main bearing, ring gear, spur gear train, and bearings; internal gravity drain passages direct the oil to the scavenge pump and return it to the reservoir.

Ram-Air Turbine

To provide immediate hydraulic power for flight control in the event of an engine power failure during fixed-wing airplane flight, a ram-air turbine-driven hydraulic pump is provided (see Figure 109). Sufficient emergency hydraulic power is supplied for flight control and for accomplishing conversion to autorotational flight. In autorotational flight, the rotor-driven hydraulic pump provides additional hydraulic power.

The ram-air turbine pump is mounted on a hinged door that is spring-loaded for opening. The pilot extends the pump into the airstream by pulling a T-handle to release the door latch. Springs and overcenter linkages open the door and lock it in position.

The variable-pitch turbine blades, sensing turbine load, vary pitch to match pump output to hydraulic power demand.

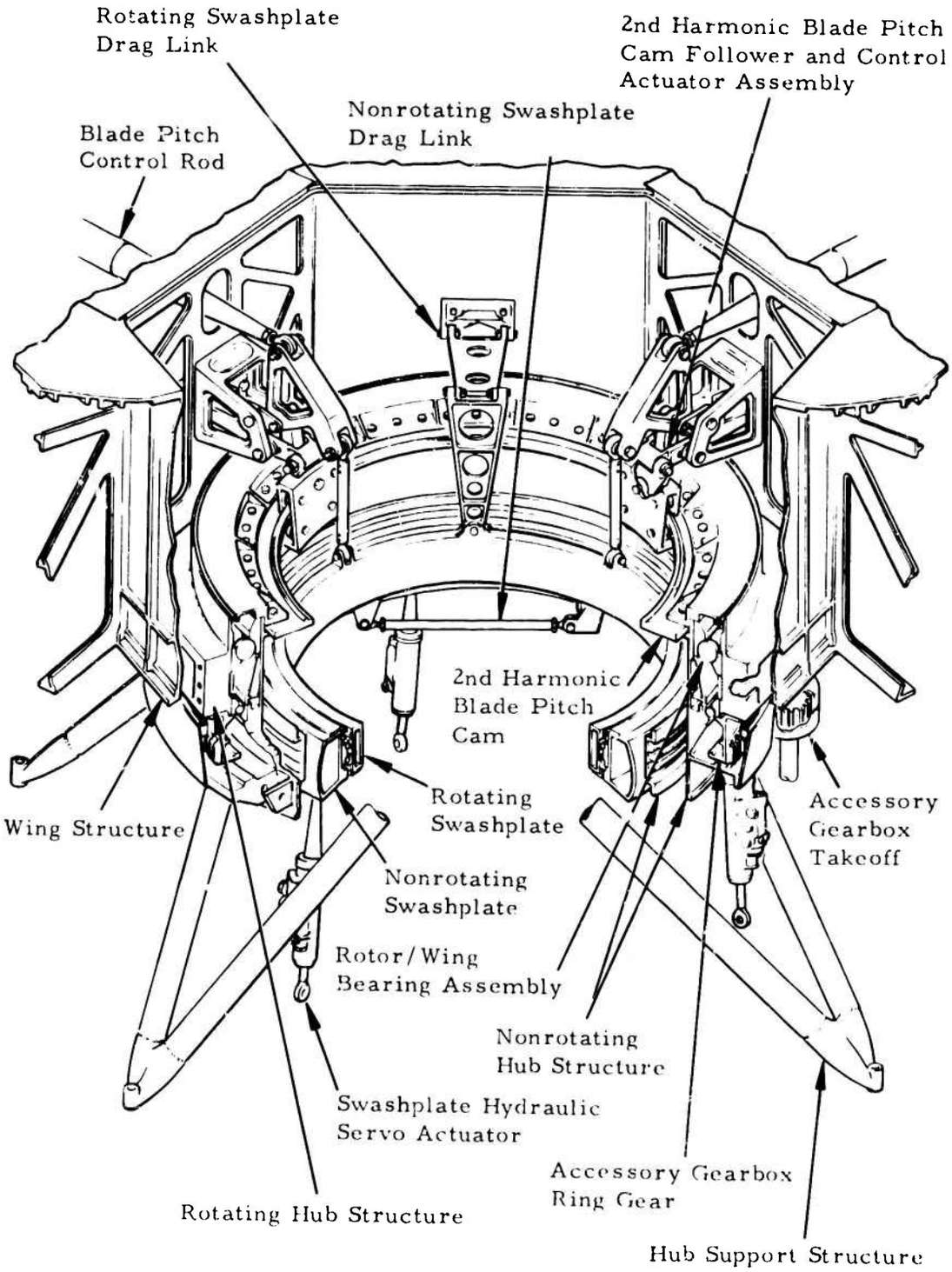

Figure 107. Hub Assembly.

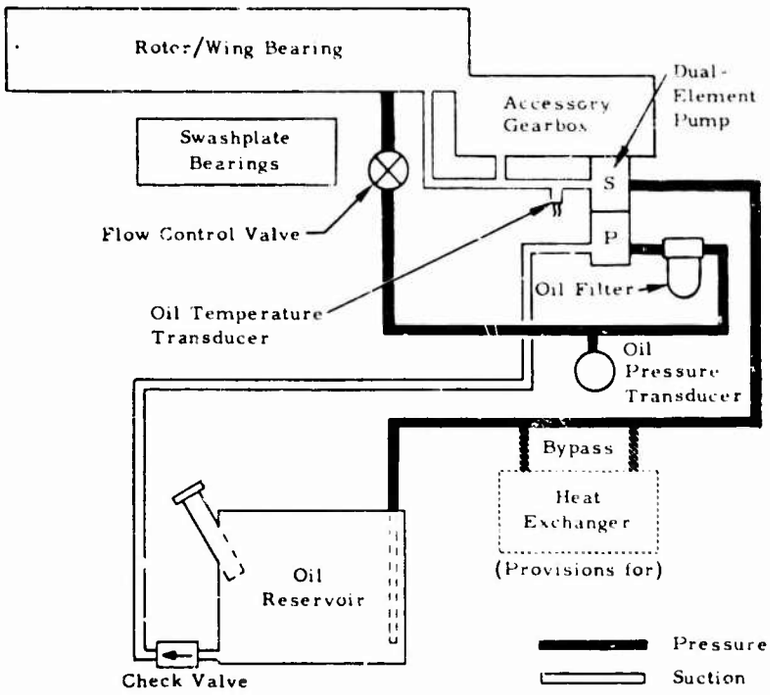

Figure 108. Rotor/Wing Lubrication System Schematic.

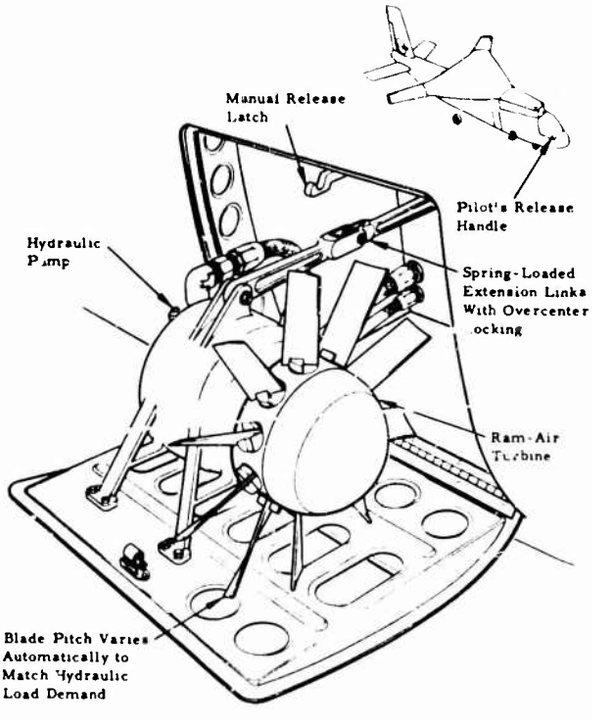

Figure 109. Ram-Air Turbine Installation.

NORMAL AND EMERGENCY OPERATING PROCEDURES

The simple design concept of the Hot Cycle Rotor/Wing CRA with its built-in safety features permits direct and uncomplicated normal and emergency operating procedures. The simplicity of the concept is further enhanced by an installation utilizing a single engine of proven performance and reliability, by the fail-safe features of two independent hydraulic systems, and by the immediate capability of autorotation from the helicopter or airplane modes, or while performing conversion. The process of converting to autorotative flight is accomplished by simply lowering the collective stick if in the helicopter mode, or by unlocking the Rotor/Wing and lowering the collective pitch to a negative angle if in the airplane mode.

As a result of this simplicity, the aircraft is controlled in any flight mode exclusively through the use of the following six major controls:

1. Cyclic stick - for lateral and longitudinal control.
2. Collective stick - for vertical control and engine control in helicopter mode.
3. Rudder pedals - for directional control.
4. Throttle lever - for engine power control in airplane mode.
5. Power divert switch - for helicopter thrust or airplane thrust.
6. Mode selector switch - for starting or stopping the Rotor/Wing in flight.

In addition to the six major controls, normal switching controls are provided in the cockpit for the control of subsidiary systems.

NORMAL OPERATING PROCEDURES

Conventional helicopter dual controls are used in the CRA. For helicopter flight, the cyclic and collective sticks are connected to the blades through a swashplate for vertical, lateral, and longitudinal control. The cockpit controls are continuously connected to the elevons and rudder, but these surfaces are largely ineffective for controlling the aircraft at low helicopter flight speeds. In the helicopter mode, the rudder pedals are used for directional control through the yaw fan, and the engine power is controlled by the rotor governor.

In the airplane mode, the collective stick is not used; the Rotor/Wing controls are deactivated, and the cyclic stick is used to control the elevons for lateral and longitudinal control; and the rudder is operated through the pedals for yaw control. The yaw fan is stopped and covered by fairing doors so that it is no longer effective. Engine power is controlled by the throttle quadrant on the console during flight in the airplane mode.

The power divert switch is used to control the position of the diverter valve to direct thrust to the blades for the helicopter mode or to the tail pipe for the airplane mode.

As an aid to the pilot, an artificial feel system is incorporated in the roll, pitch, and yaw systems for both helicopter and airplane flight. These feel forces may be trimmed to zero by using the stick-mounted beep switches.

Normal operating procedures sequencing is presented in Figure 110 and delineated in Table XXIX. Normal procedures for mode conversion from helicopter to autogyro and from autogyro to airplane are depicted in Figures 111 and 112.

EMERGENCY OPERATING PROCEDURES

The Hot Cycle Rotor/Wing concept provides capabilities under emergency conditions that combine the safe recovery features of the helicopter and the high performance airplane. The rotor can be started from the airplane mode to convert to autogyro operation using aerodynamic forces alone, and a subsequent safe landing can be made without power. The process of converting to autorotative flight is accomplished by lowering the collective stick when in the helicopter mode or by unlocking the rotor using the mode selector switch when in the airplane mode and then lowering the collective pitch to a negative setting to start the rotor. The configuration of the CRA with the cockpit forward of the rotor permits use of zero-zero ejection seats in any flight mode to effect safe evacuation of the aircraft.

Two completely independent hydraulic systems power the flight control system, and alternate power sources are available for both systems in any flight mode. In the event of an engine failure in the helicopter mode, the rotor-driven hydraulic pump supplies the power for control during autorotative flight. If an engine failure should occur while in the airplane mode, conversion to autorotation again provides the necessary control power. The ram-air turbine-driven pump supplies the hydraulic power during conversion to ensure that full hydraulic power is available while the rotor is gaining sufficient speed to drive its pump at full operating pressure.

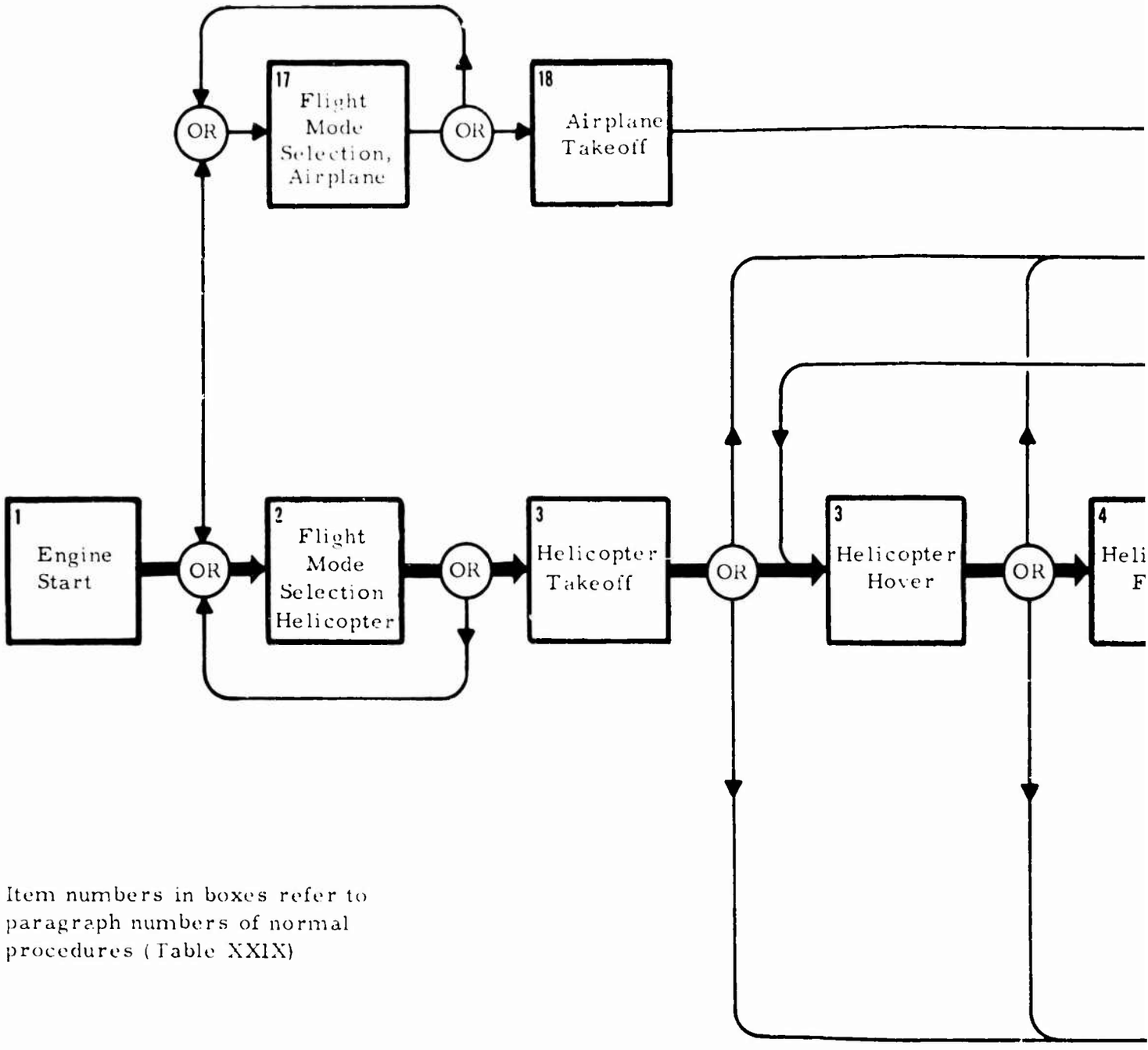

Item numbers in boxes refer to paragraph numbers of normal procedures (Table XXIX)

Figure 110. Functional Chart.

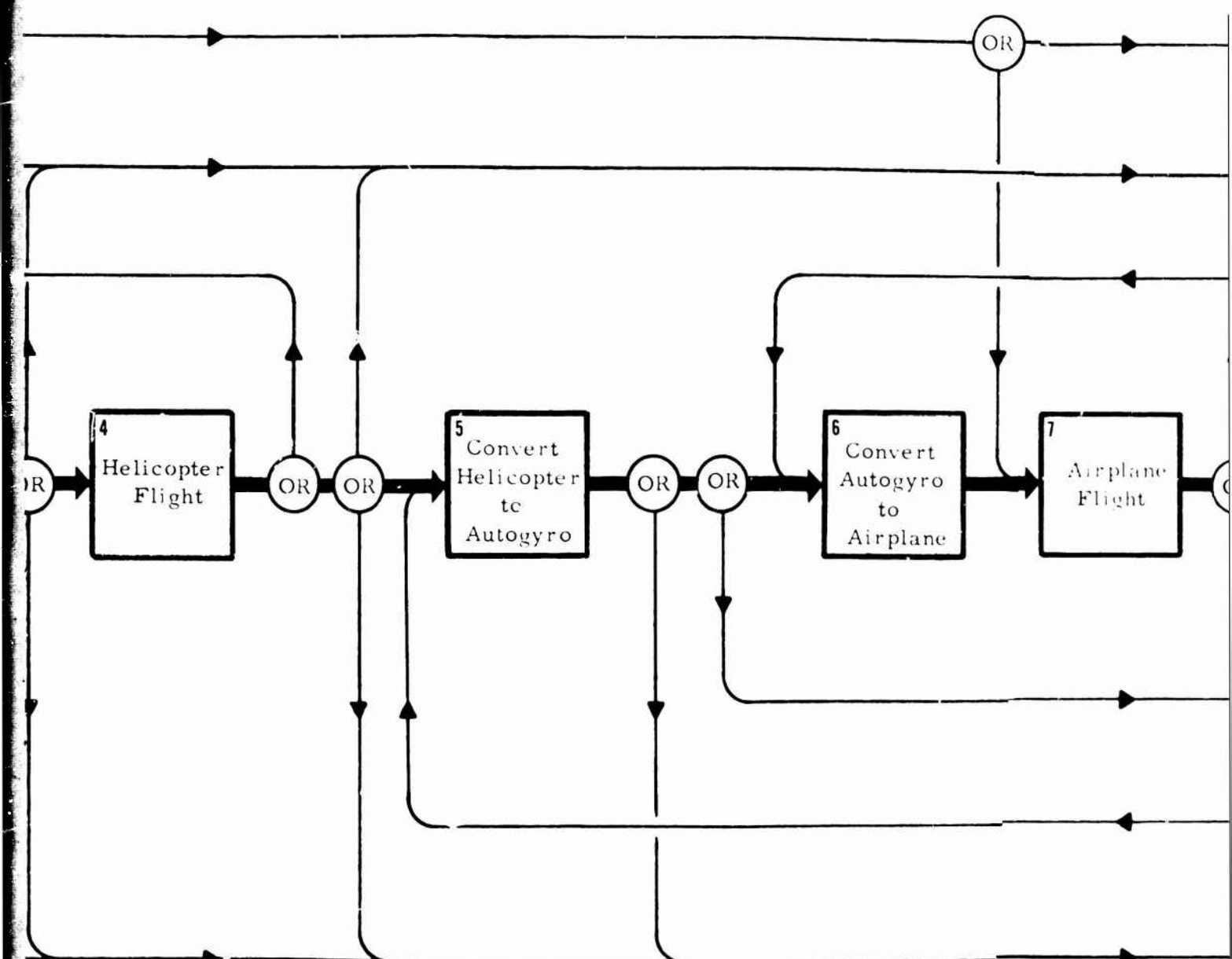
OR
4
Helicopter
Flight
OR
OR
5
Convert
Helicopter
to
Autogyro
OR
OR
6
Convert
Autogyro
to
Airplane
7
Airplane
Flight

B

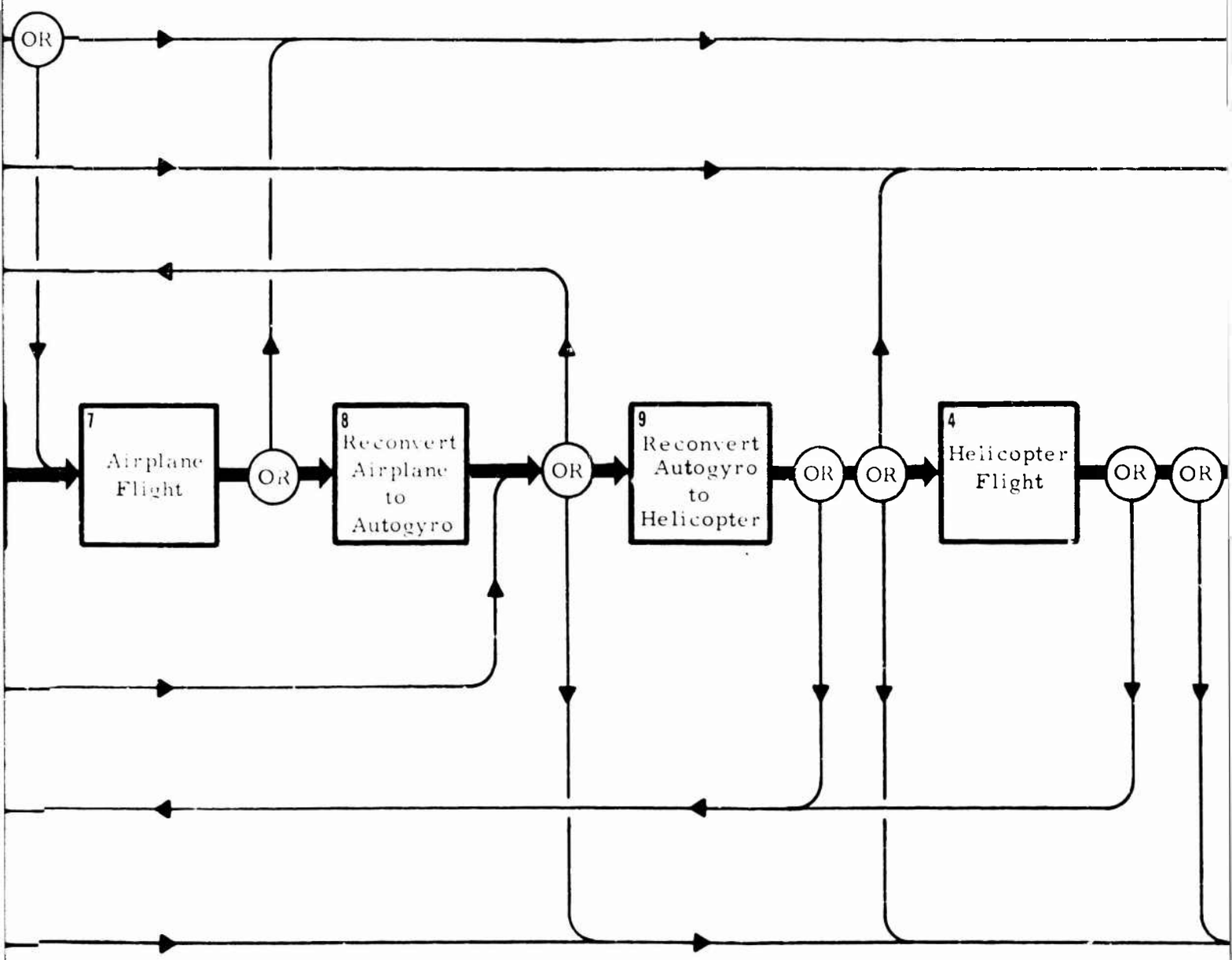
OR
7
Airplane Flight
OR
8
Reconvert Airplane to Autogyro
OR
9
Reconvert Autogyro to Helicopter
OR
OR
4
Helicopter Flight
OR
OR

C

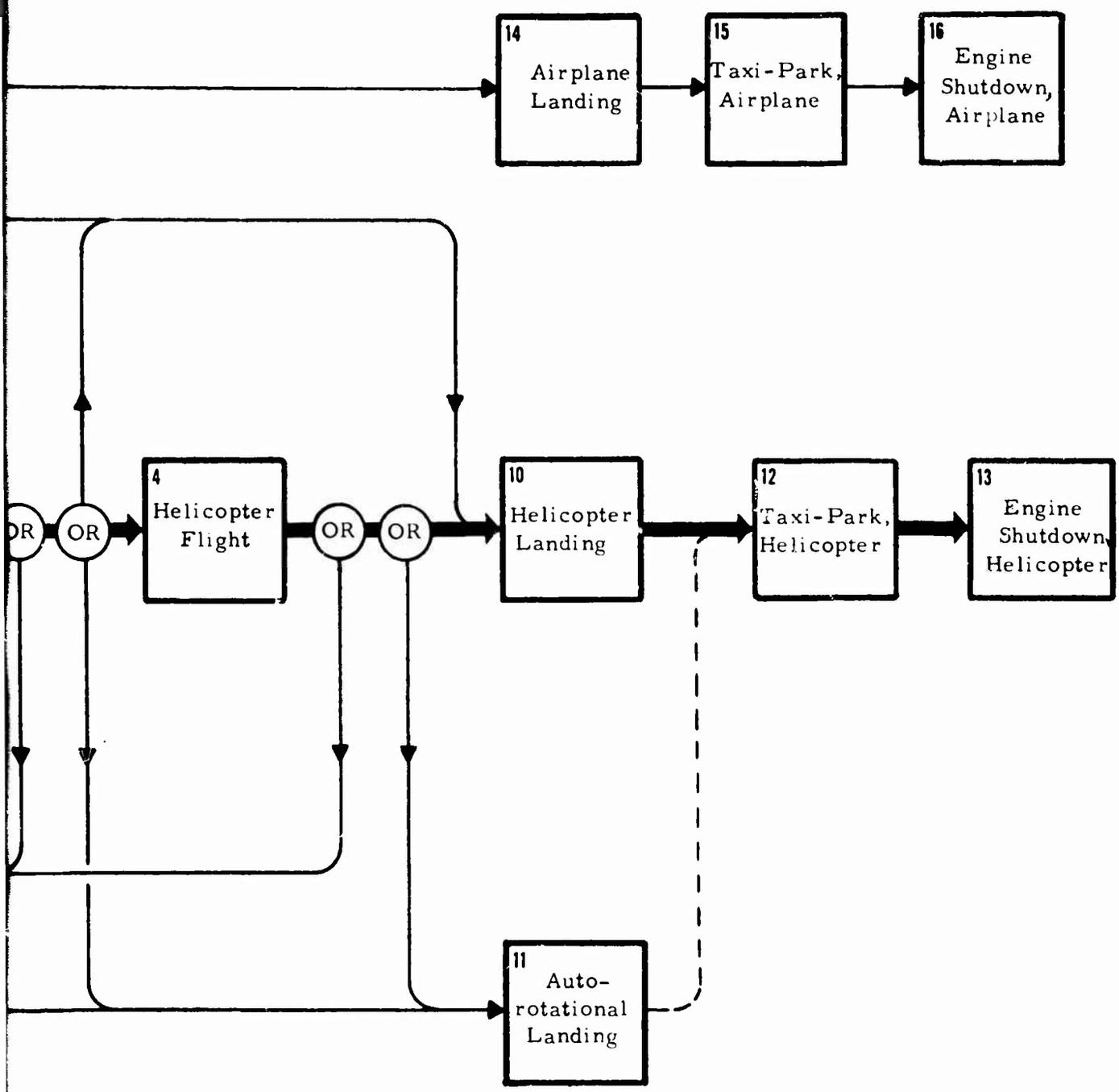
14
Airplane Landing
15
Taxi-Park, Airplane
16
Engine Shutdown, Airplane
OR
OR
4
Helicopter Flight
OR
OR
10
Helicopter Landing
12
Taxi-Park, Helicopter
13
Engine Shutdown, Helicopter
11
Auto-rotational Landing

D

TABLE XXIX. NORMAL OPERATING PROCEDURES

Mode	Operation	Action
1. Engine ground start	a. Connect engine start cart.	Provides air supply to engine air turbine
	b. Connect external electrical power (24 v).	Provides power to air starter valve and to relay providing ac power for engine.
	c. Set electrical power switch to EXTERNAL.	Check dc volts.
	d. Set main inverter switch to ON.	Check ac volts and frequency.
	e. Set radio-intercom appropriate radio switches to ON.	
	f. Push appropriate circuit breakers in.	
	g. Set power divert switch to AIRPLANE.	Sets diverter valve to tail pipe, deenergizes Rotor/Wing governing. Diverter valve linkage sets elevons to airplane trim position.
	h. Set nose wheel steering switch to DISENGAGE.	
	i. Set fuel control switch to NORMAL.	Selects primary fuel system on engine fuel control unit.
	j. Check throttle at OFF.	
	k. Set engine electrical power switch to ON.	
	l. Set fuel tank shutoff switches to OPEN.	
	m. Set fuel fire wall shutoff valve switch to OPEN.	
	n. Set fuel emergency boost pump switches individually to ON; when check is complete, set both to OFF.	Check fuel pressure low light off.
	o. Set fuel boost pump switches individually to ON; when check is complete, set both to ON.	Check fuel pressure low light off.
	p. Press warning light test switch.	Checks all warning, caution, and advisory lights.
	q. Set start switch to ON.	Opens air valve to engine air turbine starter, arms circuit to ignition switch on throttle quadrant.

TABLE XXIX - Continued

Mode	Operation	Action
	r. Advance throttle to IDLE when engine rpm (N_2) indicator reads 15 to 18 percent rpm.	Ignition initiated with throttle advance; engine light-off, indicated by exhause gas temperature and engine speed, should occur within 30 seconds after advancing throttle. Allow engine to stabilize within limits to ascertain satisfactory start. Start switch automatically releases and closes air valve when engine starter pad speed approaches 50 percent N_2.
	s. Set generator switch to ON.	Connects generator to essential bus. Check dc volts and amperes. Check ac volts and frequency.
	t. Select electrical power switch to BATTERY.	Connects battery power in circuit and disconnects external power. Provides battery charging from generator.
	u. Check hydraulic pressures (flight control and utility).	
	v. Disconnect engine start cart and external electrical power.	
2. Flight mode selection - helicopter	a. Place collective stick in 0-degree blade angle detent; center cyclic stick.	
	b. Set mode selector switch to ROTOR.	This, in sequence: (1) Retracts wing and blade locks, retracts inlet duct, deflates pneumatic seals, opens bay cooling ejector valve. (2) Opens yaw fan doors. (3) Activates Rotor/Wing controls. (4) Retracts Rotor/Wing locator.
	c. Set power divert switch to ROTOR.	Sets diverter valve to ROTOR. Sets Rotor/Wing governor references. Diverter valve linkage sets elevon trim to helicopter position.
	d. Advance throttle to obtain 100 percent Rotor/Wing rpm.	
	e. Check Rotor/Wing lube system pressure, temperature, and warning light. Check flight control hydraulic system pressure and warning light. Check utility hydraulic system pressure and warning light.	

TABLE XXIX - Continued

Mode	Operation	Action
	f. Set flight control hydraulic system checkout switch to CHECK. Release when check is complete.	Flight control system pressure gage goes to 0 and caution light illuminates. Move cyclic and rudder controls and verify operation of control surfaces.
	g. Set utility hydraulic system checkout switch to CHECK. Release when check is complete.	Utility system pressure gage goes to 0 and caution light illuminates. Move cyclic and rudder controls and verify operation of control surfaces.
3. Takeoff and hover	a. Aircraft is controlled by collective stick, cyclic stick, and rudder pedals (conventional helicopter control).	Provides longitudinal and lateral control by Rotor/Wing. Elevons are always connected to the cyclic stick as elevators and ailerons, but are ineffective. Provides directional control by yaw fan; rudder is always connected to the rudder pedals but is ineffective.
	b. Adjust Rotor/Wing rpm by rpm trim switch on collective stick grip.	Trim switch provides adjustment of Rotor/Wing rpm governing limits.
4. Helicopter flight (to approximately 140 kn)	a. Set landing gear control to UP.	Retracts main and nose landing gears.
	b. Helicopter flight controlled by cyclic and collective sticks and rudder pedals.	Provides longitudinal and lateral control by Rotor/Wing and by elevons, which become effective with increasing airspeed. Provides directional control by yaw fan and by rudder, which becomes effective with increasing airspeed.
	c. Adjust Rotor/Wing rpm by rpm trim switch if necessary.	Trim switch provides adjustment of Rotor/Wing rpm governing limits.
5. Conversion flight - helicopter to autogyro (approximately 80 to 140 kn)	a. Set power divert switch to AIRPLANE.	Sets diverter valve to tail pipe. Deenergizes Rotor/Wing governor. Diverter valve linkage sets elevon trim to airplane position.
	b. Lower collective to maintain approximately 85 percent Rotor/Wing rpm in steady autogyro flight.	Rotor/Wing autorotates. Aircraft flight attitude is nose up.
	c. Control forward thrust by throttle lever or by twist grip.	
	d. Aircraft controlled by cyclic stick and rudder pedals.	Provides longitudinal and lateral control by Rotor/Wing and by elevons. Provides directional control by yaw fan and by rudder.

TABLE XXIX - Continued

Mode	Operation	Action
6. Conversion flight - autogyro to airplane flight (approximately 100 to 170 kn).	a. Set mode selector switch to AIRPLANE.	Closes bay cooling ejector valve. Rotor/Wing speed sensor permits brake operations when Rotor/Wing has slowed down to 40-percent rpm or less. Upon reaching 5 rpm, the Rotor/Wing locator raises and engages the locking pin. After the Rotor/Wing stops, the following occur in sequence: (1) Rotor/Wing controls deactivate. (2) Wing and blade locks engage; yaw fan doors close. (3) Inlet duct raises; pneumatic seals inflate.
	b. Raises collective stick to approximately - 10 degrees to slow down Rotor/Wing. At 40-percent Rotor/Wing rpm, apply brake pressure with toe pedals. During slowdown of Rotor/Wing from 40 percent rpm, lower collective stick to reach approximately 0-degree blade pitch as Rotor/Wing reaches 5 rpm.	
	c. Maintain 1-g flight through conversion with cyclic stick motion.	
	d. Place collective stick in the stowed position	
	e. Control forward thrust by throttle lever or by twist grip.	
	f. Aircraft controlled by cyclic stick and rudder pedals.	Cyclic stick controls elevons for roll and pitch. Rudder pedals control rudder. Yaw fan blade pitch is always connected to rudder pedals, but is ineffective with yaw fan not rotating.
7. Airplane flight (approximately 100 to 500 kn)	a. Control forward thrust by throttle lever on quadrant.	
	b. Aircraft controlled by cyclic stick and rudder pedals.	
	c. Adjust feel trim switches on cyclic stick as required.	
8. Reconversion - airplane to autogyro (approximately 170 to 100 kn)	a. Reduce airspeed and altitude to be within conversion envelope.	
	b. Set mode selector switch to ROTOR.	This, in sequence: (1) Retracts wing and blade locks, retracts inlet duct, deflates pneumatic seals, opens bay cooling ejector valve. (2) Opens yaw fan doors. (3) Activates Rotor/Wing controls. (4) Retracts Rotor/Wing locator.

TABLE XXIX - Continued

Mode	Operation	Action
	c. Lower collective stick to full down (-10-degree blade pitch angle). At 75-percent Rotor/Wing rpm, gradually raise collective to the blade angle that results in approximately 85-percent Rotor/Wing rpm in steady autogyro flight.	
	d. Maintain 1-g flight with cyclic control.	
9. Reconversion - autogyro to helicopter (approximately 140 to 80 kn)	a. Set power divert switch to ROTOR.	
	b. Raise collective to maintain altitude.	
	c. Maintain 1-g flight with cyclic control.	
10. Landing - helicopter mode	a. Operate landing gear control to DOWN position.	
	b. Check nose gear steering switch to ENGAGE.	
	c. Make conventional helicopter landing.	
	d. Set power divert switch to AIRPLANE.	
11. Taxiing and parking - helicopter mode	a. Taxi to ramp position, maintaining directional control with rudder pedals for nose gear steering and with differential toe pedals for braking.	
	b. Apply landing gear parking brake.	
	In adverse weather or for long duration parking, the Rotor/Wing should be locked during rundown as follows:	
	c. Raise collective stick to +10 degrees.	
	d. Select mode selector switch to AIRPLANE. At 40-percent Rotor/Wing rpm, select Rotor/Wing brake switch to ON and hold, applying Rotor/Wing brake pressure with toe pedals to slow Rotor/Wing. After rotor stops, lower collective stick to 0 degrees.	Bay cooling ejector valve closes. Rotor/Wing speed sensor permits brake operation when Rotor/Wing has slowed down to 40-percent rpm or less. Upon reaching 5 rpm, the Rotor/Wing locator raises and engages the locking pin. After the Rotor/Wing stops, the following occur in sequence: (1) Rotor/Wing controls deactivate. (2) Wing and blade locks engage; yaw fan doors close. (3) Inlet duct raises; pneumatic seals inflate.

TABLE XXIX - Continued

Mode	Operation	Action
12. Engine shutdown - helicopter mode	a. Retard throttle to IDLE.	Allow engine to idle for a minimum of 3 minutes for cooling purposes.
	b. Retard throttle to OFF.	
	c. Observe exhaust temperature for gradual temperature drop. If exhaust temperature does not drop, indicating a fire inside the engine, connect engine start cart and press start switch to motor the engine until exhaust temperature drops.	
	d. Set fuel boost pumps switches (2) to OFF.	
	e. Set fuel fire wall shutoff switch to CLOSED.	
	f. Set fuel tank shutoff switches to OFF.	
	g. Set engine electrical power switch to OFF.	
	h. Set generator switch to OFF.	
	i. Set electrical power switch to OFF.	
	j. Set main inverter switch to OFF.	
	k. Pull circuit breakers to open position.	
	l. Set radio-intercom and radio switches to OFF.	
13. Flight mode selection - airplane (subsequent to engine ground start)	a. Place collective stick in the zero position.	
	b. Set mode selector switch to AIRPLANE.	If necessary, ground crew rotates Rotor/Wing by hand to engage Rotor/Wing locator and to accomplish subsequent sequencing of blade and wing rotor locks, and so forth.
	c. Set nose-wheel steering switch to ENGAGE.	
	d. Check hydraulic pressures (flight control and utility).	

TABLE XXIX - Continued

Mode	Operation	Action
17. Engine shut-down - airplane mode	a. Retard throttle to IDLE.	Allow engine to idle for 3 minutes minimum for cooling purposes.
	b. Retard throttle to OFF.	
	c. Set fuel boost pump switches (2) to OFF.	
	d. Set fuel fire wall shutoff valve switch to CLOSED.	
	e. Set fuel tank shutoff switches to OFF.	
	f. Set engine electrical power switch to OFF.	
	g. Set generator switch to OFF.	
	h. Set electrical power switch to OFF.	
	i. Set main inverter switch to OFF.	
	j. Pull circuit breaker to open position.	
	k. Set radio-intercom and radio switches to OFF.	

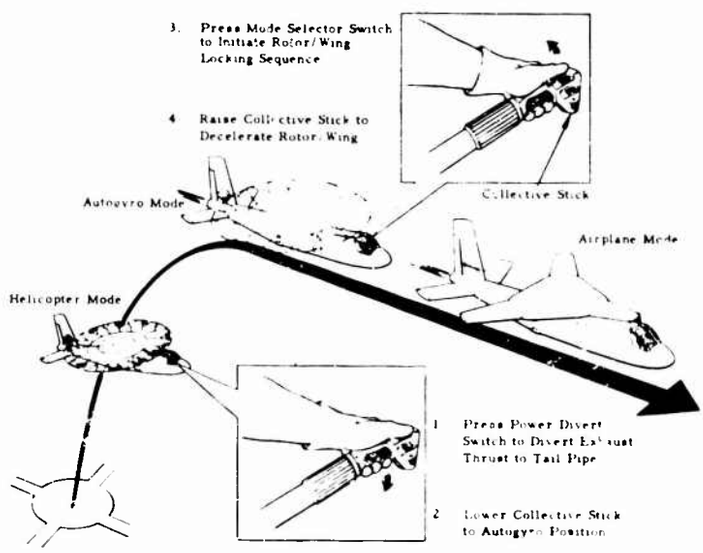

Figure 111. Mode Conversion - Helicopter to Autogyro to Airplane.

TABLE XXIX - Continued

Mode	Operation	Action
	e. Set flight control hydraulic system checkout switch to CHECK.	Flight control system pressure gage goes to 0 and caution light illuminates. Move cyclic and rudder controls and verify operation of control surfaces.
	f. Set utility hydraulic system checkout switch to CHECK. Release when check is complete.	Utility system pressure gage goes to 0 and caution light illuminates. Move cyclic and rudder controls and verify operation of control surfaces.
	g. Control engine thrust by throttle lever on quadrant.	Normal aircraft-type throttle control
14. Takeoff - airplane mode	a. Conventional airplane takeoff. Rotate aircraft at approximately 125 knots. Lift-off at approximately 150 knots	
	b. Aircraft is controlled by cyclic stick and rudder pedals.	Cyclic stick provides control of elevons as ailerons or elevator. Rudder pedals control rudder and yaw fan blade pitch (yaw fan is stopped and ineffective).
	c. Set landing gear control to UP position.	Retracts main and nose landing gears. Landing gear switch closes bay cooling ejector valve when weight off gear.
	d. Set nose gear steering switch to DISENGAGE.	
	e. Adjust feel trim switches on cyclic stick grip.	Neutralize stick and/or rudder pedal to yield pilot desired feel.
15. Landing - airplane mode	a. Set landing gear control to DOWN position	
	b. Make conventional airplane landing.	Maximum forward speed with gear down, 225 kn.
16. Taxiing and parking - airplane mode	a. Set nose gear steering to ENGAGE.	Landing gear switch opens bay cooling ejector valve with weight on gear.
	b. Taxi to ramp position, maintaining directional control with rudder pedals for nose wheel steering and with differential toe brakes as necessary.	
	c. Apply landing gear parking brake.	
	d. Set nose gear steering switch to DISENGAGE.	

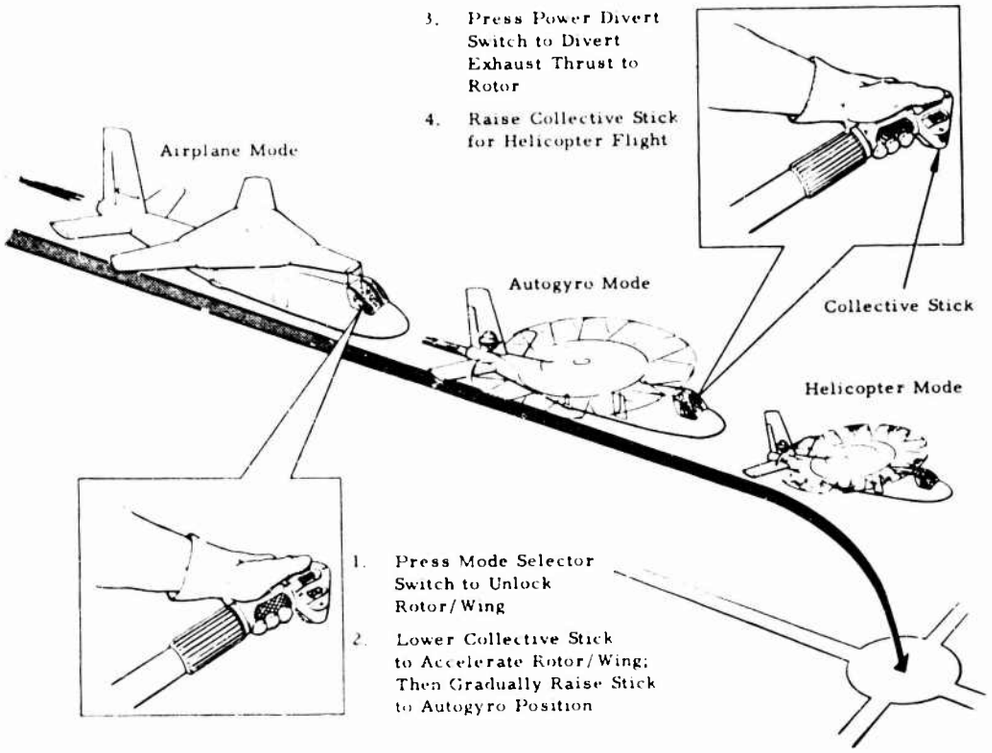

Figure 112. Mode Conversion - Airplane to Autogyro to Helicopter.

By the use of tandem actuators, the output of both hydraulic systems is used to power each of the primary controls, with one system providing continuous operating backup for the other. Should one system fail, the other continues to supply power without pilot action for uninterrupted flight control operation. This feature, plus the multiple hydraulic power sources, assures the safe emergency landing capability of the aircraft.

Electrical power is normally provided by an engine-driven generator. In case this system fails, electrical power is supplied by a battery, which has sufficient power to sustain the electrical requirements of a 15-minute period under night flying conditions.

The landing gear systems are normally operated by the utility hydraulic system failure; emergency extension of the gear is accomplished by manual release and free fall to the down-locked position. Locking is accomplished by overcenter linkages aided by springs.

The emergency operating procedures are delineated in Tables XXX, XXXI, and XXXII for helicopter, autogyro, and airplane modes.

TABLE XXX. EMERGENCY PROCEDURES (HELICOPTER MODE)

Emergency	Operation
1. Engine power loss	a. Lower collective stick to autogyro position. b. Retard throttle to OFF. c. Set power divert switch to AIRPLANE. d. Set electrical loads switch to ESSENTIAL. e. Set landing gear control to DOWN position. f. Perform normal helicopter autorotational landing.
2. In-flight engine fire Engine compartment fire warning or overheat system indicate fire or overheat condition by flashing warning light.	a. Retard throttle to IDLE. NOTE If emergency is an overheat condition, light will go out. b. Continue flight at reduced power setting and land in helicopter mode. WARNING If a fire condition exists, the warning light will remain on. Proceed to steps c through e. c. Lower collective stick to autogyro position. d. Retard throttle to OFF. e. Pull FIRE PULL handle. NOTE This will automatically close the fuel fire wall shutoff valve, close the hydraulic fire wall shutoff valves, shut down all engine electrical power, and discharge the fire extinguishing agent. f. Set power divert switch to AIRPLANE. g. Set electrical loads switch to ESSENTIAL. h. Set landing gear control to DOWN position. i. Perform normal helicopter autorotational landing.

TABLE XXX - Continued

Emergency	Operation
3. In-flight compressor stall Indications: Indications: Exhaust gas temperature (T_7) high Engine rpm (N_2) decre ; or hung up during accele. ation Exhaust gas pressure (P_7) low with no response to throttle	a. Lower collective stick to autogyro position. b. Set power divert switch to AIRPLANE. c. Retard throttle toward IDLE until T_7 setting is compatible with engine rpm or until stall ceases. d. Slowly accelerate engine until desired thrust is obtained. NOTE Actuate start ignition switch and hold for ignition (reduces the possibility of engine flameout). e. When stall condition has been corrected, release start switch and set power divert switch to ROTOR and continue helicopter flight. WARNING If compressor stall condition cannot be corrected or if altitude position limits the requirements of steps c and d, proceed to steps f through i. f. Retard throttle to OFF. g. Set electrical loads switch to ESSENTIAL. h. Set landing gear control to DOWN position. i. Perform normal helicopter autorotational landing.
4. Failure of Rotor/Wing hot gas system Rotor/Wing hot gas overheat warning system indicates overheat condition by flashing warning light Indications: Exhaust gas temperature (T_7) dropping Engine rpm (N_2) increasing Fuel flow (W_f) increasing Rotor/Wing rpm (N_R) dropping	a. Retard throttle towards IDLE. NOTE If emergency is overheat condition, light will go out. b. Continue flight at reduced power setting and land in helicopter mode. NOTE If overheat condition persists, the warning light remains on. c. Lower collective stick to autogyro position. d. Retard throttle to OFF.

TABLE XXX - Continued

Emergency	Operation
Exhaust gas pressure (P_7) dropping	e. Set power divert switch to AIRPLANE. f. Set electrical loads switch to ESSENTIAL. g. Set landing gear control to DOWN position. h. Perform normal helicopter autorotational landing.
5. High or fluctuating engine oil pressure	a. Check oil temperature. b. If temperature is normal, indicates pressure instrument failure. Flight may be continued. NOTE If sudden change from normal operating pressure in excess of 10 psi or fluctuations ±5 psi, proceed to steps c through h. c. Lower collective stick to autogyro position. d. Retard throttle to OFF. e. Set power divert switch to AIRPLANE. f. Set electrical loads switch to ESSENTIAL. g. Set landing gear control to DOWN position. h. Perform normal autorotational landing.
6. Engine oil temperature above acceptable limits	a. Reduce power setting. NOTE If temperature falls within limits, continue at a reduced power setting and land in helicopter mode. If high oil temperature continues, proceed to steps b through g. b. Lower collective stick to autogyro position. c. Retard throttle to OFF. d. Set power divert switch to AIRPLANE. e. Set electrical loads switch to ESSENTIAL. f. Set landing gear control to DOWN position. g. Perform normal helicopter autorotational landing.

TABLE XXX - Continued

Emergency	Operation
7. Landing gear hydraulic system pressure loss	a. Pull the manual release handle located on the pilot's instrument panel causing the landing gear to extend. Maximum forward speed with gear down, 225 kn.
8. In-flight major emergency	NOTE If the altitude or condition of the aircraft does not permit the time to perform the emergency procedures above, a safe ejection can be made by both crew members from any flight mode by using the procedure of step a. a. Pull D-ring, located in front of the seats between the pilot's and copilot's legs. Seats eject through the canopy. Parachutes are deployed automatically.
9. Ground escape and/or rescue	NOTE Cockpit escape and rescue panels are provided in the canopy for pilot and copilot egress. If conditions during ground operation of aircraft prevent escape from cockpit by normal methods, proceed to step a or step b. a. Set emergency exit switch to ESCAPE and evacuate aircraft through the open canopy panel. OR FOR RESCUE BY GROUND CREW, b. Open rescue access door. Set emergency exit switch to ESCAPE and evacuate crew.

TABLE XXXI. EMERGENCY PROCEDURES (AUTOGYRO MODE)

Emergency	Operation
1. Engine power loss	a. Retard throttle to OFF. b. Set electrical loads switch to ESSENTIAL. c. Set landing gear control to DOWN position. d. Perform normal helicopter autorotational landing.

TABLE XXXI - Continued

Emergency	Operation
2. In-flight engine fire Engine compartment fire warning or overheat system indicate fire or overheat condition by flashing warning light.	a. Retard throttle to IDLE. NOTE If emergency is an overheat condition, light will go out. b. Continue flight at reduced power setting. c. Set power divert switch to ROTOR. d. Set landing gear control to DOWN position. e. Perform normal helicopter landing. WARNING If a fire condition exists, the warning light remains on. Proceed to steps f and g. f. Retard throttle to OFF. g. Pull FIRE PULL handle NOTE This will automatically close the fuel fire wall shutoff valve, close the hydraulic fire wall shutoff valves, shut down all engine electrical power, and discharge the fire extinguishing agent. h. Set electrical loads switch to ESSENTIAL. i. Set landing gear control to DOWN position. j. Perform normal helicopter autorotational landing.
3. In-flight compressor stall Indications: Exhaust gas temperature (T_7) high Engine rpm (N_2) decreasing or hung during acceleration	a. Retard throttle toward IDLE until T_7 setting is compatible with engine rpm or until stall ceases. b. Slowly accelerate engine until desired thrust is obtained.

TABLE XXXI - Continued

Emergency	Operation
	NOTE
3. (Continued)	Actuate start ignition switch and hold for ignition (to reduce the possibility of engine flameout).
Exhaust gas pressure (P_7) low with no response to throttle	c. When stall condition has been corrected, release start switch and continue autogyro flight.
	WARNING
	If compressor stall condition cannot be corrected or if altitude position limits the requirements of steps a and b, proceed to steps d through g.
	d. Retard throttle to OFF.
	e. Set electrical loads switch to ESSENTIAL.
	f. Set landing gear control to DOWN position.
	g. Perform normal helicopter autorotational landing.
4. High or fluctuating engine oil pressure	a. Check oil temperature.
	b. If temperature is normal, indicates pressure instrument failure. Flight may be continued.
	NOTE
	If sudden change from normal operating pressure in excess of 10 psi or fluctuation ±5 psi, proceed to steps c through f.
	c. Retard throttle to OFF.
	d. Set electrical loads switch to ESSENTIAL.
	e. Set landing gear control to DOWN position.
	f. Perform normal autorotational landing.
5. Engine oil temperature above acceptable limits	a. Reduce power setting.
	NOTE
	If temperature falls within limits, continue at a reduced power setting. Set power divert switch to ROTOR, and land in helicopter mode. If high oil temperature continues, proceed to steps b through e.

TABLE XXXI - Continued

Emergency	Operation
	b. Retard throttle to OFF.
	c. Set electrical loads switch to ESSENTIAL.
	d. Set landing gear control to DOWN.
	e. Perform normal helicopter-type autorotational landing.
6. Landing gear hydraulic system pressure loss	a. Pull the manual release handle located on the pilot's instrument panel causing the landing gear to extend.
7. In-flight major emergency	NOTE If the altitude or condition of the aircraft does not permit the time to perform the emergency procedure as outlined, a safe ejection can be made by both crew members from any flight mode by using the following procedure.
	a. Pull D-ring, located in front of the seats between the pilot's and copilot's legs. Seats eject through the canopy. Parachutes are deployed automatically.
8. Ground escape and/or rescue	NOTE Cockpit escape and rescue panels are provided in the canopy for pilot and copilot egress. If conditions during ground operation of aircraft prevent escape from cockpit by normal methods, proceed to step a or step b.
	a. Set emergency exit switch to ESCAPE and evacuate aircraft through the open canopy panel.
	OR FOR RESCUE BY GROUND CREW
	b. Open rescue access door. Set emergency exit switch to ESCAPE and evacuate crew.

TABLE XXXII. EMERGENCY PROCEDURES (AIRPLANE MODE)

Emergency	Operation
1. Engine power loss	a. Release ram-air turbine to provide emergency hydraulic power. b. Set electrical loads switch to ESSENTIAL. c. Retard throttle to OFF. d. Reduce airspeed and altitude to be within conversion envelope. If at low altitude and high speed, initiate a zoom climb e. Set mode selector switch to ROTOR. f. Lower collective stick to full down (-10-degree blade pitch angle). At 25-percent Rotor/Wing rpm, gradually raise collective as rpm increases. g. Set landing gear control to DOWN position. h. Perform normal helicopter autorotational landing. NOTE In lieu of steps d through h, an airplane mode dead-stick landing may be made.
2. In-flight engine fire Engine compartment fire warning and overheat system indicate fire or overheat condition by flashing warning light.	a. Retard throttle to IDLE. NOTE If emergency is an overheat condition, light goes out. b. Continue flight at reduced power. WARNING If a fire condition exists, the warning light remains on. Proceed to steps c through k. c. Retard throttle to OFF. d. Pull FIRE PULL handle. NOTE This will automatically close the fuel fire wall shutoff valve, close the hydraulic fire wall shutoff valve, shut down all engine electrical power, and discharge the fire extinguishing agent.

TABLE XXXII - Continued

Emergency	Operation
	e. Release ram-air turbine to provide emergency hydraulic power. f. Set electrical loads switch to ESSENTIAL. g. Reduce airspeed and altitude within conversion envelope. If at a low altitude and high speed, initiate a zoom climb. h. Set mode selector switch to ROTOR. i. Lower collective stick to full down (-10-degree blade pitch angle). At 25-percent Rotor/Wing rpm, gradually raise collective as rpm increases. j. Set landing gear control to DOWN position. k. Perform normal helicopter autorotational landing. NOTE In lieu of steps g through k, an airplane mode dead-stick landing may be made.
3. In-flight engine compressor stall Indications: Exhaust gas temperature (T_7) high Engine rpm (N_2) decreasing or hung during acceleration Exhaust gas pressure (P_7) low with no response to throttle	a. Retard throttle toward IDLE until T_7 setting is compatible with engine rpm or until stall ceases. b. Slowly accelerate engine until desired thrust is obtained. NOTE Actuate start switch and hold for ignition to reduce possibility of engine flameout. c. When stall condition has been corrected, release start switch. WARNING If compressor stall cannot be corrected, proceed to steps d through k. d. Retard throttle to OFF. e. Release ram-air turbine to provide emergency hydraulic power. f. Set electrical loads switch to ESSENTIAL. g. Reduce airspeed and altitude within conversion envelope. If at low altitude and high speed, initiate a zoom climb.

TABLE XXXII - Continued

Emergency	Operation
	h. Set mode selector switch to ROTOR.
	i. Lower collective stick to full down (-10-degree blade pitch angle). At 25-percent Rotor/Wing rpm, gradually raise collective as rpm increases.
	j. Set landing gear control to DOWN position.
	k. Perform normal helicopter autorotational landing.
	NOTE In lieu of steps g through k, an airplane mode dead-stick landing may be made.
4. High or fluctuating engine oil pressure	a. Check oil temperature.
	b. If temperature is normal, indicates pressure instrument failure. Flight may be continued.
	NOTE If sudden change from normal operating pressure in excess of 10 psi or fluctuating ±5 psi, proceed to steps c through j.
	c. Retard throttle to OFF.
	d. Release ram-air turbine to provide emergency hydraulic power.
	e. Set electrical loads switch to ESSENTIAL.
	f. Reduce airspeed and altitude to be within conversion envelope. If at low altitude and high speed, initiate a zoom climb.
	g. Set mode selector switch to ROTOR.
	h. Lower collective stick to full down (-10-degree blade pitch angle). At 25-percent Rotor/Wing rpm, gradually raise collective as rpm increases.
	i. Set landing gear control to DOWN position.
	j. Perform normal helicopter autorotational landing.
	NOTE In lieu of steps f through j, an airplane mode dead-stick landing may be made.

TABLE XXXII - Continued

Emergency	Operation
5. Engine oil temperature above acceptable limits	a. Reduce power setting. NOTE If temperature falls within limits, continue at a reduced power setting, convert to helicopter mode, and land. If high oil temperature continues, proceed to steps b through i. b. Retard throttle to OFF. c. Release ram-air turbine to provide emergency hydraulic power. d. Set electrical loads switch to ESSENTIAL. e. Reduce airspeed and altitude to be within conversion envelope. If at low altitude and high speed, initiate a zoom climb. f. Set mode selector switch to ROTOR. g. Lower collective stick to full down (-10 degree blade pitch angle). At 25-percent Rotor/Wing rpm, gradually raise collective as rpm increases. h. Set landing gear control to DOWN position. i. Perform normal helicopter autorotational landing. NOTE In lieu of steps e through i, an airplane mode dead-stick landing may be made.
6. Engine air starts	NOTE Minimum engine speeds for engine air starts will vary with airspeed and altitude. a. Retard throttle to OFF. b. Set engine electrical power switch ON. c. Set engine anti-icing switch OFF. d. Set fuel fire wall shutoff switch OPEN. e. Set fuel boost pump switch ON. Check fuel inlet pressure. f. Advance throttle to IDLE.

TABLE XXXII - Continued

Emergency	Operation
	g. Set start switch to START and hold until light-off obtained. Air start of engine should be obtained within 20 seconds.
7. Landing gear hydraulic system pressure loss	a. Pull the manual release handle located on the pilot's instrument panel to extend the landing gear. "Maximum forward speed with gear down 225 kn."
8. In-flight major emergency	NOTE If the altitude or condition of the aircraft does not permit the time to perform the emergency procedures outlined above, a safe ejection can be made by both crew members from any flight mode by proceeding with step a.
	a. Pull D-ring, located in front of the seats between the pilot's and the copilot's legs. Seats eject through the canopy. Parachutes are deployed automatically.
9. Ground escape and/or rescue	NOTE Cockpit escape and rescue panels are provided in the canopy for pilot and copilot egress. If conditions during ground operation of aircraft prevent escape from cockpit by normal methods, proceed to step a or step b.
	a. Set emergency exit switch to ESCAPE and evacuate aircraft through the open canopy panel, OR FOR RESCUE BY GROUND CREW,
	b. Open rescue access door. Set emergency exit switch to ESCAPE and evacuate crew.

COCKPIT ARRANGEMENT

The research mission of the Hot Cycle Rotor/Wing CRA categorizes the vehicle as a visual-flight-rules aircraft with limited night flying and bad weather capabilities. The cockpit arrangement, shown in Figure 113, provides an unpressurized enclosure with two side-by-side crew stations. The pilot's station is located on the right and the copilot's station is located on the left side of the cockpit. Dual controls are provided; however, the simplicity of the configuration permits the aircraft to be flown safely by one pilot from either seat.

In designing the cockpit, careful attention was given to the safety and comfort of personnel and to the principles of human factors engineering. A simplified cockpit mock-up was fabricated to check out the cockpit arrangement (see Figure 114). The instrument panel does not restrict visibility in either the horizontal or the vertical plane (see Figure 115). The cockpit is designed completely to human factors criteria, complies with the requirements of MIL-STD-250B, and is arranged for safe operation by a single pilot.

The cockpit is large, allowing ample space for all required systems. MIL-STD-33575 dimensions are used to provide optimum control, visibility, and comfort for the pilots. A door between the cockpit and the cargo compartment provides for normal entrance and exit. The pilot stations are enclosed by a large, transparent, plastic canopy that incorporates provisions for emergency exit. Fully qualified zero-zero ejection seats are provided for both crew members (see Figure 116).

The instrument panel (see Figure 117) contains duplicate flight instruments for the pilot and copilot, together with all vital engine instruments in duplicate form. Generally, the engine and utility instruments are located on the center section of the panel for common use by both crew members or for single use by one pilot; there is equally good visibility from either seat. A centrally located console between the pilot's and copilot's stations provides maximum mutual accessibility (see Figure 118). The cockpit is air-conditioned for crew comfort, and the cockpit design includes portable oxygen breathing equipment.

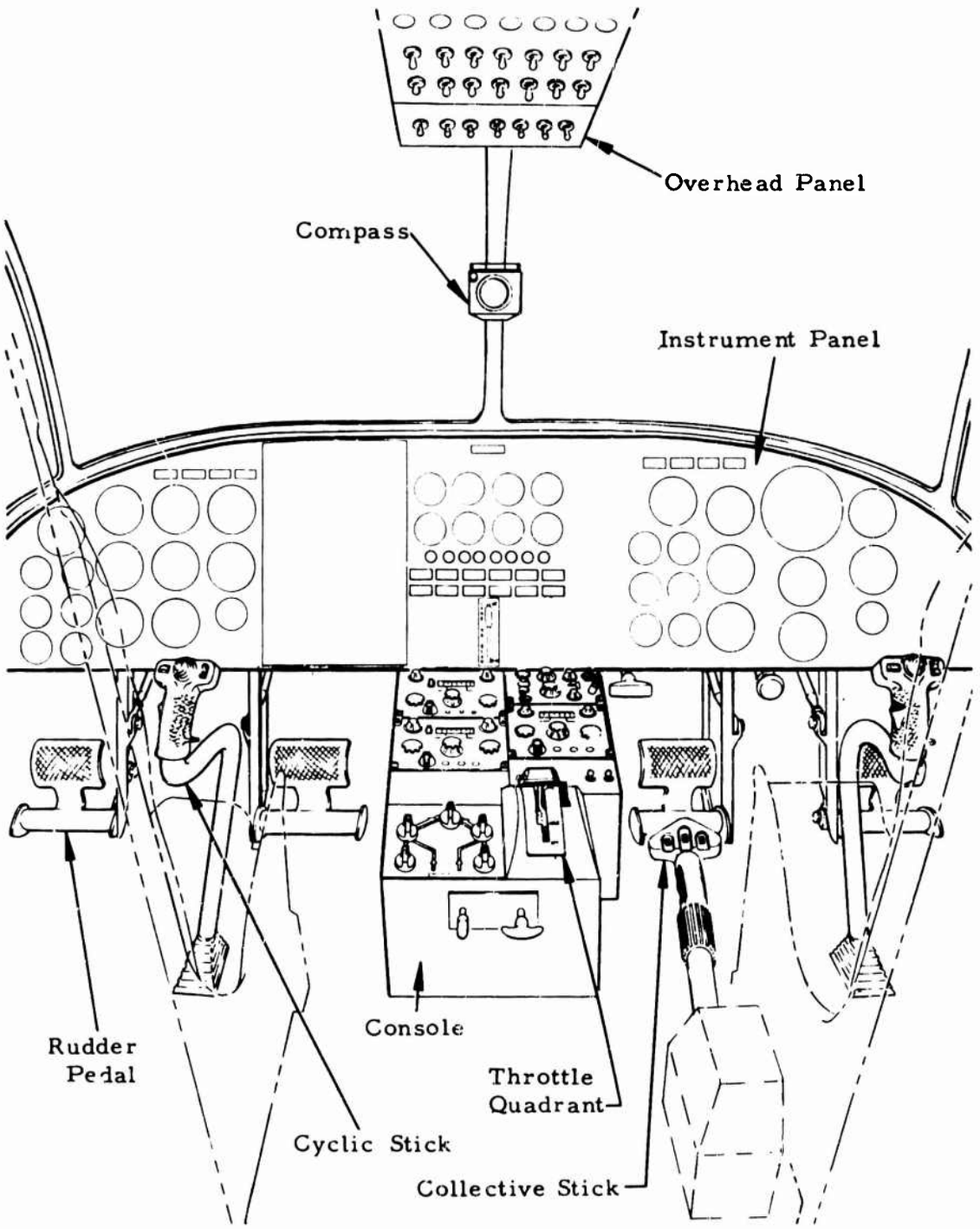

Figure 113. Cockpit Arrangement.

An overhead panel is provided, as indicated in Figure 113 and as shown in detail in Figure 119. This panel is arranged in accordance with the panel positions called for by MIL-STD-250B, as follows:

1. Emergency panel
2. Not applicable in the CRA -- (Fuel Panel)
3. Not applicable in the CRA -- (Starting Panel)
4. Light, heat, and miscellaneous panel
5. Circuit breaker panel

All panels are edge-lighted in accordance with MIL-L-007788C.

The placement of all instruments stresses maximum visibility and minimum parallax. Instrument lettering and other identifying legends and placarding are of a size to provide maximum readability. Warning and caution lights are positioned to ensure that they are within the pilot's 30-degree cone of vision. The colors and identifying legends used for these lights are ordered to ensure that the pilots have all vital information available in the shortest possible time. Also included in the cockpit are a first-aid kit, a map case, and a portable fire extinguisher.

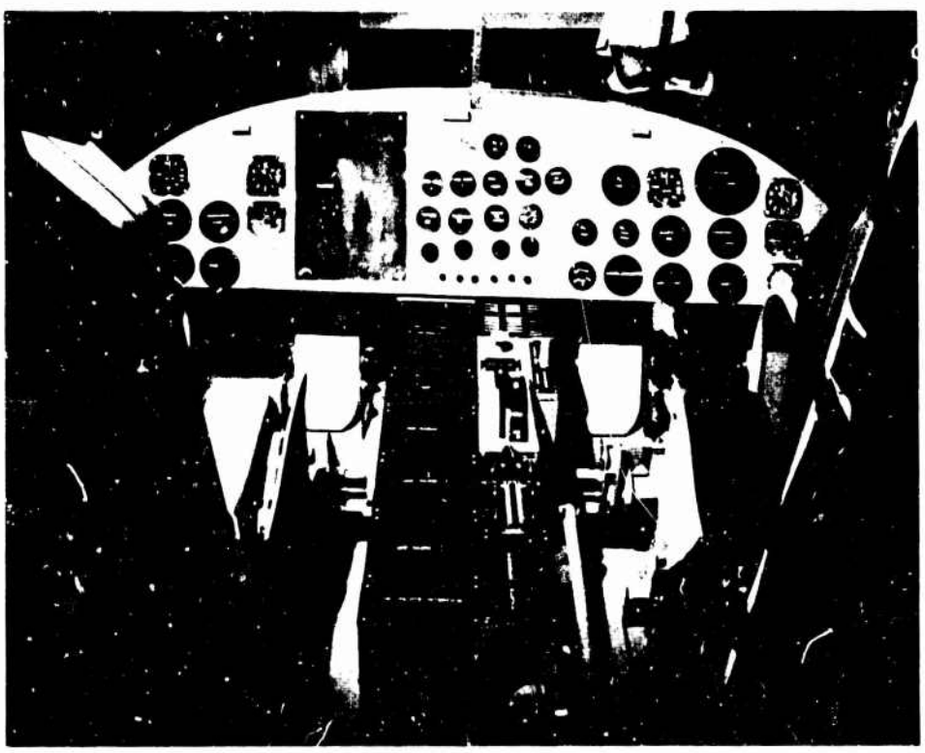

Figure 114. Cockpit Mock-Up.

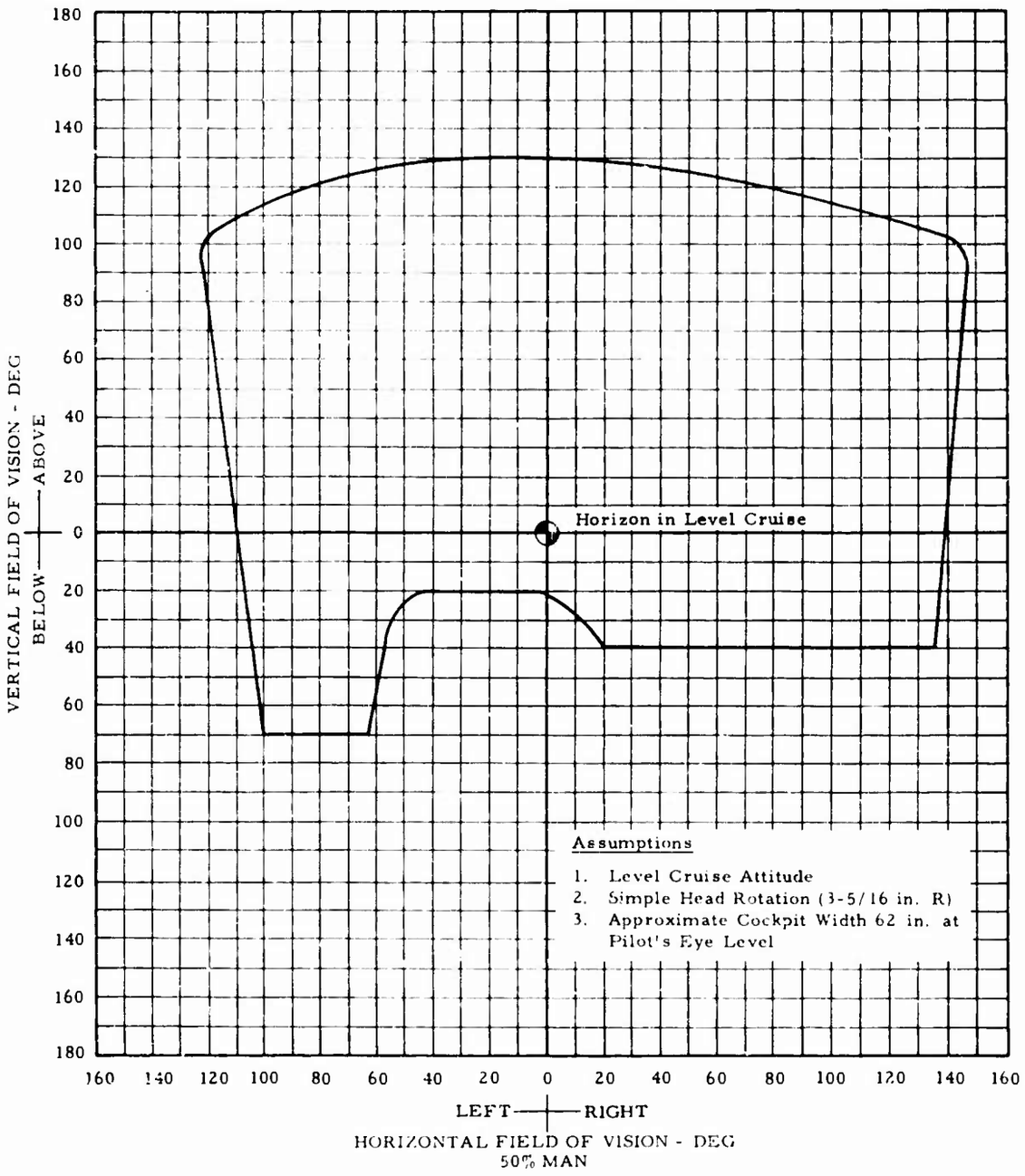

Figure 115. Cockpit Visibility.

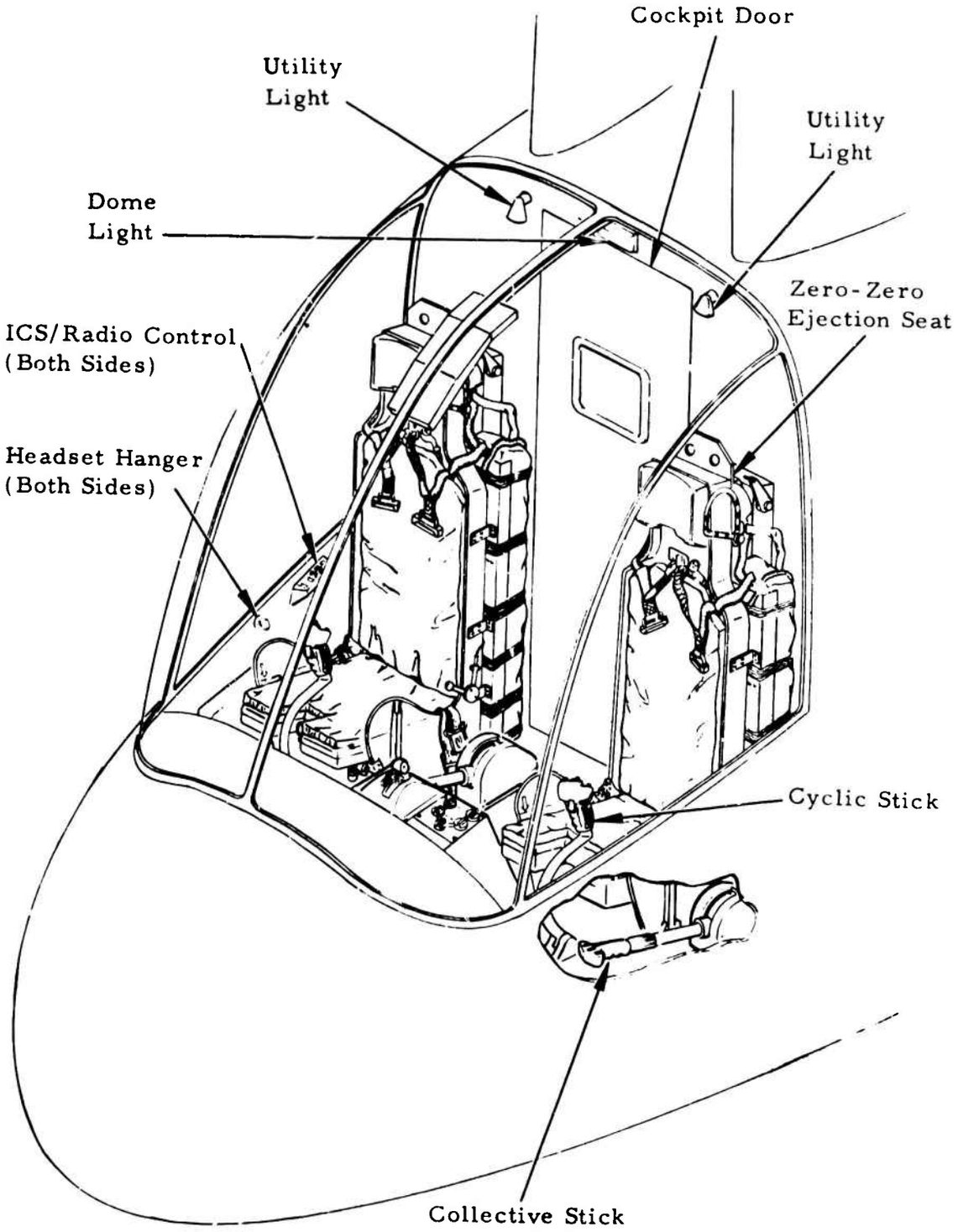

Figure 116. Cockpit Arrangement - Looking Aft.

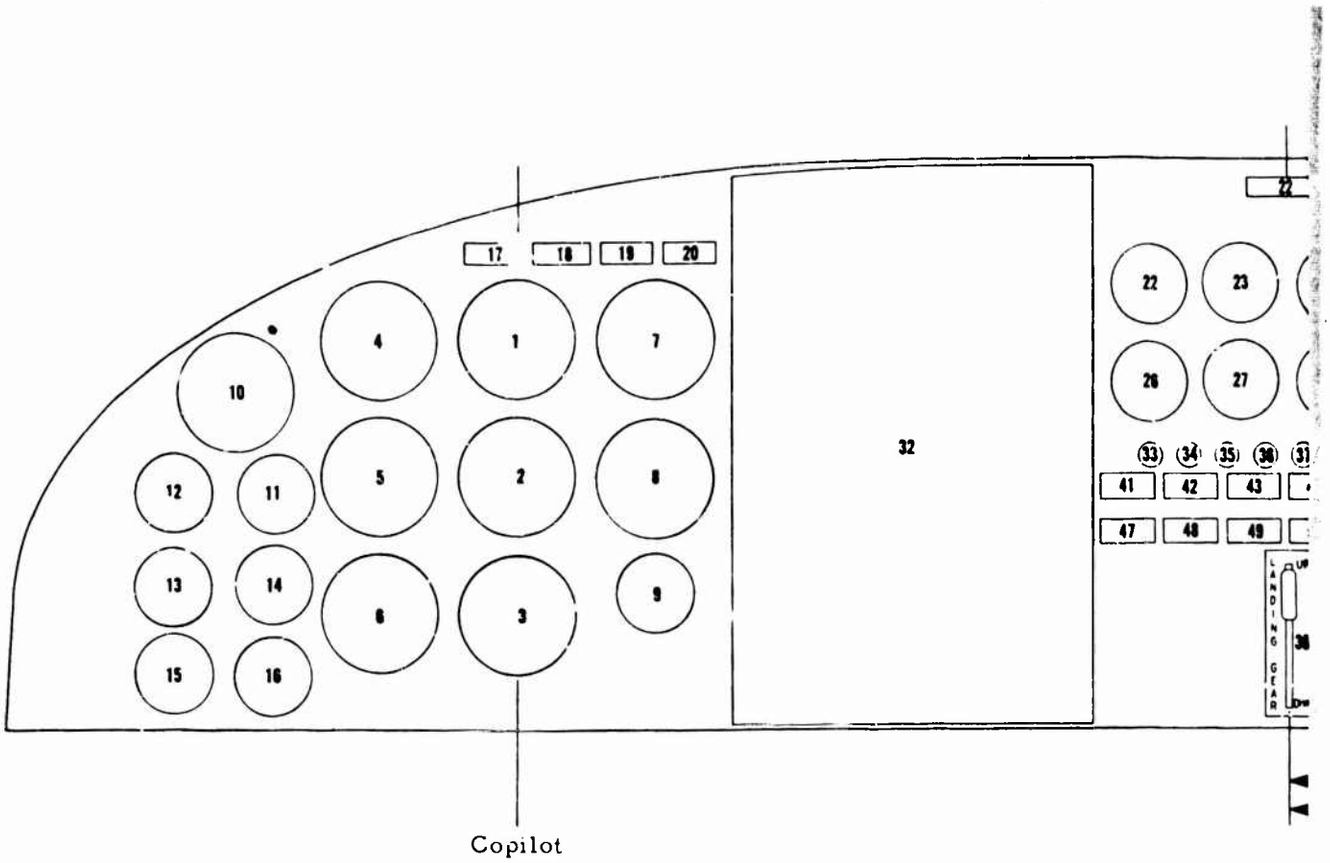

1. Attitude Gyro
2. Directional Gyro
3. ADF
4. Airspeed and Mach
5. Turn and Slip
6. Accelerometer
7. Altimeter Sensitive Aneroid
8. IVSI
9. OAT
10. N_R Tachometer
11. N_2 Tachometer
12. Fuel Flow and Totalizer
13. P_7 Turbine Discharge Pressure
14. T_7 Turbine Discharge Temperature
15. Engine Oil Temperature
16. Engine Oil Pressure
17. Fuel Pressure Low Warning Light
18. Engine Oil Level Low Warn
19. Engine Overheat Warning L
20. Rotor/Wing Overheat Warni
21. Fire Handle and Warning Li
22. Hydraulic Pressure - Utilit
23. Hydraulic Pressure - Fligh
24. Rotor/Wing Lubrication Oil
25. Rotor/Wing Lubrication Oil
26. Voltage Frequency - AC
27. Voltage Ammeter - DC
28. Fuel Quantity Indicator -
29. Fuel Cuantity Indicator - Al
30. Landing Gear Control Handl
31. Parking Brake Handle
32. Flight Test Panel
33. Diverter Valve Position Ind
34. Mode Selector Switch Positi

Figure 117. Instrument Panel.

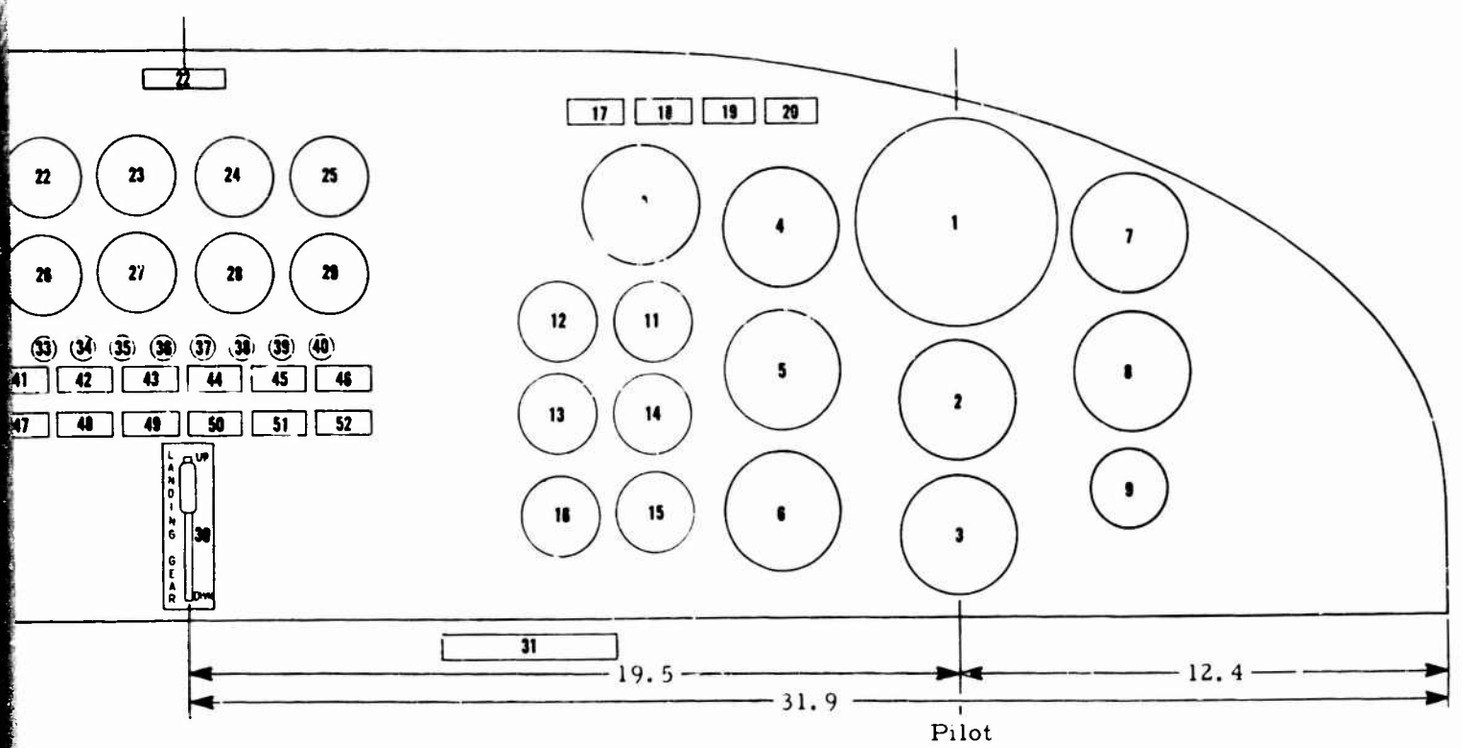

evel Low Warning Light
eat Warning Light
verheat Warning Light
nd Warning Light
essure - Utility
essure - Flight
ubrication Oil Temperature
ubrication Oil Pressure
uency - AC
eter - DC
Indicator - Forward
Indicator - Aft
Control Handle
e Handle
anel
e Position Indicator
Switch Position Indicator

35. Rotor/Wing Lock Position Indicator
36. Rotor/Wing Locator Position Indicator
37. Inlet Duct Position Indicator
38. Yaw Fan Door Position Indicator
39. Rotor/Wing Control Deactivator Position Indicator
40. Landing Gear Position Indicator
41. Parking Brake on Caution Light
42. Cargo Doors Open Caution Light
43. Hydraulic System Low Pressure Caution Light
44. Rotor/Wing Lubrication Caution Light
45. Fuel Filter Clogged Caution Light
46. Fuel Quantity Low Caution Light
47. Engine Anti-Ice Advisory Light
48. Rotor/Wing Brake Armed Advisory Light
49. Fuel Selector Advisory Light
50. External Power Advisory Light
51. AC Inverter Caution Light
52. Generator Caution Light

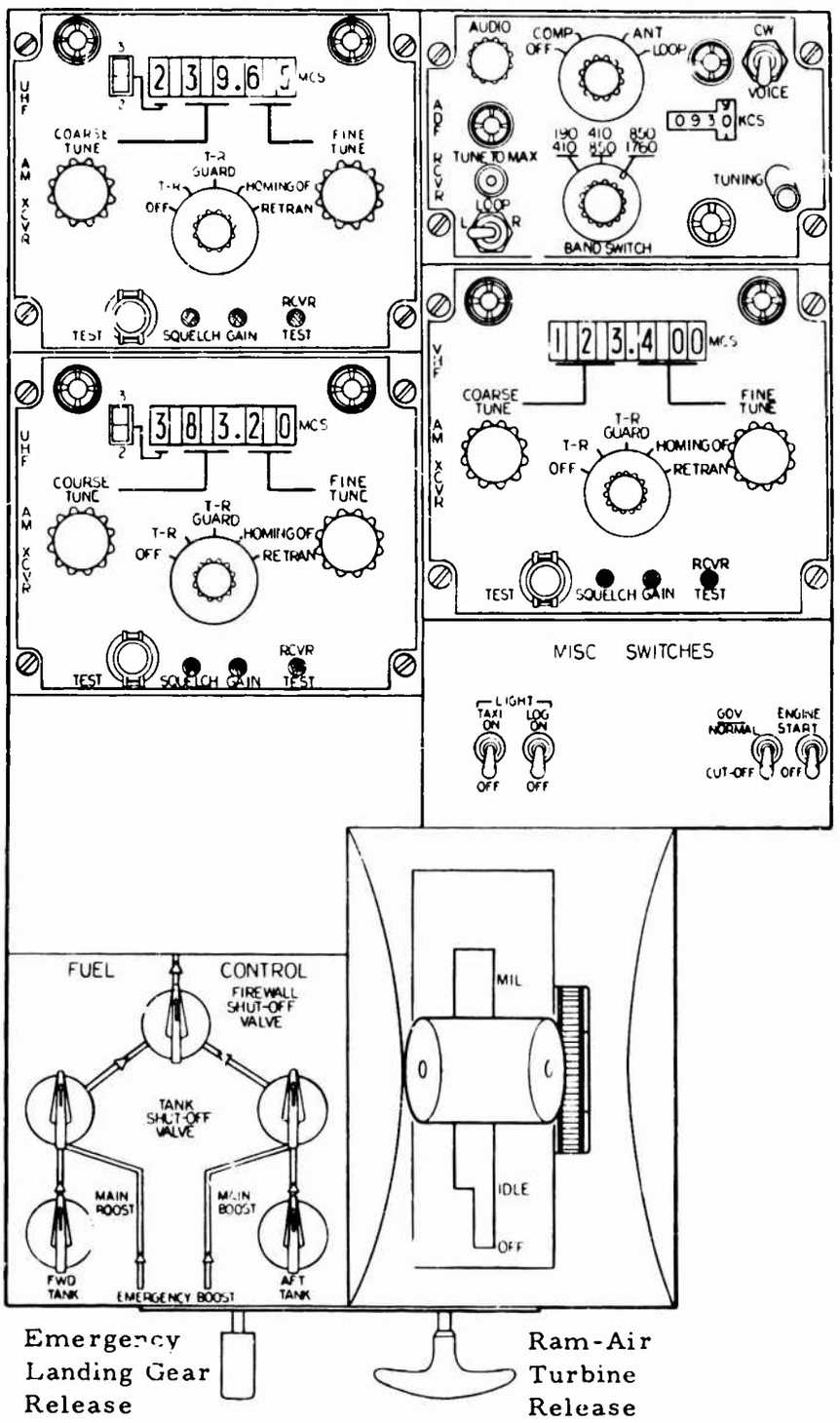

Figure 118. Console.

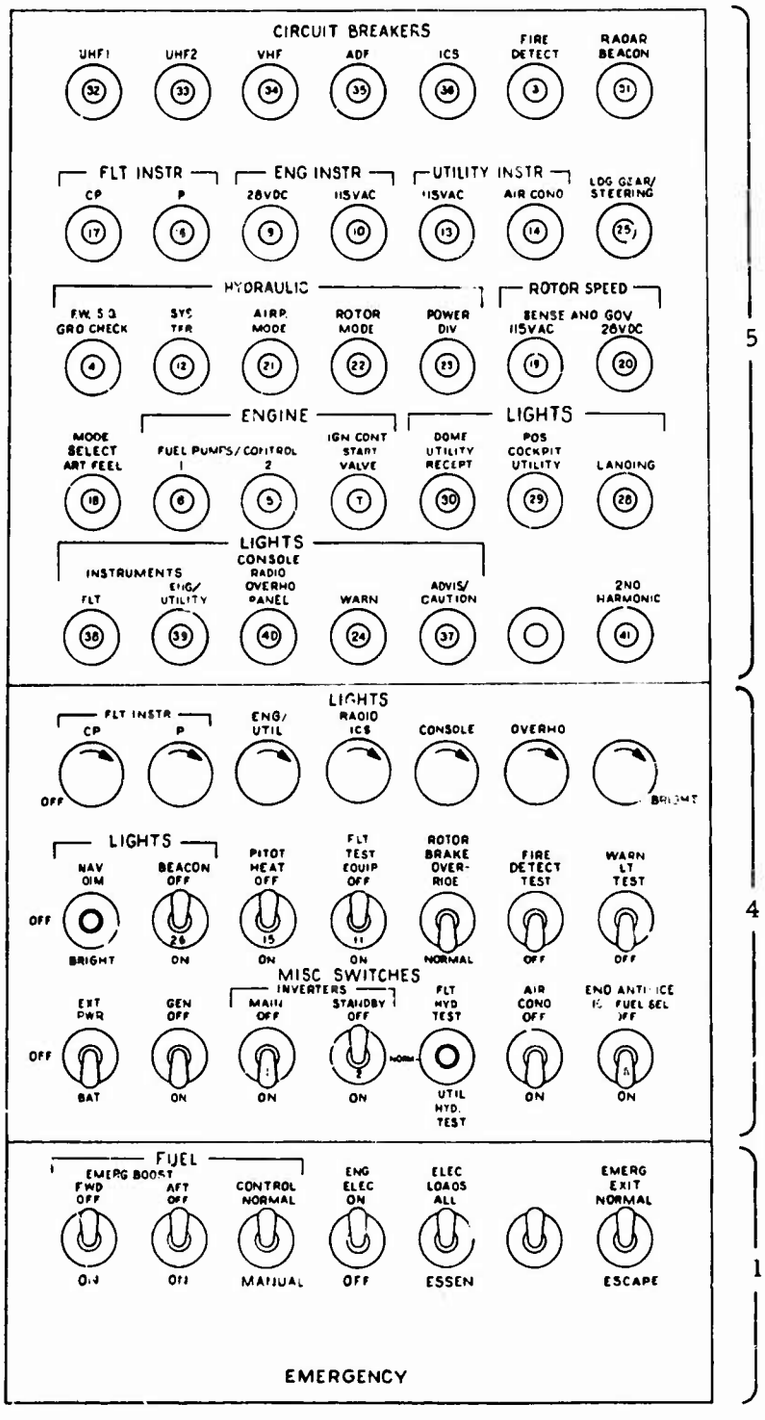

Figure 119. Overhead Panel.

REFERENCES

1. Perkins, Courtland, and Hage, Robert E., AIRPLANE PERFORMANCE STABILITY AND CONTROL, John Wiley and Sons, Inc., New York, N. Y., 1950.

2. LaForge, Sally, PERFORMANCE HANDBOOK, Hughes Tool Company - Aircraft Division, Report XA-8016, March 1966.

3. ROTOR/WING MODEL TEST REPORT, Hughes Tool Company - Aircraft Division, Report HTC-AD 63-40.

4. Head, R. E., SUMMARY TECHNICAL REPORT, ROTOR/WING CONCEPT STUDY, Hughes Tool Company - Aircraft Division, Report HTC-AD 65-15, September 1965.

5. Carpenter, Paul, EFFECTS OF COMPRESSIBILITY ON THE PERFORMANCE OF TWO FULL-SCALE HELICOPTER ROTORS, NACA TN 2277.

6. TWENTY-HOUR FOLLOW-ON FLIGHT TEST PROGRAM, XV-9A HOT CYCLE RESEARCH AIRCRAFT, Hughes Tool Company - Aircraft Division, Report HTC-AD 66-4, June 1966.

7. Head, R. E., SUPPLEMENTARY STUDY REPORT ROTOR/WING CONCEPT STUDY, Hughes Tool Company - Aircraft Division, Report HTC-AD 65-37, February 1966.

8. Briardy, F. J., COMPOSITE RESEARCH AIRCRAFT SERIES I (ROTOR/WING SERIES IV) WIND TUNNEL TEST, Hughes Tool Company - Aircraft Division, Report HTC-AD 66-5, January 1966.

9. Amer, K. B., METHOD OF STUDYING HELICOPTER LONGITUDINAL MANEUVER STABILITY, NACA TR 1200, 1954.

10. Seckel, E., STABILITY AND CONTROL OF AIRPLANES AND HELICOPTERS, Academic Press, New York, N. Y., 1964.

11. Hoak, D. E., and Carlson, J. W., USAF STABILITY AND CONTROL DATCOM, Douglas Aircraft Company, Revised July 1963.

12. Fisher, Lewis R., APPROXIMATE CORRECTIONS FOR THE EFFECTS OF COMPRESSIBILITY ON THE SUBSONIC STABILITY DERIVATIVES OF SWEPT WINGS, NACA TN 1854, 1949.

13. AIRCRAFT DESIGNERS HANDBOOK FOR TITANIUM AND TITANIUM ALLOYS, SST65-8, Prepared for Office of Deputy Administrator for Supersonic Transport Development, Federal Aviation Agency, by Battelle Memorial Institute, Contract FA-SS-65-6, August 1965.

14. PRELIMINARY TECHNICAL DATA SHEET ON CARPENTER CUSTOM 455, Carpenter Steel Corporation, Reading, Pa., 1966.

15. METALLIC MATERIALS AND ELEMENTS FOR FLIGHT VEHICLE STRUCTURES, MIL-HDBK-5, August 1962.

16. AEROSPACE STRUCTURAL METALS HANDBOOK, Vol. II, Syracuse University Press, March 1963.

17. HAYNES ALLOY NO. R-41, Union Carbide Stellite Company, Los Angeles, Calif., April 1963.

18. Frost, R. C., and Rutherford, R., SUBSONIC WING SPAN EFFICIENCY, AIA Journal, April 1963.

19. TECHNOLOGY ASSESSMENT REPORT HOT CYCLE ROTOR/WING INTRA-THEATER TRANSPORT SUPPORT SYSTEM STUDY (U), Hughes Tool Company - Aircraft Division, Report HTC-AD 67-27, May 1967 (Classified Confidential).

20. Gessow, A. and Myers, G. C., AERODYNAMICS OF THE HELICOPTER, The MacMillan Company, New York, N. Y., 1952.

21. Delany, N. K. and Sorensen, N. E., LOW SPEED DRAG OF CYLINDERS OF VARIOUS SHAPES, NACA TN 3038.

22. Hoerner, Sighard F., AERODYNAMIC DRAG, The Oherbein Press, Dayton, Ohio, 1951.

23. Shivers, James P. and Carpenter, Paul J., EFFECTS OF COMPRESSIBILITY ON ROTOR HOVERING PERFORMANCE AND SYNTHESIZED BLADE-SECTION CHARACTERISTICS DERIVED FROM MEASURED ROTOR PERFORMANCE OF BLADES USING NACA 0015 AIRFOIL TIP SECTIONS, NACA TN 4356, 1958.

24. Theodorsen and Regier, EXPERIMENTS ON DRAG OF REVOLVING DISKS, CYLINDERS, AND STREAMLINE RODS AT HIGH SPEEDS, NACA TR 793.

25. AERO-SPACE APPLIED THERMODYNAMICS MANUAL, Society of Automotive Engineers, Incorporated, Committee A-9, Aero-Space Environmental Systems, February 1960, Revised January 1962.

26. Abbott, I., and Von Doenhoenhoff, A., THEORY OF WING SECTIONS, Dover Publications, Inc., New York, N. Y., 1959.

27. FINAL REPORT DIVERTER VALVE DEVELOPMENT PROGRAM (VOLUME III), Contract No. AF 33(600)40862 Project No. 3066, General Electric Company, Cincinnati, Ohio, (date not given).

28. Bruhn, E. F., ANALYSIS AND DESIGN OF FLIGHT VEHICLE STRUCTURE, Tri-State Offset Co., Cincinnati, Ohio, 1965.

APPENDIX I

DERIVATION OF AIRPLANE DRAG POLAR

The thrust required for airplane flight was computed using the drag polars presented in Figure 120. The derivation of this set of polars from wind tunnel test data is shown in this appendix.

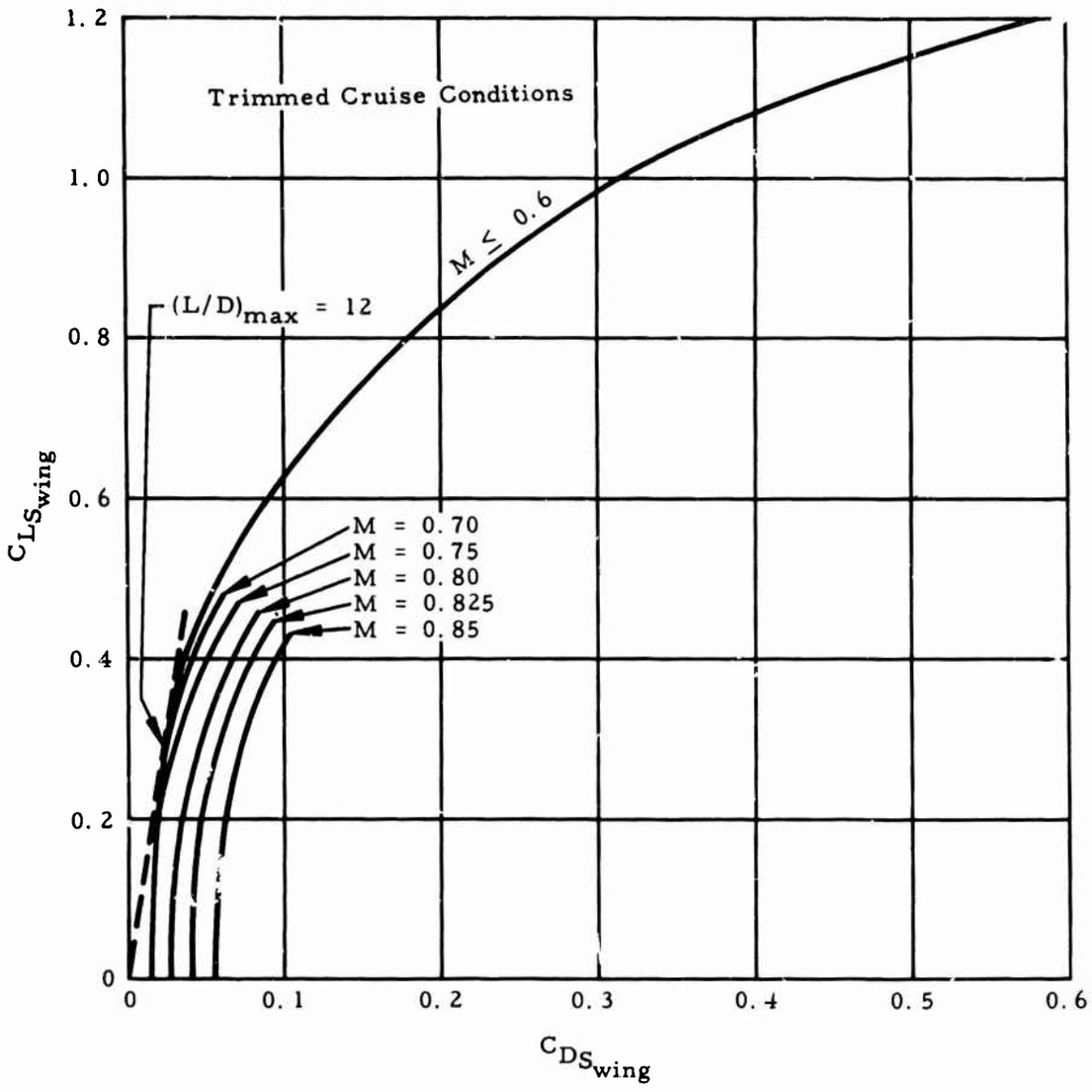

Figure 120. Drag Polars, Airplane Mode.

The airplane configuration applicable to the polars is defined by Figure 10, with the following particulars:

1. Clean airplane; that is, gear up, Rotor/Wing locked, inlet duct raised, yaw fan doors closed.

2. All seals in place; that is, wing to fuselage, inlet duct to blade.

3. Aircraft surfaces have finish and workmanship comparable with current high-speed subsonic aircraft.

4. Conservative allowances are made for roughness and leakage.

The operating conditions selected for this analysis are sea level standard atmosphere (59°F) and a Reynolds number per foot of 3.72×10^6 corresponding to V_F = 350 knots.

The general approach to the drag polar analysis for the CRA has been to match the drag polars obtained in wind tunnel tests and to extrapolate to full scale using turbulent skin friction experimental data. The shape of these experimental polars follows the form

$$C_D = C_{D_0} + \frac{C_L^2}{\pi ARe} + \Delta C_{D \text{ at } C_L} + \Delta C_{D_{MV}}$$

where the first two terms are the classical parasite and induced drag coefficients. The third term, $\Delta C_{D \text{ at } C_L}$, is common to delta-shaped or highly swept wings and is caused by a vortex generated along the swept leading edge. The fourth term accounts for the compressibility drag rise.

PARASITE DRAG ANALYSIS

An analysis of Rotor/Wing wind tunnel testing (References 4 and 8) has been made to find equivalent skin friction drag coefficients. These are then compared with the turbulent skin friction drag coefficients found by a wetted area weighted summation for model component parts at the appropriate test Reynolds number. The following sample, for Run 108-P, Reference 4, outlines the method.

First, the measured parasite drag coefficient is converted to a friction coefficient referred to total wetted area:

$$C_{f_{test}} = C_{D_{0\,test}}\left(\frac{S_{disc}}{S_{wet}}\right) = 0.0067 \times \left(\frac{40.30}{79.19}\right) = 0.00341$$

Second, a weighted Reynolds number for the entire model is computed according to the following formula:

$$(RN)^{1/5}_{calc} = \frac{\left(RN^{1/5} \times S_{wet}\right)\ components}{total\ S_{wet}}$$

The Reynolds number weighted by this method for Run 108-P is 5.65×10^6.

Third, a turbulent, flat plate C_f is computed for a model of the same component Reynolds numbers as follows:

Component	Wetted Area (Model) S_{wet} (sq ft)	Component RN	Component $\left(\begin{matrix}C_f \\ \text{turbulent} \\ \text{flat plate}\end{matrix}\right)$	Component $C_f \times S_{wet}$ (sq ft)
Fuselage	43.60	11.0×10^6	0.00288	0.12556
Wing	20.79	3.18×10^6	0.00358	0.07443
V-tail	6.05	1.36×10^6	0.00419	0.02535
H-tail	8.75	0.985×10^6	0.00280*	0.02450

Then, computing C_f as a weighted summation gives

$$C_{f_{calc}} = \frac{\left(C_f \times S_{wet}\right) components}{total\ S_{wet}} = \frac{0.24984}{79.19} = 0.003155$$

A plot of these calculated values of skin friction drag coefficient versus weighted Reynolds number is given in Figure 121. Also shown are the wind tunnel test data points. As can be seen in the figure, the test data points are somewhat above the calculated curve, as is to be expected. If a factor of 1.23 is applied to $C_{f_{calc}}$, the method will provide a conservative matching of the test data, as indicated by the dashed line. A further

*Transition value

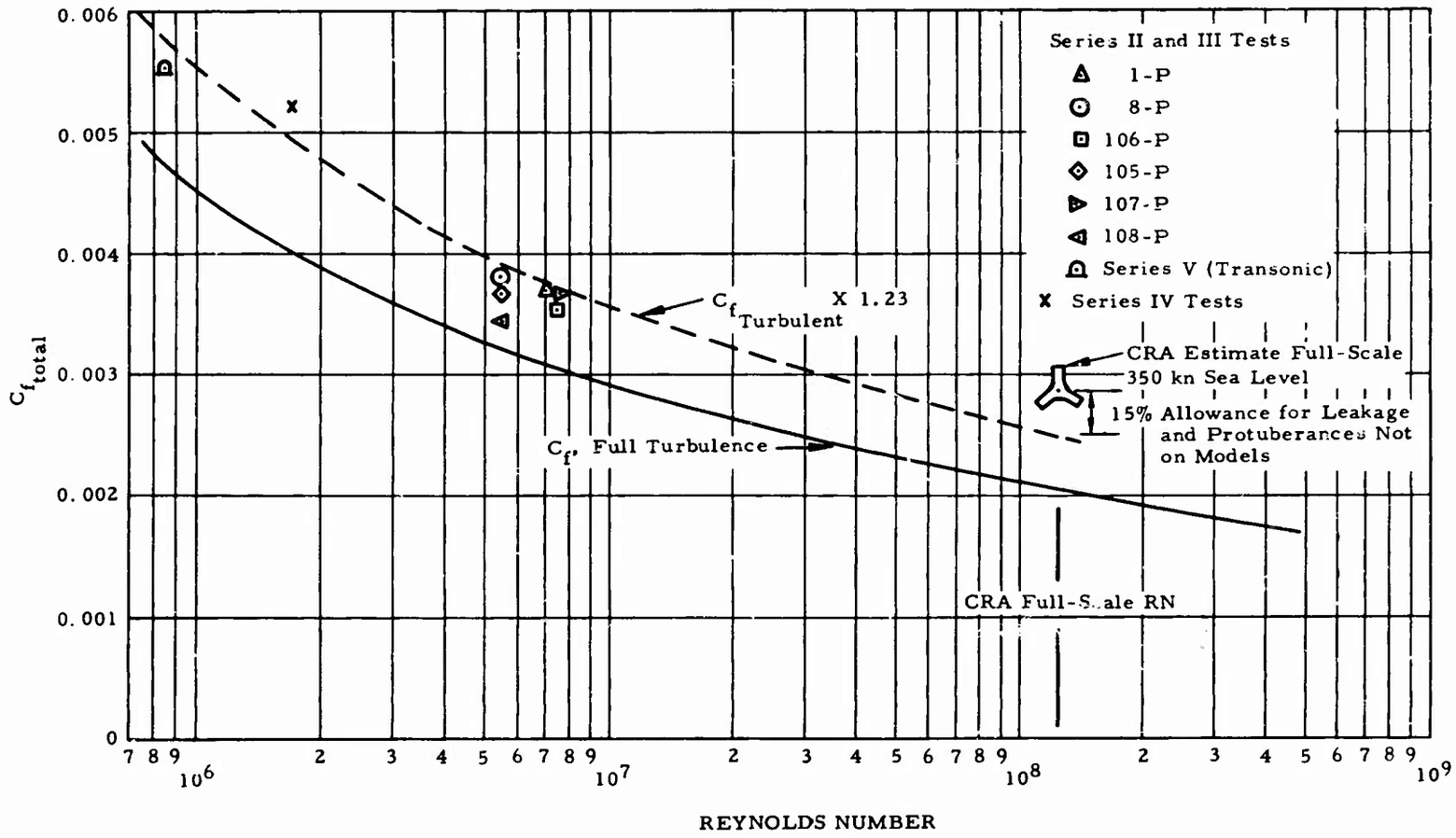

Figure 121. Estimated Comparison of Equivalent Skin Friction Drag Coefficients.

correction of 15 percent has been added to the full-scale CRA estimated C_f to account for leakage and other drag items of the full-scale airplane that were not simulated in the models.

Figure 122 shows a comparison of the CRA equivalent friction drag with that of various other aircraft on the basis of the ratio of wing area to total wetted area. Connecting lines have been drawn between several airplane data points and the corresponding C_f estimated for fuselage alone. The object of this plot is to show that for aircraft like the CRA, with a small wing, the fuselage drag is predominant. Since the fuselage Reynolds number is by far the largest of any of the aircraft components, the equivalent C_f will be weighted in this direction, and thus lowered. In fact, as the plot shows, all aircraft would approach nearly the same C_f if their wing areas were reduced to zero. The absolute level of C_f is not the criterion for good comparison, because the line of variation of C_f versus the ratio of S_{wing}/S_{wet} gives a better presentation of the situation. Thus, the CRA configuration falls in line with aircraft that have somewhat large overall values of C_f, such as the Comet, Viscount, and F3H-1. Aircraft with approximately the same C_f, such as the D558-II and F-4D, are not directly comparable because of their disproportionate ratios of wing to wetted area. In summation, the full-scale skin friction drag coefficient for the CRA is 0.0029, a conservative estimate that corresponds to an equivalent parasite drag area of 8.85 square feet.

INDUCED DRAG ANALYSIS - $\Delta C_{D \text{ at } C_L}$

The calculation of induced drag coefficient and the span efficiency factor, e, follows the classic formula, $C_L^2/\pi ARe$, at moderate angles of attack. The values for e have been determined from wind tunnel test (References 4 and 8) and plotted against Reynolds number. In this case, the Reynolds number must be based on the radius of the wing's leading edge, since this factor controls the flow imperfections involved in the e term. Figure 123 shows the values for e from test data plotted against Reynolds number. The trend line is shown from Reference 18. As can be seen, the trimmed and the tail-off data are near the trend line. When extrapolating to full-scale CRA Reynolds number, the value e = 0.895 is established.

DRAG DUE TO LEADING EDGE SEPARATION

This drag term accounts for the deviation of drag from the classic formula mentioned previously. This term is common to aircraft employing highly swept wing leading edges and is caused by premature separation at the wing

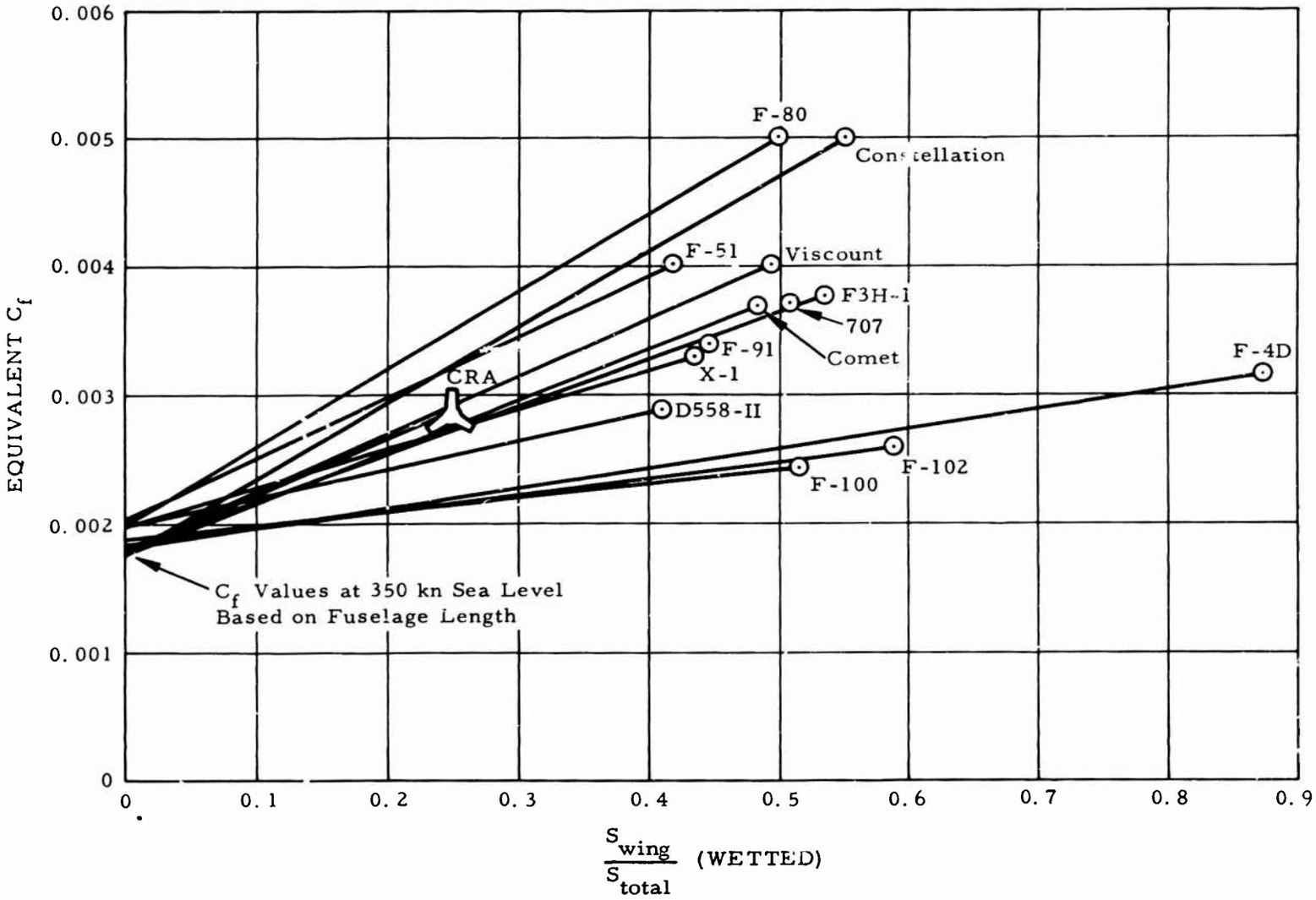

Figure 122. Comparison of Equivalent Skin Friction Drag Coefficients for Various Aircraft as a Function of the Ratio of the Wing to the Total Wetted Area.

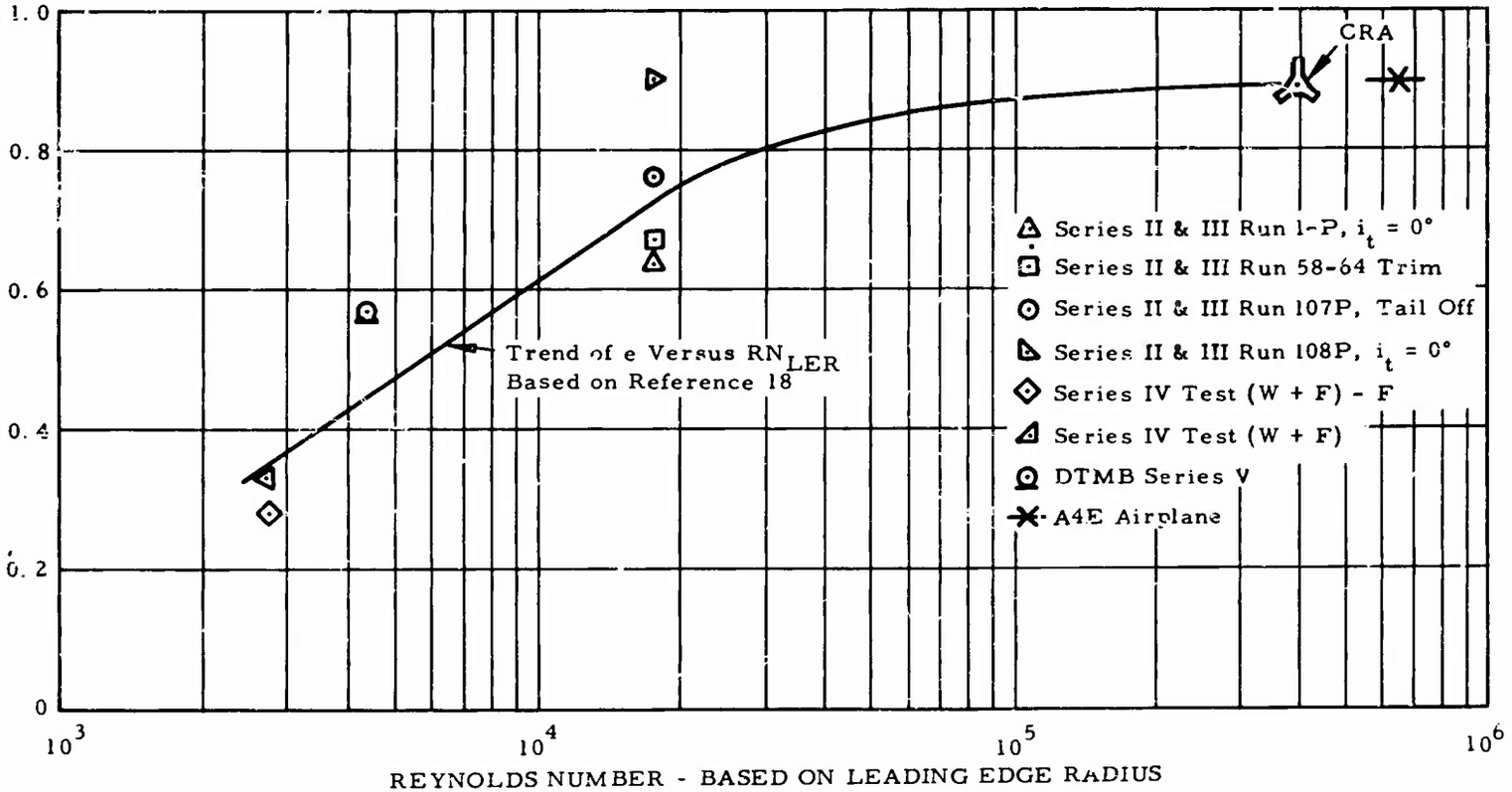

Figure 123. Wing Span Eificiency Factor, e, Derived from CRA Model Testing.

leading edge. This separation takes the form of a leading edge vortex following the spanwise direction of airflow. Figure 124 shows values of the drag increment associated with this phenomenon plotted against wing lift coefficient. Below $C_L = 0.3$, no separation occurs and drag follows the classic case. Above $C_L = 0.3$, the separation is gradual and continues to increase at a moderate rate. The test data points shown on the figure are taken from wind tunnel tests. The line used for the CRA configuration has been drawn through the test data.

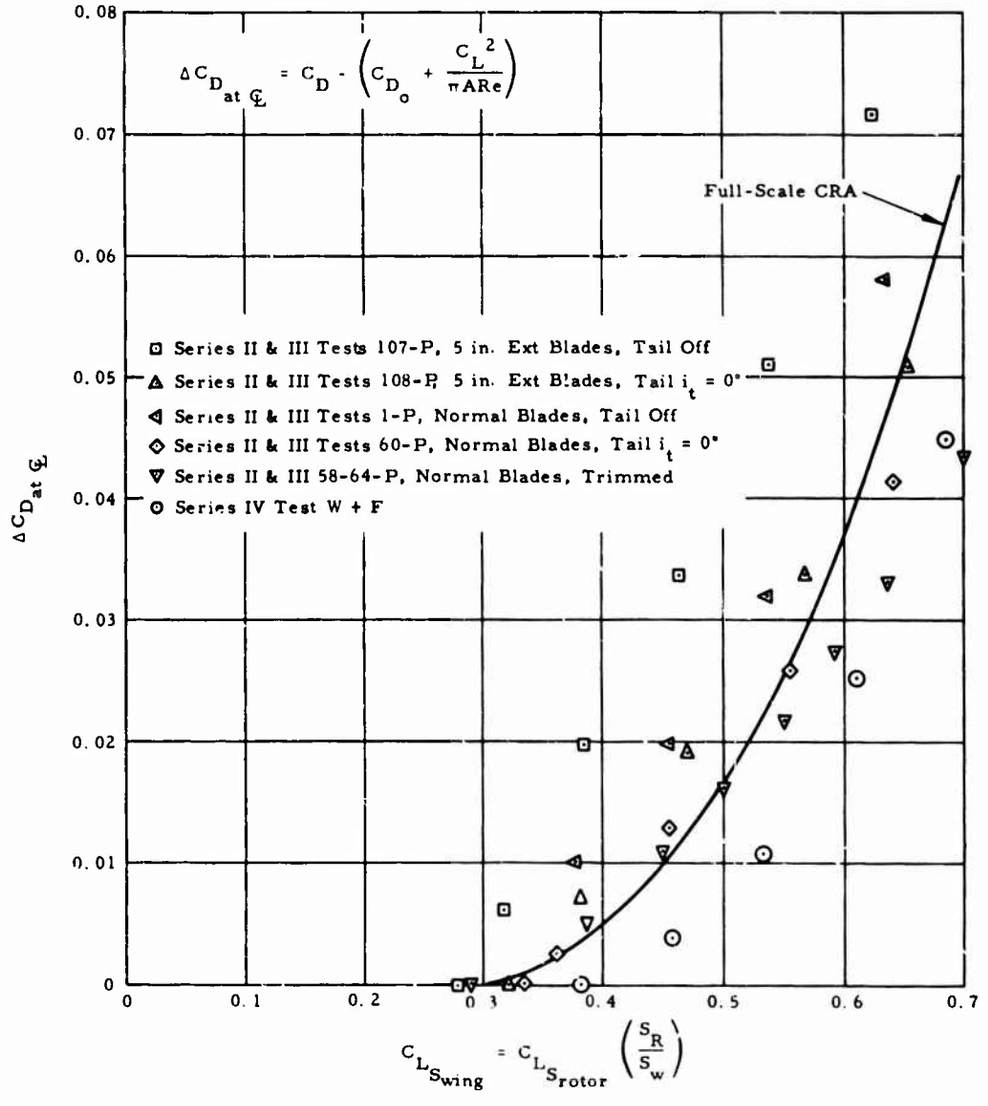

Figure 124. Data Used for Drag Increment Derivation Over and Above the Basic Induced Drag as Lift is Increased Beyond $C_L \approx 0.3$.

DRAG DUE TO TRIM

The effects of trimming the wind tunnel test drag polars to zero pitching moment have been analyzed and found to be small. This is indicated by the data shown in Figure 125, where the aircraft center of gravity is assumed to be on the Rotor/Wing centerline. In essence, this is a conservative approach, because the tail surface, with its large aspect ratio, produces lift at less penalty in drag than does the wing. In normal operation at cruise conditions, the load on the tail is small. Thus, drags associated with center of gravity positions other than at the rotor centerlines are very small and are neglected.

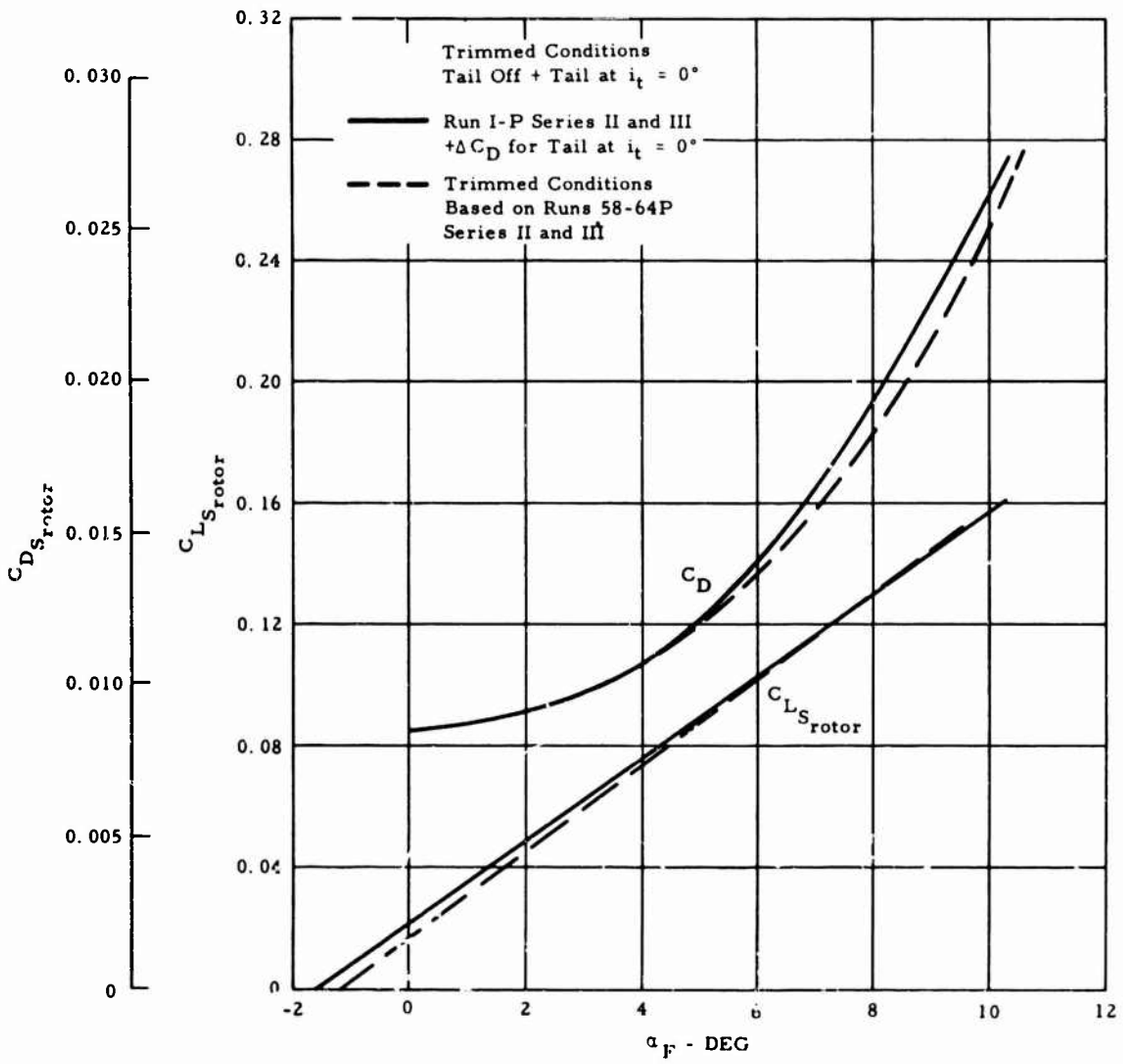

Figure 125. Comparison of C_L and C_D Versus α_F.

DRAG DUE TO COMPRESSIBILITY

An empirical method for determination of drag divergence Mach number for the various portions of an aircraft has been developed (see Reference 19). These equations are:

$$M_{D_{wing}} = 1 - \left(0.15 + \frac{t/c}{1.2} - 0.15e^{-20(t/c)} + 0.13C_L\right)(\cos \Lambda)^2$$

$$M_{D_{fuselage}} = 0.98 - \frac{0.74}{l/d}$$

Thus, for the CRA wing,

$$\left(\frac{t}{c}\right)_{max} = 0.213 \text{ (blade section)}$$

$$C_{L_{S_{wing}}} = 0.15 (M = 0.75 \text{ at } 30,000 \text{ ft})$$

$$\Lambda = 0.35°$$

$$M_{D_{wing}} = 1 - \left(0.15 + \frac{0.213}{1.2} - 0.15 \times 2.71828^{-20 \times 0.213} + 0.13 \times 0.15\right)(\cos 35)^2$$

$$= 1 - (0.3448)(0.671)$$

$$M_{D_{wing}} = 0.769$$

For the CRA fuselage,

$$\frac{l}{d} = 10.5$$

Thus,

$$M_{D_{fuselage}} = 0.98 - \frac{0.74}{10.5} = 0.91$$

For the CRA horizontal tail,

$$\frac{t}{c} = 0.15$$

$$C_{L_{S_{tail}}} = 0.035 \text{ (trim at M = 0.75, 30,000 ft)}$$

$$\Lambda = 18°$$

$$M_{D_{tail}} = 1 - \left(0.15 + \frac{0.15}{1.2} - 15e^{-20 \times 0.15} + 0.13 \times 0.035\right) (\cos 18)^2$$

$$M_{D_{tail}} = 0.754$$

For the CRA vertical tail,

$$\frac{t}{c} = 0.15$$

$$C_L = 0$$

$$\Lambda = 17°$$

$$M_D = 1 - \left(0.15 - \frac{0.15}{1.2} - 0.15 \times 2.71828^{20 \times 0.15}\right)(\cos 17)^2$$

$$= 1 - (0.2675)(0.915)$$

$$M_{D_{vt}} = 0.755$$

Drag rise test data from Series V wind tunnel tests are presented in Figure 126 for comparison with the values used in constructing the polars of Figure 120. Note that the model results are taken literally at C_D greater than 0.02, and that the CRA polars do not reflect the tendency of the test points to show a gradual drag increase over the Mach number region of approximately 0.1 just prior to the drag break. This tendency is common to models tested at relatively low Reynolds numbers. It is not typical of tests of full-scale airplanes. In fact, full-scale airplane drag tests normally show a decreasing C_{D_0} as Mach number increases toward the drag break, as a result of the Reynolds number increase that accompanies the Mach number increase.

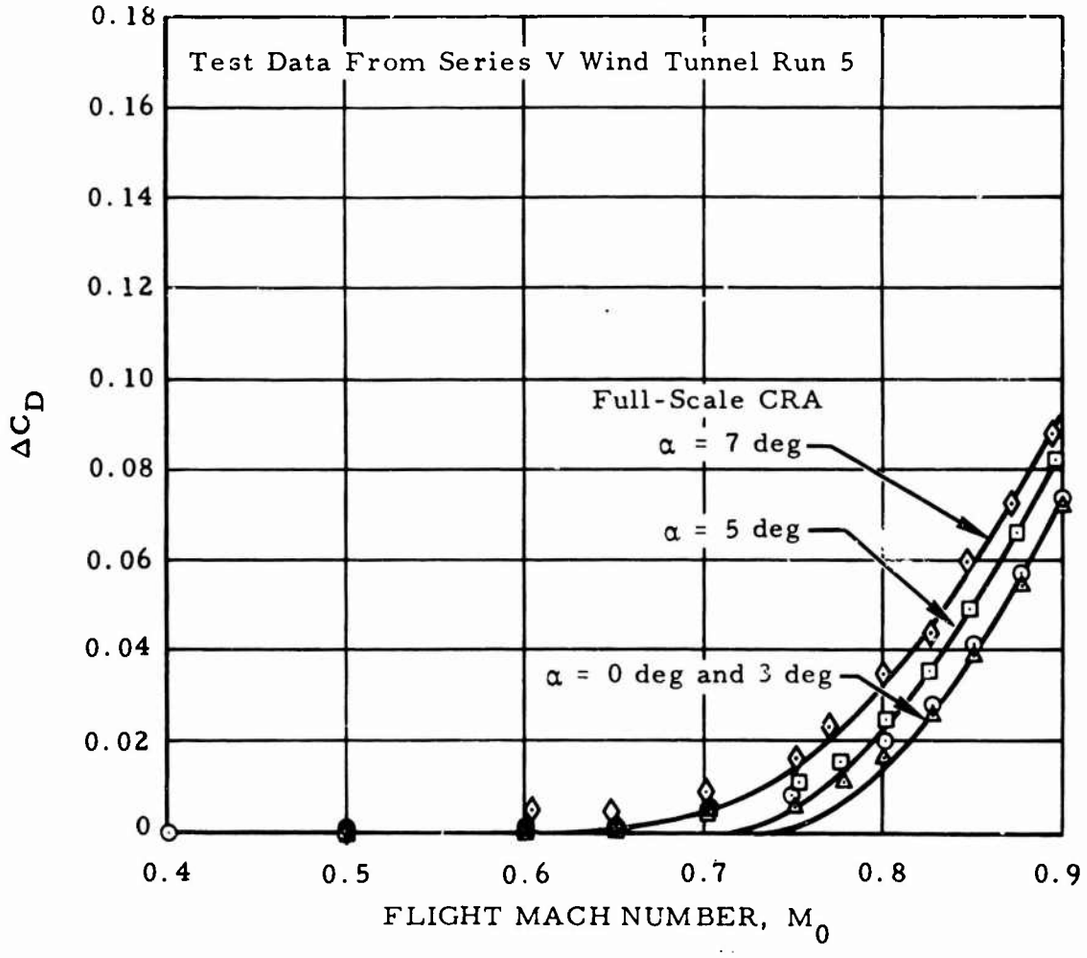

Figure 126. Drag Rise Versus Mach Number.

APPENDIX II

METHOD OF COMPUTING HOVERING POWER REQUIRED

Hovering power required for the aircraft is computed using the method of Reference 20, modified slightly to handle the large centerbody of the Rotor/Wing. This method has been verified by whirl tower tests of a model Rotor/Wing and of a conventional rotor and is discussed later in this appendix. The entire calculational procedure is outlined in Figure 127.

FUSELAGE DOWNLOAD

The aircraft download in hover will be greatest out of ground effect, based on data in and out of ground effect shown in Appendix D of Reference 4. The fuselage download arises from the Rotor/Wing slipstream determined by net Rotor/Wing thrust concentrated in an annulus defined by an inner radius of 0.55 percent R and an outer radius (less tip loss) of 0.97 percent R. It is assumed that full slipstream velocity has been achieved at the fuselage surface $(Z/D) \approx 0.06$. These Rotor/Wing slipstream characteristics have been generally confirmed by unpublished wake survey measurements made of the Rotor/Wing during Reference 4 tower testing.

The detail calculation for fuselage download is as follows:

1. Wake Velocity and Dynamic Pressure

Net rotor thrust coefficient for sea level standard hovering OGE is

$$\frac{C_T}{\sigma} = 0.0492$$

Therefore, assuming 5-percent download,

$$T_{net} = 20{,}671 \text{ pounds}$$

$$v_{wake} = 2\sqrt{\frac{T_{rotor}}{2\rho\pi(R^2 - r^2_{\text{blade root}})}} = 2\sqrt{\frac{20{,}671}{2 \times 0.002378 \times 1263}} = 117.2 \text{ fps}$$

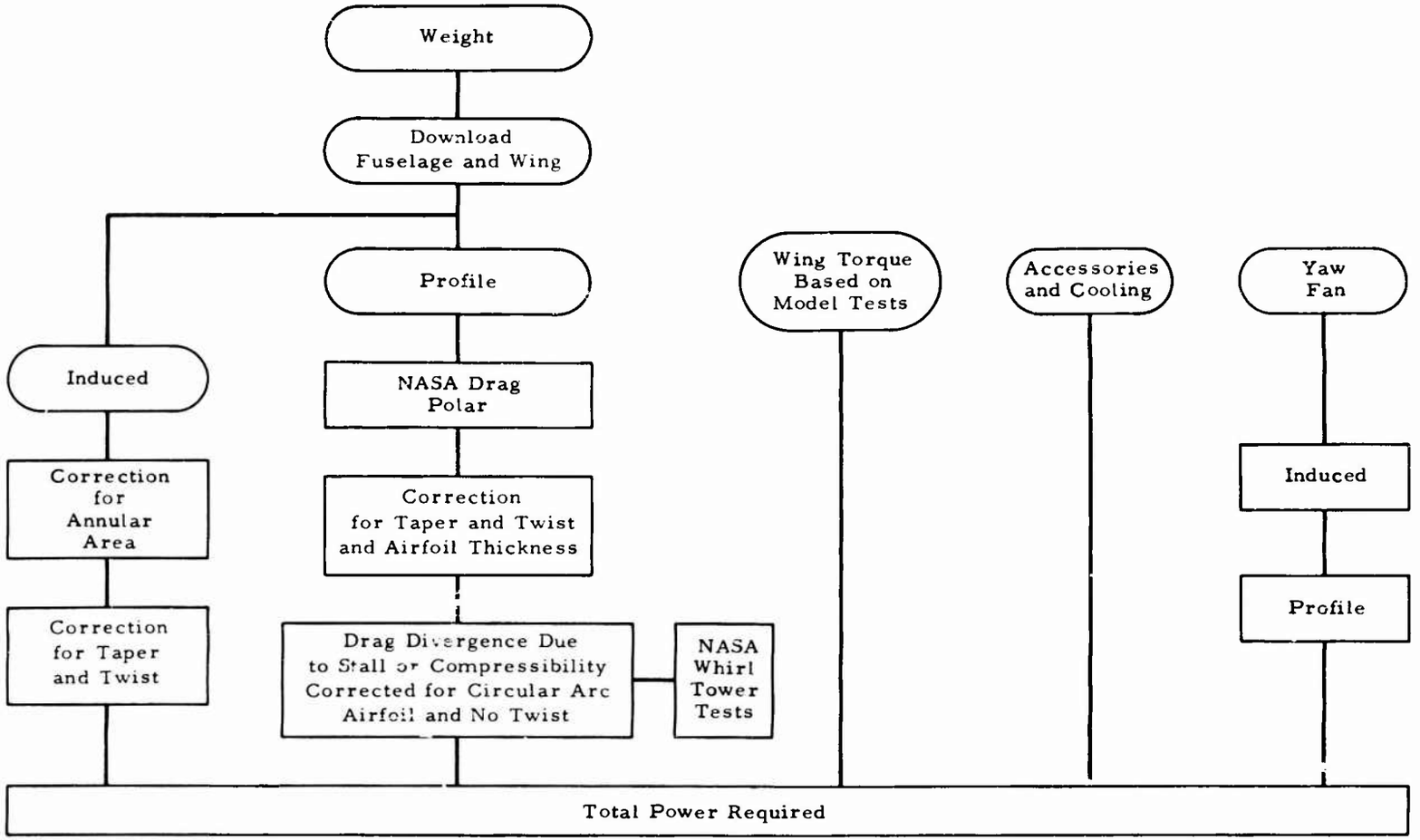

Figure 127. Factors Affecting Hover Power Required.

$$q_{wake} = \left(\frac{0.002378}{2}\right)(117)^2 = 16.35 \text{ lb/sq ft}$$

2. Download on Forward Fuselage

The Rotor/Wing wash extends from fuselage station 112 to fuselage station 238. In this area, the fuselage generally is a smooth rectangular box with rounded corners. The fuselage dimensions in this area are:

1. Average width, b = 77.5 inches
2. Average depth, c = 100 inches
3. Corner radius, r = 15 inches

Thus,

$$\frac{c}{b} = 1.29$$

$$\frac{r}{b} = 0.194$$

$$S_0 = 67.8 \text{ sq ft}$$

$$RN_b = \frac{0.00238 \times 117 \times 8.34 \times 10^7}{3.745} = 6.21 \times 10^6$$

Using data from Reference 21 interpolated, $C_{D_0} = 0.5$. Therefore,

$$\text{Download} = C_{D_0} qS_0 = 0.5 \times 16.35 \times 67.8 = 555 \text{ lb}$$

3. Download on Aft Fuselage

The Rotor/Wing wash extends from fuselage station 568 to fuselage station 694. Here again, the fuselage is generally a smooth rectangular box with rounded corners. The fuselage dimensions in this area are:

1. Average width, b = 62.5 inches
2. Average depth, c = 87 inches
3. Corner radius, r = 15 inches

Thus,

$$\frac{c}{b} = 1.39$$

$$\frac{r}{b} = 0.24$$

$$S_0 = 54.8 \text{ sq ft}$$

$$RN_b = 4.99 \times 10^6$$

$$C_{D_0} = 0.46 \text{ (Reference 21)}$$

Therefore,

$$\text{Download} = C_{D_0} qS_0 = 0.46 \times 16.35 \times 54.6 = 411 \text{ lb}$$

4. Total Fuselage Download

$$T_{\text{fuselage}} = 555 + 411 = 966 \text{ lb}$$

$$\frac{T_{\text{fuselage}}}{T_{\text{rotor net}}} = \frac{966}{20,671} \times 100 = 4.46 \text{ percent}$$

Conservatively, 5-percent download has been used in the hovering power computations.

INDUCED POWER

The induced power is computed using the basic momentum equation

$$C_Q = \frac{C_T^{3/2}}{\sqrt{2B^2}}$$

shown in step (4), page 85, of Reference 20. In order to properly represent the large reduction in effective area due to the wing, the equation

has been modified by replacing the tip loss factor B by the value $\sqrt{A_d/A}$, where A is the total disc area and A_d is the annular area swept by the blades, excluding the outer 3 percent for tip loss. This has the effect of assuming that the lift is carried only in the annular area from 55- to 97-percent radius. In addition, a coefficient, c_i, of 1.04 has been applied to correct for planform and taper. This factor was obtained from the table on page 85 of Reference 20 for blades with zero twist and 2.3:1 taper. The resulting equation used for induced torque coefficient is

$$C_{Q_i} = \frac{c_i C_T^{3/2}}{\sqrt{2\frac{A_d}{A}}} = \frac{c_i C_T^{3/2}}{\sqrt{2(B^2 - r/R^2_{\text{blade root}})}}$$

PROFILE POWER

The profile torque coefficient is computed using the basic equation (36) on page 83, of Reference 20, written in a slightly different form:

$$\frac{C_{Q_0}}{\sigma} = \frac{\delta_0}{8} + \left(\frac{2\delta_1}{3a}\right)\left(\frac{C_T}{\sigma B^2}\right) + \left(\frac{4\delta_2}{a^2}\right)\left(\frac{C_T}{\sigma B^2}\right)^2$$

The values of δ are given by the NACA polar, which is based on conventional airfoils such as an NACA 0012 airfoil.

$$C_{D_0} = 0.0087 - 0.0216\alpha_r + 0.4\alpha_r^2$$

which results in

$$\frac{C_{Q_0}}{\sigma} = \left[0.0010875 - 0.002513\left(\frac{C_T}{\sigma B^2}\right) + 0.0487316\left(\frac{C_T}{\sigma B^2}\right)^2\right]$$

The solidity used in the above equation is based on a weighted effective chord from 55- to 100-percent radius; the tip loss factor B of 0.97 handles the tip loss.

The weighted effective chord is given by

$$c_e = \frac{\int_{0.55}^{1} cx^2 \, dx}{\int_0^1 x^2 \, dx}$$

where $x = \frac{r}{R}$

and $\sigma = \frac{bc_e}{\pi R}$

As in the induced power, the factor for planform and twist c_i is applied. The drag polar used in the profile torque equation is based on 12-percent-thick airfoils; therefore, a factor is added to account for the increased drag of a thicker airfoil. The average thickness is assumed to be the thickness at the radius at which the geometric chord is equal to the effective weighted chord. This value is then 14.4 percent. Airfoil data of Reference 22 indicate an approximate 2.3-percent increase in drag coefficient with each 1-percent increase in airfoil thickness. Therefore, the profile torque is increased by 6 percent to provide an allowance for increased drag over that of the conventional NACA airfoil.

NACA whirl tower tests presented in Reference 23 for a rotor with an NACA 0015 airfoil are used to determine a profile power correction due to stall and compressibility, if required. These data are modified in the following manner for the Rotor/Wing configuration.

It is conservatively assumed that the drag rise due to stall for the circular arc airfoil will occur approximately 1 degree in angle of attack earlier than for an NACA 0015 airfoil. To account for this, the average C_L is increased by an equivalent of 1 degree when entering the profile power-Mach number charts of Reference 23.

The rotor of Reference 23 had -5.5 degrees of twist, whereas the CRA Rotor/Wing is untwisted. Reference 5, which presents whirl tower test data for both a twisted and untwisted model rotor, shows that at a constant Mach number, the angle for drag divergence is increased by 1 degree for an untwisted blade compared with one with -8 degrees of twist. Thus, the tip angle of attack of an untwisted blade is effectively 1 degree higher, rather than the expected 2 degrees higher, for a blade with -8 degrees of twist. To apply the drag-divergence data of Reference 23 to the Rotor/Wing

configuration hover, the average lift coefficient is conservatively increased by an equivalent of 2 degrees angle of attack (1 degree for lack of twist; 1 degree to account for the circular arc airfoil), assuming the blade lift curve slope is 0.1 per degree.

The drag divergence data of Reference 23 have been replotted in Reference 2, in terms of C_T/σ. The value of the factor determined from these data is identified as C_{stall}.

The resulting equation for profile torque used for Rotor/Wing performance is

$$C_{Q_0} = C_{stall}\,(1.06)\,c_i\,\sigma\left[0.0010875 - 0.0025131\left(\frac{C_T}{\sigma B^2}\right) + 0.0487316\left(\frac{C_T}{\sigma B^2}\right)^2\right]$$

WING HOVER TORQUE

Hovering torque for the Rotor/Wing at sea level has been derived on the basis of whirl tower testing of Appendix D of Reference 4, and is

$$C_{Q_{wing}} = 0.000044$$

The analysis used to obtain this value is as follows.

1. Triangular Model Wing Torque Evaluation (HTC Whirl Test, Reference 4)

Triangular wing torque was analyzed by treating it as a combination of torque from a circular disc centerbody and three blade segments attached as indicated in Figure 128. Test conditions prevailing were:

$$n = 23.85 \text{ rps}$$

$$R_{blade} = 3.33 \text{ ft}$$

Sea level standard

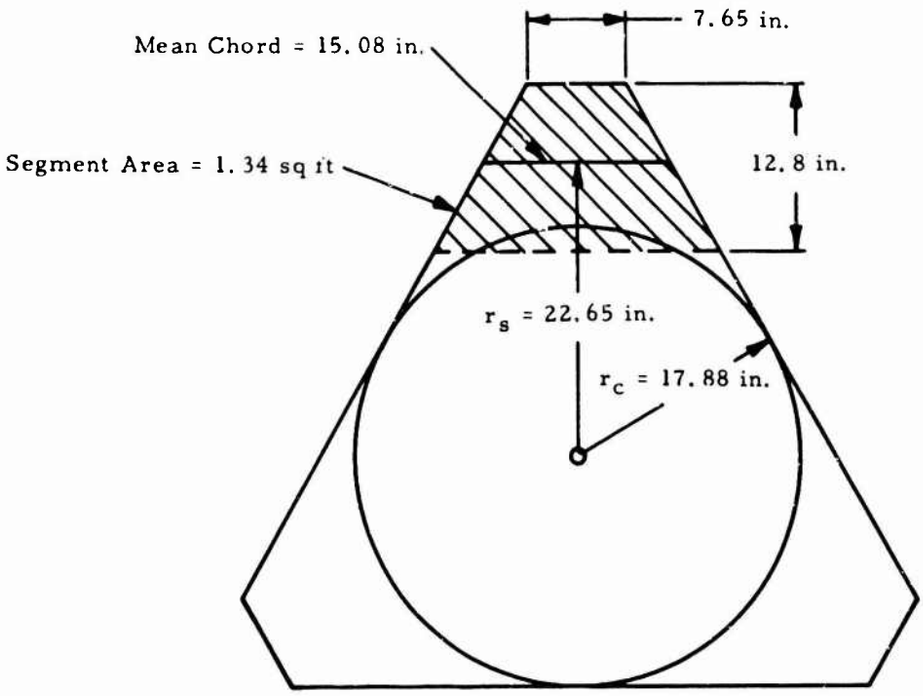

Figure 128. Dimensional Characteristics, Triangular Model Wing.

Torque for the circular midsection is calculated using rotating disc theory and data of Reference 24.

$$\text{Disc Reynolds number, } RN_{r_c} = \frac{V_{r_c}}{\nu} = \frac{2\,r_c\,n r_c}{\nu}$$

$$= \frac{2\pi(23.85)}{0.000157}\,\frac{17.88^2}{12} = 2.12 \times 10^6$$

Using the equation and terminology of Reference 24 for full turbulent flow, we have a torque coefficient varying with RN_{r_c}; thus,

$$C_{Q_c} = \frac{0.146}{RN_{r_c}^{1/5}} = \frac{0.146}{18.47} = 0.00791$$

Thus, centerbody torque is

$$Q_c = C_{Q_c} \frac{\rho}{2} \left(\Omega r_c\right)^2 r_c^3 = 1.55 \text{ ft-lb}$$

Now the complete wing torque is Q_{wing} = 13.03 ft-lb (Reference 4) and segment torque is $Q_s = Q_{wing} - Q_c$ = 11.48 ft-lb.

A relationship is now found between the segment drag coefficient (as indicated by the torque just found) and turbulent flat plate section drag.

Thus, let

$$Q_s = DXr_s = 3\left(C_{D_0} \times q_{r_s} S_s r_s\right)$$

Then

$$C_{D_0} = \frac{11.48}{3\left(\frac{0.002378}{2}\right)(2\pi \times 1.88 \times 23.85)^2 \times (1.34 \times 1.888)} = 0.016$$

$$RN_s = \frac{V_s \times C}{\nu} = \frac{282.5}{0.000157}\left(\frac{15.08}{12}\right) = 2.28 \times 10^6$$

From turbulent section drag data (Figure 66 of Reference 25),

$$C_{D_{min}} = 0.0078$$

Thus, the segment drag coefficient relationship to flat plate is

$$C_{D_0} = \left(\frac{0.016}{0.0078}\right) C_{D_{min}} = 2.05 \times C_{D_{min}}$$

It is assumed that full-scale wing torque may be estimated using full-scale Reynolds number in the disc torque equation, and the segment drag coefficient will be 2.05 x $C_{D_{min}}$.

2. CRA Wing Torque Estimation

The wing torque coefficient for use in the CRA hover performance calculation procedure is derived below.

The wing is treated in the same manner as in the triangular model torque evaluation (a circular center section with blade root segments as shown schematically in Figur 129).

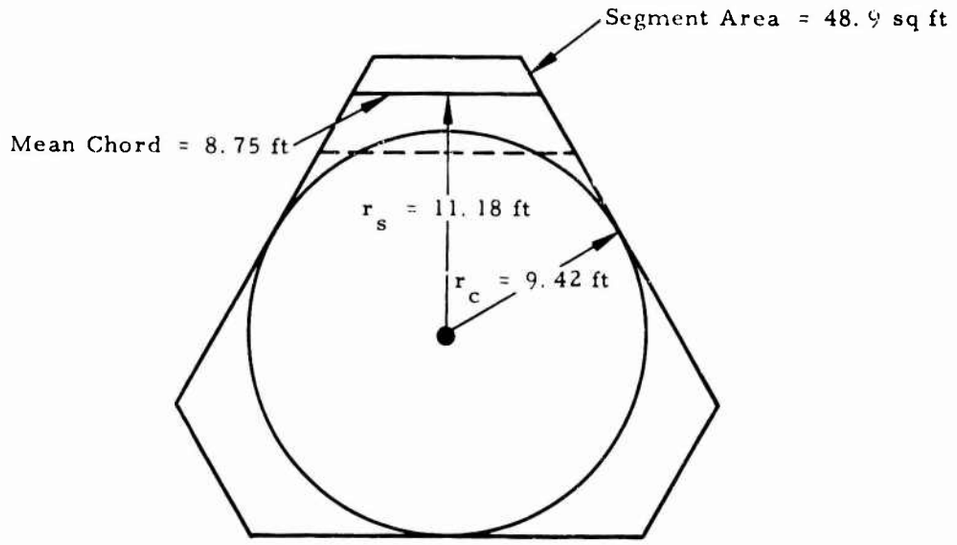

Figure 129. Dimensional Characteristics, CRA Wing.

The torque on the center section is calculated as follows:

$$RN_{r_c} = \frac{V_{r_c} r_c}{\nu} = \frac{2\pi \times 9.42 \times 4.59 \times 9.42}{0.000157} = 1.625 \times 10^7$$

$$C_{Q_c} = \frac{0.146}{RN_{c_r}^{1/5}} = \frac{0.146}{(1.625 \times 10^7)^{1/5}} = 0.00525$$

and

$$Q_c = C_{Q_c} \frac{1}{2} \rho V_{r_c}^2 r_c^3 = 0.00525 \frac{0.002378}{2} (271)^2 (9.42)^3$$

$$= 383 \text{ ft-lb}$$

The segment torque, Q_s, is calculated as follows:

$$RN_{r_s} = \frac{V_{r_s} C}{\nu} = \frac{(2\pi \times 11.18 \times 4.59) \times 8.75}{0.000157} = 1.795 \times 10^7$$

From Figure 66 of Reference 26, $C_{d\ min} = 0.0055$

Thus,

$$C_{D_0} = 2.05 \times 0.0055 = 0.01129$$

$$Q_s = 3D_0 r_s = 3 C_{D_0} q_{r_s} S_s r_s$$

$$= 3 \times 0.01129 \times \frac{(0.002378)(322)^2}{2} \times 48.9 \times 11.18$$

$$= 2,280 \text{ ft-lb}$$

The CRA wing torque coefficient for hovering is therefore

$$Q_{total} = 2,280 + 383 = 2,663 \text{ ft-lb}$$

and the wing torque in rotor terminology is

$$C_Q = \frac{Q}{\rho \pi \Omega^2 R^5} = \frac{2663}{0.002378 \pi (2 \pi 4.59)^2 (25)^2} = 0.000044$$

This is the value of C_Q used in the CRA hover performance calculation procedure.

Comparison of Model Wing Torque Coefficient and CRA Estimate

Whirl tower test data for the triangular and trisector wings (Reference 4) are shown in Figure 130. The model data were obtained at the r/R values indicated by the data point. By varying the rotor blade radius, the variation of C_Q versus r/R indicated is obtained. The radius ratio for the CRA is 0.55, which locates the calculated hovering point close to the extrapolated model triangular wing data, as seen in Figure 130. Apparently, even though there is a large drop in moment and drag coefficients as a result of the increase in Reynolds number from model to full scale, the increased wing area (see Figure 131) of the CRA wing for the same r/R offsets this.

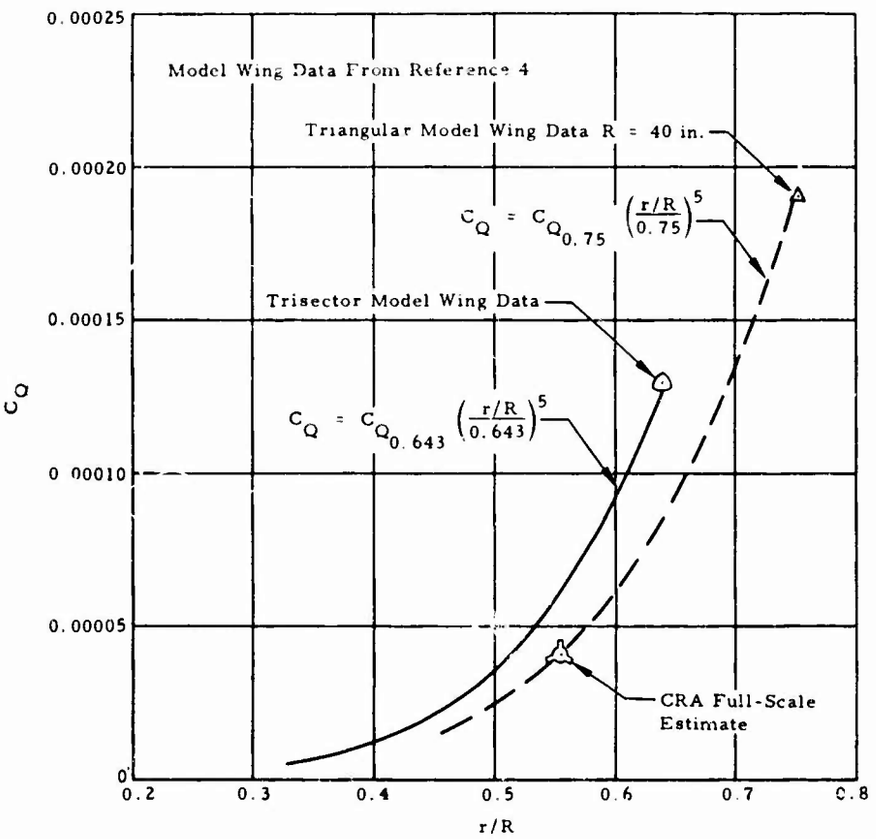

Figure 130. Variation of Wing C_Q with r/R, Hovering Conditions.

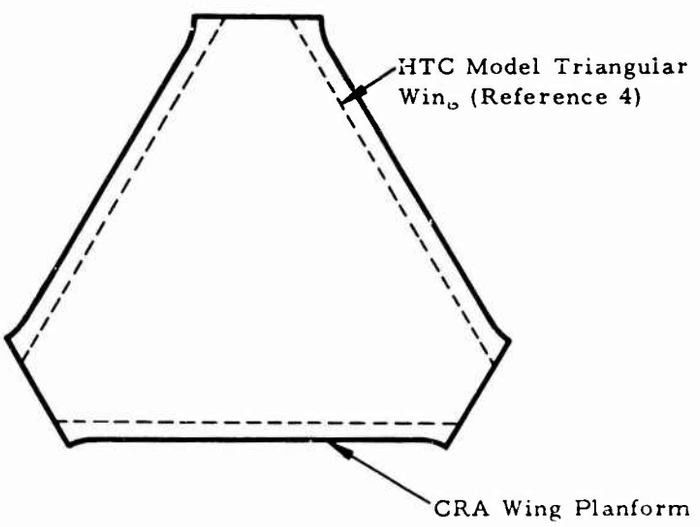

Figure 131. Relative Proportions of CRA Wing and Model Triangular Wing.

The trisector wing data shown in Figure 130 are used for forward flight helicopter performance calculations.

ACCESSORY AND COOLING POWER REQUIREMENTS

During helicopter flight, the Rotor/Wing provides power to drive various accessories and to cool a portion of the engine compartment, the wing, and the blades. The accessory power extracted is 4 horsepower. The rotor pumping power required for cooling is estimated to be 30 horsepower in the section entitled Propulsion System.

YAW FAN

The Rotor/Wing also drives the yaw fan. Inasmuch as the Rotor/Wing is tip driven, the yaw fan thrust during steady flight is used only to counteract the torque required to drive the accessories and yaw fan. By estimating the yaw fan power, the necessary thrust can be computed. The yaw fan power is estimated to be approximately 1 percent of Rotor/Wing power based on the method of Reference 2, assuming a mechanical drive efficiency of 95 percent. The method used to compute the power absorbed by the yaw fan is presented in detail in Reference 2. A brief discussion is presented below.

The yaw fan induced power is computed from the method of Reference 20, using an annular area obtained after applying a 3-percent radius tip and root loss to the blades. The blades are untwisted and untapered, so the correction factor for twist and taper from Reference 20 is applied to the induced power.

The yaw fan profile power is computed using equation 33 on page 83 of Reference 20. The blade loading is based on a thrust-weighted solidity with a tip and root loss of 3 percent, and the torque is based on a torque-weighted solidity over the entire blade.

The drag divergence factor derived from flight tests of the Hughes Model 269A tail rotor blade, presented in Reference 2, was used when necessary.

GROUND EFFECT

Whirl tests of the model Rotor/Wing indicated that the ground effect was greater than that of a conventional rotor. The model data and a wheel height above the ground of 6 feet are used in computing the ground effect.

VERTICAL CLIMB

The vertical climb rate is computed using equation 36 on page 83 of Reference 20, modified to apply to the Rotor/Wing configuration. In this method, the total power required for climb equals the sum of the profile power, the induced power reduced to account for the vertical in-flow into the Rotor/Wing, and the power required to lift the aircraft at the climb velocity. The increased download on the fuselage and elevons is also accounted for.

The profile power computation method is unchanged from the method used during steady hovering flight. The induced torque coefficient is computed by the following equation, which is consistent with the steady hovering analysis:

$$C_{Q_i} = \frac{1}{2} C_T \sqrt{\left(\frac{V_v}{\Omega R}\right)^2 + \frac{2C_T}{\left(\frac{A_d}{A}\right)}} + \frac{1}{2}\left(\frac{V_v}{\Omega R}\right) C_T$$

where C_T is based on total rotor thrust, including the effects of download.

WHIRL TOWER MODEL SUBSTANTIATION OF HOVERING PERFORMANCE COMPUTATIONAL METHOD

Data from whirl tower tests of models of a conventional helicopter rotor with NACA 0015 blades, called herein the reference rotor, and of a Rotor/Wing with circular arc blades are used to substantiate the power-computing method.

A $C_T - C_Q$ curve from tests of the reference rotor is shown in Figure 132. A profile power factor (PPF) for the model is determined by comparing these test data with a similar curve calculated by the NACA performance method (Reference 20). The PPF thus determined is shown in Figure 133 and is the result of the low Reynolds number of the small-scale model, since both the model and the theory have NACA 0015 blades.

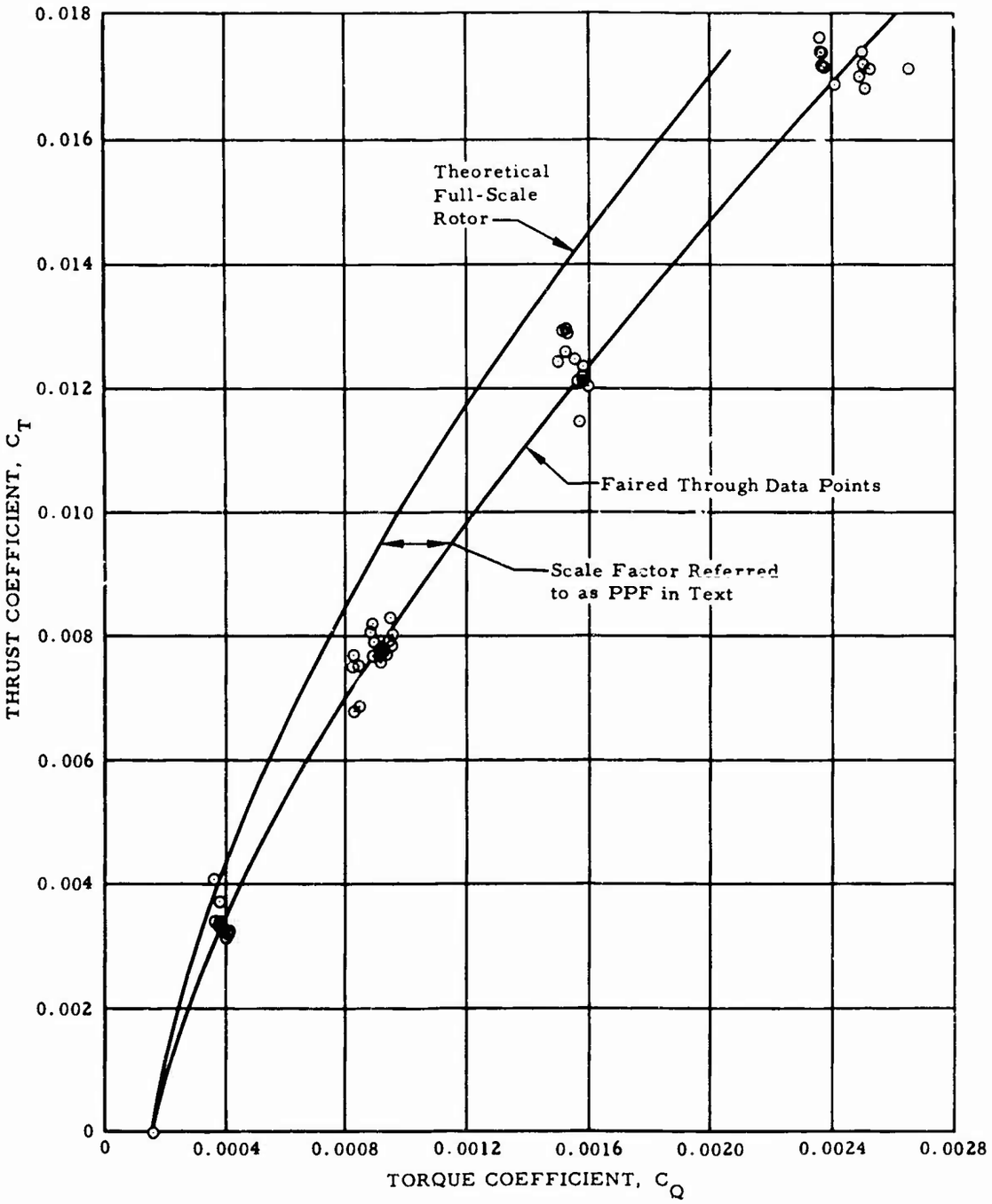

Figure 132. Thrust and Torque Coefficients, Reference Rotor.

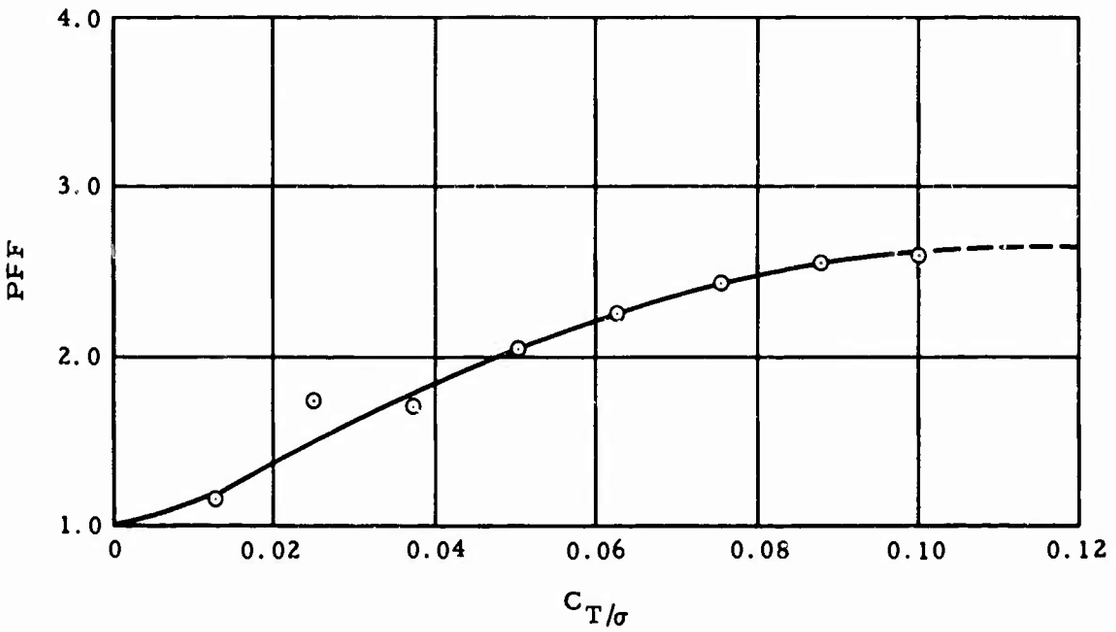

Figure 133. Profile Power Scale Factor, Whirl Test of Reference Rotor.

When the profile power factor determined in this way is applied to the hovering computational method devised for the Rotor/Wing configuration, the good agreement between model test data and C_T - C_Q predicted for the Rotor/Wing model is shown in Figure 134. Thus, the validity of the performance prediction method is confirmed. This method is then used for full-scale aircraft performance prediction, by making the PPF equal to unity to account for the scale change.

Computation of the Model Scale Factor (PPF)

Whirl tower data of the reference rotor form the basis of this computation. The dimensions of the reference rotor are:

Rotor diameter, D = 80 in.
Rotor radius, R = 40 in. = 3.33 ft
Rotor chord, c = 6.66 in. = 0.555 ft

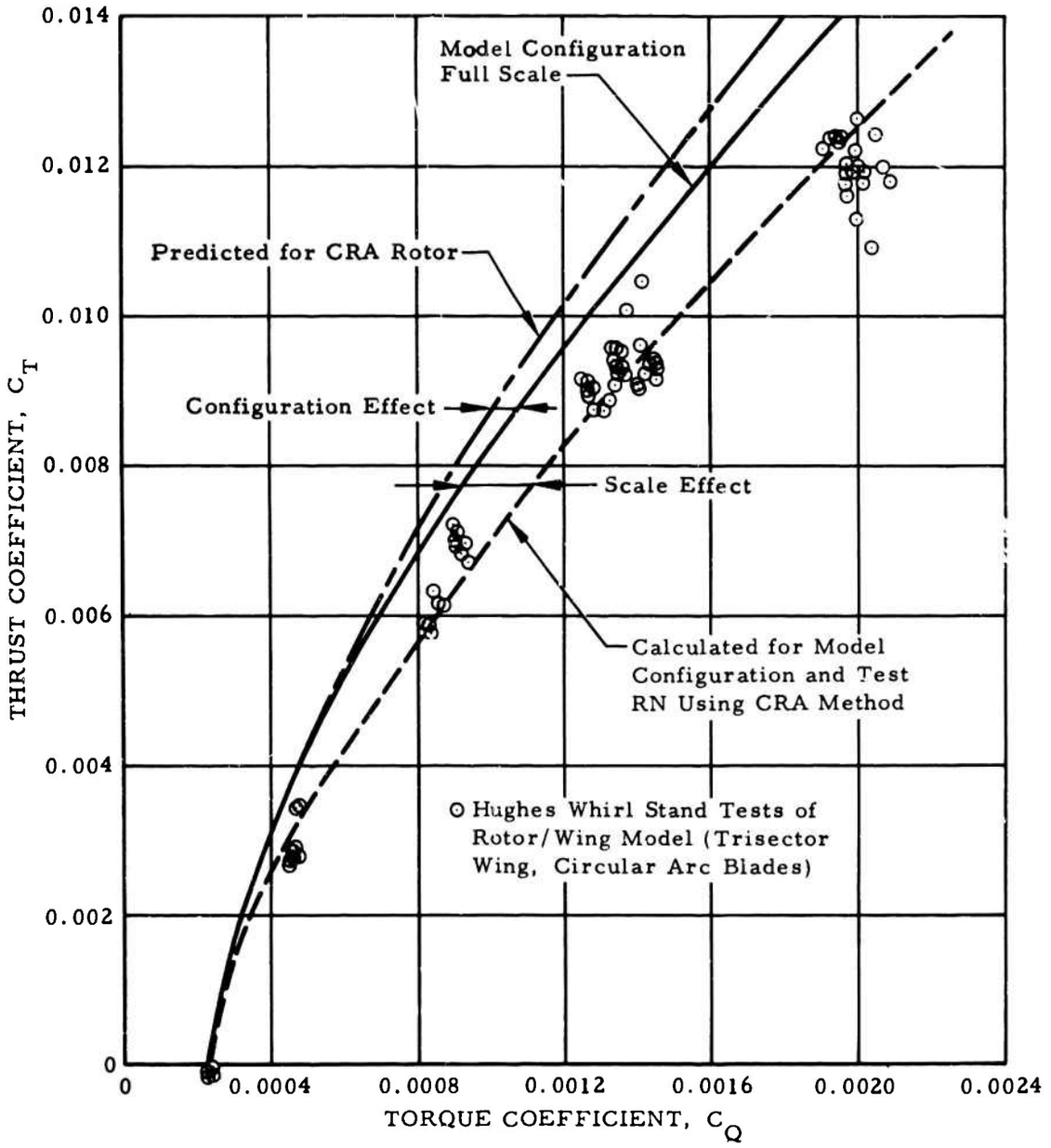

Figure 134. Comparison, CRA Rotor Hover Power and Model Test Data.

The main rotor solidity σ is calculated from the equation

$$\sigma = \frac{(b)(c)}{\pi R}$$

where b is the number of blades.

Thus,

$$\sigma = \frac{(3)(0.555)}{(3.1416)(3.33)} = 0.159$$

The induced torque coefficient C_{Q_i} is calculated from the equation

$$C_{Q_i} = \frac{c_i C_T^{3/2}}{\sqrt{2}\, B} = \frac{c_i C_T^{3/2}}{1.3716}$$

where

B = 0.97, representing a 3 percent tip loss

C_T = rotor thrust coefficient

c_i = factor for zero twist and untapered blades (function of $C_T/\sigma B^2$).

The theoretical profile torque coefficient is calculated from the equation

$$C_{Q_{0_{theory}}} = c_i C_{t/c} \sigma \left[0.0010875 - 0.002513\left(\frac{C_T}{\sigma B^2}\right) + 0.0487316\left(\frac{C_T}{\sigma B^2}\right)^2\right]$$

where $C_{t/c}$ = 1.07 (profile thickness factor for a 15-percent-thick blade).

The following equation relates the test torque coefficients of the reference rotor in hover:

$$C_{Q_{test}} = C_{Q_i} + C_{Q_{0_{test}}}$$

Solving for the test profile torque coefficient,

$$C_{Q_{0_{test}}} = C_{Q_{test}} - C_{Q_i}$$

The scale factor (or PPF) is the ratio of the test profile torque coefficient to the theoretical profile torque coefficient. Thus,

$$PPF = \frac{C_{Q_0}{}_{test}}{C_{Q_0}{}_{theory}}$$

Table XXXIII summarizes the calculations for the model scale factor (PPF) for various values of C_T and C_T/σ.

TABLE XXXIII. MODEL SCALE FACTORS

C_T	0.002	0.004	0.006	0.008	0.010	0.012	0.014	0.016
$C_{T/\sigma}$	0.01258	0.02515	0.03774	0.05031	0.06289	0.07547	0.08805	0.10063
$C_T/\sigma B^2$	0.01337	0.02672	0.04011	0.05347	0.06684	0.08021	0.09358	0.10695
c_i	1.022	1.030	1.037	1.045	1.052	1.06	1.068	1.075
C_{Q_i}	0.0000651	0.0001899	0.0003514	0.0005452	0.0007672	0.0010159	0.001289	0.001586
$C_{Q_{0theory}}$	0.0001848	0.0001849	0.0001879	0.0001942	0.0002037	0.0002163	0.0002324	0.0002486
$C_{Q_{test}}$	0.00028	0.000450	0.000670	0.000 94	0.001230	0.00154	0.00188	0.00223
$C_{Q_{0test}}$	0.000215	0.000260	0.000319	0.000395	0.000460	0.000524	0.000590	0.000644
$PPF = \frac{C_{Q_0}{}_{test}}{C_{Q_0}{}_{theory}}$	1.162	1.731	1.697	2.036	2.244	2.425	2.545	2.587

The model scale factor (PPF) as a function of C_T/σ is plotted in Figure 133. The faired curve is used in the computation of the model Rotor/Wing C_T - C_Q curve.

Computation of Rotor/Wing Model C_T - C_Q

Assuming the same profile power scale factor, this computation is as follows.

The dimensions of the Rotor/Wing model are as follows:

Rotor radius, R = 42.95 in. 3.579 ft

Radial distance to the inboard root of the blade, r 25.77 in. 2.148 feet

Rotor disc area, $A = \pi R^2 = 40.245$ sq ft

Annular area swept by the blades only

$$A_d = \pi(0.97R^2 - r^2) = \pi(3.472^2 - 2.148^2)$$

$$A_d = 23.376 \text{ sq ft}$$

The equivalent Rotor/Wing tip and root loss factor is $\sqrt{A/A_d}$, thus

$$\sqrt{\frac{A}{A_d}} = 0.762$$

Calculating the equivalent blade chord on a thrust basis,

$$C_e = \frac{c(R^3 - r^3)}{R^3} = \frac{(6.6)(45.844 - 9.911)}{45.844}$$

$$C_e = 5.173 \text{ in.} = 0.431 \text{ ft}$$

The Rotor/Wing solidity can then be calculated from the equation

$$\sigma = \frac{(b)(C_e)}{\pi R} = \frac{(3)(0.431)}{(3.14)(3.579)} = 0.115$$

The induced torque coefficient for the Rotor/Wing is calculated from the equation

$$C_{Q_i} = \frac{c_i C_T^{3/2}}{\sqrt{2\frac{A_d}{A}}} = 0.9278\, c_i C_T^{3/2}$$

and the profile torque coefficient from the equation

$$C_{Q_0} = (PPF)(c_i)\, C_{t/c}\, \sigma\left[0.0010875 - 0.0025131\left(\frac{C_T}{\sigma B^2}\right) + 0.0487316\left(\frac{C_T}{\sigma B^2}\right)^2\right]$$

where PPF is the profile power scale factor previously determined from tests of the reference rotor (Figure 133) and c_i and $C_{t/c}$ are the same as for the reference rotor, as both blades are untwisted and untapered and 15 percent thick.

From test data, blades off, the wing torque coefficient, C_{Q_w} 0.0001.

The total torque coefficient C_Q for the Rotor/Wing in hover is therefore

$$C_Q \quad C_{Q_i} + C_{Q_0} + C_{Q_w}$$

Table XXXIV summarizes the calculations for the Rotor/Wing model C_T versus C_Q.

TABLE XXXIV. ROTOR/WING MODEL COMPUTATION OF C_Q

C_T	0	0.002	0.004	0.006	0.008	0.010	0.012
$C_{T/\sigma}$	0	0 0174	0.0348	0.0522	0.0696	0.0869	0.1043
$C_{T/\sigma B^2}$	0	0.0185	0.0370	0.0555	0.0740	0.0924	0.1108
c_i	1.014	1.025	1.037	1.048	1.059	1.070	1.081
PPF	1.00	1.30	1.70	2.07	2.35	2.54	2.62
C_{Q_0}	0.0001357	0.0001714	0.0002297	0.0002907	0.0003510	0.0004137	0.0004724
C_{Q_i}	0	0.0000561	0.0002434	0.0004519	0.0007030	0.0009927	0.0013184
C_Q	0.0002357	0.0003575	0.0005131	0.0007426	0.0011548	0.0015064	0.0018908

APPENDIX III

CALCULATION OF POWER AVAILABLE

PRESSURE LOSS CALCULATION FOR HELICOPTER FLIGHT

Engine Inlet Loss

A bellmouth with a 4-inch radius of curvature is used. Three aerodynamically shaped struts of 0.45-inch thickness and 3-inch chord length are used for protection of the electric wires leading to the generator. The pressure loss due to the struts is calculated with a loss coefficient, Kt = 0.007. The bellmouth velocity head is calculated using the flow function.

$$\frac{W\sqrt{T}}{AP} = \frac{135\sqrt{519}}{(618)(14.7)} = 0.339$$

where W = 135 lb/sec

T = 519°R

A = 618 sq in.

P = 14.7 psia

K = 1.4

Therefore, the Mach number is M = 0.4 and the velocity head to total pressure ratio is $(q/P_T) = 0.104$. The pressure loss due to the struts is then,

$$\frac{\Delta P}{P} = (0.007)(0.104) = 0.0008$$

Bellmouth-Intake Loss

The intake loss coefficient is Kt = 0.01, and the pressure loss is

$$\frac{\Delta P}{P} = Kt\ \frac{q}{P} = (0.01)(0.104) = 0.00104$$

The total engine inlet loss is the sum of the strut and intake loss.

$$\frac{\Delta P}{P} = 0.0018$$

Pressure Loss -- Engine Exit to Rotor Inlet

The losses for the diverter valve are taken from Reference 27, which gives the following pressure and leakage losses

$$\frac{\Delta P}{P} = 0.035 \quad \text{at Mach Number} \quad M = 0.5$$

$$\frac{\Delta W}{W} = 0.0088$$

For the present case, the flow function and the Mach number are

$$\frac{W\sqrt{T}}{AP} = \frac{140}{381.1} = 0.367 \quad \text{at} \quad M = 0.465$$

As the pressure loss is proportionate to the Mach number squared, the diverter valve pressure loss is

$$\frac{\Delta P}{P} = 0.035 \left(\frac{0.465}{0.5}\right)^2 = 0.0304$$

The leakage loss is taken as

$$\frac{\Delta W}{W} = 0.0088$$

The single exit pipe from the diverter valve splits up into 3 pairs of pipes, with one pair leading into each blade. The momentum rate ratio G_2/G_1 is established from continuity.

$$\rho_2 A_2 V_2 = \frac{1}{6} \rho_1 A_1 V_1$$

$$\frac{G_2}{G_1} = \frac{\rho_2 V_2}{\rho_1 V_1} = \frac{1}{6} \frac{A_1}{A_2}$$

$$\frac{G_2}{G_1} = \frac{1}{6} \frac{A_1}{A_2} = \frac{452.4}{6(70.9)} = 1.065$$

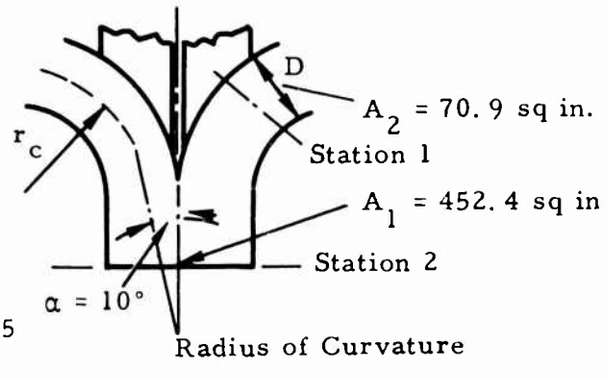

The angle between the main stream and the individual pipe is approximately 10 degrees.

The hub split up loss coefficient is found with the help of Reference 25 and is Kt = 0.04. The flow function, Mach number, and the velocity head pressure at the inlet to the hub are:

$$\frac{W\sqrt{T}}{AP} = \frac{140}{452.4} = 0.309$$

then

$$M = 0.375$$

$$\frac{q}{P} = 0.088$$

The split up pressure loss is then

$$\frac{\Delta P}{P} = Kt \frac{q}{P_T} = (0.04)(0.088) = 0.0035$$

The pressure loss for the 90-degree turn into rotor is found similarly.

The flow function at the rotor duct inlet is

$$\frac{W\sqrt{T}}{AP} = \frac{1}{6}\left(\frac{140}{70.9}\right) = 0.33$$

then

$$M = 0.405$$

$$\frac{q}{P} = 0.102$$

From Reference 25 the loss coefficient for $r_c/D = 1.65$ is $Kt_{90°} = 0.11$ and the turning pressure loss is

$$\frac{\Delta P}{P} = (0.11)(0.102) = 0.0112$$

The total pressure loss from engine to rotor inlet is the sum of losses of the diverter valve, split up and turning

$$\frac{\Delta P}{P} = \left(\frac{\Delta P}{P}\right)_{div} + \left(\frac{\Delta P}{P}\right)_{split} + \left(\frac{\Delta P}{P}\right)_{turn} = 0.0304 + 0.0035 + 0.0112 = 0.0451$$

Rotor Duct Pressure Losses

The state of the gas along the rotor duct is broken down into four sections indicated in Figure 135. The friction losses along the duct are included in the basic equations outlined in Rotor Power Calculations, page 281. Only additional coefficients for split-up and turning losses are calculated here.

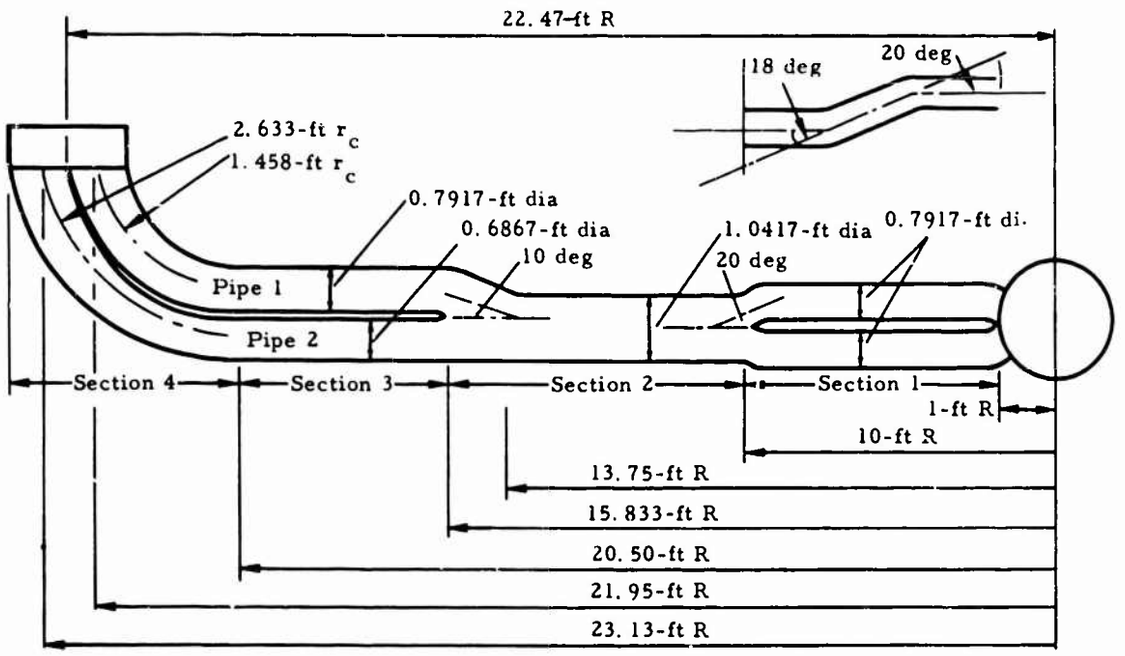

Figure 135. Rotor Duct Schematic.

Pressure Loss Coefficients of Section 1 (Figure 135)

The turning losses at the junction of the two separate pipes into a single pipe are found in Reference 25 for the turning angles of 18 and 20 degrees and a radius of curvature to diameter ratio of 2.0.

$$Kt_{18°} = 0.023$$

$$Kt_{20°} = 0.024$$

$$Kt' = Kt_{18°} + Kt_{20°} = 0.047$$

The merging loss coefficients are established next. The subscripts a and b indicate the single duct, and c, the merged duct. The cross-sectional areas are

$$A_a = A_b = 70.9 \text{ sq in.}$$

$$A_c = 122.8 \text{ sq in.}$$

The angle between the single duct δ and β is 20 degrees. The merging loss coefficient is found with the following equation taken from Reference 25.

$$Kt_c = \lambda + \left(\frac{G_c}{G_a}\right)^2 - 2\left(\frac{A_a}{A_c}\right)\cos\beta - \left(\frac{G_b}{G_a}\right)^2\left(2\,\frac{A_b}{A_c}\cos\delta\right)$$

The parameters in the present case are

$$\lambda = 0.95$$

$$2W_a = 2\rho_a V_a A_a = \rho_c V_c A_c$$

$$\frac{G_c}{G_a} = \frac{2(70.9)}{122.8} = 1.152$$

$$\frac{A_a}{A_c} = \frac{70.9}{122.8} = 0.576$$

$$\frac{\rho_c V_c}{\rho_a V_a} = 2\left(\frac{A_a}{A_c}\right) = \frac{G_c}{G_a}$$

$$\frac{G_b}{G_a} = 1.0$$

$$2\left(\frac{A_b}{A_c}\right)\cos\delta = 1.075$$

$$2\left(\frac{A_a}{A_c}\right)\cos\beta = 1.075$$

$$Kt_c = 0.95 + (1.152)^2 - 1.075 - 1.075 = 0.127$$

$$Kt_a = Kt_b = \frac{Kt_c}{2} + Kt' = \frac{0.127}{2} + 0.047 = 0.11$$

$$Kt_a = Kt_b = 0.11$$

Pressure Loss Coefficient at End of Section 2 (Figure 135)

The split-up-loss coefficient can be readily found with the angle between the two single ducts as 10 degrees and the momentum rate is assumed as

$$\frac{G_b}{G_a} = \frac{\rho_b V_b}{\rho_a V_a} = 1.0$$

Then the loss coefficient is Kt = 0.04.

Pressure Loss Coefficients at End of Section 4 (Figure 135)

Each of the two pipes has two guide vanes built in as reinforcements against duct buckling. These vanes reduce the turning losses, but increase the friction losses. The ducts start as round and continuously change their cross section in the 90-degree turn, and finally fit into the rectangular nozzle inlet.

The computer program calculates the duct flow area from a single input diameter chosen to produce the right flow velocities. The friction losses, however, have to be calculated from the hydraulic diameter, which is not necessarily equal to the input diameter used for the area calculation. To compute the friction losses for the subdivided pipe with a single diameter, an equivalent friction factor is established.

$$\frac{4fL}{\bar{D}}\,\bar{q} = \frac{1}{3}\left[\left(\frac{4fL_1}{D_1}\right)q_1 + \left(\frac{4fL_2}{D_2}\right)q_2\left(\frac{4fL_3}{D_3}\right)q_3\right] = \left(\frac{4f_e L}{D}\right)\bar{q}$$

$$f_e \cong \frac{fD}{3}\left(\frac{1}{D_1} + \frac{1}{D_2} + \frac{1}{D_3}\right)$$

These are two pipes, each subdivided into three channels (see Figure 135). Assuming that each channel has a square cross section, the hydraulic diameters D_1, D_2, and D_3 are equal, and the equivalent friction factor reduces to

$$f_e = f \frac{D}{D_1}$$

The total cross-sectional area of pipe 1 is 56.4 square inches, and the corresponding diameter D = 8.49 inches. The hydraulic diameter of each channel is

$$D_1 = \frac{4 \text{ area}}{\text{perimeter}} = \frac{4a^2}{4a} = a = \sqrt{\frac{A_{total}}{3}} = \sqrt{\frac{56.4}{3}} = 4.36 \text{ in.}$$

where a is the length of one side of the square. Similarly, the hydraulic diameter D_1 for the channels of pipe 2 are

$$D_1 = \sqrt{\frac{A_{total}}{3}} = \sqrt{\frac{41.6}{3}} = 3.72 \text{ in.}$$

The equivalent friction factor for pipe 1 is

$$f_e = f\left(\frac{D}{D_1}\right) = 0.003 \left(\frac{8.49}{4.36}\right) = 0.00583$$

for pipe 2

$$f_e = 0.003 \left(\frac{7.29}{3.72}\right) = 0.00585$$

The equivalent friction factor for pipe 1 and pipe 2 is approximately equal to 0.00585.

The turning loss coefficient (referred to inlet Mach number of pipe) for pipe 1 for a radius of curvature to diameter ratio of

$$\frac{r_c}{D} = \frac{12(1.458)}{4.36} = 4$$

is equal to

$$Kt_{inlet} = 0.05$$

The computer program calculates the pressure loss at the beginning of section 4 and the turning losses therefore are referred to the inlet in the following manner.

$$\Delta P = Kt_{inlet}\, q_{inlet} = Kt_{exit}\, q_{exit}$$

$$K'_{exit} = Kt_{inlet}\left(\frac{q_{inlet}}{q_{exit}}\right) = Kt_{inlet}\left(\frac{M_{inlet}}{M_{exit}}\right)^2$$

$$Kt_{exit} = 0.05\left(\frac{0.5}{0.8}\right)^2 = 0.0195$$

$$Kt_1 = 0.02$$

Similarly for pipe 2,

$$\frac{r_c}{D} = \frac{12(2.633)}{3.72} = 8.5$$

$$Kt_{inlet} = 0.02$$

$$Kt_{exit} = 0.02\left(\frac{0.5}{0.8}\right)^2 = 0.0078$$

$$Kt_2 = 0.008$$

PRESSURE LOSS CALCULATION FOR FORWARD FLIGHT

Engine Inlet Loss

The inlet diffuser has a rectangular shape and a total length of 147 inches. The engine bellmouth is mounted at the end of the diffuser.

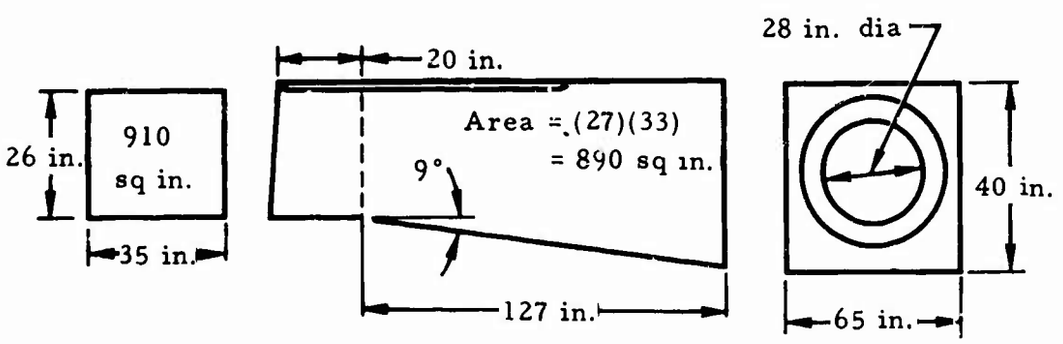

The cross-sectional area at the inlet is 910 square inches and the hydraulic diameter is

$$D_h = \frac{2A}{a + b} = \frac{2(910)}{26 + 35} = 29.8 \text{ in.}$$

The cross-sectional area at the end of the diffuser is,

$$\text{Area} = 65 \times 40 = 2,600 \text{ sq in.}$$

and the hydraulic diameter

$$D_h = \frac{2(2600)}{65 + 40} = 49.5 \text{ in.}$$

The average hydraulic diameter for the diffuser is then

$$D_{av} = \frac{29.8 + 49.5}{2} = 39.65$$

and

$$\frac{4fL}{D_{av}} = \frac{4(0.03)(147)}{39.65} = 0.0445$$

The hydraulic diameter at the start of the ramp is

$$D_h = \frac{2(890)}{27 + 33} = 29.7 \text{ in.}$$

The diffuser equivalent cone half angle is

$$\tan \alpha = \frac{D_{h_{exit}} - D_{h_{inlet}}}{2L} = \frac{49.5 - 29.8}{2(127)} = 0.0775$$

$$\alpha = 4^\circ 26 \text{ ft}$$

The diffuser pressure loss coefficient is then found from Reference 25 as Kt = 0.031 for an area ratio of

$$\frac{A_1}{A_2} = \frac{890}{2600} = 0.342$$

For a flow function of

$$\frac{W\sqrt{T}}{AP} = \frac{209}{890} = 0.235$$

The Mach number is M = 0.265 and the velocity head to total pressure ratio is q/P = 0.048.

The friction and diffusion pressure losses are

$$\frac{\Delta P}{P} = (0.0445 + 0.031)(0.048) = 0.0036$$

The boundary layer losses ahead of the diffuser inlet are taken as a constant 1.5 percent of the average free stream Mach number M = 0.4 and the velocity head to total pressure ratio is q/P = 0.104.

$$\frac{\Delta P}{P} = (0.015)(0.104) = 0.0016$$

The total loss is the sum of the boundary layer loss and diffuser loss

$$\left(\frac{\Delta P}{P}\right)_{total} = 0.0036 + 0.0016 = 0.0052$$

Engine Exhaust Loss

The diverter valve loss and leakage for straight through operation according to General Electric data (Reference 27)

$$\frac{\Delta P}{P} = 0.031 \quad \text{at } M = 0.5$$

$$\frac{\Delta W}{W} = 0.0067$$

For a flow function of

$$\frac{W\sqrt{T}}{AP} = \frac{140}{381.1} = 0.367$$

The Mach number is M = 0.465 and the velocity head to total pressure ratio q/P = 0.131.

The pressure loss is then

$$\frac{\Delta P}{P} = \left(\frac{\Delta P}{P}\right)_{M=0.5} \left(\frac{M}{0.5}\right)^2 = 0.031 \left(\frac{0.465}{0.5}\right)^2 = 0.0268$$

and the leakage loss is

$$\frac{\Delta W}{W} = 0.0067$$

Tail Pipe Pressure Loss

The friction factor is assumed as 0.003; the length of the tail pipe is 426 inches and the diameter 22 inches. The friction loss coefficient is then

$$\frac{4fL}{D} = \frac{4(0.003)(426)}{22} = 0.233$$

The pressure loss coefficient for two 20-degree turns in the tail pipe assembly is

$$\frac{r_c}{D} = 2.0$$

$$Kt_{20°} = 0.0255$$

The friction and turning pressure loss is

$$\frac{\Delta P}{P} = \left(\frac{4fL}{D} + 2Kt_{20°}\right) \frac{q}{P} = (0.233 + 0.051)(0.131) = 0.0372$$

Total exhaust loss (diverter valve + tail pipe) is

$$\left(\frac{\Delta P}{P}\right)_{total} = 0.0268 + 0.0372 = 0.064$$

HEAT LOSSES IN ROTOR AND TAIL PIPE

The heat losses are taken from the cooling system analysis.

The heat losses for helicopter operation are

Rotor/Wing	3 x 49,000	=	147,000
Rotor blades	3 x 27,000	=	81,000
Diverter valve		=	30,800
Total heat loss		=	258,800 btu/hr

The gas temperature drop due to heat losses is

$$\Delta T = \frac{\text{Heat loss}}{W(c_p)} = \frac{258,800}{(3600)(137)(0.276)} = 1.9°F$$

The gas temperature is

$$T_{gas} = 1621°R$$

and

$$\frac{\Delta T}{T} = \frac{1.9}{1621} = 0.00117$$

The gas temperature loss from engine to rotor tip is

$$\frac{\Delta T}{T} = 0.12 \text{ percent}$$

The heat losses for forward flight are

Diverter valve	=	30,800
Tail pipe	=	218,000
Total heat loss	=	248,800 btu/hr

The gas temperature drop due to heat losses is

$$\Delta T = \frac{248,800}{(3600)(137)(0.276)} = 1.8°F$$

and

$$\frac{\Delta T}{T} = \frac{1.8}{1621} = 0.0011$$

The gas temperature loss from engine to tail nozzle is

$$\frac{\Delta T}{T} = 0.11 \text{ percent}$$

The thrust loss due to heat loss is

$$\frac{\Delta F}{F} = \frac{1}{2}\left(\frac{\Delta T}{T}\right) = \frac{1}{2}(0.11 \text{ percent}) = 0.055 \text{ percent}$$

SINGLE-LINE TURBINE CHARACTERISTIC

The single-line turbine characteristic is based on the assumption that the change of the external and internal engine performance is proportional to the change of the inlet pressure and temperature. This method, which is commonly known as "referring" to a standard ambient pressure and temperature, is satisfactory for up to approximately 20,000-foot altitude. For higher altitudes, Reynolds and specific heat effects produce significant deviations from the single-line operation.

The single-line approach is used only for the helicopter powe. alculation.

The performance parameters are referred to the standard ambient conditions of $P_o = 14.7$ psia; $T_o = 59°F = 518.7°R$. The parameters are:

P_2/δ	Compressor inlet pressure
T_2/θ	Compressor inlet temperature
P_7/δ	Turbine exhaust pressure
T_7/θ	Turbine exhaust temperature
$W_f/\delta\sqrt{\theta}$	Fuel flow
$W_A\sqrt{\theta}/\delta$	Air flow

where

$$\delta = \frac{\text{ambient pressure} + \Delta P_{ram} - \Delta P_{loss}}{14.7}$$

$$\theta = \frac{\text{ambient temperature} + \Delta T_{ram} + \Delta T_{hot\ exhaust}}{518.7}$$

In reverse, the single-line characteristic can be used to find the actual fuel flow, air flow, and exhaust gas conditions at any ambient condition. A power setting is determined by the actual turbine inlet temperature. It can also be assumed that the actual exhaust temperature is approximately constant with a constant turbine inlet temperature. The temperature ratio T_7/T_2 can be formed, and the operating point on the referred single-line characteristic can be determined.

Sample Calculation:

We find the gas conditions for a 95°F day at 6,000 foot altitude static and for the military rating in the following manner:

The pressure at 6,000 feet is $P_a = 11.8$ psia and

$$\delta = \left(\frac{11.8}{14.7}\right)(0.998) = 0.7998$$

The engine inlet loss is

$$\frac{\Delta P}{P} = 0.002$$

The ambient temperature is $T_a = 95°F$

The engine inlet temperature is raised 4 degrees by mixing of exhaust gases with fresh air

$$T_2 = 99°F = 558.7°R$$

and

$$\theta = \frac{558.7}{518.7} = 1.0771$$

$$\sqrt{\theta} = 1.0378$$

The actual exhaust temperature at military rating is $T_7 = 1621°R$. The engine temperature ratio is

$$\frac{T_7}{T_2} = \frac{1621}{558.7} = 2.901$$

All the referred parameters can be found from the single-line characteristic (see Figure 136) by establishing the referred thrust for the temperature ratio

$$T_7/T_2 = 2.901$$

$$P_7/P_2 = 2.455$$

$$W_A\sqrt{\theta}/\delta = 129.5 \text{ lb/sec}$$

$$/\delta\sqrt{\theta} = 6568 \text{ lb/hr}$$

The actual exhaust pressure, airflow, and fuel flow are found by unreferring the above values.

$$P_7 = (P_7/P_2)\,P_2 = (2.455)(11.8)(0.998) = 28.9 \text{ psia}$$

$$W_A = (W_A\sqrt{\theta}/\delta)(\delta/\sqrt{\theta}) = (129.5)\left(\frac{0.7998}{1.0378}\right) = 99.8 \text{ lb/sec}$$

$$W_f = (W_f/\delta\sqrt{\theta})\,\delta\sqrt{\theta} = (6568)(0.7998)(1.0378) = 5452 \text{ lb/hr}$$

ROTOR POWER CALCULATION

The change in Mach number along the rotating duct can be expressed by the following differential equation:

$$\frac{dM}{dr} = \frac{M(1+KM^2)\left(1+\frac{K-1}{2}M^2\right)}{2T(1-M^2)}\frac{dT}{dr} + \frac{2KfM^3\left(1+\frac{K-1}{2}M^2\right)}{D(1-M^2)}$$

$$- \frac{\Omega^2 rM\left(1+\frac{K-1}{2}M^2\right)}{gRT(1-M^2)} - \frac{M\left(1+\frac{K-1}{2}M^2\right)}{(1-M^2)}\frac{dA/A}{dr} \qquad (1)$$

The above equation has been derived by John R. Henry (NACA TN-3089) with the help of the following equations:

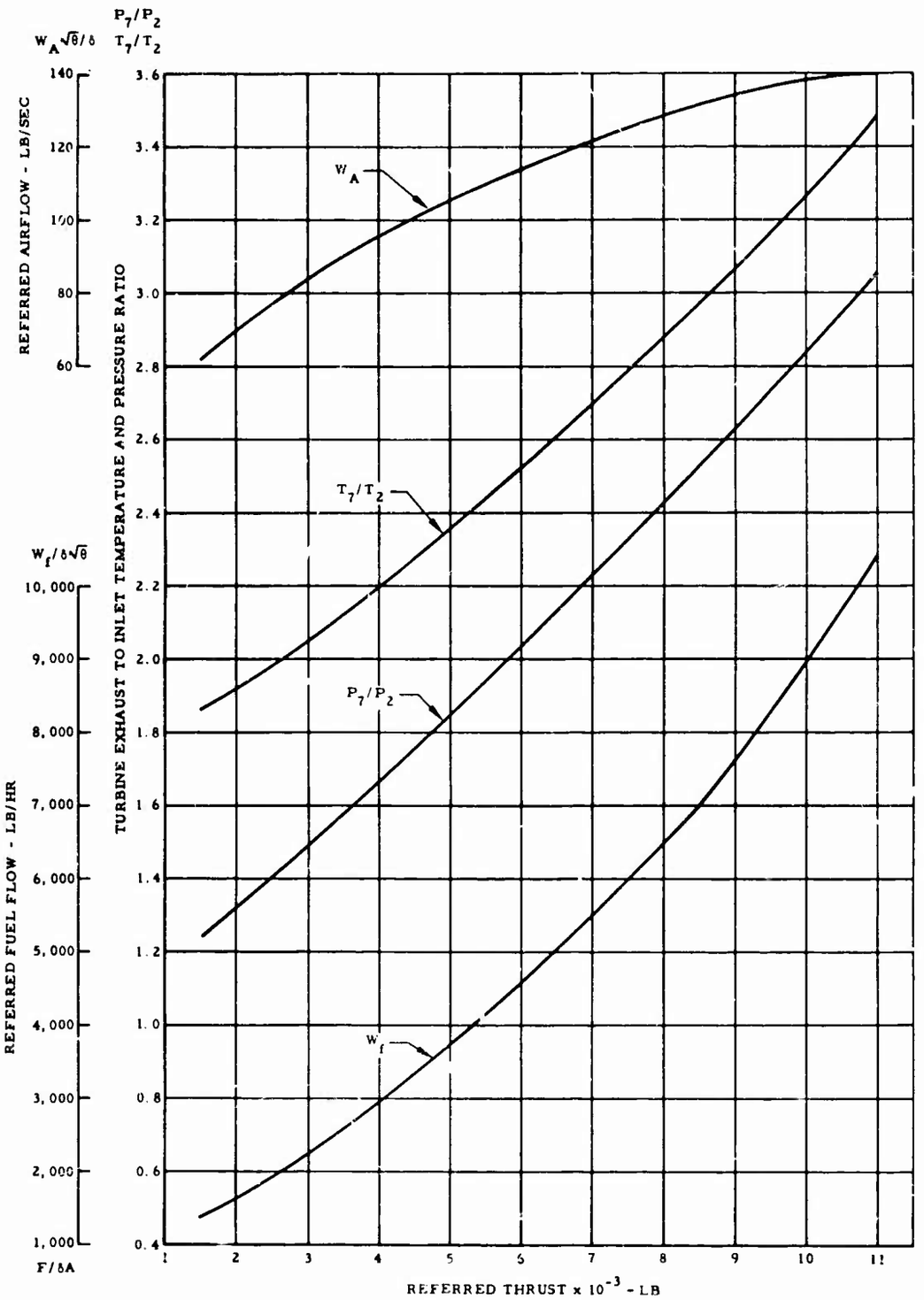

Figure 136. J52-P-8A Engine Single-Operating Line.

Momentum

$$\rho AVdV = -Adp - 4A \frac{f}{D} \frac{\rho V^2}{2} dr + \Omega^2 \rho Ar\, dr \tag{2}$$

Equation of State

$$\frac{dP_s}{P_s} = \frac{d\rho}{\rho} + \frac{dT_s}{T_s} \tag{3}$$

Mach Number Relation

$$\frac{dM^2}{M^2} = \frac{dV^2}{V^2} - \frac{dT_s}{T_s} \tag{4}$$

Continuity

$$\frac{d\rho}{\rho} + \frac{dA}{A} + \frac{dV}{V} = 0 \tag{5}$$

Isentropic Stagnation Relations

$$\frac{T}{T_s} = 1 + \frac{K-1}{2} M^2 \tag{6}$$

and

$$\frac{P}{P_s} = \left(1 + \frac{K-1}{2} M^2\right)^{\frac{K}{K-1}} \tag{7}$$

From the energy equation an expression for the change in total temperature due to centrifugal forces can be obtained. The energy balance

$$dm\, c_p\, dT = dm\, r\Omega^2\, dr$$

reduces to

$$\frac{dT}{dr} = \frac{r\Omega^2}{c_p} = \frac{K-1}{gKR} r\Omega^2 \tag{8}$$

The differential Equation (1) is solved numerically. Using Equation (8) and the following definition

$$F_B = \frac{1 + \frac{K-1}{2} M^2}{1 - M^2} \tag{9}$$

equation (1) can be written in differential form

$$\Delta M = C\left(\frac{F_B M(K-1)}{2TgKR}\right)(1 + KM^2)\,\Omega^2 r \Delta r + \left(\frac{2KfM^3 F_B}{D}\right)\Delta L$$

$$- \frac{\left(1 + \frac{K-1}{2} M^2\right)\Omega^2 F_B rM}{gRT} \Delta r - MF_B\left(\frac{\Delta A}{A}\right) \tag{10}$$

The coefficient C has been added to correct for heat losses. The second term of the equation represents the friction loss. The increment Δr has been replaced by ΔL to allow calculations of deviations of the ducting from the radial direction.

The total change of the Mach number over any section of the ducting is the sum of all increments.

$$M_2 = M_1 + \sum_{r_1}^{r_2} \Delta M \tag{11}$$

The temperature for the next integration step is found from

$$T_2 = T_1 + C\left(\frac{K-1}{2gKR}\right)\Omega^2\left(r_2^2 - r_1^2\right) \tag{12}$$

The total pressure at the end of the section is calculated from continuity and the stagnation relation at both ends.

$$\frac{P_2}{P_1} = \frac{A_1 M_1}{A_2 M_2}\left(\frac{1 + \frac{K-1}{2} M_2^2}{1 + \frac{K-1}{2} M_1^2}\right)^{\frac{K+1}{2(K-1)}} \sqrt{\frac{T_2}{T_1}} \tag{13}$$

If two or more unequally sized ducts are joined, the mixed total temperature is calculated by mass weighing enthalpy and the mixed total pressure is calculated by mass weighing entropy. Assuming constant specific heat,

$$T_m = \frac{W_1 T_1 + W_2 T_2}{W_1 + W_2} \tag{14}$$

Mixed entropy at constant mixed temperature

$$\int_{S_1}^{S_m} W_1 dS + \int_{S_2}^{S_m} W_2 dS = 0 \rightarrow S_m = \frac{W_1 S_1 + W_2 S_2}{W_1 + W_2} \tag{15}$$

The entropy change is a function of the temperature and pressure change

$$ds = c_p \frac{dT}{T} - R \frac{dP}{P} \tag{16}$$

The entropy for $dT/T = 0$ is

$$s = -R\ell nP \tag{17}$$

Mass Weighing the entropy

$$-R\ell nP_m = \frac{-RW_1 \ell nP_1 - RW_2 \ell nP_2}{W_1 + W_2} \tag{18}$$

we can establish the mixed pressure for two flows as

$$P_m = e^{\frac{W_1 \ell nP_1 + W_2 \ell nP_2}{W_1 + W_2}} \tag{19}$$

Pressure losses due to turbulence occurring at sharp turns, flow mixing, and splitting are calculated separately as a function of the local velocity head. The losses are taken into account at the end of each blade section. (See page 270 for the calculation of the turbulence losses.)

If the gas conditions are known at the entrance to the nozzles, the power is calculated from the enthalpy drop across the nozzle.

$$\Delta h = \frac{K}{K-1} gRT \left[1 - \left(\frac{P_a}{P} \right)^{\frac{K-1}{K}} \right]$$

The isentropic velocity is

$$V_{is} = \sqrt{2\Delta h}$$

The actual nozzle velocity is

$$V_{actual} = C_{ve} V_{is}$$

Shaft Horsepower

$$SHP = \frac{W_{total}}{g(550)} (V_{actual} - V_R) V_R$$

where V_R = rotational velocity of nozzle centerline, ft/sec.

The calculations outlined above have been programmed for the IBM computer 7094. Experiences with the XV-9A Research Vehicle have indicated that the temperature increases due to centrifugal forces were cancelled by heat losses. The calculations for this proposal have been made assuming a constant gas temperature. However, it should be noted that this is a conservative assumption in view of the fact that the ducting on the CRA will be insulated, and the heat losses are expected to be lower than for the XV-9A vehicle. The friction factor of f = 0.003 has been established for the XV-9A ducting and is used for all the present calculations. A sample calculation of rotor horsepower for 6,000-foot altitude and a 95°F ambient temperature is presented in Table XXXV.

The complete table of rotor power available is given in Table XXXVI. The rotor power corrections for engine power extraction and bleed are given in Table XXXVII.

TABLE XXXV. SAMPLE CALCULATION FOR ROTOR POWER AT 6,000-FOOT ALTITUDE 95°F DAY MILITARY RATING

Section	Location	Radius (ft)	Pressure (psia)	Mach Number	$W\sqrt{T}/P$ (sq in. - $°R^{1/2}$/sec)	Flow (lb/sec)	$\overline{P}_T/P_{T_7}$	Area (sq ft)
Engine	Exit	-	28.866	-	141.27	100.395	1.0	2.64
Section 1	Inlet	1.0	27.564	0.425	48.881	33.465	0.9549	0.9846
Pipe 1	Exit	10.0	27.185	0.4257	-	16.733	-	0.4923
Pipe 2	Exit	10.0	27.185	0.4257	-	16.733	-	0.4923
Section 1	Exit	-	27.185	0.4257	49.563	33.465	0.9418	0.9846
Section 2	Inlet	10.0	27.185	0.5250	49.563	33.465	0.9418	0.8523
Section 2	Exit	15.833	27.315	0.5166	49.327	33.465	0.9463	0.8523
Section 3	Inlet	15.833	27.315	0.5125	49.327	33.465	0.9463	0.8626
Pipe 1	Exit	20.5	27.702	0.5024	-	19.097	-	0.4923
Pipe 2	Exit	20.5	27.650	0.5037	-	14.368	-	0.3704
Section 3	Exit	-	27.680	-	48.677	33.465	0.9589	0.8626
Section 4	Inlet	20.5	27.680	0.50625	48.677	33.465	0.9589	0.8626
Pipe 1	Exit	21.96	27.866	0.7582	-	19.097	-	0.3931
Pipe 2	Exit	23.13	27.5[illegible]	0.8376	-	14.368	-	0.2899
Section 4	Exit	22.47	27.724	-	48.[illegible]00	33.465	0.9604	0.6830

The station designations follow the schematic shown in Figure 135
The calculations use a constant gas temperature T_7 = 1621°R
Nozzle calculation:

$$V_{is} = \left\{2g \frac{K}{K-1} RT \left[1 - \left(\frac{P_a}{P}\right)^{\frac{K-1}{K}}\right]\right\}^{\frac{1}{2}} = \left\{(2)(32.2)\left(\frac{1.334}{1.334-1}\right)(53.34)(1621)\left[1 - \left(\frac{11.77}{27.72}\right)^{\frac{1.334-1}{1.334}}\right]\right\}^{\frac{1}{2}} = 2072 \text{ ft/sec}$$

$$V_{actual} = C_{ve} \times V_{is} = (0.96)(2072) = 1989 \text{ ft/sec}$$

$$SHP = \frac{W_{total}}{g(550)} \left(V_{actual} - V_R\right)V_R = \frac{100.4}{(550)(32.2)} (1989 - 649)\, 649 = 4925 \qquad \frac{\Delta SHP}{SHP} = 0.0008$$

The power correction due to compressor bleed and power extraction is given in Table XXXVII. Finally, rotor shaft horsepower is equal to SHP = 4921.

TABLE XXXVI. ROTOR PERFORMANCE

Power does not include mechanical losses and power extractions from the rotor shaft.

Altitude (ft)	$T_{ambient}$ (°F)	Rotor (hp)	Fuel Flow (lb/hr)	Rating
Sea Level	Standard	7,044	7,894	Military
5,000	Standard	6,238	7,052	Military
10,000	Standard	5,470	6,255	Military
15,000	Standard	4,741	5,505	Military
20,000	Standard	4,080	4,801	Military
Sea Level	95	6,137	6,836	Military
3,000	95	5,503	6,131	Military
6,000	95	4,921	5,487	Military
9,000	95	4,390	4,897	Military
12,000	95	3,906	4,359	Military
Sea Level	Standard	7,044	7,894	Military
Sea Level	Standard	6,006	6,566	Normal
Sea Level	Standard	5,222	5,758	Part Load
Sea Level	Standard	3,316	3,869	Part Load
Sea Level	Standard	1,199	1,952	Part Load
Sea Level	95	6,137	6,836	Military
Sea Level	95	5,096	5,743	Normal
Sea Level	95	4,356	4,968	Part Load
Sea Level	95	2,537	3,206	Part Load
Sea Level	95	541	1,414	Part Load
6,000	95	4,921	5,487	Military
6,000	95	4,087	4,612	Normal
6,000	95	3,494	3,990	Part Load
6,000	95	2,035	2,575	Part Load
6,000	95	437	1,138	Part Load

Blade tip velocity V_R = 720 ft/sec

Inlet temperatures are taken 4°F above ambient temperatures to account for hot gas mixing

Inlet pressure loss, $\Delta P/P = 0.002$

Friction coefficient, $f = 0.003$

Nozzle velocity coefficient, $C_{ve} = 0.96$

Diverter valve leakage loss, $\Delta W/W = 0.0088$

Low rotor power extraction, HP = 6.7 (engine)

High-rotor power extraction, HP = 34 (engine)

Pressure loss from engine exhaust to rotor inlet, $\Delta P/P = 0.0451$

High compressor bleed. $\Delta W/W = 0.0015$

Two guide vanes are used in each turn before the nozzle

TABLE XXXVII. ROTOR POWER CORRECTION

Altitude (ft)	$T_{ambient}$ (°F)	RHP - Loss ($\Delta SHP/SHP$)	Fuel Loss ($\Delta W_f/W_f$)	Rating
Sea Level	Standard	0.0014	-0.0044	Military
5,000	Standard	0.0011	-0.0055	Military
10,000	Standard	0.0006	-0.0066	Military
15,000	Standard	0.0001	-0.0082	Military
20,000	Standard	-0.0006	-0.0101	Military
Sea Level	95	0.0014	-0.0049	Military
3,000	95	0.0011	-0.0056	Military
6,000	95	0.0008	-0.0064	Military
9,000	95	0.0007	-0.0069	Military
12,000	95	0.0006	-0.0074	Military
Sea Level	Standard	0.0014	-0.0044	Military
Sea Level	Standard	0.0013	-0.0051	Normal
Sea Level	Standard	0.0012	-0.0058	Part Load*
Sea Level	Standard	0.0004	-0.0083	Part Load
Sea Level	Standard	-0.0004	-0.0108	Part Load
Sea Level	95	-0.0014	-0.0049	Military
Sea Level	95	0.0013	-0.0055	Normal
Sea Level	95	0.0008	-0.0068	Part Load
Sea Level	95	0.0003	-0.0082	Part Load
Sea Level	95	-0.0002	-0.0096	Part Load
6,000	95	0.0008	-0.0064	Military
6,000	95	0.0004	-0.0077	Normal
6,000	95	0.0	-0.009	Part Load
6,000	95	-0.0005	-0.0104	Part Load
6,000	95	-0.001	-0.0132	Part Load

Correction Due To:

Power Extraction from Engine

Low Rotor: $HP = 6.7 (HP_{extr}/HP_{engine}) = 0.00223$

High Rotor: $HP = 34 (HP_{extr}/HP_{engine}) = 0.01153$

High Compressor Bleed: $\Delta W/W = 0.0015$

*The part load power setting corresponds to Table XXXVI.

THRUST CALCULATION FOR FORWARD FLIGHT

The thrust calculations have been made according to the instructions of the engine manufacturer. The pressure loss estimations are taken from calculations on pages 274 to 277. Power extractions of 13 horsepower for hydraulic pumps are taken from the high rotor shaft and 6.7 horsepower for generator drive from the low engine rotor.

The thrusts and fuel flow for sea level, 15,000, 25,000, 35,000 feet altitude at standard day, and 6,000 feet altitude at a 95° F day are given in Tables XXXVIII through XLII.

The performance correction factors are given in Tables XLIII through XLVII.

The nozzle velocity coefficient is assumed to be the same as that for the standard Pratt and Whitney engine nozzle.

TABLE XXXVIII. THRUST AT SEA LEVEL, STANDARD DAY

CRA Model 485

V_{true} (kn)	Jet Thrust (lb)						Fuel Flow (lb/hr)					
	0	100	200	300	400	500	0	100	200	300	400	500
Military	8940	8275	7950	7810	7810	7890	7975	7575	7705	7990	8345	8770
Normal	7850	7260	6970	6860	6870	6915	6630	6400	6630	6940	7340	7725
70% Normal	5435	5020	4820	4745	4750	4780	4275	4345	4560	4840	5170	5530
40% Normal	3035	2800	2680	2635	2635	2655	2465	2620	2810	3025	3265	3510

TABLE XXXIX. THRUST AT 15,000 FEET ALTITUDE, STANDARD DAY

CRA Model 485

V_{true} (kn)	Jet Thrust (lb)					Fuel Flow (lb/hr)				
	100	200	300	400	500	100	200	300	400	500
Military	5370	5275	5380	5635	5955	4855	5080	5440	5935	6435
Normal	4710	4605	4735	4950	5230	4070	4255	4645	5095	5570
70% Normal	3265	3190	3280	3430	3625	2690	2860	3150	3505	3885

TABLE XL. THRUST AT 25,000 FEET ALTITUDE, STANDARD DAY										
CRA Model 485										
V_{true} (kn)	Jet Thrust (lb)					Fuel Flow (lb/hr)				
	200	300	400	500	600	200	300	400	500	600
Military	3850	3855	4060	4395	4850	3680	3835	4165	4640	5240
Normal	3310	3365	3565	3860	4285	3005	3220	3550	3980	4560
70% Normal	2295	2335	2475	2680	2980	1980	2175	2430	2735	3140
1000 lb Rating	907	907	907	907	907	820	885	955	1020	1089

TABLE XLI. THRUST AT 35,000 FEET ALTITUDE, STANDARD DAY										
CRA Model 485										
V_{true} (kn)	Jet Thrust (lb)					Fuel Flow (lb/hr)				
	200	300	400	500	600	200	300	400	500	600
Military	2560	2680	2945	3260	3600	2405	2650	3030	3445	3870
Normal	2255	2345	2580	2880	3155	1995	2195	2525	2935	3340
70% Normal	1565	1625	1795	2000	2195	1310	1460	1690	1960	2225
1000-lb Rating	937	938	933	933	922	826	888	958	1023	1092

TABLE XLII. THRUST AT 6,000 FEET ALTITUDE, 95° DAY												
CRA Model 485												
V_{true} (kn)	Jet Thrust (lb)						Fuel Flow (lb/hr)					
	100	200	300	400	500	600	100	200	300	400	500	600
Military	5687	5373	5047	5124	5290	-	5317	5458	5542	5744	5911	-

TABLE XLIII. PERFORMANCE CORRECTION AT SEA LEVEL, STANDARD DAY

Diverter Valve Leakage Loss $\Delta W/W = 0.0067$
Low Rotor Power Extraction HP = 6.7
High Rotor Power Extraction HP = 13.0

V_{true} (kn)	Jet Thrust Loss ($\Delta F/F$)						Fuel Flow Loss ($\Delta W_f/W_f$)						Inlet Loss ($\Delta P/P$)	Exhaust Loss ($\Delta P/P$)
	0	100	200	300	400	500	0	100	200	300	400	500		
Military	0.0389	0.0410	0.0420	0.0425	0.0426	0.0423	0.0029	0.0028	0.0029	0.0030	0.0031	0.0033	0.005	0.064
Normal	0.0425	0.0449	0.0461	0.0470	0.0469	0.0464	0.0027	0.0028	0.0027	0.0028	0.0030	0.0031	0.00465	0.064
70% Normal	0.0535	0.0564	0.0580	0.0589	0.0588	0.0583	0.0006	0.0007	0.0008	0.0009	0.0011	0.0013	0.0035	0.064
40% Normal	0.0741	0.0789	0.0830	0.0859	0.0858	0.0842	-0.0016	-0.0015	-0.0012	-0.0010	-0.0008	-0.0006	0.0021	0.0575

TABLE XLIV. PERFORMANCE CORRECTION AT 15,000 FEET ALTITUDE, STANDARD DAY

Diverter Valve Leakage Loss $\Delta W/W = 0.0067$
Low Rotor Power Extraction HP = 6.7
High Rotor Power Extraction HP = 13.0

V_{true} (kn)	Jet Thrust Loss ($\Delta F/F$)					Fuel Flow Loss ($\Delta W_f/W_f$)					Inlet Loss ($\Delta P/P$)	Exhaust Loss ($\Delta P/P$)
	100	200	300	400	500	100	200	300	400	500		
Military	0.0288	0.0302	0.0306	0.0302	0.0282	0.0013	0.0016	0.0017	0.0020	0.0024	0.005	0.064
Normal	0.0335	0.0341	0.0333	0.0318	0.0306	-0.0007	-0.0009	-0.0011	-0.0014	-0.0017	0.0047	0.064
70% Normal	0.0438	0.0447	0.0437	0.0916	0.0401	-0.0015	-0.0012	-0.0009	-0.0006	-0.0002	0.0035	0.064

TABLE XLV. PERFORMANCE CORRECTION AT 25,000 FEET ALTITUDE, STANDARD DAY

Diverter Valve Leakage Loss $\Delta W/W$ = 0.0067
Low Rotor Power Extraction HP = 6.7
High Rotor Power Extraction HP = 13.0

V_{true} (kts)	Jet Thrust Loss ($\Delta F/F$)					Fuel Flow Loss ($\Delta W_f / W_f$)					Inlet Loss ($\Delta P/P$)	Exhaust Loss ($\Delta P/P$)
	200	300	400	500	600	200	300	400	500	600		
Military	0.0289	0.0285	0.0221	0.0255	0.0233	-0.0001	-0.0002	-0.0004	-0.0013	-0.0019	0.005	0.064
Normal	0.0316	0.0312	0.0298	0.0277	0.0257	0.0009	0.0007	0.0001	0.0006	0.0011	0.0047	0.064
70% Normal	0.0412	0.0405	0.0385	0.0359	0.0326	0.0036	0.0031	0.0029	0.0018	0.0011	0.0035	0.064
[illegible]% Rating	0.0863	0.0862	0.0862	0.0862	0.0862	0.0061	0.0057	0.0049	0.0045	0.0037	0.0023	0.058

TABLE XLVI. PERFORMANCE CORRECTION AT 35,000 FEET ALTITUDE, STANDARD DAY

Diverter Valve Leakage $\Delta W/W$ = 0.0067
Low Rotor Power Extraction HP = 6.7
High Rotor Power Extraction HP = 13.0

V_{true} (kts)	Jet Thrust Loss ($\Delta F/F$)					Fuel Flow Loss ($\Delta W_f / W_f$)					Inlet Loss ($\Delta P/P$)	Exhaust Loss ($\Delta P/P$)
	200	300	400	500	600	200	300	400	500	600		
Military	0.0278	0.0247	0.0244	0.0226	0.0205	0.0028	0.0024	0.0013	0.0004	-0.0006	0.005	0.064
Normal	0.0298	0.0284	0.0264	0.0240	0.0226	0.0040	0.0034	0.0022	0.0013	0.0001	0.0047	0.064
70% Normal	0.0380	0.0368	0.0336	0.0309	0.0284	0.0075	0.0068	0.0057	0.0044	0.0030	0.0035	0.064
[illegible]% Rating	0.0603	0.0550	0.0602	0.0604	0.0608	0.0104	0.0096	0.0088	0.0078	0.0067	0.0028	0.060

TABLE XLVII. PERFORMANCE CORRECTION AT 6,000 FEET ALTITUDE, 95° DAY

Diverter Valve Leakage Loss $\Delta W/W$ = 0.0067
Low Rotor Power Extraction HP = 6.7
High Rotor Power Extraction HP = 13.0

V_{true} (kts)	Jet Thrust Loss ($\Delta F/F$)					Fuel Flow Loss ($\Delta W_f / W_f$)					Inlet Loss ($\Delta P/P$)	Exhaust Loss ($\Delta P/P$)
	100	200	300	400	500	100	200	300	400	500		
Military	0.0446	0.0479	0.0498	0.0488	0.0417	0.0024	0.0023	0.0023	0.0023	0.0025	0.005	0.064

APPENDIX IV

PRELIMINARY STRUCTURAL ANALYSIS

ROTOR/WING BLADE ANALYSIS

Table XLVIII presents a summary of rotor blade total stresses Only the outboard portion of the blade is considered critical.

TABLE XLVIII. SUMMARY OF BLADE STRESSES, FATIGUE CASE

Spar Cap Stresses for Blade Stations 189 to 280 (Titanium)				
Blade Station	Centrifugal Force Stress (lb/sq in.)	Flapwise Bending Stress (lb/sq in.)	Chordwise Bending Stress (lb/sq in.)	Total Spar Cap Stress (lb/sq in.)
189	18,300	6500 ±4100	± 970	24,800 ±5070
201	18,500	7500 ±4710	± 780	26,000 ±5490
220	20,600	9400 ±5100	± 675	30,000 ±5775
240	19,200	8750 ±5000	± 460	27,950 ±5460
260	13,900	6600 ±3280	±1000	20,500 ±4280
280	-	-	-	-

Skin Stresses, Combined Shear and Direct for Blade Stations 189 to 280						
	Titanium			Aluminum		
Blade Station	q_{max} (lb/in.)	f_s (lb/sq in.)	Maximum Combined* (lb/sq in.)	q_{max} (lb/in.)	f_s (lb/sq in.)	Maximum Combined* (lb/sq in.)
189	±60	±2100	25,000 ±6250	±28	±1400	15,500 ±4000
201	±55	±2040	26,000 ±6560	±26	±1300	16,200 ±4120
220	±51	±2040	30,000 ±6770	±25	±1250	18,750 ±4200
240	±45	±2040	28,000 ±6520	±22	±1100	17,500 ±3920
260	±35	±2060	20,500 ±5600	±19	± 950	12,800 ±3140
280	±16	±1000	-	± 8	± 400	-

*Maximum combined endurance stress based on distortion energy theory is

$$\sigma_e = \sqrt{\sigma^2 + 3\tau^2}$$

Table XLIX presents the maximum tension at overspeed, and maximum compression at normal rpm. The ultimate tensile stresses used for titanium are F_{tu} = 175,000 lb/sq in. at room temperature, and F_{tu} = 158,000 at 200°F.

TABLE XLIX. SUMMARY OF BLADE STRESSES AT 3-G MANEUVER LOADS

Maximum Tension at Overspeed						
Blade Station	Centrifugal Force Stress (lb/sq in.)	Flapwise Bending, f (lb/sq in.)	Chordwise Bending, f (lb/sq in.)	Total, f (lb/ sq in.)	F_{tu}	Margin of Safety
180	43,000	43,600	15,600	102,200	158,000	+0.55
201	43,500	48,000	11,900	103,400	158,000	+0.53
220	48,200	56,500	9,800	114,500	158,000	+0.38
240	45,200	43,000	6,200	94,400	158,000	+0.67
260	32,500	27,000	13,200	72,700	158,000	> 1
280	-	-	-	-	-	-

Maximum Compression at Normal rpm				
Blade Station	Centrifugal Force Stress (lb/sq in.)	Flapwise Bending (lb/sq in.)	Chordwise Bending (lb/sq in.)	Total F_c (lb/sq in.)
189	25,450	43,600	15,600	30,750
201	25,750	48,000	11,900	34,150
220	30,900	56,500	9,800	35,400
240	28,800	43,000	6,200	20,400
260	20,850	27,000	13,200	19,350
280	-	-	-	-

WING ANALYSIS

A plan view and a typical cross section of the wing are shown in Figure 137. The blade retention system is shown schematically in Figure 138, with view AA showing the retention strap pack.

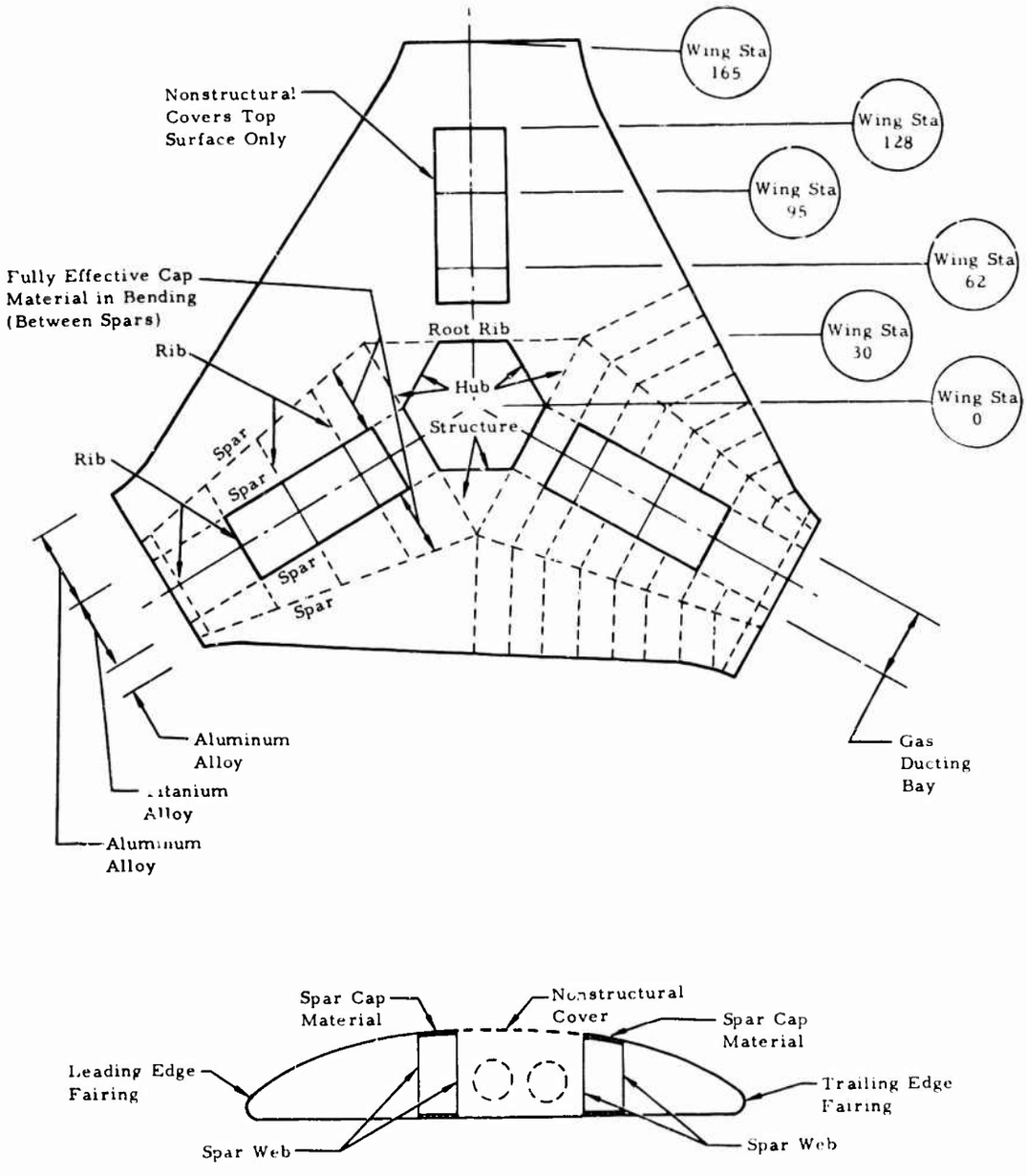

Figure 137. Plan View and Cross Section of Wing.

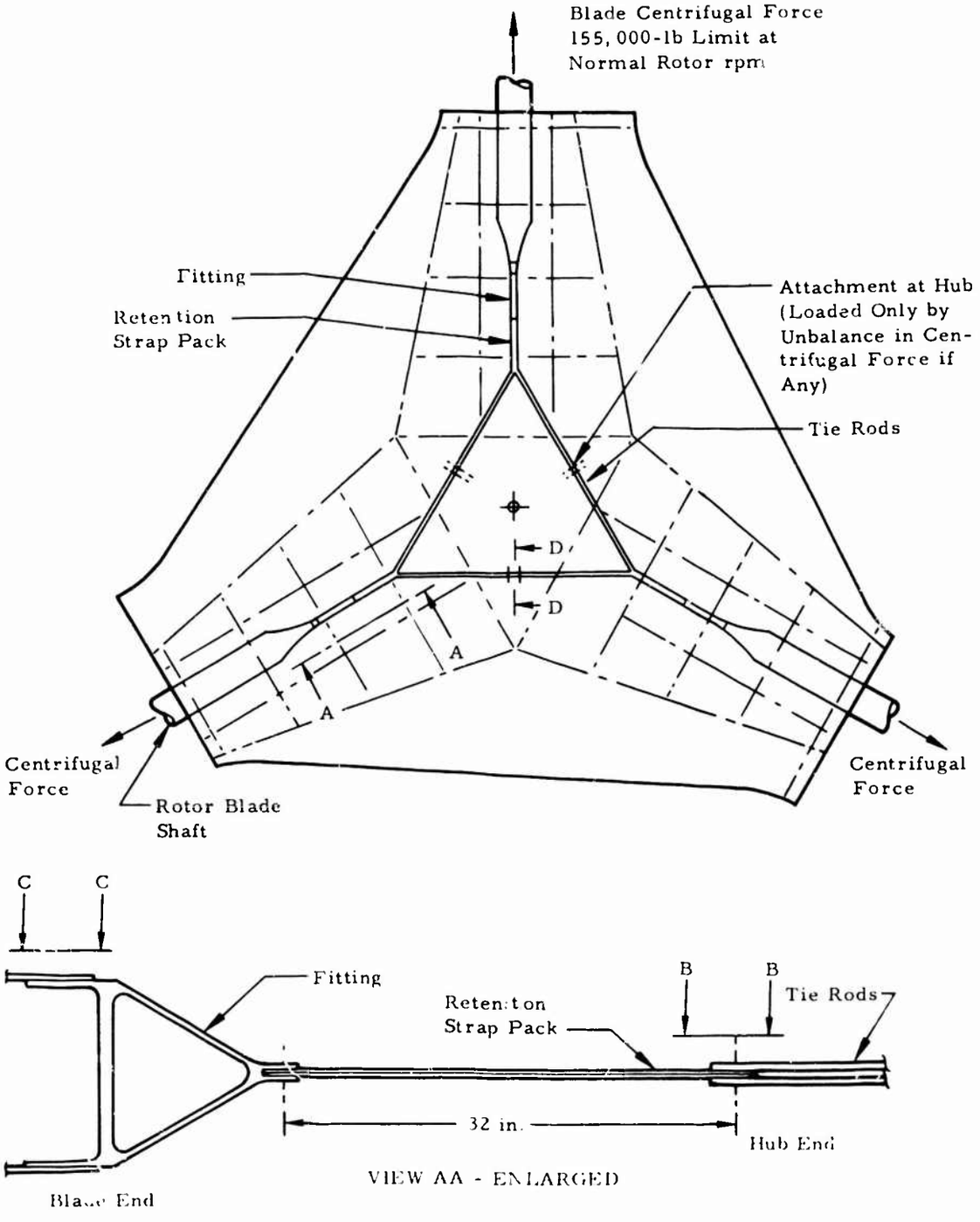

Figure 138. Blade Retention System.

ANALYSIS OF SHEAR FLOWS

A unit analysis of the shear flows acting at a typical wing station 62 is shown in Figure 139. View A shows the areas of the wing cross-section and dimensions at wing station 62. The shear flows are indicated for a unit 1000-pound vertical load View B, and for a unit 1000-pound pitching moment in View C.

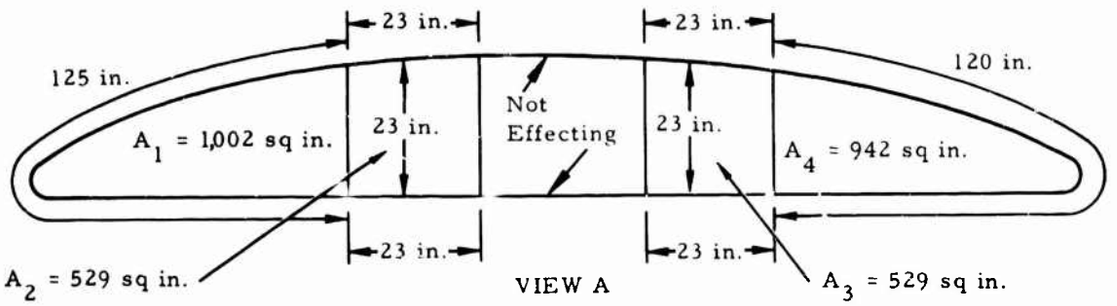

VIEW A

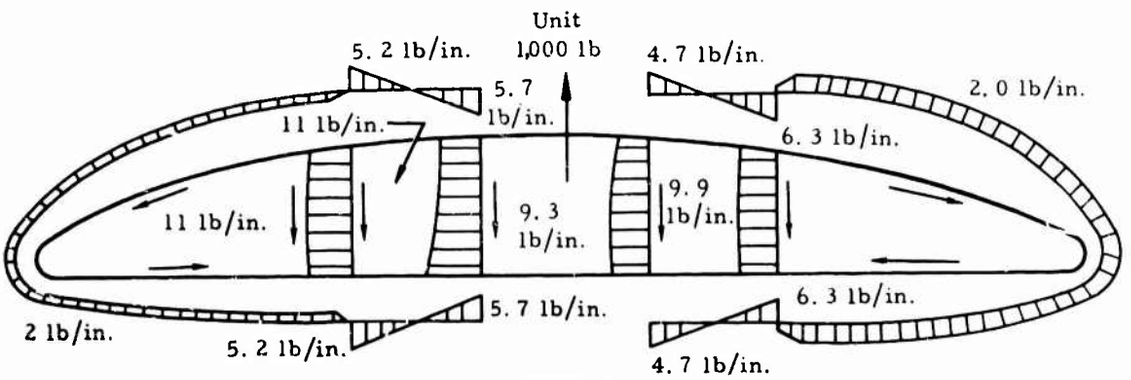

VIEW B

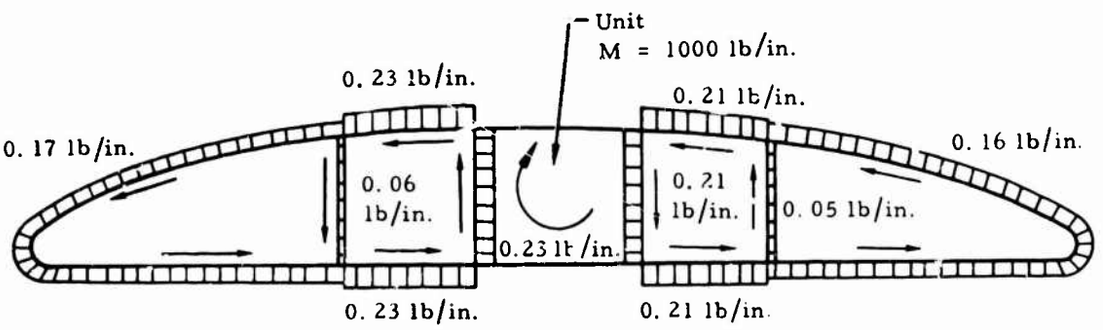

VIEW C

Figure 139. Shear Flows at Wing Station 62.

Table L gives the typical shear flows for wing station 60, calculated for 3-g maneuvers in helicopter flight and for 4-1/2-g maneuvers in the airplane mode. The stressed items are identified by number in the following cross-section of wing station 60.

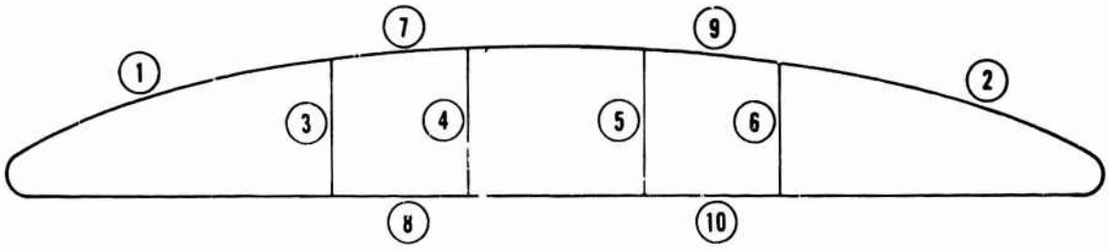

TABLE L. TYPICAL SHEAR FLOWS FOR WING STATION 60

Stressed Item	Description	Shear Due to 1000-lb Unit Vertical Load (lb/in.)	Shears × Unit Values	Shear Due to 1000-in.-lb Pitch (lb/in.)	Torsion × Unit Values	Total Ultimate Shear Flow (lb/in.)
3-g Maneuver - Helicopter Mode						
1	Leading edge	- 2.0	- 81	-0.17	- 40	-121
2	Trailing edge	+ 2.0	+ 81	-0.16	- 36	+ 45
3	Spar web	-11.0	-445	-0.06	- 14	-459
4	Spar web	-11.0	-445	+0.23	+ 54	-391
5	Spar web	- 9.3	-376	0.21	- 50	-426
6	Spar web	- 9.9	-402	+0.05	+ 12	-390
7	Spar caps	- 5.2	-211	-0.23	- 54	-265
8	Spar caps	- 5.2	-211	-0.23	- 54	-265
9	Spar caps	- 4.7	-191	-0.21	- 50	-241
10	Spar caps	- 4.7	-191	-0.21	- 50	-241
4-1/2-g Maneuver - Airplane Mode						
1	Leading edge	- 2.0	- 75	-0.17	-204	-279
2	Trailing edge	+ 2.0	+ 75	-0.16	-192	-117
3	Spar web	-11.0	-412	-0.06	- 72	-484
4	Spar web	-11.0	-412	+0.23	+276	-136
5	Spar web	- 9.3	-348	-0.21	-252	-600
6	Spar web	- 9.9	-371	+0.05	+ 60	-311
7	Spar cap	- 5.2	-195	-0.23	-276	-471
8	Spar cap	- 5.2	195	-0.23	-276	-471
9	Spar cap	- 4.7	176	-0.21	252	-428
10	Spar cap	- 4.7	-176	-0.21	-252	-428
Shears × Unit Values $\frac{27,000}{1000}$ × 1-1/2 × Unit Value						
Torsion × Unit Values $\frac{187,000}{1000}$ × 1-1/2 × Unit Values						

ANALYSIS OF RIB AT STATION 62

An analysis of the rib at station 62 in the hot duct bay for 4-1/2-g maneuver condition in the airplane mode for the highest wing torsion shows the following limit loads (see Figure 140):

V_1 = 5,560 lb $\qquad$ V_2 = 5,560 lb

M_1 = 90,294 in.-lb $\qquad$ M_2 = 262,564 in.-lb

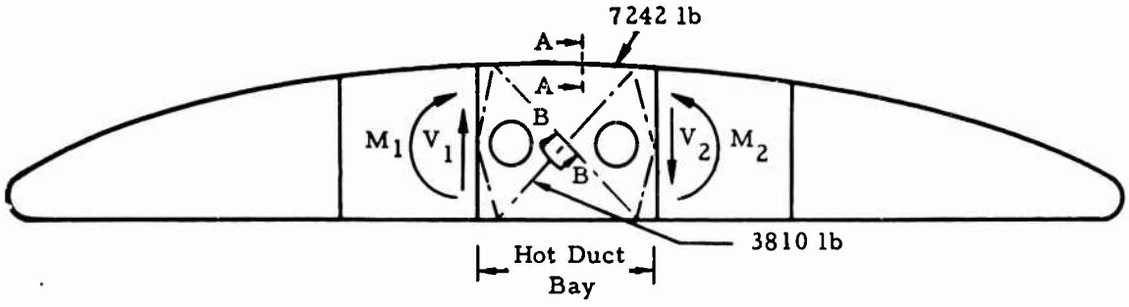

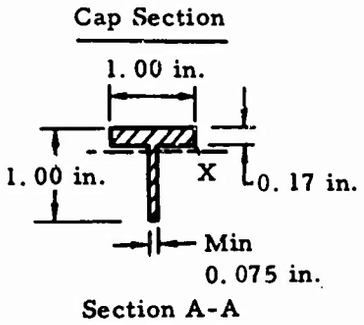

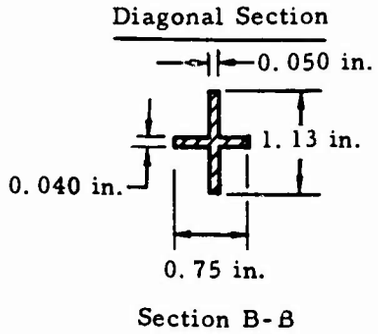

Figure 140. Rib Section (Titanium) in Hot Duct Area.

The material used is titanium. The stresses of the cap section (section A-A in Figure 140) are:

$$\text{Area} = 1.00(0.17) + (1.00 - 0.17)(0.075) = 0.232 \text{ sq in.}$$

$$f_c = \frac{P}{A} = \frac{7242(1.5)}{0.232 \text{ sq in.}} = 46,800 \text{ psi ultimate}$$

$$\frac{L}{r_{xx}} = \frac{19 \text{ in.}}{1.5(0.23)} = 55$$

The allowable stress at 300°F for $(L/\rho_{xx}) = 55$ is found from Figure C2.15 of Reference 28 and is

$$f_{c_{300°F}} = 47,000 \text{ psi}$$

Similarly, the section stress and allowable stresses for the diagonal section B-B of Figure 140 are:

$$\text{Area} = 0.75(0.04) + (1.13 - 0.04)(0.05) = 0.085 \text{ sq in.}$$

$$f_c = \frac{P}{A} = \frac{3810.0(1.5)}{0.085} = 67,300 \text{ psi ultimate}$$

$$\frac{L}{\rho} = \frac{15}{0.34} = 44$$

The allowable stress at 300°F for $L/\rho = 44$ is equal to 68,000 psi.

Analysis of Outer Wing Rib at Wing Station 159.5

The shear flows due to torsion, M, are found by applying the following equations:

$$2AG\theta = \Sigma q\, L/t$$

$$M = \Sigma 2\, Aq$$

The vertical load, V, is assumed to be distributed equally to each of the four webs in the static condition. In Figure 141, AL indicates aluminum and Ti indicates titanium.

The vertical webs are of aluminum and have the following thicknesses:

$$w_1 = 0.09 \text{ in.}$$

$$w_2 = w_3 = w_4 = 0.06 \text{ in.}$$

The shear flow,

$$q = \frac{H}{2(83 \text{ in.})}$$

due to horizontal loads acts aft in unison with the shear flows shown due to the vertical loads (Figure 142).

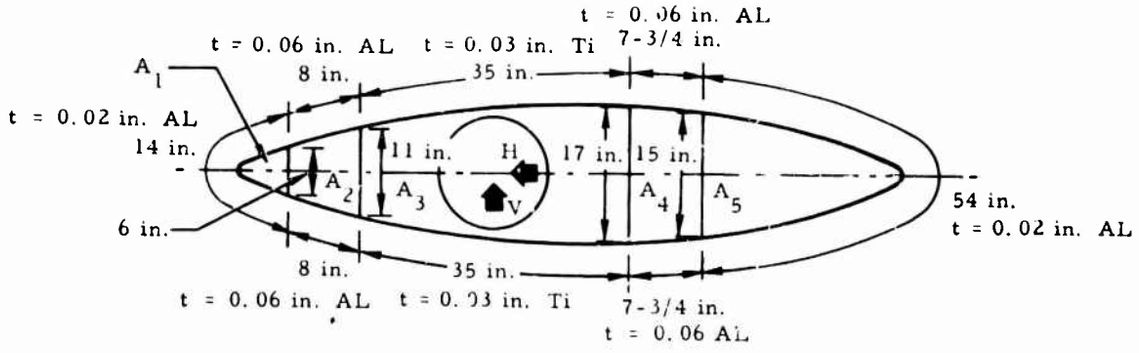

A_1 = 22.0 sq in.
A_2 = 69.0 sq in.
A_3 = 529.0 sq in.
A_4 = 124.0 sq in.
A_5 = 247.0 sq in.

Figure 141. Structural Arrangement at Rib-Wing Station 159.5.

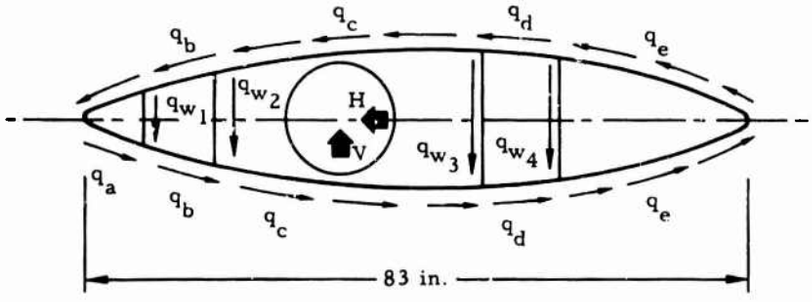

Figure 142. Shear Flow Schematic at Rib-Wing Station 159.5.

Table LI is an analysis of the fatigue condition and the 3-g helicopter limit load on the outer wing rib at wing station 159.5. The calculation of shear flows q on the rib due to the horizontal force H is equal to:

$$q = \frac{H}{2(83 \text{ in.})}$$

TABLE LI. FATIGUE AND 3 G LIMIT LOADS ON WING RIB AT STATION 159.5

Unit q Due to V		Fatigue Condition			3 g Limit Loads		
		q Due to V = 10,250 ±6,300 lb (lb/in.)	q Due to H = 22,154 ±2,238 lb (lb/in.)	Total q (lb/in.)	q Due to V = 58,000 lb (lb/in.)	q Due to H = 45,154 lb (lb/in.)	Total q Limit (lb/in.)
q_a	+0.00932V	+ 96 ±59	+134 ±14 -134 ∓14	+230 ±73 - 38 ±45	+ 540	+272 -272	+712 +268
q_b	+0.00271V	+ 28 ±17	+134 ±14 -134 ∓14	+162 ±31 -106 ±3	+ 157	+272 -272	+429 -115
q_c	+0.000674V	+ 7 ±4	+134 ±14 -134 ∓14	+141 ±18 -127 ∓10	+ 39	+272 -272	+311 -233
q_d	-0.000569V	- 6 ∓4	+134 ±14 -134 ∓14	+128 ±10 -140 ∓18	- 33	+272 -272	+239 -305
q_e	-0.002735V	- 28 ∓17	+134 ±14 -134 ∓14	+106 ∓3 -162 ∓31	- 159	+272 -272	+113 -431
q_{w_1}	+0.03589V	+368 ±226	0	+368 ±226	+2080	0	+2080
q_{w_2}	+0.02066V	+206 ±127	0	+206 ±127	+1200	0	+1200
q_{w_3}	+0.013477V	+138 ±85	0	+138 ±85	+ 782	0	+ 782
q_{w_4}	+0.014434V	+148 ±91	0	+148 ±91	+ 850	0	+ 850

(+) Sign indicates the direction agrees with directions shown on Figure 142 for the q values.

The rib shear and bending moments at wing station 159. 5 are shown in Figure 143.

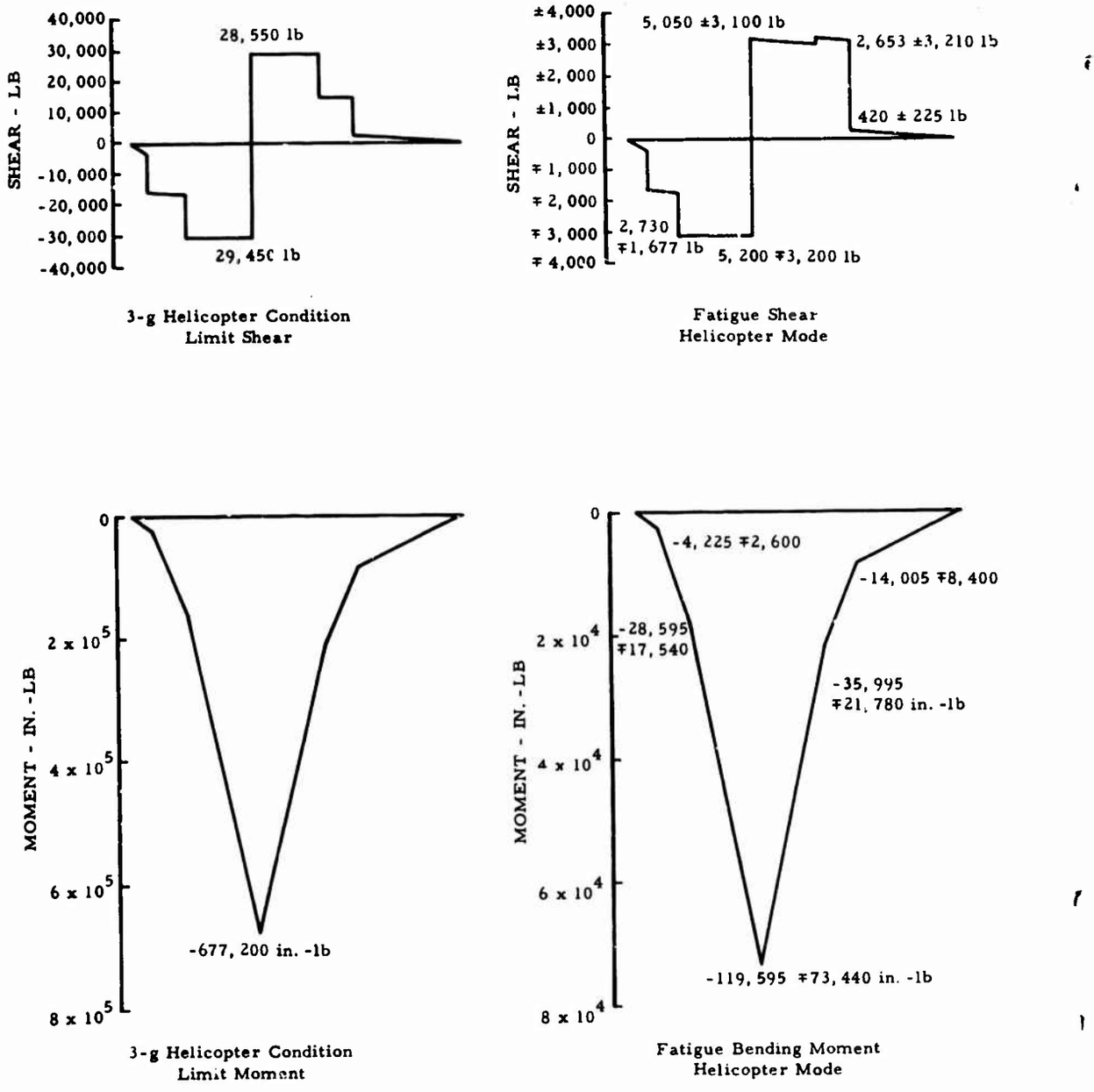

Figure 143. Rib Shear and Bending Moments of the Outer Wing (Station 159. 5).

MAXIMUM BENDING MOMENT AND SHEAR

The maximum bending moment and shear occurs in the rib at the bearing support (see Figure 144):

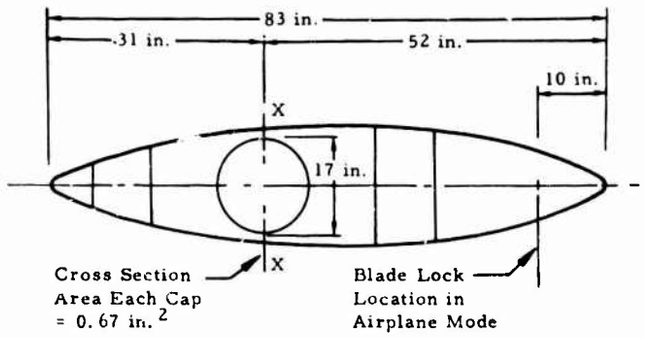

Material: Titanium

Allowable Stresses:

$F_B = (165,000)(0.91) = 150,000$ psi

$F_{cyclic} = 25,000 \pm 7,500$

Stresses at Section X-X							
Condition	Rib Moment (in.-lb)	Horizontal Bearing Loads (lb)	$\frac{M}{D} = \frac{M}{17}$ (lb)	$\frac{H}{2} \times \frac{52}{83}$ (lb)	$\frac{M}{17} + \left(\frac{H}{2} \times \frac{52}{83}\right)$ (lb)	$f = \frac{T}{A}$ $\left(\frac{M}{17} + \frac{H}{2} \times \frac{52}{83}\right)$ (psi)	Allowable Stress, F_c (psi)
Fatigue condition	-119,595 ±73,440	22,154 ±2,238	+7,040 ±4,320	6,940 ±700	+13,980 ±5,020	21,000 ±7,500	25,000 ±7,500
3-g maneuver helicopter mode	-677,200 limit	45,154	+40,000	+14,100	+54,100 x 1-1/2	81,000 ultimate	150,000

Figure 144. Rib Wing Station 159.5.

In the 4-1/2-g maneuver condition, airplane mode, the vertical limit load is V = 24,715 pounds limit (bearing load) on this rib, which is less than the 58,000 pound limit load from the 3-g helicopter maneuver conditions. When the blade is latched to the rib, the blade torque in 4-1/2-g airplane mode is 162,000 inch-pounds. For the 3-g helicopter mode, the shear flow limit is

$$q = \frac{T}{2A} = \frac{162,000}{2(515)} = 157 \text{ in.-lb}$$

Therefore, the airplane mode is not critical.

APPENDIX V

SUMMARY TABULATION

CONFIGURATION

1.	Overall dimensions	
	Wing span (Rotor/Wing turning)	50.0 ft
	Wing span (Rotor/Wing stopped)	44.9 ft
	Length	70.67 ft
	Height (from static ground line)	26.7 ft
	Tread	10.5 ft
	Rotor/Wing ground clearance	13.25 ft
2.	Rotor/Wing	
	Rotor diameter	50.0 ft
	Rotor disc area	1964 sq ft
	Rotor disc loading	10 lb per sq ft
	Blade solidity	0.165
	Rotor/Wing planform area (includes 2 blades only)	526 sq ft
	Aspect ratio (includes 2 blades only)	3.95
	Number of blades	3
	Blade area (each blade)	60.6 sq ft
	Blade coning angle	1.0 deg
	Blade twist	0 deg
	Blade hinge line angle (plan view)	3.43 deg fwd
	Design blade tip speed	720 fps
	Design rotor rpm	275
	Blade airfoil section	Modified circular arc
	Blade tip chord	50.0 in.
	Blade tip thickness	7.0 in.
	Blade root chord	80.0 in.
	Blade root thickness	17.0 in.
	Collective pitch range	-10 deg to +18 deg
	Cyclic pitch (first harmonic)	±15 deg (longitudinal and lateral)
	Cyclic pitch (second harmonic)	±2.5 deg
3.	Yaw fan	
	Diameter	4.7 ft
	Number of blades	6
	Blade chord	6.2 in.
	Disc area	17.3 sq ft
	Solidity ratio	0.42
	Blade twist	0 deg
	Airfoil section	NACA 0015
	Collective pitch range	±20 deg
	Design tip speed	720 fps
	Maximum power	235 hp
	Distance between Rotor/Wing and fan center lines	30.3 ft
	RPM (Rotor/Wing at 275 rpm)	2,930
4.	Vertical tail	
	Span	15.5 ft
	Area	137 sq ft
	Tip chord	81 in.
	Root chord	131 in.
	Aspect ratio	1.75
	Leading edge sweep angle	17 deg
	Root airfoil section	NACA 64_2A016
	Tip airfoil section	NACA 64_2A012
	Rudder hinge line	70 percent chord
	Rudder travel	±15 deg
5.	Horizontal tail	
	Span	27.83 ft
	Area	184 sq ft
	Tip chord	69 in.
	Root chord	90 in.
	Aspect ratio	4.20
	Leading edge sweep angle	18.5
	Root airfoil section	NACA 64_2A015
	Tip airfoil section	NACA 64_2A010
	Simultaneous elevon range	+5 deg to -20 deg
	Differential elevon range	±15 deg
	Simultaneous elevon trim travel	15 deg
6.	Fuselage	
	Length	70.67 ft
	Width	6.67 ft
	Height	10.6 ft
	Ground clearance (gross weight)	27 in.
	Cargo compartment	
	Basic length	14.5 ft
	Basic width	5.5 ft
	Basic height	6.0 ft
	Total length	26.2 ft
7.	Cockpit	
	Pilot	Right side
	Copilot	Left side
	Ejection seats	Installed
	Cyclic stick movement	±6 in. (longitudinal and lateral)
	Collective stick movement	9.5 in. up to 0.5 in. down
	Rudder pedal movement	±3.25 in.
	Rudder pedal adjustment	±3 in.

PERFORMANCE

1.	Airplane mode (design gross weight)	
	Maximum speed	490 kn
	Rate of climb	7,500 ft/min
	Service ceiling	> 35,000 ft
	Range (3,000-lb payload)	460 n mi
	Ferry range	2,575 n mi
	Stall speed	102 KEAS
	Limit dive speed	500 KEAS
2.	Helicopter mode (design gross weight)	
	Hover ceiling (OGE, 95°F)	13,100 ft
	Hover ceiling (OGE, std day)	19,500 ft
	V_{ne}	150 kn
	Rate of climb	6,500 fpm
	Rate of descent (autorotation)	2,200 fpm
	Forward cg limit	15 in.
	Aft cg limit	0 in.
	Lateral cg limit	±8 in.
	Maximum design rotor speed (power on)	275 rpm (red line)
	Maximum design rotor speed (power off)	275 rpm (red line)
	Design limit rotor speed (power on)	344 rpm
	Design limit rotor speed (power off)	344 rpm

WEIGHT

1.	Empty weight	13,169 lb
2.	Design gross weight (disc loading 10 psf)	19,635 lb
3.	Alternate gross weight	30,000 lb

DESIGN MANEUVER LOAD FACTOR (Design Gross Weight)

1.	Helicopter	+3.0 g, -0.5 g
2.	Airplane	+4.5 g, -1.0 g

SYSTEMS

Electrical

28-volt dc (primary)
115-volt single-phase 400-cycle
28-volt single-phase 400-cycle (for instrumentation)

Hydraulic

Flight and auxiliary per MIL-H-5440 Type II 3000 psi

APPENDIX V

MARY TABULATION

6. Fuselage

Length	70.67 ft
Width	6.67 ft
Height	10.6 ft
Ground clearance (gross weight)	27 in.
Cargo compartment	
Basic length	14.5 ft
Basic width	5.5 ft
Basic height	6.0 ft
Total length	26.2 ft

7. Cockpit

Pilot	Right side
Copilot	Left side
Ejection seats	Installed
Cyclic stick movement	±6 in. (longitudinal and lateral)
Collective stick movement	9.5 in. up to 6.5 in. down
Rudder pedal movement	±3.25 in.
Rudder pedal adjustment	±3 in.

PERFORMANCE

1. Airplane mode (design gross weight)

Maximum speed	490 kn
Rate of climb	7,500 ft/min
Service ceiling	>35,000 ft
Range (3,000-lb payload)	460 n mi
Ferry range	2,575 n mi
Stall speed	102 KEAS
Limit dive speed	500 KEAS

2. Helicopter mode (design gross weight)

Hover ceiling (OGE, 95°F)	13,100 ft
Hover ceiling (OGE, std day)	19,500 ft
V_{ne}	150 kn
Rate of climb	6,500 fpm
Rate of descent (autorotation)	2,200 fpm
Forward cg limit	15 in.
Aft cg limit	0 in.
Lateral cg limit	±8 in.
Maximum design rotor speed (power on)	275 rpm (red line)
Maximum design rotor speed (power off)	275 rpm (red line)
Design limit rotor speed (power on)	344 rpm
Design limit rotor speed (power off)	344 rpm

WEIGHT

1. Empty weight	13,169 lb
2. Design gross weight (disc loading 10 psf)	19,635 lb
3. Alternate gross weight	30,000 lb

DESIGN MANEUVER LOAD FACTOR (Design Gross Weight)

1. Helicopter	+3.0 g, -0.5 g
2. Airplane	+4.5 g, -1.0 g

SYSTEMS

Electrical

28-volt dc (primary)
115-volt single-phase 400-cycle
28-volt single-phase 400-cycle (for instrumentation)

Hydraulic

Flight and auxiliary per MIL-H-5440 Type II 3000 psi

Landing Gear

1. Landing gear

Tread	10.5 ft
Wheel base	24 ft 1 in.
Main gear	
Stroke	10 in.
Wheel size	11.00-12

2. Nose gear (steerable)

Stroke	10 in.
Steering angle	±40 degrees
Wheel size	4.4-10

Communication

1. AN/ARC-116 UHF-AM transceiver	2 units
2. AN/ARC-115 VHF-AM transceiver	1 unit
3. C-6533/ARC intercom panel	2 units
4. RH-101 headset microphone	2 units

Navigation

1. AN/ARN-LF/MF ADF	1 unit
2. AN/ARN compass system	1 unit

POWER PLANT

No. and model	(1) J52-P-8A(Model JT8B-3)
Manufacturer	Pratt & Whitney

Guaranteed SL Static Ratings

	Thrust (lb)	SFC (max) (lb/hr/lb of Thrust)
Maximum	9,300	0.86
Military	9,300	0.86
Normal	8,200	0.81
90% Cruise	7,380	0.79
75% Cruise	6,150	0.78

Gas conditions

	T°(R)	T°(F)	Press Ratio	Press (psig)	Gas Flow (lb/sec)
SLS normal	1,512	1052	2.47	21.6	131.8
SLS Mil.	1,621	1161	2.70	25.0	137.4

Fuel

Capacity (two 1,500-lb tanks)	3,000 lb
Grade or specification	JP-4 (MIL-J-5624)

Oil

Capacity 36 lb (MIL-L-7808 or MIL-L-23699)

EQUIPMENT AND FURNISHINGS

Zero-Zero ejection seats

UNCLASSIFIED
Security Classification

DOCUMENT CONTROL DATA - R & D

(Security classification of title, body of abstract and indexing annotation must be entered when the overall report is classified)

1. ORIGINATING ACTIVITY (Corporate author) Hughes Tool Company - Aircraft Division Culver City, California	2a. REPORT SECURITY CLASSIFICATION Unclassified 2b. GROUP

3. REPORT TITLE

HOT CYCLE ROTOR/WING COMPOSITE RESEARCH AIRCRAFT

4. DESCRIPTIVE NOTES (Type of report and inclusive dates)
Final Report

5. AUTHOR(S) (First name, middle initial, last name)
C. R. Smith

6. REPORT DATE August 1968	7a. TOTAL NO. OF PAGES 337	7b. NO. OF REFS 28
8a. CONTRACT OR GRANT NO. DA 44-177-AMC-338(T) b. PROJECT NO. Task 1F163204D15704 c. d.	9a. ORIGINATOR'S REPORT NUMBER(S) USAAVLABS Technical Report 68-31 9b. OTHER REPORT NO(S) (Any other numbers that may be assigned this report) HTC-AD 67-85	

10. DISTRIBUTION STATEMENT
This document has been approved for public release and sale; its distribution is unlimited.

11. SUPPLEMENTARY NOTES	12. SPONSORING MILITARY ACTIVITY U. S. Army Aviation Materiel Laboratories Fort Eustis, Virginia

13. ABSTRACT

A preliminary design study of a Hot Cycle Rotor/Wing Composite Research Aircraft is described. The Hot Cycle Rotor/Wing uses a single lightweight lifting surface which functions as both a rotor for takeoff and a fixed wing for horizontal flight. The Rotor/Wing is essentially an equilateral delta wing with short feathering blades at the three corners. The rotor is powered by a tip-jet Hot Cycle drive, and the turbojet exhaust is diverted from the rotor to provide forward propulsion.

The Hot Cycle Rotor/Wing provides the advantages of hovering efficiency, low downwash velocity, and helicopter-like flying qualities for vertical and low-speed flight, in addition to the high-speed capability and cruise efficiency of the jet airplane. Its simplicity and light weight are made possible through the combined use of the all-pneumatic Hot Cycle drive system and the dual-purpose Rotor/Wing lift system. This eliminates the need for heavy and complex mechanical drive components and anti-torque tail rotor; it permits flight as a helicopter and as an airplane without recourse to duplicate lifting systems or to folding, tilting, or retracting of lift systems to effect conversion.

DD FORM 1 NOV 68 1473 REPLACES DD FORM 1473, 1 JAN 64, WHICH IS OBSOLETE FOR ARMY USE.

UNCLASSIFIED
Security Classification

14. KEY WORDS	LINK A		LINK B		LINK C	
	ROLE	WT	ROLE	WT	ROLE	WT
Hot Cycle Rotor/Wing VTOL Aircraft Composite Research Aircraft (CRA)						